

**Intercollicular Modulation of Auditory Processing
in the Inferior Colliculus**

Llwyd David Orton BSc. (Hons)

**Submitted for the degree of Doctor of Philosophy
Institute of Neuroscience, Newcastle University**

July 2013

Abstract

The inferior colliculi (ICs) are the principal nuclei of the auditory midbrain. Each IC processes converging inputs from numerous brainstem nuclei as well as from thalamus and cortex. The ICs are interconnected in mirror image by one of the largest afferent inputs to each IC, the commissure of the inferior colliculus. There is exiguous knowledge about how each IC influences the processing of auditory information in its contralateral counterpart. This thesis investigates how one IC modulates the neural representation of sounds in the contralateral IC. To this end, I established and validated an experimental model in anaesthetised guinea pig whereby neuronal activity in one IC was selectively and reversibly deactivated. Cryoloop cooling produced temperature changes sufficient to deactivate spiking activity in the dorsal half of one IC, whilst leaving other centres in the auditory pathway unaffected. Single units were recorded in one IC before, during and after deactivation of the other IC. The characteristic frequency (CF) of IC neurons was unaffected during cooling, but the threshold of the population was raised. The area of non-V-shaped frequency response areas (FRAs) changed more than V-shaped FRAs. Differential changes were also observed in the firing rate of units with different temporal response patterns. Onset responders increased their firing rate whilst the firing of Chopper units was reduced. The temporal firing patterns of all neurons were unchanged by cooling. Changes in first spike latency (FSL) were negatively correlated with changes in firing rate. These data indicate that each IC differentially modulates the frequency selectivity, sensitivity, firing rate and FSL, but not the temporal firing pattern or CF of neurons in the contralateral IC. These findings demonstrate that the analysis of auditory stimuli in each IC is dependent on intercollicular processing. The ICs should therefore be viewed as working cooperatively rather than independently.

**Dedicated to the memory
of Our Ian and Our Andy**

Acknowledgements

It has been a privilege to pursue my post-graduate studies within the Institute of Neuroscience at Newcastle University. I will be forever indebted to my advisor, Professor Adrian Rees. His knowledge, patience and expert supervision have guided me through the completion of this thesis. He exemplifies all that an academic scholar should be. The research we have undertaken has fascinated me, but our friendship is what I will treasure from my time in his laboratory.

During my first year in Newcastle, I was fortunate to learn under the tutelage of Dr. David Pérez-González, from whom I garnered a wealth of information. I also spent a lot of time in that year working with visiting Professor Paul Poon. His enthusiasm and enquiring mind continue to influence me. Other researchers in the department who have helped me over the last four years are Dr. Claudia Racca, Dr. Sasha Gartside, Dr. Richard McQuade, and Dr. Fiona LeBeau.

I wish to thank my parents for their support: To my mum - thank you for giving everything you had to provide the best for me. I am truly thankful for the sacrifices you made. To my dad – no words can convey what you mean to me. Miles upon miles of bricks were laid and repointed so that I could have this opportunity, and for that I have a gratitude that I cannot express.

To Dominic Barber, my best mate for the best part of two decades, I would like to express numerous thanks. Thanks for standing by me no matter what. Thanks for always being hilarious. Thanks for never doubting me. Thanks for not letting me forget how important friendship is. Thanks for being the brother I never had.

Finally, but most importantly, to my beautiful bride Laura - your love, support and encouragement have inspired me to complete this journey. No matter what the future may bring, you make me happier than I could ever have dreamed. My love is eternally yours.

Table of Contents

Chapter 1. Introduction.....	1
1.1 Overview.....	1
1.2 Position of the Inferior Colliculi in the Auditory Pathway	3
1.3 Anatomy of the Inferior Colliculi	5
1.4 Neuronal Morphologies in the IC and Fibrodendritic Laminae	7
1.5 Afferent Projections to the Inferior Colliculi.....	9
1.5.1 Cochlear nuclei.....	11
1.5.2 Superior olivary complex.....	13
1.5.3 Nuclei of the lateral lemniscus.....	16
1.5.4 Medial geniculate body.....	20
1.5.5 Auditory cortex.....	21
1.6 Efferent Targets of the Inferior Colliculi.....	23
1.6.1 Medial geniculate body.....	23
1.6.2 Nuclei of the lateral lemniscus.....	24
1.6.3 Superior olivary complex.....	24
1.6.4 Cochlear nuclei.....	25
1.7 Physiology of the Inferior Colliculi.....	27
1.7.1 Tonotopy.....	27

1.7.2	<i>Temporal responses of inferior colliculus neurons</i>	29
1.7.3	<i>Binaural integration in the inferior colliculus</i>	29
1.7.4	<i>Response latency in the inferior colliculus</i>	30
1.8	The Commissure of the Inferior Colliculus	31
1.8.1	<i>Anatomy of the commissure of the inferior colliculi</i>	31
1.8.2	<i>Neurochemical nature of the CoIC</i>	35
1.8.3	<i>Functional influence of the CoIC</i>	37
1.8.4	<i>Gaps in our understanding of CoIC mediated processing of sound</i>	40
1.9	Aims of this Thesis	41
1.9.1	<i>Hypotheses</i>	41
1.9.2	<i>Organisation of this thesis</i>	41
Chapter 2.	Materials and Methods	43
2.1	Overview of Methodology	43
2.2	Animal Model	43
2.3	Anaesthetic Protocol	43
2.4	Surgical Procedure	44
2.5	The Cryoloop and Cooling System	45
2.6	Stimulus Generation and Presentation	48
2.7	Electrodes	50

2.8 Electrophysiological Recordings.....	50
2.9 Termination of Experiments	51
2.10 Histological Processing and Analysis	52
2.11 Data Analysis	52
2.12 Statistical Analyses	52
Chapter 3. Temperature change and electrophysiological deactivation with cryoloop cooling.....	55
3.1 Introduction	55
3.2 Methods	57
<i>3.2.1 Thermocouple measurements.....</i>	<i>57</i>
<i>3.2.2 Electrophysiological recordings and analyses.....</i>	<i>57</i>
3.3 Results	59
<i>3.3.1 Cooling produced a thermal gradient around the cryoloop.....</i>	<i>59</i>
<i>3.3.2 Cooling caused small temperature changes in the contralateral IC.....</i>	<i>62</i>
<i>3.3.3 Temperature changes across both ICs in the coronal plane</i>	<i>64</i>
<i>3.3.4 The ipsilateral cochlea and cochlear nuclei were not cooled.....</i>	<i>66</i>
<i>3.3.5 Neuronal deactivation in the cooled IC.....</i>	<i>68</i>
<i>3.3.6 Complete deactivation of a unit in the dorsal IC.....</i>	<i>69</i>
<i>3.3.7 Neuronal deactivation halfway down the tonotopic axis of the IC.....</i>	<i>71</i>

3.3.8	<i>Cooling did not deactivate neurons in the ventral IC</i>	73
3.3.9	<i>Multi-unit responses to cooling matched those of single units</i>	75
3.3.10	<i>Neural deactivation was restricted to the dorsal IC</i>	77
3.3.11	<i>Histological analysis of cooled tissue</i>	79
3.3.12	<i>Moderate cooling occasionally induced neuronal hyperactivity</i>	81
3.3.13	<i>Differential modulation of LFP components in the IC contralateral to cooling</i>	83
3.4	Discussion	85
3.4.1	<i>Restricted cooling efficacy matches previous data</i>	86
3.4.2	<i>Cooling did not deactivate other nuclei in the auditory system</i>	87
3.4.3	<i>Cooling deactivated the dorsal IC</i>	88
3.4.4	<i>Cooling did not damage tissue</i>	89
3.4.5	<i>Moderate cooling induced increases in firing rate</i>	90
3.4.6	<i>Changes in LFPs in the IC contralateral to cooling suggest a commissural selective deactivation</i>	92
3.5	Conclusion	94
Chapter 4. Modulation of Frequency Response Areas by Deactivation of the Contralateral IC		
		95
4.1	Introduction	95
4.2	Methods	99

4.2.1 Experimental procedure.....	99
4.2.2 Measurement of changes induced by cooling.....	99
4.2.3 Analyses of FRAs.....	100
4.3 Results.....	101
4.3.1 Classification of FRAs.....	102
4.3.2 Stability of FRAs over time.....	105
4.3.3 Classification of FRA types in this dataset.....	108
4.3.4 Frequency distribution of units.....	109
4.3.5 Increases in area of V-shaped monotonic FRAs.....	111
4.3.6 Decreases in area of V-shaped monotonic FRAs.....	113
4.3.7 Lack of change in area of V-shaped monotonic FRAs.....	115
4.3.8 The population of V-shaped monotonic FRA areas were unchanged by cooling of the contralateral IC.....	117
4.3.9 Cooling did not change the area of non-V-shaped non-monotonic FRAs.....	119
4.3.10 One of two Low Tilt units reached criterion.....	121
4.3.11 Cooling reduced the area of most Narrow FRAs.....	123
4.3.12 Contralateral IC cooling increased the area of all Closed FRAs.....	125
4.3.13 A high proportion of Multi-peaked FRAs changed to criterion.....	127

4.3.14 Broad FRAs had the largest areas of any FRA type and reduced in area.....	130
4.3.15 Area changes of non-V-Shaped FRAs were bidirectional.....	132
4.3.16 V-shaped and non-V-shaped FRAs had similar distributions of control FRA areas.....	134
4.3.17 Area changes of non-V-shaped FRAs were larger than V-shaped...135	
4.3.18 Changes in absolute area were significantly different between V-shaped and non-V-shaped FRAs.....	136
4.4 Discussion	141
4.4.1 FRA classification in the IC.....	142
4.4.2 FRA formation in the IC.....	143
4.4.3 Comparison of V-shaped and non-V-shaped FRA area changes.....	145
4.4.4 Changes in V-shaped FRAs.....	145
4.4.5 Changes in non-V-shaped FRAs.....	146
4.4.6 Changes in Multi-peaked FRAs were more than opposite.....	147
4.4.7 Broad FRAs are a distinct FRA type which were modulated differently than other FRA types.....	150
4.4.8 No commissural selectivity for monaural or binaural stimuli.....	151
4.5 Conclusion.....	152
Chapter 5. Changes in Parameters of Tuning and Selectivity Derived from FRAs Induced by Contralateral IC Deactivation.....	153

5.1 Introduction	153
5.1.1 <i>Characteristic frequencies of IC neurons and tonotopy</i>	153
5.1.2 <i>Threshold as a measure of IC neuron sensitivity to sound</i>	154
5.1.3 <i>Bandwidth as a measure of frequency selectivity in IC neurons</i>	155
5.2 Methods	158
5.2 Results	161
5.2.1 <i>Contralateral cooling did not change the CF of IC neurons</i>	161
5.2.2 <i>Threshold was modulated by contralateral IC deactivation</i>	163
5.2.3 <i>Threshold changes were similar to monaural or binaural stimulation</i>	171
5.2.4 <i>Control tuning bandwidths of FRAs 10 dB above threshold</i>	173
5.2.5 <i>Control tuning bandwidths of FRAs 40 dB above threshold</i>	175
5.2.6 <i>Cube root transformation made bandwidth independent of CF</i>	177
5.2.7 <i>Some FRA types had significantly different bandwidths at 40 dB above threshold</i>	179
5.2.8 <i>Changes in tuning bandwidth induced by contralateral IC deactivation</i>	180
5.2.9 <i>Changes in Q_{10} during contralateral IC cooling</i>	180
5.2.10 <i>Changes in cube root₁₀ during contralateral IC cooling</i>	183
5.2.11 <i>Changes in Q_{40} during contralateral IC cooling</i>	185

5.2.12 Changes in cube root ₄₀ during contralateral IC cooling.....	188
5.2.13 Initial bandwidth did not influence changes in bandwidth during cooling.....	190
5.2.14 Bandwidth changes 10 and 40 dB re threshold were uncorrelated .	192
5.2.15 Bandwidth changes were unrelated to control CF.....	194
5.2.16 Bandwidth changes were unrelated to control threshold.....	196
5.2.17 Bandwidth changes were not different in response to contralateral or binaural stimulation	198
5.4 Discussion	200
5.4.1 Clustering of units with similar CF in this study.....	200
5.4.2 Unchanged CF during contralateral IC cooling shows the influence of ascending afferent input to the IC.....	201
5.4.3 Threshold shifts correlated with FRA area changes and were larger in non-V-shaped FRAs than V-shaped FRAs.....	203
5.4.4 The cube root transform may be a useful measure of bandwidth in auditory neurons.....	205
5.4.5 Bandwidth changes showed no pattern or difference with level.....	206
5.5 Conclusion	209
Chapter 6. Effects of Contralateral IC Deactivation on Temporal Response Properties of IC Neurons	210
6.1 Introduction	210

6.2 Methods	213
6.3 Results	215
<i>6.3.1 Summary of the units included in this dataset</i>	215
<i>6.3.2 The firing rate of Onset units increased during contralateral IC deactivation</i>	218
<i>6.3.3 The majority of Build-up responses were unchanged</i>	221
<i>6.3.4 The firing rate of Chopper units decreased while ISI increased</i>	223
<i>6.3.5 Most Pauser units decreased in firing rate</i>	228
<i>6.3.6 On-sustained units expressed a range of changes</i>	231
<i>6.3.7 Sustained units changed firing rate during contralateral IC deactivation</i>	235
<i>6.3.8 Offset and Onset-Offset PSTHs tended to change in firing rate</i>	236
<i>6.3.9 Summary of changes in firing rate of all units by PSTH type</i>	237
<i>6.3.10 The FRA of a unit had no relationship to its PSTH</i>	239
<i>6.3.11 Changes in firing rate were not dependent on stimulation type</i>	242
<i>6.3.12 Firing rate and first spike latency were negatively related</i>	244
<i>6.3.13 First spike latency significantly increased across all units</i>	249
<i>6.3.14 The firing rate of the population of responses was not changed by contralateral IC deactivation</i>	250
<i>6.3.15 Units which were unchanged in firing rate had higher CFs than those that changed</i>	250

6.4 Discussion	251
<i>6.4.1 Technical limitations of this study</i>	251
<i>6.4.2 Effects of contralateral IC deactivation on firing rate</i>	253
<i>6.4.3 Differential changes in firing rate between PSTH morphologies</i>	256
<i>6.4.4 PSTH morphology was unchanged by the cooling paradigm</i>	258
<i>6.4.5 FRA and PSTH changes showed no correlation</i>	259
<i>6.4.6 Magnitude of rate changes were similar to either stimulation type</i> ...	260
<i>6.4.7 Changes in firing rate and FSL implicate the CoIC in temporal integration</i>	260
6.5 Conclusion	265
Chapter 7. General Discussion	266
7.1 Summary of Findings.....	266
7.2 Cooling as a Means by which to Investigate the CoIC	266
7.3 What Influence does the CoIC have on the Processing of Auditory Stimuli in the IC?.....	271
7.4 Possible Functional Roles for the CoIC in the Auditory System.....	273
7.5 Future Work Using Current Methods	276
7.6 Future Work Using Different Methods.....	276
References.....	279

List of Figures

Chapter 1

- 1.1 Photograph of the caudal guinea pig brain showing the location of the right IC with respect to other nuclei in the auditory system.
- 1.2 Schematic diagram of the unilateral ascending and commissural pathways of the auditory system.
- 1.3 Histologically stained sections of rat and human ICs stained for Nissl substance and Calcium binding proteins which highlight the shape, macrostructure and sub-nuclei of the IC.
- 1.4 Diagrammatical representations of the neurons in the IC, and the shape of the fibrodendritic laminae of the IC.
- 1.5 Summary schematic of the afferent projections to one IC with the relative size and neurochemical nature of each projection shown.
- 1.6 Schematic showing the binaural brainstem networks involved in the processing of azimuthal sound localisation stimuli.
- 1.7 Coronal Nissl stained sections showing the location of the nuclei of the lateral lemniscus relative to the IC.
- 1.8 Diagrammatical representation of the descending efferent projections of the IC.
- 1.9 Histological sections and diagrams showing the reciprocal interconnections of the ICs via the CoIC in rat, guinea pig and mouse.
- 1.10 Distribution of GABAergic and putative glutamatergic CoIC projecting IC neurons.
- 1.11 Data from prior investigations into the physiology of the CoIC.

Chapter 2

- 2.1 Photograph of the cryoloop used in the cooling experiments.
- 2.2 Schematic diagram of the hydraulic cooling system.

Chapter 3

- 3.1 Diagram and graph of the temperature measurements made through the IC in contact with the cryoloop and comparison with previous data recorded in guinea pig cortex (Coomber *et al.*, 2011).
- 3.2 Temperature measurements in the IC contralateral to cooling as a function of different durations of cooling.
- 3.3 Temperature measurements made through both ICs during cryoloop cooling.
- 3.4 Temperature measurements in the cochlea and cochlear nucleus ipsilateral to cooling.
- 3.5 Peri-stimulus time histogram (PSTH) showing reversible deactivation of a single unit in the dorsal region of the cooled IC.
- 3.6 Examples of changes in firing rate, PSTH and FRA of a single unit in the cooled IC throughout a step-wise cooling cycle.
- 3.7 PSTHs showing no change in firing rate of a unit in the ventral region of the cooled IC.
- 3.8 PSTHs of multi-units recorded at four depths spanning the dorso-ventral axis of the cooled IC.
- 3.9 Summary data of all single and multi-units recorded in the cooled IC as a function of CF.
- 3.10 Histological verification of the lack of trauma imparted to the brain by repeated cryoloop cooling.
- 3.11 Examples of the initial increase in firing rate of a neuron in the cooled IC before reversible deactivation at lower temperatures.
- 3.12 Averaged LFPs in the IC contralateral to cooling showing reversible changes in IC related potentials while potentials due to afferent projections were unchanged by cooling.

Chapter 4

- 4.1 Examples of each of the FRA types found in this study.
- 4.2 Multiple Narrow FRAs recorded from one neuron over 1 hour showing the repeatability and stability of the FRA recording method.
- 4.3 CFs of all units in this study and the relative proportions of each FRA type.
- 4.4 Example of a V-shaped FRA which increased in area during contralateral IC deactivation.
- 4.5 Example of a V-shaped FRA which decreased in area during contralateral IC deactivation.
- 4.6 Example of a V-shaped FRA which was unchanged in area during contralateral IC deactivation.
- 4.7 Summary of the changes induced in FRA area of all V-shaped monotonic FRAs found in this study.
- 4.8 Example of a V-shaped non-monotonic FRA which was unchanged in area during contralateral IC deactivation.
- 4.9 Example of a Low Tilt FRA which was unchanged in area during contralateral IC deactivation.
- 4.10 Example of a Narrow FRA which reduced in area during contralateral IC deactivation.
- 4.11 Example of a Closed FRA which increased in area during contralateral IC deactivation.
- 4.12 Example of a Multi-peaked FRA which decreased in area during contralateral IC deactivation.
- 4.13 Example of a Broad FRA which decreased in area during contralateral IC deactivation.
- 4.14 Summary of the changes induced in FRA area of all non-V-shaped FRAs found in this study.
- 4.15 Changes in FRA area of all units classified as being V-shaped and non-V-shaped groups.

Chapter 5

- 5.1 V-shaped FRA showing how the measures of CF, threshold and bandwidth were made.
- 5.2 CF of all FRAs in the control and contralateral IC cool stages.
- 5.3 Threshold of all FRAs in the control condition.
- 5.4 Changes in threshold of all FRAs and population analyses grouped by FRA type.
- 5.5 Changes in threshold grouped by control threshold and control CF.
- 5.6 Comparison of changes in threshold to contralateral monaural and binaural diotic stimuli.
- 5.7 Q_{10} and square root₁₀ measures of bandwidth for all control FRAs.
- 5.8 Q_{40} and square root₄₀ measures of bandwidth for all control FRAs.
- 5.9 Cube root₁₀ and cube root₄₀ transform of bandwidths for all control FRAs.
- 5.10 Changes in Q_{10} of all FRAs and population analyses grouped by FRA type.
- 5.11 Changes in cube root₁₀ of all FRAs and population analyses grouped by FRA type.
- 5.12 Changes in Q_{40} of all FRAs and population analyses grouped by FRA type.
- 5.13 Changes in cube root₄₀ of all FRAs and population analyses grouped by FRA type.
- 5.14 Changes in $Q_{10/40}$ and cube root_{10/40} as a function of grouped control bandwidth measures.
- 5.15 Comparison of Q and cube root measures of bandwidth and comparison of the change in bandwidth measures 10 dB and 40 dB re threshold.
- 5.16 Changes in bandwidth at 10 and 40 dB re threshold grouped according to control CF.
- 5.17 Changes in bandwidth at 10 and 40 dB re threshold grouped according to control threshold.
- 5.18 Comparison of changes in bandwidth at 10 and 40 dB re threshold to contralateral monaural and binaural diotic stimuli.

Chapter 6

- 6.1 Examples of each of the PSTH types found in this study.
- 6.2 Example of an Onset type PSTH response that reversibly increased in firing rate to both contralateral monaural and binaural diotic stimuli during contralateral IC cooling.
- 6.3 Example of a Build-up type PSTH response that was unchanged in firing rate to both contralateral monaural and binaural diotic stimuli during contralateral IC cooling.
- 6.4 Example of a Chopper type PSTH response that reversibly decreased in firing rate to both contralateral monaural and binaural diotic stimuli during contralateral IC cooling.
- 6.5 Examples of reversible increases in inter-stimulus interval in two Chopper units in response to both contralateral monaural and binaural diotic stimuli during contralateral IC cooling.
- 6.6 Example of a Pauser type PSTH response that reversibly decreased in firing rate to both contralateral monaural and binaural diotic stimuli during contralateral IC cooling.
- 6.7 Examples of three On-sustained type PSTH response units, each of which responded differently to contralateral IC cooling.
- 6.8 Summary of changes in firing rate of all units according to PSTH type.
- 6.9 Control and change in firing rate of each unit according to FRA type, plus changes in firing rate of each unit and comparison of change in firing rate and change in FRA area.
- 6.10 Comparison of changes in firing rate to both contralateral monaural and binaural diotic stimuli during contralateral IC cooling.
- 6.11 Examples of On-sustained type PSTH responses correlated changes in firing rate and first spike latency during contralateral IC cooling. Also shown is the frequency distribution of control latencies and correlation of changes in firing rate and changes in first spike latency.

List of Tables

Chapter 4

- 4.1 Stability of FRA measures over the course of an hour of recording.
- 4.2 Number and proportion in the population of each type of FRA found in this study.
- 4.3 Distributions of V-shaped and non-V-shaped FRA areas in the control condition.
- 4.4 Number and proportion of each FRA type that changed by more than 50 % irrespective of the direction of change.

Chapter 5

- 5.1 Changes in threshold imparted by contralateral IC cooling to all FRAs found in the study, classified according to FRA type.
- 5.2 Comparison of bandwidth changes using Q and cube root at both 10 and 40 dB re threshold that were induced by contralateral IC cooling.

Chapter 6

- 6.1 Relationship of changes in firing rate during contralateral IC cooling to control firing rate.
- 6.2 Relationship between FRA type and PSTH type in the population of neurons.
- 6.3 Changes in first spike latency of different PSTH types with statistical analyses.

Chapter 1. Introduction

1.1 Overview

Considerable progress has been made over the past century in elucidating the anatomical structures and physiological mechanisms responsible for transforming sound stimuli into the auditory percepts we experience. Despite the advances that have been made, many fundamental questions remain. This thesis will report the findings of an experimental study that sought to investigate some of the roles that the commissure of the inferior colliculus (CoIC) plays in auditory processing. The CoIC is a fibre tract that interconnects the two inferior colliculi (ICs) - the principal auditory nuclei of the midbrain. We know little about the contribution of the CoIC to sound processing.

The auditory system is remarkable in its ability to decipher the spectral, temporal and spatial properties of sounds. In marked contrast to the two other orientating senses, vision and somatosensation, the auditory sense organs do not possess a topographic representation of the spatial location of sounds on the receptor surface. As such, the auditory system has an abundance of pre-cortical complexity, including many sub-thalamic nuclei. These nuclei extract and analyse different components of auditory stimuli, such as the spectro-temporal features of a sound, or perform binaural analyses, which allow for determination of the spatial location of a sound source. Different characteristics of sounds are analysed separately in these parallel pathways before being brought together and processed in the ICs.

This Introduction will provide an overview of the anatomical and physiological organisation of the ICs and discuss their afferent and efferent connections, with focus on the CoIC. The Introduction will culminate by drawing together the current gaps in our knowledge about the CoIC and outline the aims of this thesis and how it will seek to address some of these questions.

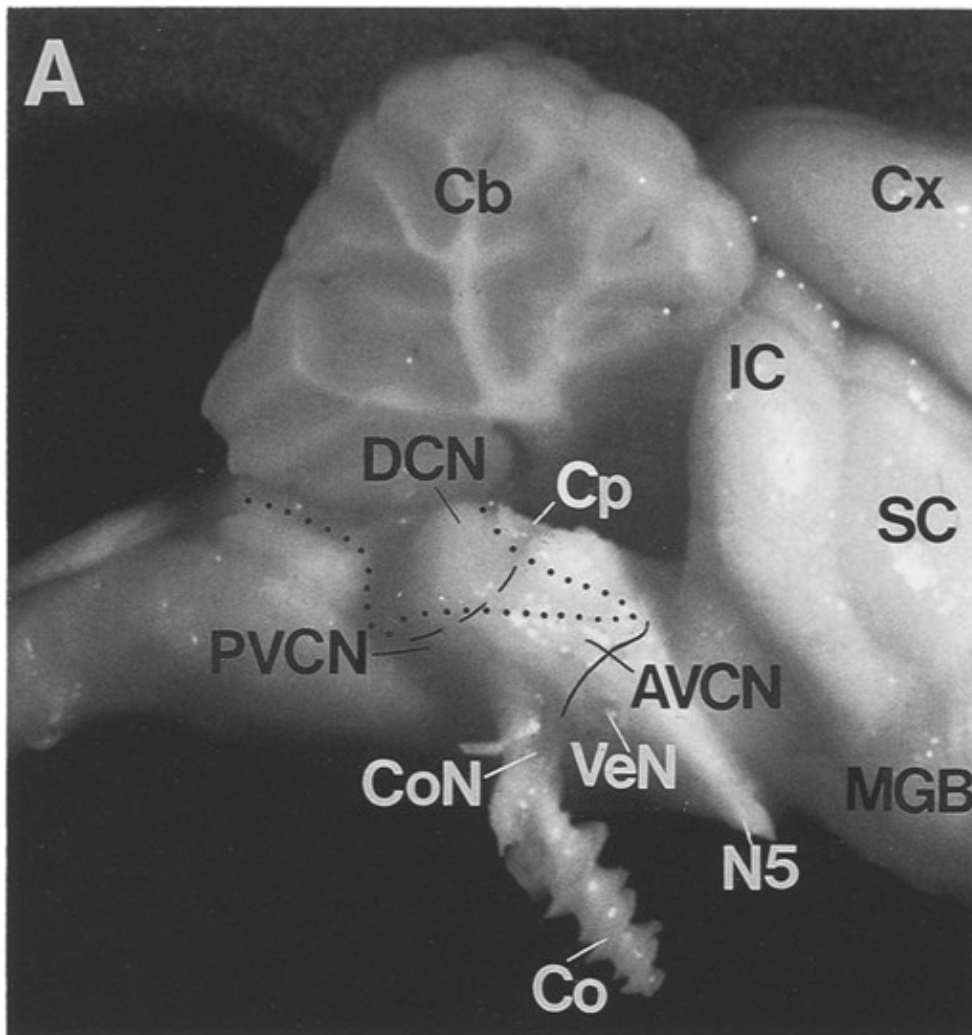


Figure 1.1 Lateral view of the guinea pig hindbrain following dissection of the right cerebellar and right cortical hemispheres. Cb = cerebellum; Cp = cerebellar peduncles; Cx = cortex; IC = inferior colliculus; SC = superior colliculus; MGB = medial geniculate body; DCN = dorsal cochlear nucleus; PVCN = postero-ventral cochlear nucleus; AVCN = antero-ventral cochlear nucleus; CoN = cochlear nerve; VeN = vestibular nerve; N5 = trigeminal nerve; Co = cochlea. Note the large size of the IC relative to the other labelled structures in the ascending auditory pathway (From Hackney *et al.* (1990)).

1.2 Position of the Inferior Colliculi in the Auditory Pathway

The ICs, two cupola shaped structures that protrude dorsally from the tectum, are the largest sub-cortical nuclei in the mammalian brain. They form the caudal half of the corpora quadrigemina - the superior colliculi forming the rostral half. The colliculi are distinct in the brain, having anatomical and physiological properties which are distinct from other subcortical structures and both the cortex and cerebellum. Figure 1.1 shows the gross anatomy of the ascending auditory system of the guinea pig after dissection of the right cerebellum and right cortex. The IC can be visualised as a promontory which resides at a crucial point between the ascending afferent projections of the cochlear nuclei (CN) and the medial geniculate body of the thalamus (MGB; Hackney *et al.*, 1990). The IC receives the output of all auditory brainstem nuclei and processes these before passing its output to the MGB (Calford and Aitkin, 1983) which in turn innervates the auditory cortex (AC).

The position of the IC within the ascending auditory pathway, and the ascending projections it receives from one cochlea via the other principal nuclei of the brainstem auditory system, are shown in figure 1.2. The efferent projections of numerous auditory brainstem structures terminate within the ICs where they are processed and transmitted to the MGB. For simplicity, this schematic only presents the ascending and commissural projections, and ignores the extensive descending projections which reciprocate with the projections of almost all ascending afferent nuclei.

The large size and high metabolic demands of the IC (Reivich *et al.*, 1969; Gross *et al.*, 1987), coupled with its position in the auditory system, suggests the IC is a crucial locus in auditory processing. The ICs are the final sub-cortical auditory nuclei that innervate one another bilaterally (Fig. 1.2).

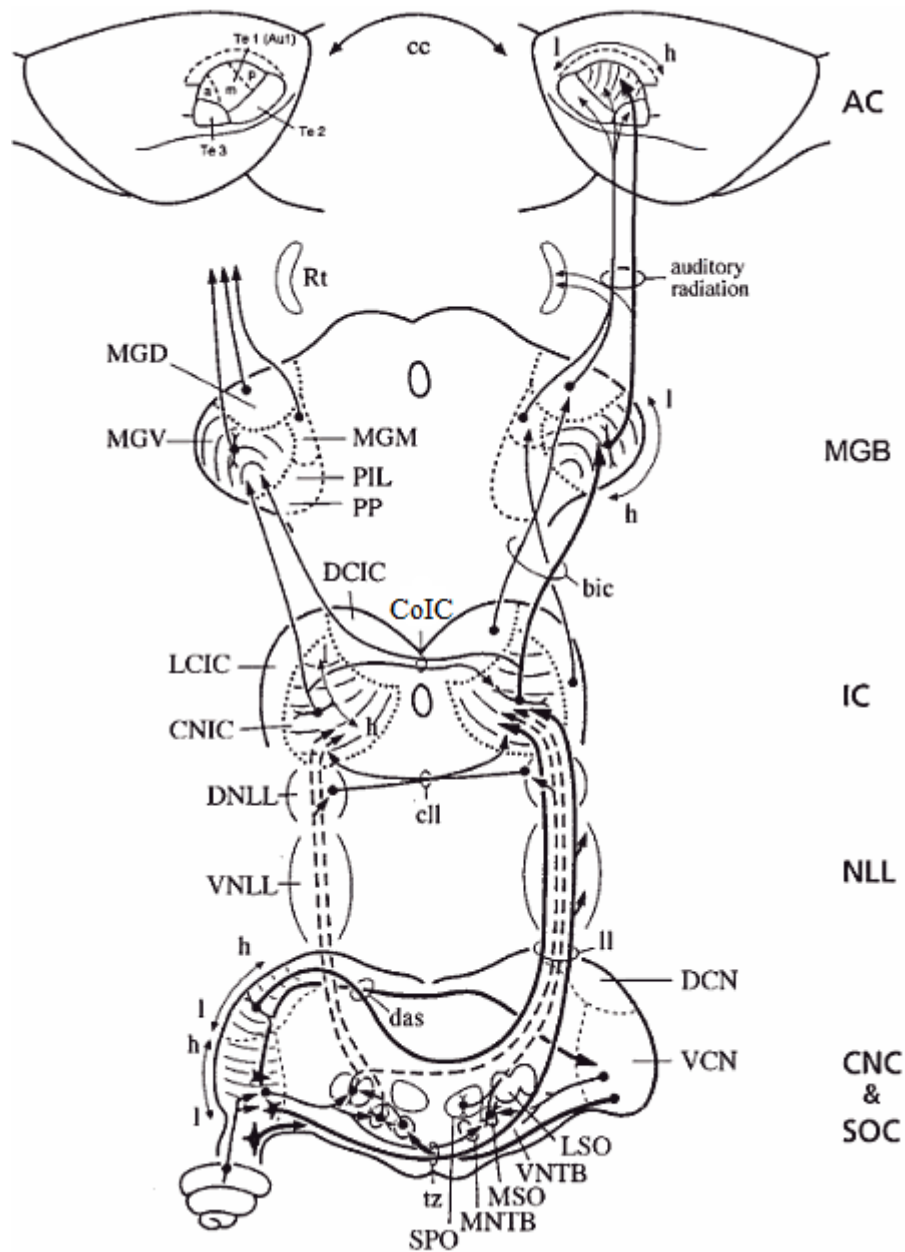


Figure 1.2 Schematic of the ascending and commissural auditory pathways in rat - with input from one cochlea for simplicity. Line weight indicates the strength of connections. Note how the right IC receives its predominant input from the left CN. The CoIC is the final sub-cortical point of bilateral interaction in the auditory system (From Malmierca and Hackett (2010)).

1.3 Anatomy of the Inferior Colliculi

The size and shape of the ICs vary between species, possibly due to the varying auditory environments within which each species has evolved. However, all mammalian ICs have a central nucleus (CNIC; Ramon y Cajal (1995)), which is surrounded by a shell which can be divided into the rostro-laterally located lateral cortex (LCIC) and the dorso-caudally located dorsal cortex (DCIC; Morest and Oliver, 1984).

The CNIC can be distinguished from the cortices by the expression of calcium binding proteins. There are high numbers of parvalbumin containing neurons in CNIC with few in the cortices; while in contrast, calbindin and calretinin are expressed throughout LCIC and DCIC whereas the CNIC is almost bereft of any such somata (Coleman *et al.*, 1992; Lohmann and Friauf, 1996; Tardif *et al.*, 2003). Staining for cytochrome oxidase (CO), the terminal electron acceptor in the electron transport chain of mitochondria, allows visualisation of the differential oxidative capacity of neural regions within the IC. There are high levels of CO in CNIC, but little in the cortices (Gonzalez-Lima and Cada, 1994; Cant and Benson, 2006). Neuronal nitric oxide synthase is also expressed in much higher levels in DCIC and LCIC than CNIC (Coote and Rees, 2008). There is extensive interlacing of different neuronal morphologies at the borders of DCIC and CNIC which has led to difficulties in delineating the border between these sub-nuclei (Coote and Rees, 2008; Malmierca *et al.*, 2011). Amongst the species variations in sub-nucleus composition of the IC are a much larger LCIC in rat than cat, while cat IC has a much larger low frequency CNIC than rat (Loftus *et al.*, 2008). Considerable effort has been made to determine the precise borders of each sub-nucleus in the IC, but there is currently no consensus of opinion on the issue.

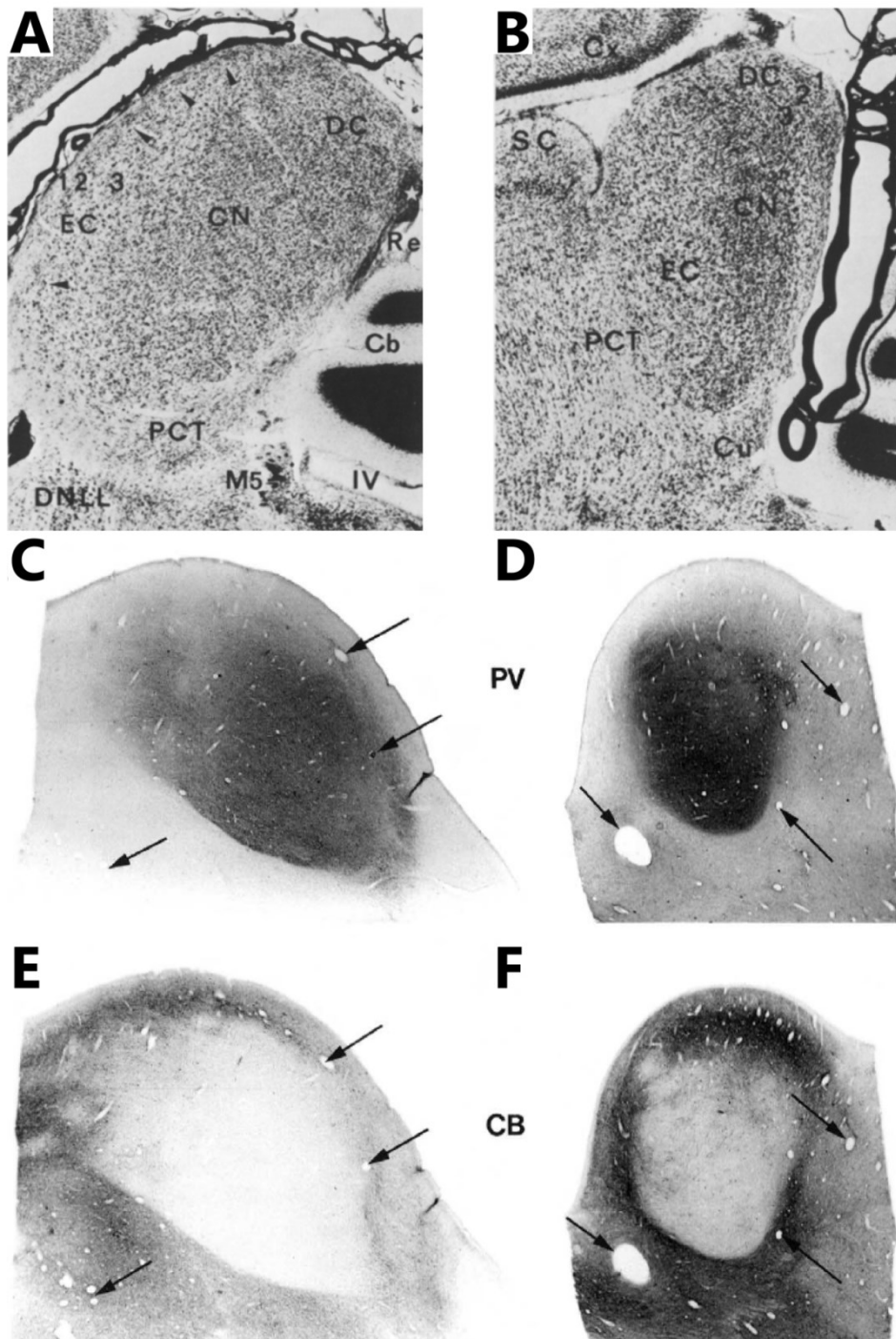


Figure 1.3 (A) Nissl stained coronal section through rat IC with major subdivisions labelled. (B) Parasagittal Nissl stained section through rat IC. Note the higher cell density in the CNIC. (C-F) Human IC sections stained for calcium binding proteins parvalbumin (C & D) and calbindin (E & F) in the coronal (C & E) and parasagittal planes (D & F). Note high levels of parvalbumin and lack of calbindin in the CNIC with the opposite in the cortices. This is one of several ways by which the sub-nuclei of the IC can be distinguished. Arrows indicate blood vessels found in adjacent sections between C & E, and D & F. (A & B from Faye-Lund and Osen (1985); C to F from Tardif *et al.* (2003)).

1.4 Neuronal Morphologies in the IC and Fibrodendritic Laminae

Golgi's black reaction has provided detailed information as to the neuronal morphologies in the IC (Rockel and Jones, 1973a; Rockel and Jones, 1973b; Rockel and Jones, 1973c; Morest and Oliver, 1984; Faye-Lund and Osen, 1985; Meininger *et al.*, 1986). In the CNIC there are two neuronal morphologies: disc shaped cells and stellate cells (Fig. 1.4A). Disc shaped cells have planar dendrites which form stacked rows, oriented in parallel, and constitute the majority of CNIC neurons (Oliver, 1984b; Oliver *et al.*, 1991). The parallel dendritic arbours and axons of disk-shaped cells are intertwined with the ascending fibres of the lateral lemniscus. These fibre and dendrite bundles course in a ventro-lateral to dorso-medial orientation throughout the CNIC and DCIC and form fibrodendritic laminae. Stellate cells form a smaller percentage of neurons in CNIC. The dendritic arborisations of stellate cells are thicker, more extensive, and more spherical than disc shaped cells (Oliver, 1984b). Stellate cells have dendrites which are oriented perpendicular to the dendrites of disc shaped cells, and can span more than one lamina (Oliver, 1984b; Malmierca *et al.*, 2011).

The orientation of the lamina in LCIC turns to an orientation perpendicular to that of the CNIC and DCIC. The laminae are stacked atop one another with lower frequency laminae (Fig. 1.4C) having a smaller area than high frequency (Fig. 1.4E) laminae (Saldaña and Merchán, 1992; Malmierca *et al.*, 1995). Each lamina contains extensive intrinsic fibres. Whether some neurons within a lamina are interneurons or have collateralised projecting axons to other nuclei is an unresolved issue (Miller *et al.*, 2005; Wallace *et al.*, 2012). The dendrites of IC neurons course throughout and interconnect all sub-nuclei of the IC but only within one lamina (Saldaña and Merchán, 1992; Malmierca *et al.*, 1995; Miller *et al.*, 2005). Some of these projections course from ventro-lateral to dorso-medial regions of a lamina, possibly providing a substrate for intra-laminar processing (Miller *et al.*, 2005).

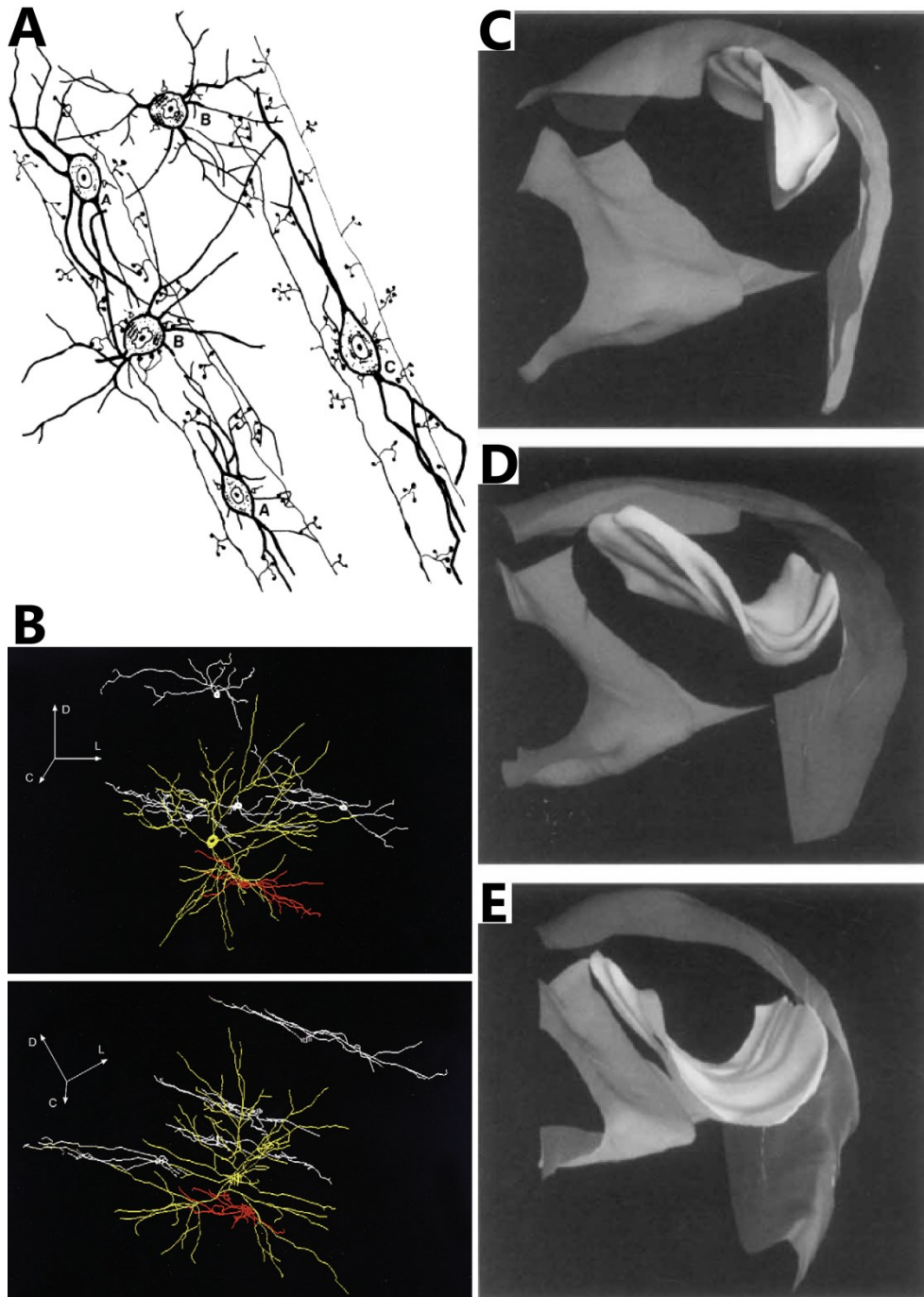


Figure 1.4 (A) Drawings of Golgi stained CNIC neurons in cat. Neurons labelled A and C are small and large disk-shaped cells respectively which course in parallel with the lemniscal axons. Neurons labelled B are stellate cells with dendrites which are oriented orthogonal to the laminae. (B) Two views of 3D reconstructions of Golgi stained neurons in rat at the border of DCIC and CNIC. Disk shaped cells are shown in white, stellate cells are shown coloured. (C,D,E) 3D reconstructions of laminae with CFs of 0.5 (C), 6 (D), and 21 (E) kHz in guinea pig. Note the change in shape and size as the CF of the laminae increased. (A) from Oliver (1984b); (B) from Malmierca *et al.* (2011); (C) From Malmierca *et al.* (1995).

1.5 Afferent Projections to the Inferior Colliculi

Sounds which arrive at the tympanic membrane undergo frequency analysis that takes the form of a travelling wave on the basilar membrane of the cochlea (von Békésy, 1960). This mechanical displacement is transduced by inner hair cells which innervate bipolar neurons of the auditory nerve (AN). Outer hair cells provide a mechanical response to stimulation that underlies cochlear amplification, a feedback mechanism that allows for the precise sensitivity and exquisite frequency resolution of the cochlea (Ashmore, 1987). All AN fibres are frequency selective - a characteristic which is inherited from the frequency specific deflection of a point on the basilar membrane. The frequency selectivity of AN fibres can be defined by their frequency threshold curves (FTCs) which determines the firing rate of sound driven spikes as a function of frequency and level over the audiogram of the animal (Kiang, 1965). All AN fibres have V-shaped frequency tuning. An AN fibre can be defined at its most sensitive and selective point by its characteristic frequency (CF) and the minimum threshold point in the FTC. The AN is tonotopic – i.e. organised according to frequency (Keithley and Schreiber, 1987). This pattern of organisation is a fundamental characteristic of all central auditory nuclei. Each AN enters the brainstem and terminates in the CN which is the first point in the central auditory pathway.

Each IC receives afferent ascending auditory projections from many brainstem nuclei (Brunso-Bechtold *et al.*, 1981), including: the CNs, the superior olivary complexes (SOCs), and the nuclei of the lateral lemniscus (NLLs). In addition to these ascending sources of auditory input, each IC is also innervated by descending auditory projections from both MGBs, and both ACs. Each afferent structure contains multiple subdivisions, each with a distinct projection pattern to the IC (Fig. 1.5).

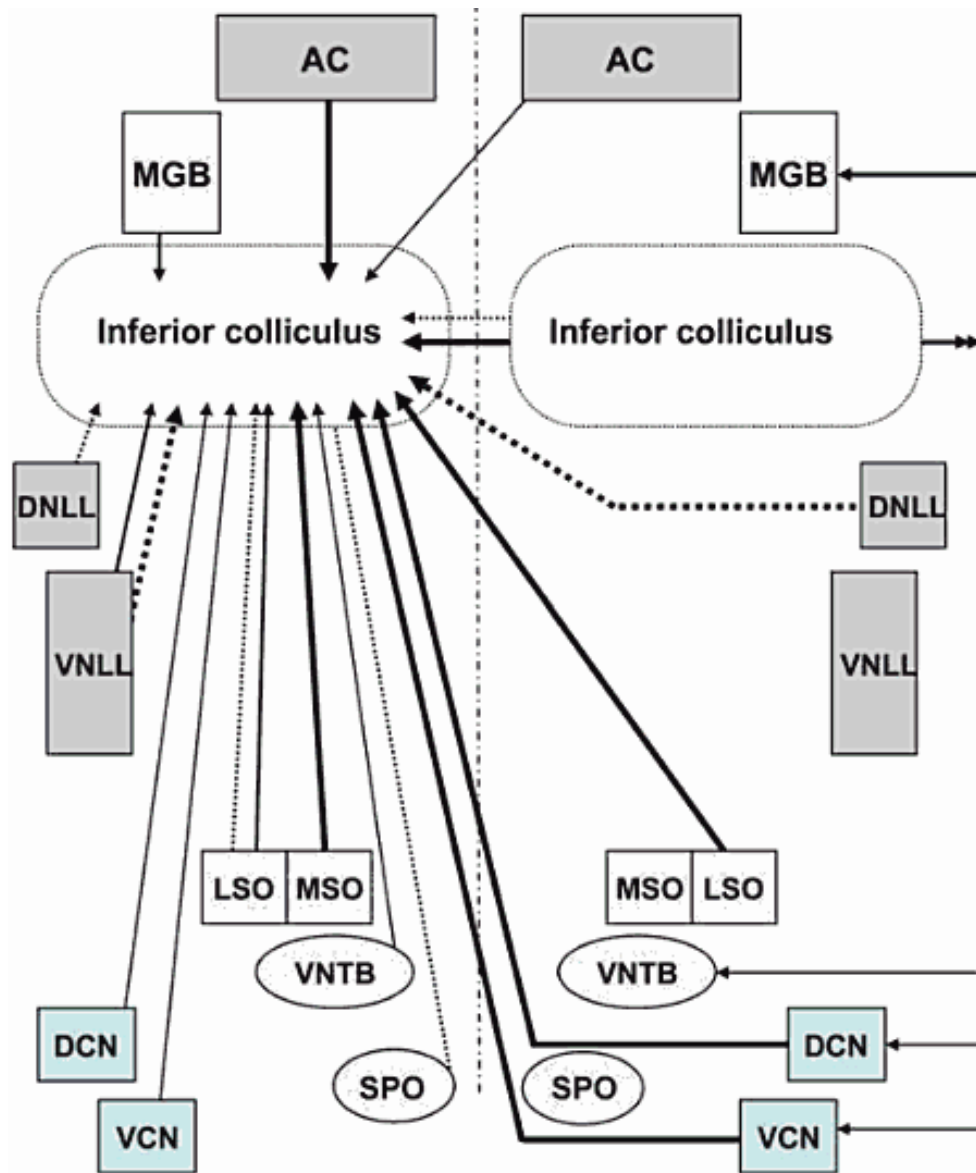


Figure 1.5 Summary diagram of the auditory projections received by each IC. One IC receives projections from five groups of nuclei, each of which can be divided into constituent sub-nuclei. These nuclei process and provide different aspects of auditory information to the IC. Solid lines represent excitatory projections. Dashed lines represent inhibitory projections. Line weight indicates relative size of each projection. VCN = ventral cochlear nucleus; DCN = dorsal cochlear nucleus; SPO = superior paraolivary nucleus; VNTB = ventral nucleus of the trapezoid body; MSO = medial superior olive; LSO = lateral superior olive; VNLL = ventral nucleus of the lateral lemniscus; DNLL = dorsal nucleus of the lateral lemniscus (From Malmierca (2004)).

1.5.1 Cochlear nuclei

Fibres of the AN terminate exclusively within the CN (Powell and Cowan, 1962; Osen, 1970). These fibres bifurcate into an ascending branch which terminates in the AVCN and a descending branch which terminates in the DCN by way of the PVCN (De No, 1933). The AVCN and PVCN are commonly grouped together under the broader term of the ventral cochlear nucleus (VCN). The bifurcation maintains the tonotopic arrangement of the AN within all subdivisions of the CN (Rose *et al.*, 1959; Sando, 1965; Osen, 1970). These branches represent the initial separation of the parallel processing pathways, each involved in the extraction and analysis of a distinct aspect of auditory stimuli.

The CN has between nine (Osen, 1969), and fourteen (Brawer *et al.*, 1974) distinct neuronal morphologies depending upon the anatomical method used to classify them. The DCN is structured as a miniature cerebellar circuit (Oertel and Young, 2004). Only the large fusiform and giant cells project directly to the contralateral IC (Ryugo *et al.*, 1981; Moore, 1988). The analyses performed in the DCN include forming a representation of spectral notches introduced into the incident sound stimulus by interference with waves reflected from the pinnae and the head (Young *et al.*, 1992). Spectral notch cues underlie a mechanism for sound localisation in the vertical plane (Oldfield and Parker, 1984).

Most, if not all Type I multipolar neurons throughout the VCN project monosynaptically to the contralateral IC (Josephson and Morest, 1998) via the thin fibre component of the trapezoid body (Warr, 1966; Osen, 1972). Direct projections from VCN are more numerous than those from DCN (Adams, 1979; Schofield and Cant, 1992). Type I neurons have narrow frequency tuning and respond to tones with a 'chopper' pattern of regularly spaced spikes (Rhode and Smith, 1986; Palmer *et al.*, 1996). These neurons may be involved in the analysis of complex auditory stimuli (Rhode and Smith, 1986), including speech sounds

over a wide range of stimulus levels (Blackburn and Sachs, 1989; May *et al.*, 1998).

The efferent projections of contralateral CN neurons terminate monosynaptically in the CNIC and form one of the largest ascending inputs to the IC. Terminations originating from all subdivisions of the contralateral CN are asymmetric, with round synaptic vesicles and are therefore thought to be excitatory (Oliver, 1984a; Oliver, 1985; Oliver, 1987; Alibardi, 1998). These projections maintain the tonotopic organisation with neurons in the low frequency regions of the CN projecting to dorsal IC, while high frequency CN neurons have projections which terminate in the ventral IC (Osen, 1972; Adams, 1979). There are also some cells in all regions of the CN which project to the ipsilateral, dorsolateral IC (Strominger *et al.*, 1977; Oliver, 1984a; Oliver, 1987).

The CNIC is the major target of ascending contralateral CN input (Osen, 1972) with fewer projections terminating in DCIC (Oliver, 1984a; Coleman and Clerici, 1987). Projections from the DCN also innervate the LCIC (Ryugo *et al.*, 1981; Coleman and Clerici, 1987). All projections from the CN to the IC are topographically organised (Ryugo *et al.*, 1981; Oliver, 1984a; Oliver, 1987).

1.5.2 Superior olivary complex

The encoding of sound location in the azimuthal plane is inherited in IC from processing in the SOC. The nuclei of the SOC receive afferent projections from both CNs. The analysis of interaural time differences (ITDs) underlies sound localisation of low frequency stimuli. ITDs are first encoded in the medial superior olive (MSO; Goldberg and Brown (1969); Masterton *et al.* (1975)). Interaural level differences (ILDs), allow localisation of high frequency sounds, and are first processed in the S-shaped lateral superior olive (LSO; Boudreau and Tsuchitani (1968)), before being passed up the IC. There are several peri-olivary nuclei in the SOC which are involved in sub-collicular auditory processing which will not be considered further here.

Cells in the MSO receive bilateral excitatory innervation from spherical bushy cells of the AVCN with a tonotopic organisation which over represents low frequencies (Harrison and Warr, 1962; Cant and Casseday, 1986). MSO neurons act as coincidence detectors, firing when afferent input from both sides arrives simultaneously (Goldberg and Brown, 1969; Yin and Chan, 1990). Different MSO neurons have different best-ITDs at which their firing is maximal (Goldberg and Brown, 1969; Yin and Chan, 1990). The ITD tuning of MSO neurons is derived from the temporal linear summation of the afferent excitatory input to the cell, with nonlinear weighting of synaptic size determining spike output (van der Heijden *et al.*, 2013). In addition to coincident binaural excitation, the MSO receives glycinergic inhibition from the lateral nucleus of the trapezoid body (LNTB) and medial nucleus of the trapezoid body (MNTB; Grothe and Sanes (1993)). This glycinergic inhibition selectively innervates the somata of MSO principal neurons (Clark, 1969; Kapfer *et al.*, 2002). Both the presence and precise timing of this inhibition are essential for normal MSO function (Brand *et al.*, 2002; Pecka *et al.*, 2008). This inhibition arrives prior to direct excitation which produces the exquisite temporal resolution by which MSO principal

neurons encode ITD (Roberts *et al.*, 2013). A schematic representation of the afferent projections to MSO is presented in figure 1.6A.

The vast majority of MSO neurons project ipsilaterally to the dorsolateral CNIC (Fig. 1.6C; Oliver *et al.* (1995)). Projections from MSO to IC are almost entirely glutamatergic although GABAergic neurons have been described (Helfert *et al.*, 1989; Kumoi *et al.*, 1993). Neurons in IC which are sensitive to low frequency sounds are thought to receive inputs from the MSO (Aitkin and Schuck, 1985).

Neurons in the LSO are inhibited by stimuli at the contralateral ear but excited by the ipsilateral ear, an inhibitory-excitatory property termed an IE interaction. These responses are formed due to LSO cells receiving monosynaptic excitation from spherical bushy cells in the ipsilateral CN, while excitatory globular bushy cells in the contralateral CN cross the midline and innervate the contralateral MNTB by means of the Calyx of Held (Cant and Casseday, 1986). The MNTB in turn sends glycinergic inhibition to the LSO. These inputs, coupled with a frequency representation biased to high frequencies, allow LSO neurons to encode ILDs (Fig. 1.6B). The IE representation of the LSO is flipped to become EI in the IC due to both a direct excitatory projection from LSO to the contralateral CNIC and dorsal nucleus of the lateral lemniscus (DNLL), and an inhibitory glycinergic (Saint Marie *et al.*, 1989) ipsilateral projection to the CNIC and DNLL (Glendenning and Masterton, 1983). Over 95 % of LSO projections do not collateralise (Glendenning and Masterton, 1983). Rather they represent mirror opposite pathways to the IC; a fact supported by the differential sources of LSO projections to IC, with the excitatory contralateral projection arising from the medial portion, and the inhibitory ipsilateral projection originating in the lateral limb (Fig. 1.6B). The EI representation of azimuthal space inherited in IC from LSO allows for representation of auditory stimuli in the contralateral hemifield (Irvine, 1986).

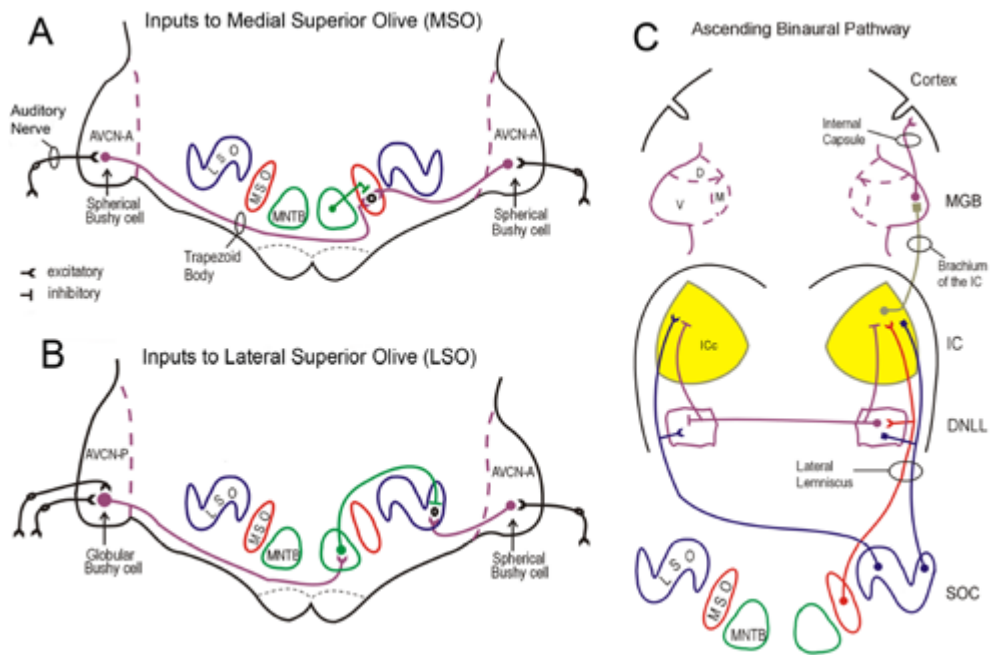


Figure 1.6 Schematic of the ascending binaural processing nuclei in the brainstem and their projections to the ICs. (A) Coincidental binaural projections from spherical bushy cells of the CN, along with contralaterally driven MNTB glycinergic inhibition, permit low frequency ITD encoding in the MSO. (B) High frequency ILDs are formed from ipsilateral excitatory and contralateral inhibitory inputs to the LSO. (C) Both MSO and LSO project extensively to the CNIC (From Yin and Kuwada (2010)).

1.5.3 Nuclei of the lateral lemniscus

The NLL are comprised of the ventral (VNLL) and dorsal (DNLL) nuclei. The VNLL is often further subdivided into dorsal and ventral divisions. Species such as bat and rat have a further nucleus which resides between the DNLL and VNLL which is termed the intermediate nucleus (Fig. 1.7). The nature of this specialised nucleus is superfluous to the study at hand and will not be discussed further.

The VNLL is cylindrical in shape, extending along the dorso-ventral axis and curving towards the midline as it descends ventrally (Fig. 1.7). Somata in the VNLL are stellate and vertically oriented (Merchán and Berbel, 1996). Projections to the VNLL arise from the ipsilateral MNTB and contralateral VCN (Kelly *et al.*, 2009). Neurons in the VNLL provide an inhibitory, be that glycinergic or GABAergic, input to the IC (Winer *et al.*, 1995), with some neurons expressing both neurotransmitters (Riquelme *et al.*, 2001). The VNLL projects ipsilaterally, providing one of the largest sources of inhibition to the IC, with widespread terminations in the CNIC and DCIC (Whitley and Henkel, 1984). These projections are tonotopically organised (Benson and Cant, 2008).

Neurons of the VNLL respond binaurally (Batra and Fitzpatrick, 2002), owing to bilateral inputs from VCN. The VNLL also receives contralateral innervation from both globular and spherical bushy cells of the VCN and ipsilateral inhibition is provided to the VNLL by the MNTB. The ventral VNLL is distinct from the DNLL owing to the selective innervation of neurons in VNLL by octopus cells in the contralateral PVCN, a characteristic which implicates this region in temporally precise processing (Glendenning and Hutson, 1998). Responses in the VNLL are heterogeneous with most having V-shaped or U-shaped frequency tuning, while more than a third have multi-peaked tuning. All have sharp tuning near threshold (Zhang and Kelly, 2006). Onset and sustained responses are both present, with the former having a shorter latency (Zhang and Kelly, 2006). This

projection may influence the processing of frequency modulation (FM) in the IC (Huffman *et al.*, 1998; Pollak *et al.*, 2011).

Neurons in the DNLL are almost exclusively GABAergic (Adams and Mugnaini, 1984; Saint Marie *et al.*, 1997). As with all the central auditory nuclei, the DNLL is topographically organised according to frequency. High frequencies are represented dorsally and ventrally, while low frequency responsive cells are centrally located (Bajo *et al.*, 1998; Bajo *et al.*, 1999; Shneiderman *et al.*, 1999). Each DNLL receives bilateral LSO and ipsilateral MSO and VNLL projections (Pollak *et al.*, 2003).

The DNLL provides a significant inhibitory contribution to the contralateral CNIC and DCIC and DNLL via the commissure of Probst, with a less numerous projection to the ipsilateral IC (Brunso-Bechtold *et al.*, 1981; Kelly *et al.*, 2009). Winer *et al.* (1995) found that larger neurons within the DNLL stained weakly for GABA and formed the contralaterally projecting efferents, while smaller cells had stronger staining and projected to the ipsilateral IC. DNLL projections terminate in the contralateral IC along the laminae in alternating bands of high and low density. Single neurons maintain the tonotopic organisation by terminating within one frequency band lamina only (Henkel *et al.*, 2003).

DNLL neurons are responsive to both ITDs and ILDs (Brugge *et al.*, 1970; Bajo *et al.*, 1998) with binaurally excited cells more common than those inhibited by the ipsilateral ear (Siveke *et al.*, 2006). Cutting of the commissure of Probst, which removed 90 to 95 % of contralaterally projecting DNLL neurons, induced a large deficit in the ability to localise broadband noise in the azimuthal plane, although some localisation ability remained (Ito *et al.*, 1996). This lesion technique was also employed by van Adel *et al.* (1999) who found that after transection, ipsilateral stimuli were no longer effective in suppressing evoked responses. This study was a follow up to a prior investigation in which unilateral lesions of the DNLL were found to be as detrimental to sound localisation as bilateral lesions

(Kelly *et al.*, 1996). From this it can be inferred that the commissural projections from one DNLL to the other and/or the contralateral IC are essential for the accurate localisation of sound stimuli.

Blocking contralateral but not ipsilateral DNLL input by kynurenic acid injection reversibly reduced inhibition and shifted the ILD functions (Li and Kelly, 1992) and ITD functions (Kidd and Kelly, 1996) of CNIC neurons. These findings suggest DNLL mediated contralateral inhibition forms EI properties in *IC de novo*, producing responses which may detect ILDs from moving stimuli or multiple stimuli in different positions (Burger and Pollak, 2001). DNLL processing doubles the efficacy of ITD encoding relative to the MSO by increasing the dynamic range and reducing neuronal variability (Pecka *et al.*, 2010) which may improve signal extraction from noise (Meffin and Grothe, 2009). This process may involve inhibitory interactions (Yang *et al.*, 1992) which sharpen ITD representation in DNLL relative to MSO (Kuwada *et al.*, 2006) and may help sharpen further the ITD representation in the IC (Yin and Kuwada, 2010). The DNLL, while having no response selectivity to communication calls itself (Bauer *et al.*, 2002), aids the formation of the high selectivity for communication calls observed in IC (Pollak, 2013).

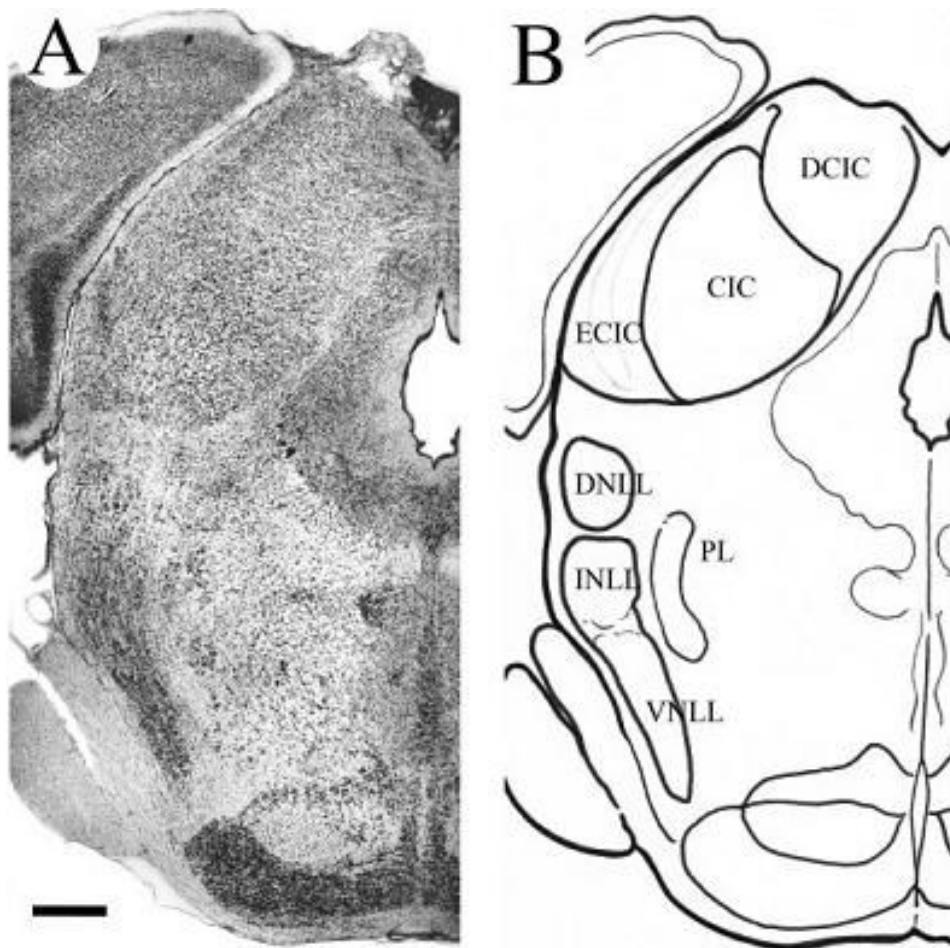


Figure 1.7 Coronal section through the rat midbrain showing the position of the NLL relative to the IC. (A) Cresyl violet stained section showing the cytoarchitecture of the midbrain. (B) Approximate outline of the borders of the NLL and IC in the midbrain. Note the dense staining of the VNLL and the large size of the IC with respect to the NLL (From Kelly *et al.* (2009)).

1.5.4 Medial geniculate body

The MGB has been defined anatomically in a similar manner to the IC, with tripartite sub-division composed of medial (mMGB), dorsal (dMGB) and ventral (vMGB) divisions (Clerici and Coleman, 1990). Descending connections from MGB to IC were first described by (Adams, 1980). This projection is predominantly ipsilateral and innervates all divisions of the IC with the tonotopic projection from vMGB to CNIC forming the largest component (Winer *et al.*, 2002). Neurons in the medial and dorsal (non-tonotopic) divisions were found to project to the IC by Kuwabara and Zook (2000). This study found that the magnocellular region of mMGB formed the largest contribution to LCIC and DCIC, with a smaller projection from dMGB. This pathway may therefore represent a non-tonotopic projection which is segregated from the tonotopic pathway. Numerous other midbrain nuclei also project to the IC, including bilateral projections from the brachium of the IC (Winer *et al.*, 2002).

1.5.5 Auditory cortex

Descending connections from almost all divisions of AC innervate the IC. The highest densities of these connections originate in ipsilateral primary auditory cortex (A1) and terminate topographically in DCIC and LCIC with a smaller number of projections terminating in the ipsilateral CNIC and contralateral DCIC and CNIC (Winer *et al.*, 1998; Bajo and Moore, 2005; Bajo *et al.*, 2007). These projections are some of the largest sources of afferent input to the IC (Fig. 1.5). Secondary AC projects ipsilaterally to the cortices of the IC but not the CNIC, thus maintaining the separation of tonotopic and non-tonotopic pathways to IC (Winer *et al.*, 1998; Bajo *et al.*, 2007).

Projections from AC originate from glutamatergic (Feliciano and Potashner, 1995) pyramidal cells in layer V (Games and Winer, 1988; Winer and Prieto, 2001) and target IC neurons of which only 4 % are inhibitory (Nakamoto *et al.*, 2013). Two projecting cell types have been described. Neurons with large apical dendrites which terminate in cortical layer I and fire calcium dependent spikes in rhythmic bursts (Slater *et al.*, 2013) are termed intrinsic bursting (IB) cells. These cells have dense terminations in DCIC and LCIC (Bajo and Moore, 2005), have broad frequency tuning, long response latencies and comprise around half of descending projections (Turner *et al.*, 2005). The other cell type known to project to IC are regular spiking (RS) neurons. These cells have shorter apical dendrites and fewer axonal arborisations. These cells fire regularly and receive stronger GABAergic inhibition (Hefti and Smith, 2000). RS cells innervate the CNIC tonotopically (Bajo and Moore, 2005). They are highly selective for frequency and form around a third of descending projections (Turner *et al.*, 2005; Sun *et al.*, 2013). A further difference between the two descending cell types is that IB neurons possess an I_h mediated sag in response to prolonged current injection while RS neurons do not (Slater *et al.*, 2013). These differences suggest differential processing streams from AC to IC.

Electrical stimulation of AC elicited excitatory post-synaptic potentials (EPSPs), inhibitory post-synaptic potentials (IPSPs), or a combination of both with EPSPs leading in DCIC (Mitani *et al.*, 1983). Such stimulation produced short latency excitatory responses in around half of DCIC units recorded, with some neurons also showing a later inhibitory component (Syka and Popelář, 1984). It has been shown that the representation of ILDs (Nakamoto *et al.*, 2008) and harmonic stimuli (Nakamoto *et al.*, 2010) in IC are both strongly influenced by corticofugal projections. The ability to relearn an orienting behaviour to sound stimuli of varying azimuthal location was lost after unilateral ear occlusion and targeted neuron death in layer V of AC (Bajo *et al.*, 2009) – a finding which implicates corticofugal projections in such learning. Anderson and Malmierca (2013) showed that stimulus specific adaptation in the IC is influenced, but does not depend on the corticofugal pathway. The corticofugal pathway has also been demonstrated to cause CF shifts in IC neurons due to electrical stimulation of the AC (Yan and Suga, 1998; Ma and Suga, 2001).

1.6 Efferent Targets of the Inferior Colliculi

The IC sends its principle efferent projection to the MGB. There are also reciprocal efferent projections to each of the auditory brainstem nuclei which innervate the IC.

1.6.1 Medial geniculate body

The IC projects to all subdivisions of MGB via the brachium of the IC. The vMGB receives the majority of its afferent terminals from the CNIC. Its neurons exhibit sharp frequency tuning with short response latencies (Calford *et al.*, 1983; Edeline *et al.*, 1999) and are organised tonotopically (Kudo and Niimi, 1978). The CNIC also innervates the mMGB and dMGB, although these projections are highly variable between different species (Calford and Aitkin, 1983; Oliver, 1984b). The DCIC projects strongly to the dMGB - a region which has numerous sub-divisions, each of which is also variable between species. Neurons in dMGB typically exhibit broad tuning. The LCIC sends a projection to both dMGB and mMGB, the latter of which produces both short and long latency responses (Anderson and Linden, 2011).

The projection to MGB from IC is almost entirely ipsilateral (Rouiller and De Ribaupierre, 1985; González-Hernández *et al.*, 1991). Both disc shaped and stellate cells project to MGB, with disk-shaped forming the majority of these (Oliver, 1984b; Oliver *et al.*, 1999). Dependent on the species studied, anywhere from twenty to forty five percent of these projection neurons are GABAergic with the remainder presumed glutamatergic (Winer *et al.*, 1996; Peruzzi *et al.*, 1997). Both GABAergic and glutamatergic projections to MGB can emanate from either disc shaped or stellate cells (Merchán *et al.*, 2005). Two thirds of MGB neurons receive IPSPs, with the overwhelming majority of these arriving in conjunction with an EPSP - the remaining third receive EPSPs only (Peruzzi *et al.*, 1997).

As the MGB receives a large proportion of its afferent input from IC, it has a longer latency (Klug *et al.*, 2000) and a lower maximum frequency with which it can synchronise to temporally modulated stimuli (Langner, 1992) than IC, suggesting integration at the level of the MGB. One interesting transformation from IC to MGB is an increase in the number of onset responding cells, which may represent a functional shift between the two nuclei (Edeline *et al.*, 1999).

1.6.2 Nuclei of the lateral lemniscus

Descending efferent projections from the CNIC course through the lateral lemniscus and terminate in the ipsilateral DNLL and VNLL (Fig. 1.8; Moore and Goldberg (1966); Caicedo and Herbert (1993); Thompson and Thompson (1993); Malmierca *et al.* (1996)). The projection to the DNLL is tonotopic while no such obvious pattern was reported in VNLL. This may be due to the complex topographical organisation of the VNLL, with the identification of a tonotopic organisation only being described later (Malmierca *et al.*, 1998; Benson and Cant, 2008).

1.6.3 Superior olivary complex

The innervation of the SOC by the IC emanates from the LCIC and CNIC and is almost exclusively ipsilateral (Fig. 1.8; Vetter *et al.* (1993)). Like descending projections from AC to IC, these projections are exclusively glutamatergic (Saint Marie, 1996). The majority of these fibres target the ventral nucleus of the trapezoid body (VNTB). Neurons in the CNIC project in a tonotopic manner while LCIC projections are more diffuse. The ipsilateral dorsal periolivary region, superior paraolivary nucleus (SPN), LNTB and MNTB are also innervated by IC projections (Carey and Webster, 1971; Malmierca *et al.*, 1996). A fascinating finding is that colliculo-olivary projections selectively target SOC neurons which in turn project to CN (Schofield and Cant, 1999) or cochlea (Vetter *et al.*, 1993), and not back to IC (Schofield, 2002). This suggests a functional role other than a

simple feedback loop between SOC and IC, but rather an integrative, multi-level modulatory pathway. The functional implications of this network are tantalising but poorly understood.

1.6.4 Cochlear nuclei

The fusiform cells of DCN are the primary target of tonotopic CNIC and non-tonotopic LCIC efferents to CN (Saint Marie, 1996; Schofield, 2001) although all layers of DCN receive some innervation (Caicedo and Herbert, 1993; Malmierca *et al.*, 1996). These descending projections are bilateral and glutamatergic (Fig. 1.8). These diffuse projections may therefore mediate direct feedback to the IC via fusiform and giant cells, or indirect modulation of the DCN via the granular cell region. Stellate cells of LCIC and both cell morphologies in CNIC project to DCN, with the former representing a significant projection (Schofield, 2001). The VCN receives scant innervation from IC (Saint Marie, 1996). The small cap region may receive sparse terminals, but these may represent fibres of passage (Malmierca *et al.*, 1996). This is a curious finding given the extensive monosynaptic innervation of multipolar cells of VCN to IC. As feedback to VCN from IC is mediated via SOC, this implies a possible role in sound localisation for these projections.

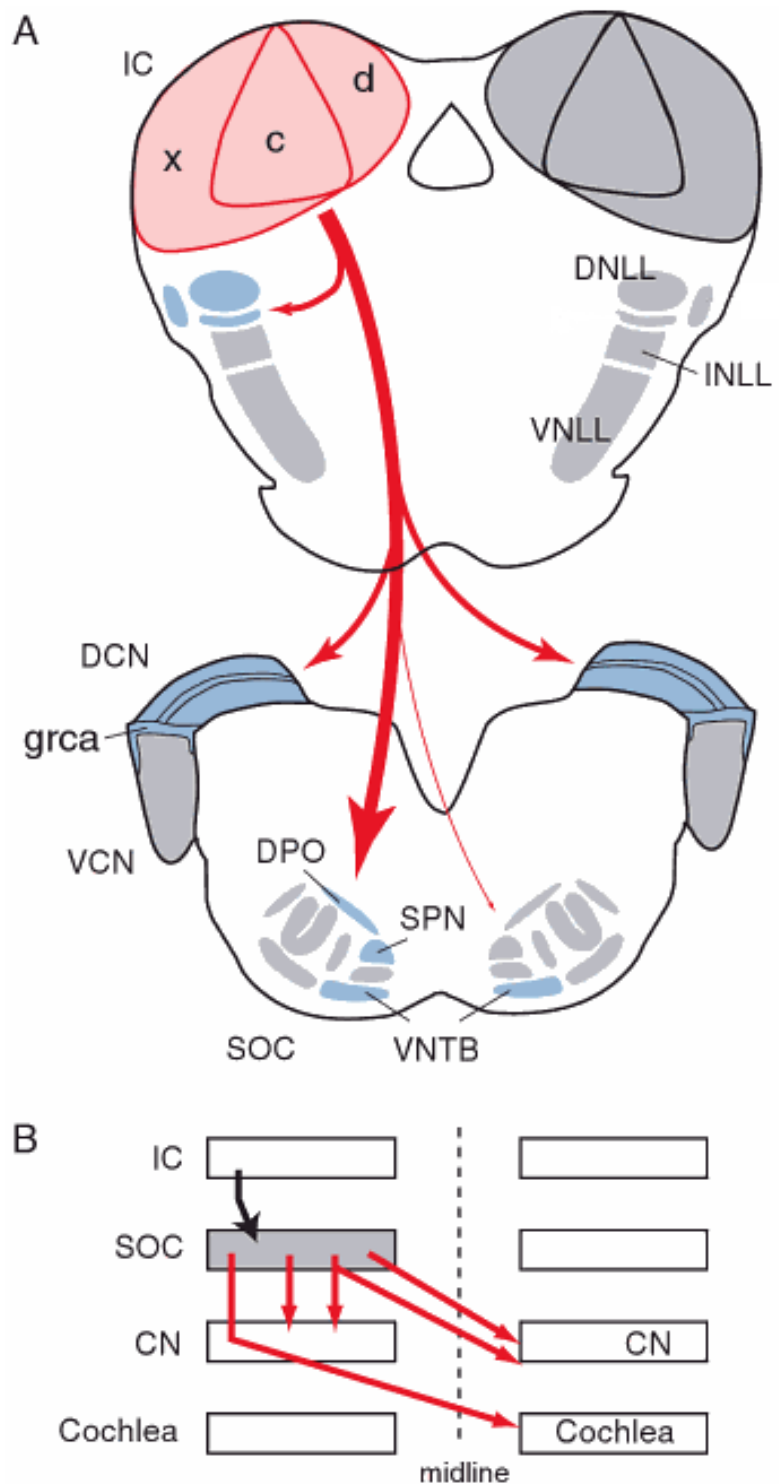


Figure 1.8 Summary diagrams of the descending connections of one IC (Red arrows). Line weight indicates relative size of each projection. (A) The IC innervates the ipsilateral DNLL and non-principal nuclei of the SOC, and both DCNs. (B) Neurons in SOC which receive IC innervation project to the CN and cochlea but not back to the IC (From Schofield (2010)).

1.7 Physiology of the Inferior Colliculi

The many afferent sources of projections to the IC, combined with a wide array of conductive ion channels expressed in IC neurons, produce a variety of cellular responses in response to stimulation in IC neurons. This section will provide a brief overview of the properties that characterise the responses of IC neurons.

1.7.1 Tonotopy

The organising principle of the CNIC in all mammals is the topographical representation of stimulus frequency. Neurons in the dorsal CNIC respond best to low frequency tones (the term 'low' here refers to tones in the lower range of each species' respective audiogram). As microelectrodes are advanced ventrally through the CNIC, neurons respond best to tones of increasing frequency (Rose *et al.*, 1963; Aitkin *et al.*, 1970; Clopton and Winfield, 1973; Merzenich and Reid, 1974). The anatomical substrates of this organisation are the fibrodendritic laminae (Malmierca *et al.*, 1995), each of which is comprised of neurons which respond to a band of frequencies, a property which produces discontinuous stepwise jumps in CF rather than a continually changing axis of frequency (Schreiner and Langner, 1997; Malmierca *et al.*, 2008), and allows the alternative nomenclature – frequency band laminae (Merzenich and Reid, 1974; Schreiner and Langner, 1997). Frequency band laminae may consist of just two to three neurons stacked aside each other (Malmierca *et al.*, 2008).

The representation of frequency in the LCIC is less clearly defined and more variable across species. A high to low frequency axis was found in cat from lateral to medial locations along the LCIC (Rose *et al.*, 1963; Clopton and Winfield, 1973), while in mouse the tonotopic axis appears to be much less defined but possibly in the opposite direction to cat (Stiebler and Ehret, 1985). The LCIC is a multisensory region which receives afferent projections from the dorsal column nuclei and trigeminal nuclei and somatosensory evoked and

modulated responses are common in LCIC (Aitkin *et al.*, 1975). The lack of clear tonotopy may be influenced by the multimodal processing demands and integrations performed in LCIC.

The frequency organisation of the DCIC is less clear. Early studies suggested that frequency representation in the DCIC progressed from high to low CFs in the dorso-ventral axis, with a reversal of the tonotopic maps at the border with CNIC (Merzenich and Reid, 1974). This may have been due to the borders used to define the sub-nuclei in the reference atlas of the time (Berman, 1968). This finding has been countered by evidence suggesting that the laminae of the CNIC extend into the DCIC, forming a continuous frequency representation between the two regions both functionally (Fitzpatrick, 1975) and anatomically (Romand and Ehret, 1990; Malmierca *et al.*, 2011). As the DCIC and CNIC are difficult to distinguish anatomically (Malmierca *et al.*, 2011) or physiologically, it may be that there is gradual change along a lamina rather than a clearly delineated border.

The frequency selectivity of neurons in CNIC has been extensively described (Rose *et al.*, 1963; Casseday and Covey, 1992; Ramachandran *et al.*, 1999; LeBeau *et al.*, 2001; Hernández *et al.*, 2005; Palmer *et al.*, 2013). Neurons in CNIC exhibit a range of frequency responses which represent transformations from the V-shaped responses of AN fibres. In DCIC and LCIC, responses have been described less thoroughly. Units in the cortices tend to be much broader and irregularly shaped, with little frequency selectivity undertaken, while CNIC neurons are more sharply tuned, with shorter latency responses and vigorous responses are seen in response to pure tone stimuli (Aitkin *et al.*, 1975; Willott and Urban, 1978; Syka *et al.*, 2000). A more thorough introduction to frequency response types in the IC is presented in Chapter 4.

Frequency band laminae may be the functional modules which form the representation of critical bands. Each lamina has a CF range of around one

critical bandwidth and the distance to each neighbouring lamina is also approximately one critical bandwidth (Schreiner and Langner, 1997; Ehret and Schreiner, 2005). Processing of stimuli within a critical band may therefore be mediated by disk-shaped cells, while stellate cells may allow for spectral integration across frequencies. This organisation may allow for representation of complex spectral features at the level of the IC.

1.7.2 Temporal responses of inferior colliculus neurons

There are at least six temporal response types *in vitro*, which appear to have no relationship to cellular morphology (Peruzzi *et al.*, 2000; Sivaramakrishnan and Oliver, 2001). This picture is more complicated *in vivo*, where even more response types have been identified (Bock *et al.*, 1972; Rees *et al.*, 1997; Wallace *et al.*, 2012). These response types have been broadly grouped into responses which discharge spikes in a phasic manner at the onset or offset of stimuli, or responses which discharge spikes throughout the stimulus - of which there are several subtypes. *In vivo* and *in vitro* studies suggest these responses are generated both by the intrinsic channels of the cell, and the confluence of afferent synaptic input the cell receives, both of which are highly variable in IC. The range of temporal response types allows from complex integrations of input to be encoded in IC spike trains (Peruzzi *et al.*, 2000). The specific types and functional implications of temporal response characteristics in IC are discussed in more detail in Chapter 6.

1.7.3 Binaural integration in the inferior colliculus

Because the IC receives inputs from first order (SOC) and second order (NLL) binaural nuclei, it is a crucial nucleus for the processing of binaural stimuli. These interactions underlie sound localisation in the azimuthal plane through the analysis of ITDs and ILDs.

Most IC neurons exhibit binaural interactions (Rose *et al.*, 1966; Moore *et al.*, 1983). These interactions are manifest as either the facilitation of responses to binaural stimulation compared to stimulation of only the contralateral ear (so called excitatory-excitatory or EE responses), or inhibitory binaural interactions with respect to contralateral stimulation alone (excitatory-inhibitory, EI responses). Some IC neurons do not exhibit binaural modulation of firing rate (EO responses). Examples of these response types have been observed in all preparations studied to date (Aitkin *et al.*, 1972; Popelar and Syka, 1982; Pollak *et al.*, 2002).

1.7.4 Response latency in the inferior colliculus

The latency of units in the IC is determined by the processing time of its afferent projections. The population of IC neurons have a wide range of latencies. The shortest responses occur in the ventral IC with a latency of 4 to 5 ms, which correlates closely with wave V of the auditory brainstem response (Harrison and Palmer, 1984). First spike latency (FSL) in the CNIC decreases in the dorso-ventral axis (Harrison and Palmer, 1984) and as stimulus level increases (Hind *et al.*, 1963; Kuwada *et al.*, 1984; Semple and Kitzes, 1985). The responses of phasic units tend to be shorter than temporally sustained units (Kuwada *et al.*, 1984). First spike latency may be an important signalling feature of sound localisation cues (Chase and Young, 2007; Zohar *et al.*, 2011) and amplitude modulations (Langner *et al.*, 1987) in IC. Latency responses are discussed further in Chapter 6.

1.8 The Commissure of the Inferior Colliculus

The role of the CoIC in the processing of auditory stimuli is the main subject of study in this thesis. As such, our current knowledge of the anatomy, pharmacology and physiology of the CoIC will be described in detail.

The ICs are the highest sub-cortical nuclei in the auditory system which innervate one another bilaterally via a commissure. The CoIC may provide more afferent innervation to each IC than any other single source (Moore, 1988). The CoIC is a curvilinear fibre bundle which courses symmetrically between the ICs. The CoIC interconnects the ICs dorsally and rostrally, forming a direct projection from neurons in one IC to those in the opposite IC. The commissure is hypothesised to be a major source of bilateral processing at the level of the midbrain in the auditory system.

1.8.1 Anatomy of the commissure of the inferior colliculi

The CoIC is comprised of heavily myelinated fibres. The number of CoIC projecting fibres increases dorsally, medially and rostrally throughout the IC, producing a myeloarchitecture of increasing density. The majority of fibres which project via the CoIC emanate from the IC (Faye-Lund and Osen, 1985).

Coleman and Clerici (1987) categorised the projections from one IC to the other as arising from 'homotopic points' to which DCIC and LCIC as well as CNIC contribute. In a key study, Saldaña and Merchán (1992) investigated the intercollicular projections of the IC in rat. Using Phaseolus vulgaris-leucoagglutinin (PHA-L) as an anterograde tracer, they made deposits in the CNIC, DCIC and LCIC and identified the respective targets of each in the contralateral IC. Injections into the CNIC formed 'plexuses' along the tonotopic laminae both ipsi and contralaterally. The authors subdivided these plexuses into two on each side, one in the LCIC and the other that coursed through both CNIC and DCIC. However, it could be argued that other than the change in

orientation and thickness between the medial and lateral wings of these laminar plexuses, they formed one continuous laminar sheet rather than two separate subdivisions (Fig. 1.9).

Malmierca *et al.* (1995) produced similar findings in guinea pig using the anterograde tracer biocytin. They confirmed the finding of Saldaña and Merchán (1992) that the DCIC shows remarkable similarity to the CNIC in its tonotopic interconnectivity via the CoIC. This work has since been extended and the commissure found to connect the two colliculi in a tonotopic manner with predominantly a point to point connectivity but with diffuse projections throughout the injected lamina and the mirror opposite lamina (Malmierca *et al.*, 2009). Furthermore, the DCIC and CNIC projections are different. The CNIC sends a projection to the contralateral frequency matched lamina, with a bias towards the mirror image point from which the projection originated. The DCIC may have two types of projections, one type which projects tonotopically to the contralateral CNIC while another type projects exclusively to the contralateral DCIC in a diffuse manner (Malmierca *et al.*, 2009).

Rockel and Jones (1973a) used a degeneration technique to lesion one DCIC and found only cells in a symmetric position to the lesion were affected. This study had the methodological drawback of not being able to disambiguate the lesion of the DCIC from the descending MGB and AC coursing through the DCIC. Brunso-Bechtold *et al.* (1981) corroborated this finding and also suggested that the DCIC formed the heaviest and perhaps only component of the CoIC. This study was also hampered by the methodological constraints of the lesion technique employed. Earlier work had already shown that the lateral CNIC and LCIC project commissurally (Carey and Webster, 1971), a finding that has been corroborated since (Saldaña and Merchán, 1992; Malmierca *et al.*, 1995; Malmierca *et al.*, 2009).

Kudo and Niimi (1978) found that a few fibres within the CoIC do not originate from the IC. Using tract tracing they discovered that depositing retrograde horseradish peroxidase (HRP) tracers in MGB labelled both the ipsilateral IC and contralateral IC. Oliver (1984b), replicated this finding, describing 'scattered' cells which project to MGB from the contralateral IC.

Corticofugal fibres from the AC have also been found to contribute to the commissure (Saldaña *et al.*, 1996; Winer *et al.*, 2002; Bajo and Moore, 2005; Bajo *et al.*, 2007). Further tracing studies have identified that ascending neurons from the DNLL (Bajo *et al.*, 1993), SPN (Saldaña *et al.*, 2009), tectal longitudinal column (Aparicio *et al.*, 2010) and sagulum (Henkel and Shneiderman, 1988) project through the CoIC.

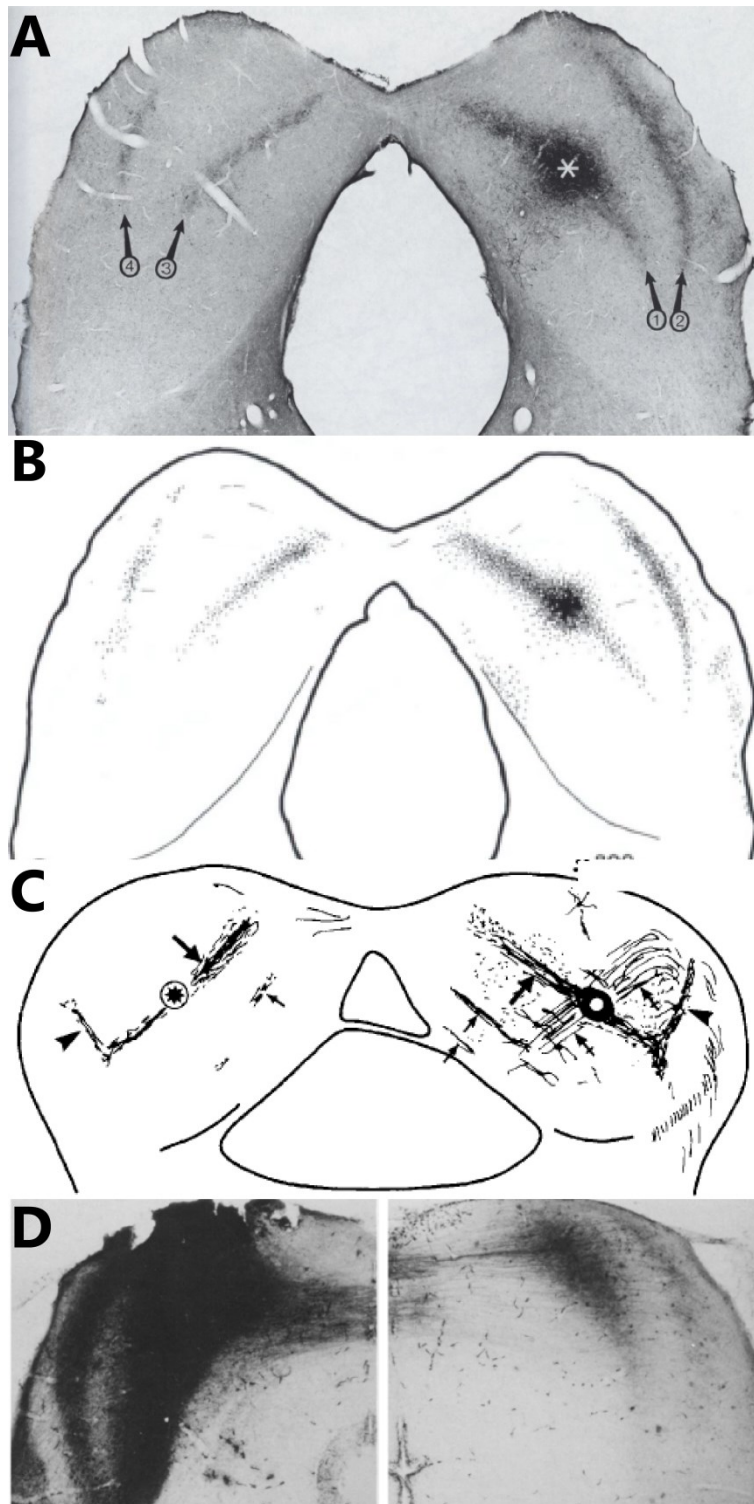


Figure 1.9 (A) Coronal section through rat IC. PHA-L injected into the CNIC on one side (star) produced staining throughout the ipsilateral lamina and the mirror symmetric contralateral lamina via the CoIC. (B) Camera lucida drawing of A. (C) Biocytin injection in guinea pig and (D) HRP injection in mouse also showed similar staining patterns (A & B from Saldaña and Merchán (1992); C from Malmierca *et al.* (1995); D from González-Hernández *et al.* (1986)).

1.8.2 Neurochemical nature of the CoIC

Glutamate is the principal excitatory neurotransmitter in the IC (Adams and Wenthold, 1979) and the majority of commissural projections, most of which emanate from disc shaped cells are glutamatergic (Saint Marie, 1996). A variable proportion of CoIC projecting neurons were found to be GABAergic in rat, with approximately 20 % in dorsal CNIC, and as few as 3 % in ventral CNIC (Fig. 1.10; González-Hernández *et al.* (1996)). A later study challenged this finding as no CoIC projecting cells were found to be GABAergic in CNIC (Zhang *et al.*, 1998). Both of these studies used albino rat as their model species, but the latter used restricted injections into central CNIC while the former employed huge injections and thus found more stained cells. Owing to the nucleotopic organisation of the IC, small injections are valuable when combined with physiological recording as they may provide functional and anatomical correlates of CoIC projections, but they may not provide a global picture of CoIC projections. Thus Zhang *et al.* (1998) may not have captured the GABAergic component of the projection. The percentage of GABAergic CoIC projection neurons is estimated in pigmented rat to be ~20% based on double labelling of cells from an injection in central CNIC (Fig. 1.10; Hernández *et al.* (2006)). While the CoIC clearly contains a GABAergic component, the density and number of these neurons varies between different regions within and between laminae of the IC and between sub-nuclei. Whether these inhibitory neurons act mono- or poly-synaptically is an important issue that remains to be determined. Electrophysiological mapping, combined with discrete injections of tracers, may elucidate more information about the functional and anatomical nature of CoIC projections (Malmierca *et al.*, 2009). The possible contribution of other neurochemicals to CoIC projections has not been investigated.

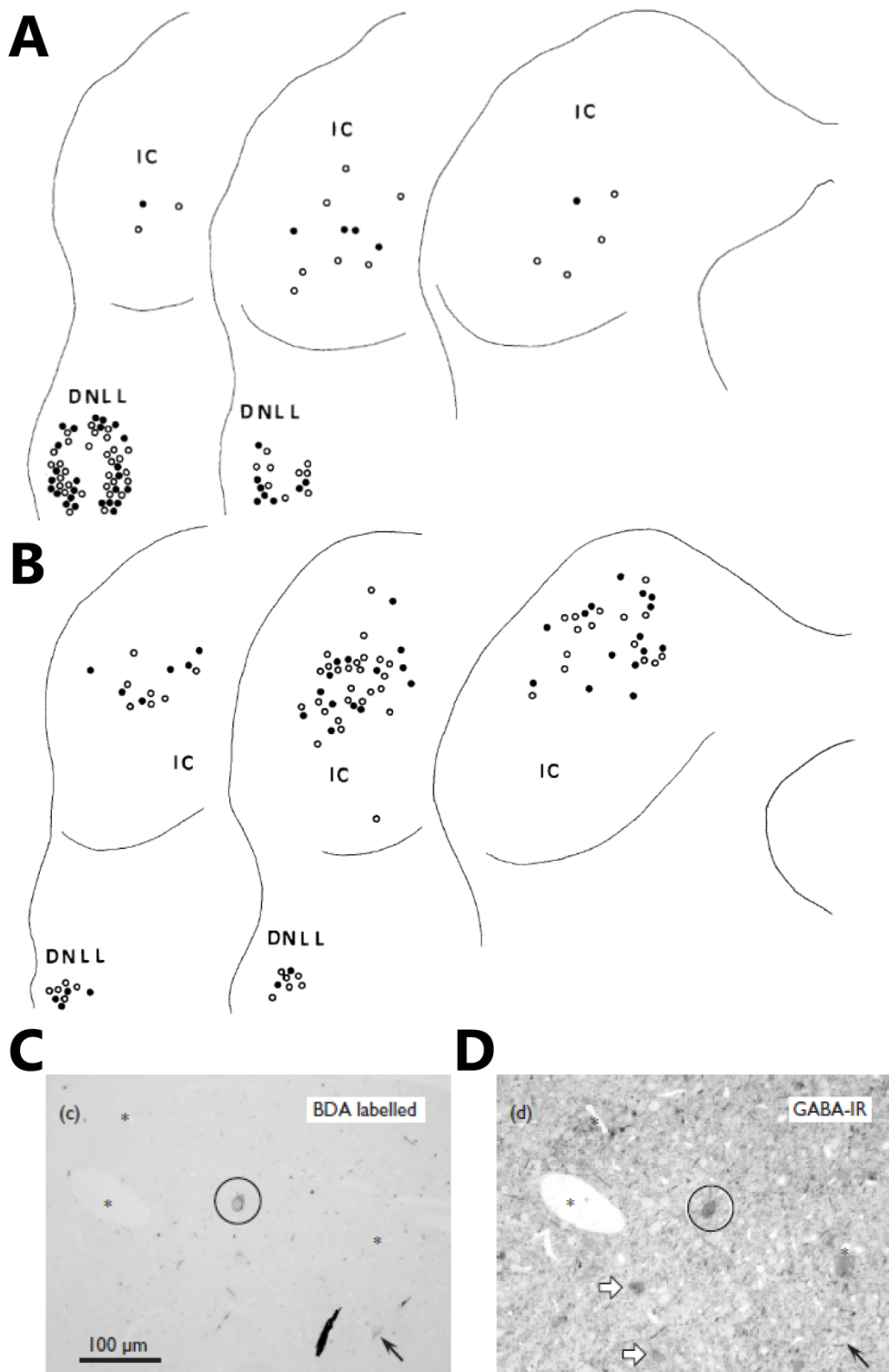


Figure 1.10 (A) Camera lucida illustrations of HRP and GABA (filled circles) and HRP only (open circles) positive somata in the IC following injection in contralateral ventral CNIC and (B) dorsal CNIC. GABAergic CoIC projecting nuclei were more common in dorsal CNIC. (C) Semithin consecutive sections showing a retrogradely stained, biotin positive soma (circled) after injection in the contralateral CNIC. (D) The same neuron was GABAergic. (A & B from González-Hernández *et al.* (1996); C & D from Hernández *et al.* (2006)).

1.8.3 Functional influence of the CoIC

In spite of the extensive size and therefore likely importance of the CoIC for processing in the IC, there is a paucity of information as to what functional influence intercollicular processing has on the analysis of sound. Two studies were first to glimpse the functional influence of CoIC mediated interactions *in vivo*, both of which utilised pressure injection of kynurenic acid, a blocker of glutamatergic transmission, while recording single units in a mirror opposite position in the contralateral IC of anaesthetised rat (Malmierca *et al.*, 2003; Malmierca *et al.*, 2005). The first of these investigations found that the frequency response areas (FRAs) of the majority of neurons were modulated by contralateral IC block, with both excitatory and inhibitory effects observed (Fig. 1.11C & D; Malmierca *et al.* (2003)). However, the pressure injection method is technically difficult and the low number of neurons recorded in the study limits its interpretability. A further study by Malmierca *et al.* (2005), found that 97% of sampled neurons either increased or decreased in firing rate following contralateral IC blockade (Fig. 1.11E & F), however, the sample size was again small.

The pressure injection technique suffers several drawbacks. One being that the effects of drug application were restricted to the injection site and did not suppress activity in a large region of the IC. Another hindrance is that in spite of the small volume of drug injected, it is not possible to infer how far it travelled to have an effect and as such the precise region that is disrupted by glutamatergic blockade could not be determined. Finally, the mechanical distortion effect of physical pressure injection caused the loss of a high proportion of units. This highlights the need for a technique which can derive a high throughput of cells, so that a sizable population of units can be studied. This would allow for inferences to be made of population activity, rather than speculation on the basis of a few example units. So while these studies provide

an enticing insight into intercollicular processing, there remains a large gap in our understanding of the functional influence of the connections mediated by the CoIC in auditory processing.

Electrical stimulation of the CoIC of the rat *in vitro* produced a short latency IPSP, followed by a short latency EPSP and then slow, polysynaptic IPSPs in mid-sized multipolar (stellate) neurons which projected throughout the ipsilateral IC or through the CoIC (Fig. 1.11A; Smith (1992)). The excitation was not changed by NMDA blockers, implying AMPA and/or Kainate receptors as the target of the synaptic glutamate. Both the short and long latency inhibitory components were removed by blocking the actions of GABA. Another *in vitro* study, conducted in gerbil, supported the finding that complexes of synaptic events were produced in response to CoIC stimulation (Fig. 1.11B; Moore *et al.* (1998)). Both lemniscal and CoIC mediated currents were found in almost all cells. Inhibitory GABAergic currents were found to dominate excitatory currents, with 38 % of cells receiving no glutamatergic current at all in response to CoIC stimulation. The dominance of inhibition was thought to be largely mediated through poly-synaptic, interneuron mediated currents.

Two recent reports have described the effects of electrically stimulating one IC while recording single units in the contralateral IC *in vivo*. When electrical stimulation was synchronised with auditory stimuli at a repetition rate of 2 Hz it produced an almost entirely inhibitory effect on contralateral IC neurons (Mei *et al.*, 2012). Driving the contralateral IC with tetanic stimulation produced inhibition and sharpening of frequency tuning in the vast majority of contralateral IC neurons and shifted the frequency representation of contralateral V-shaped neurons towards that of the electrically stimulated neuron's CF (Fig. 1.11G & H; Cheng *et al.* (2013)). These data appear to show a key role for the CoIC in the processing of auditory stimuli and possible plastic effects between the colliculi.

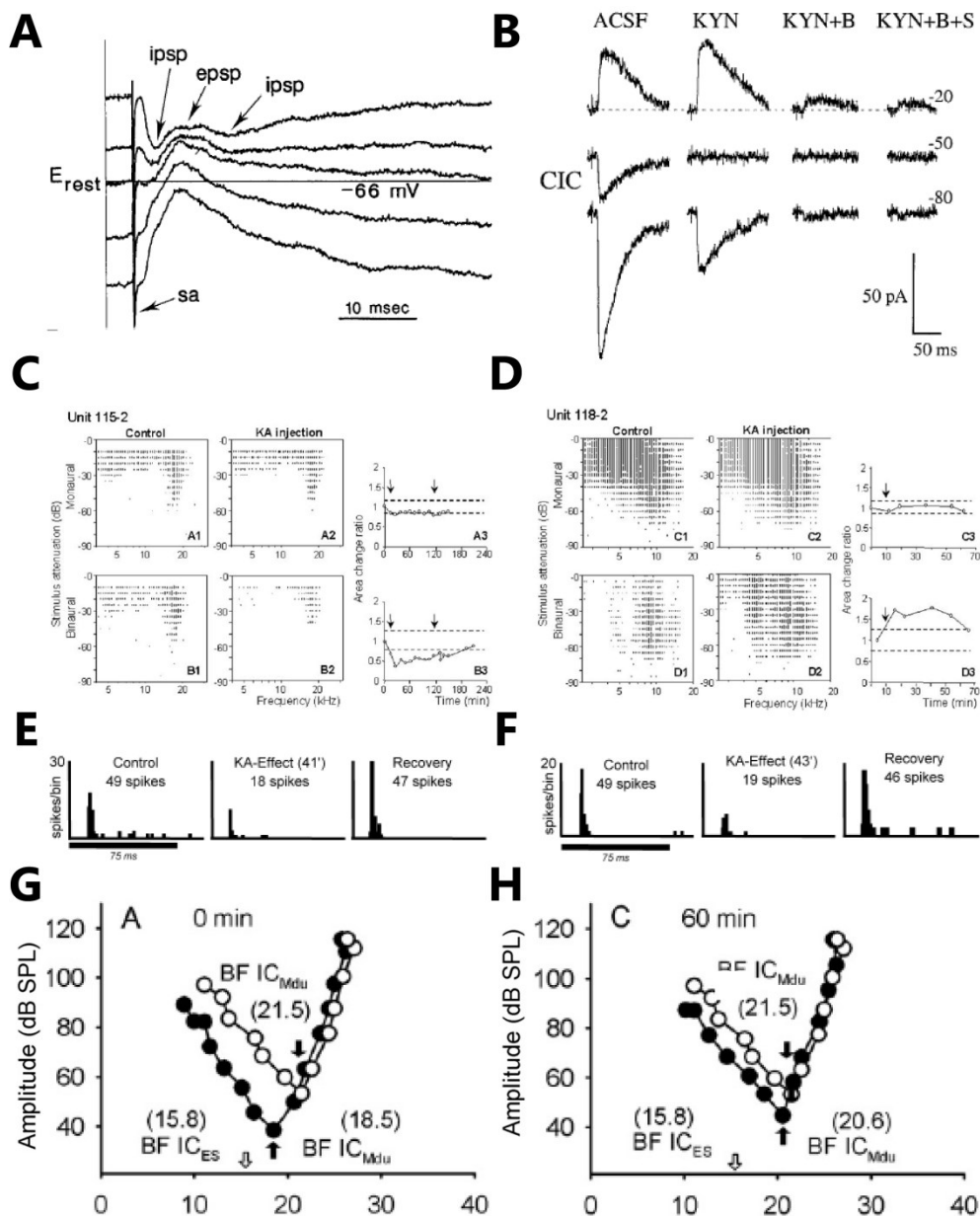


Figure 1.11 (A) Intracellular potentials from an IC neuron in response to CoIC stimulation. Short latency IPSPs were followed by an EPSP and a polysynaptic IPSP. (B) Whole cell recordings from an IC neuron to CoIC stimulation. Blocking glutamate reduced inward current. Bicuculline eliminated all remaining currents. (C) V-shaped FRA that was unchanged to contralateral ear stimulation during contralateral IC deactivation, but decreased to binaural stimulation. (D) A Broad FRA that was unchanged to contralateral stimulation but increased to binaural stimulation. (E) Contralateral and (F) binaural stimulated PSTH responses that were reversibly suppressed by contralateral IC deactivation. (G) Electrical stimulation of the contralateral IC induced a shift in CF that (H) recovered after an hour. (A from Smith (1992); B from Moore *et al.* (1998); C & D from Malmierca *et al.* (2003); E & F from Malmierca *et al.* (2005); G & H from Cheng *et al.* (2013)).

1.8.4 Gaps in our understanding of CoIC mediated processing of sound

Our knowledge of CoIC mediated influences on auditory processing within the IC is in its infancy. While the general anatomy is quite well understood, there remains a dearth of investigations into what CoIC projecting terminations do. The findings of Malmierca *et al.* (2003) and Cheng *et al.* (2013) indicate that the spectral responses of IC neurons can be strongly influenced by CoIC fibres. FRAs in the IC have many different morphologies, but almost all cells reported to date during commissural deactivation have had a V-shaped morphology. The frequency analyses performed by different shaped FRAs are important (Palmer *et al.*, 2013). Whether the CoIC has any influence on these response properties of IC cells is unknown. Furthermore, detailed measurements of fundamental parameters of FRAs have not been described in response to CoIC modulation.

While Malmierca *et al.* (2005) and Mei *et al.* (2012) have found evidence that firing rates of most IC neurons are influenced by commissural input, the specific and differential effects on the several temporal response types in IC have not yet been investigated. The various temporal response characteristics of IC neurons likely have different functional roles that may be differentially influenced by CoIC input. The finding that inhibition is dominant via the CoIC is interesting, as while there is a GABAergic component of CoIC fibres, the majority in CNIC are excitatory (González-Hernández *et al.*, 1996; Hernández *et al.*, 2006). The findings of Mei *et al.* (2012), that electrical stimulation of one IC produced almost entirely inhibitory effects in the contralateral IC, contradicts the known anatomical projections of the CoIC, the majority of which are excitatory. The finding of Mei and colleagues is important to corroborate as it has significant functional implications.

The CoIC has been hypothesised to undertake a significant role in complex auditory analysis and sound localisation. While it is intriguing to speculate as to

these possible mechanisms, a thorough grounding in responses to simple stimuli is important before any higher level stimuli are analysed in great detail.

1.9 Aims of this Thesis

This thesis will address some of the outstanding questions as to the functions of the CoIC *in vivo*.

1.9.1 Hypotheses

The main hypotheses to be tested in this thesis are:

- That commissural projections contribute to the FRA shapes of a large proportion of IC neurons in the contralateral IC. Furthermore, the extensive inhibitory component of dorsally located CoIC projecting neurons is involved in creating FRAs which are formed by inhibition.
- That the firing rates and the structure of temporal response properties of most IC neurons can be modulated by commissural projections. The effects on firing rate of contralateral IC deactivation are hypothesised to be predominantly excitatory, based on by a previous study which reported a near entirely inhibitory effect of stimulating the contralateral IC (Mei *et al.*, 2012).

1.9.2 Organisation of this thesis

- Chapter 2 describes the general methods employed in the experiments performed in the course of the study.
- Chapter 3 is aimed at testing the hypothesis that cryoloop cooling is a suitable model by which one IC can be selectively deactivated while recording neurons in the contralateral IC. One of the limitations of investigations into the role of commissural connections thus far has been the lack of a practical model by which one IC can be deactivated in a

reversible manner so that changes in sound driven responses in the contralateral IC can be recorded.

The remaining Chapters describe experiments that employed cryoloop cooling of one IC while recording single units in the contralateral IC in response to contralateral and binaural stimulation.

- Chapter 4 seeks to corroborate the previous finding that the CoIC input modulates the FRAs of IC neurons in a larger sample of units than was previously possible. Furthermore, these experiments tested whether there are differences between the changes observed on different FRA types.
- Chapter 5 presents the changes in numerous measures which can be derived from FRAs such as CF, threshold and bandwidth, during contralateral IC deactivation by cryoloop cooling.
- Chapter 6 will address the effects of cooling one IC on the temporal response properties of single units in the contralateral IC with the aim of conducting the first systematic evaluation of changes in the firing rate and temporal structure of a large population of IC neurons in response to contralateral IC deactivation.
- Chapter 7 provides a general discussion of this work in the context of previous studies and proposes further experiments to advance knowledge in the field.

Chapters 3 to 6 all have the structure of a full research report. The topic of each Chapter will be introduced with any information pertinent to that Chapter. The specific methods employed will next be described. This will be followed by any results and these will then be discussed.

Chapter 2. Materials and Methods

2.1 Overview of Methodology

This Chapter will outline the general methods implemented in all experiments conducted in this study. Details pertinent only to the methods and analyses employed within a specific results Chapter will be described in the methods section of that Chapter.

2.2 Animal Model

Experiments were performed in accordance with the terms and conditions of a licence issued by the UK Home Office under the Animals (Scientific Procedures) Act of 1986, and with the approval of the Local Ethical Review committee of Newcastle University. All 63 experiments were performed on adult guinea pigs (*Cavia porcellus*), 38 of which were male and 25 female. Animals used were at least 14 weeks old and ranged in weight from 421 to 1,100 g (median (\tilde{x}) = 795 g; Interquartile range (IQR) = 607 to 909 g). Animals were housed in cages with 0.5 m high wire mesh walls (floor area 1 m X 0.5 m). Bedding was comprised of hay and wood shavings. Animals were fed food pellets *ad libitum*, and their diet was supplemented daily with apples, pears and oranges. Vitamin C was added to the unrestricted water supply.

2.3 Anaesthetic Protocol

Anaesthesia was induced with urethane (1 g/kg as 20 % solution, intraperitoneal injection (i.p.)) and supplemented by the analgesic and dissociative Hypnorm (fentanyl citrate 0.315 mg/ml and fluanisone 10 mg/ml; 1 ml/kg, intramuscular injection (i.m.)). Atropine sulphate monohydrate (0.05 mg/kg, subcutaneous injection (s.c.)) was given following induction of anaesthesia to suppress bronchial secretions. Anaesthesia was maintained with further doses of

Hypnorm (1/3 original dose) on indication of a pedal reflex in response to a pinch of the hind paw.

2.4 Surgical Procedure

A tracheotomy was performed in all experiments. A hard plastic cannula was inserted into a stoma in the trachea and secured with suture. The cannula acted as a tracheostomy tube through which the animal could be artificially ventilated. Animals were allowed to respire spontaneously. If breathing became laboured the animal was artificially respired with medical air via a modified small animal ventilator (Harvard Apparatus) which maintained end-tidal CO₂ at ~5 %. Core temperature was monitored with a rectal probe and maintained at 38±1 °C with a thermostatically controlled electric blanket (Harvard Apparatus).

Experiments were conducted inside a single walled, sound attenuating room (IAC). Animals were placed in a stereotaxic frame (Kopf) in which the standard ear bars were replaced by hollow polymethyl methacrylate conical specula, the apices of which were placed in the auditory meatuses allowing visualisation of the tympanic membranes. This 'closed acoustic system' modification from standard stereotaxy held the head in place and allowed sound stimuli to be delivered to the animal.

A dorsal midsagittal incision was made along the scalp. The skin was reflected and the tissues overlying the skull were abraded. A hole was trephined 10.5 mm caudal and 2.5 mm left of bregma. Rongeurs were used to extend the diameter of the craniotomy to ~5 mm, centred on the initial trephine hole. The dura mater was retracted and the cortical tissue overlying the left IC was aspirated with a glass Pasteur pipette attached to a vacuum pump until the dorsal surface of the left IC was visualised. This procedure caused no trauma to the IC.

A second craniotomy was made at a mirror image location on the contralateral side. The dura was retracted but the cortex on this side was left in place.

Electrode penetrations were made through the cortex in a mirror opposite position to the visualised IC.

2.5 The Cryoloop and Cooling System

The cryoloop and cooling system used in this study were modified from the method described by Lomber *et al.* (1999). A cryoloop was constructed by forming a loop from 23 gauge stainless steel tubing (Fig. 2.1 inset). Each end of the tubing was soldered inside a 19 gauge needle which served as inlet and outlet points of the cryoloop (Fig. 2.1). The tip of a type T (copper-constantan) thermocouple (Omega) was secured to the cryoloop tip to allow monitoring of the cryoloop temperature with a digital thermometer (HH506RA, Omega).

A peristaltic pump (Gilson) drew -80 °C ethanol (cooled in a deep freeze) from a reservoir. The ethanol was pumped through Tygon R-1000 tubing (Cole-Parmer) into a cooling coil of fluorinated ethylene propylene tubing (Cole-Parmer) coiled inside a vacuum flask containing more -80 °C ethanol. The ethanol then passed through the cryoloop and back to the reservoir (Fig. 2.2). Regulating the pump speed controlled the flow rate through the system and thereby enabled the temperature at the cryoloop tip to be maintained at a desired value.

The cryoloop was curved to maximise contact with the dorso-lateral surface of the exposed IC. This maximised the extent of cooling in areas in which the density of neurons projecting via the CoIC to the contralateral IC is known to be highest (Saldaña and Merchán, 1992; Malmierca *et al.*, 1995; Malmierca *et al.*, 2009). At no time was the temperature allowed to drop below 2 °C. This prevented cryo-trauma from occurring in the cooled IC. Measurements of the temperature within the IC were made using a needle thermocouple (Hyp-0, Omega) which was advanced into the IC in a ventral direction from the dorsal aspect.

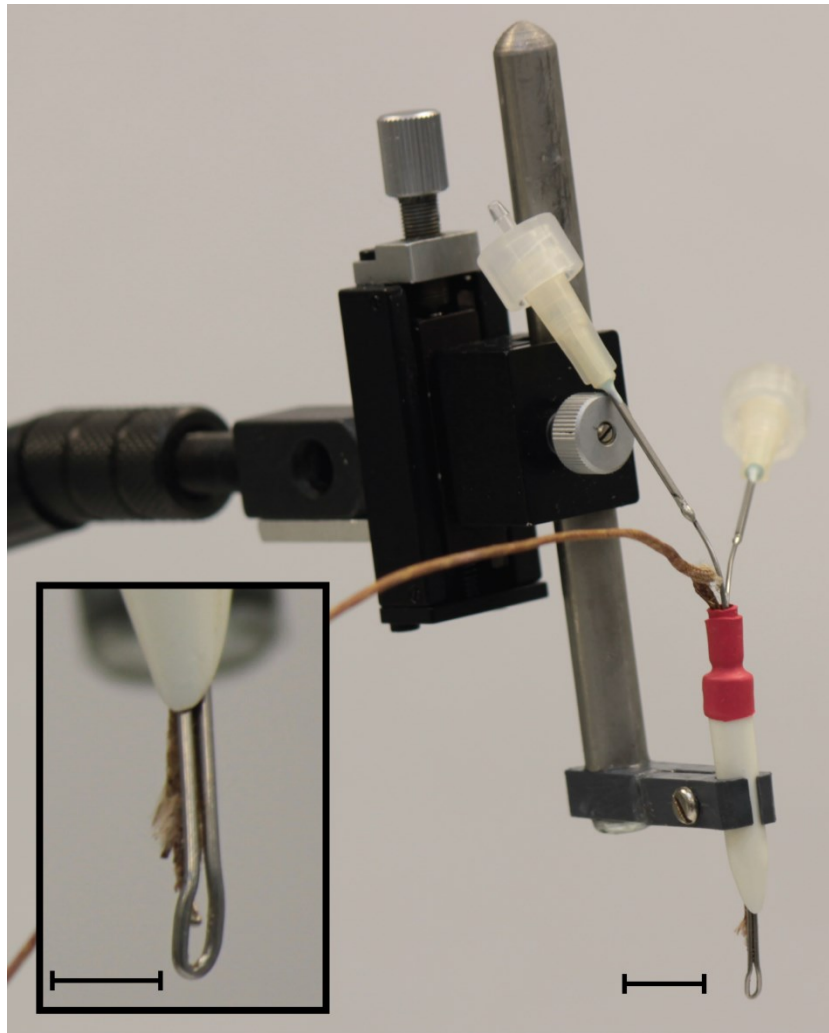


Figure 2.1 Photograph of the cryoloop used to cool the IC held in a micromanipulator. Two 19 gauge needles soldered to each end of the cryoloop tubing acted as inlet and outlet ports for the coolant. The manipulator allowed precise placement of the loop in contact with the exposed IC. Inset: zoomed in view of the cryoloop. Placing the thermocouple tip at the bifurcation of the loop allowed precise monitoring of the cryoloop temperature. The surface of the cryoloop was placed in contact with the dorso-rostral aspect of the exposed IC. Scale bars = 5 mm.

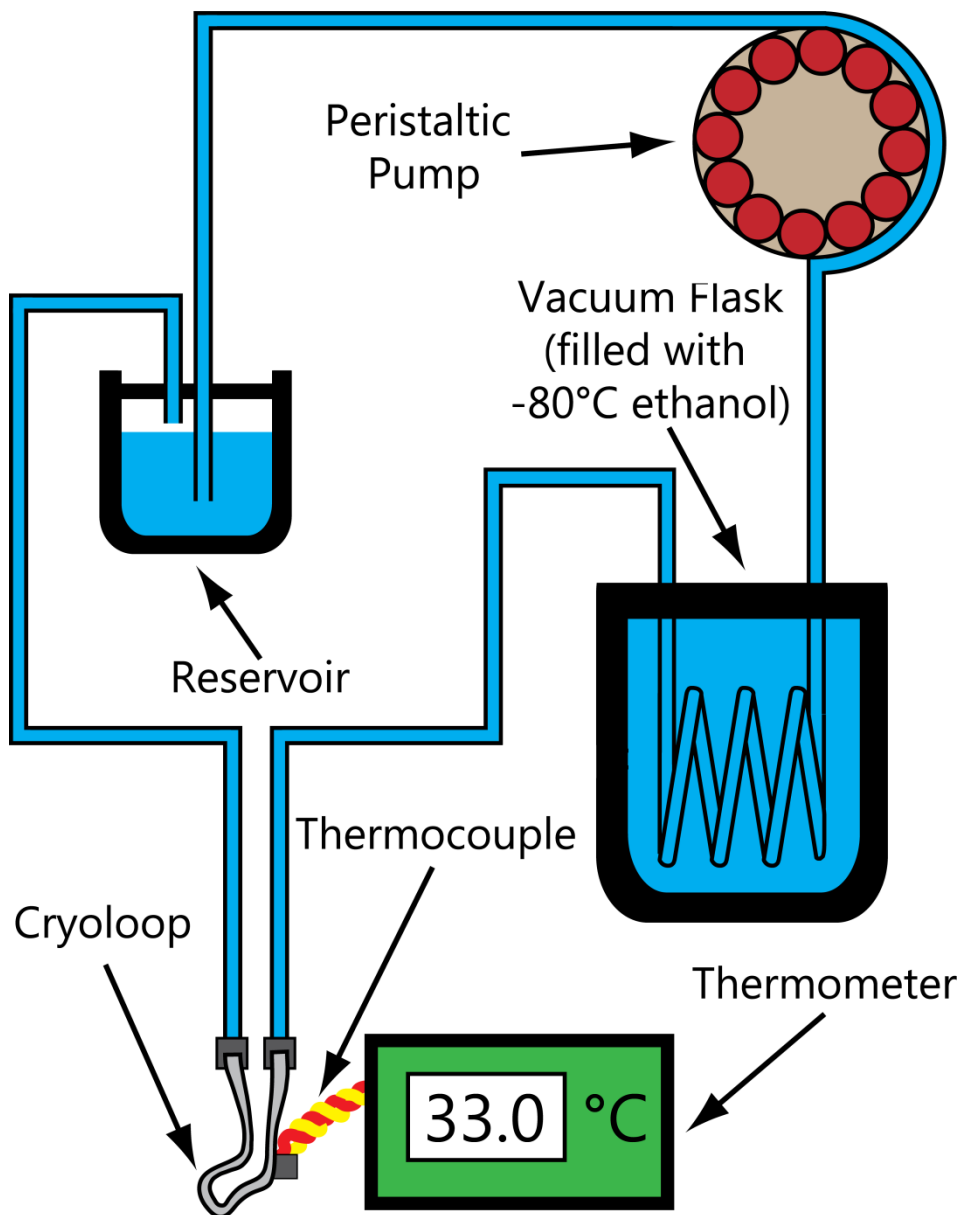


Figure 2.2 Schematic representation of the cooling system (adapted from Lomber et al. (1999)). A peristaltic pump drew ethanol at $-80\text{ }^{\circ}\text{C}$ from a reservoir and pumped it through the hydraulic system. The ethanol was cooled by passing it through a coil within a sealed vacuum flask filled with $-80\text{ }^{\circ}\text{C}$ ethanol before it passed through the cryoloop. A thermocouple was attached to the cryoloop to allow precise monitoring of the temperature imparted to the tissue. Control of flow rate allowed precise control of the tissue temperature.

2.6 Stimulus Generation and Presentation

Pure tone and click stimuli were generated digitally by Tucker-Davis Technologies System 2 (TDT2) hardware which was controlled by custom-written software that allowed the frequency and level of stimuli to be varied in real time. Stimulus waveforms were generated with a sampling frequency of 100 kHz. Pure tones were cosine² ramped to shape the initial and final 5 ms of the tone stimuli. Search stimuli were 50 ms bursts of pure tones, roved manually between 0.1 to 20 kHz and between 0 to 99 dB attenuation, and presented at a repetition rate of 4 Hz.

Stimuli were delivered through Sony MDR 464 earphones housed in an alloy enclosure and coupled to damped probe tubes (4 mm diameter) that fitted into the Perspex specula (Rees *et al.*, 1997). The output of the system was calibrated using a Bruel & Kjaer Type 4134 1/8 inch microphone, a Type 2639 preamplifier and Type 2610 measuring amplifier with the appropriate K factor correction. The microphone was seated in a small tubing coupler that sealed the narrow end of the speculum holding each speaker. The output was measured in steps of:

1. 50 Hz between 100 and 600 Hz;
2. 100 Hz between 600 and 1,000 Hz;
3. 125 Hz between 1,000 and 1,500 Hz.;
4. 500 Hz between 1,500 and 12,000 Hz;
5. 1,000 Hz between 12,000 Hz and 16,000 Hz.

The maximum output of the system was approximately flat from 0.1 to 9 kHz (100 ± 8 dB SPL) and then fell with a slope so that the maximum output of the system at 16 kHz was 78 dB from both the left and right speakers (Fig. 2.3). Second and third harmonic components in the signal were ≤ 60 dB of the fundamental at the highest output level.

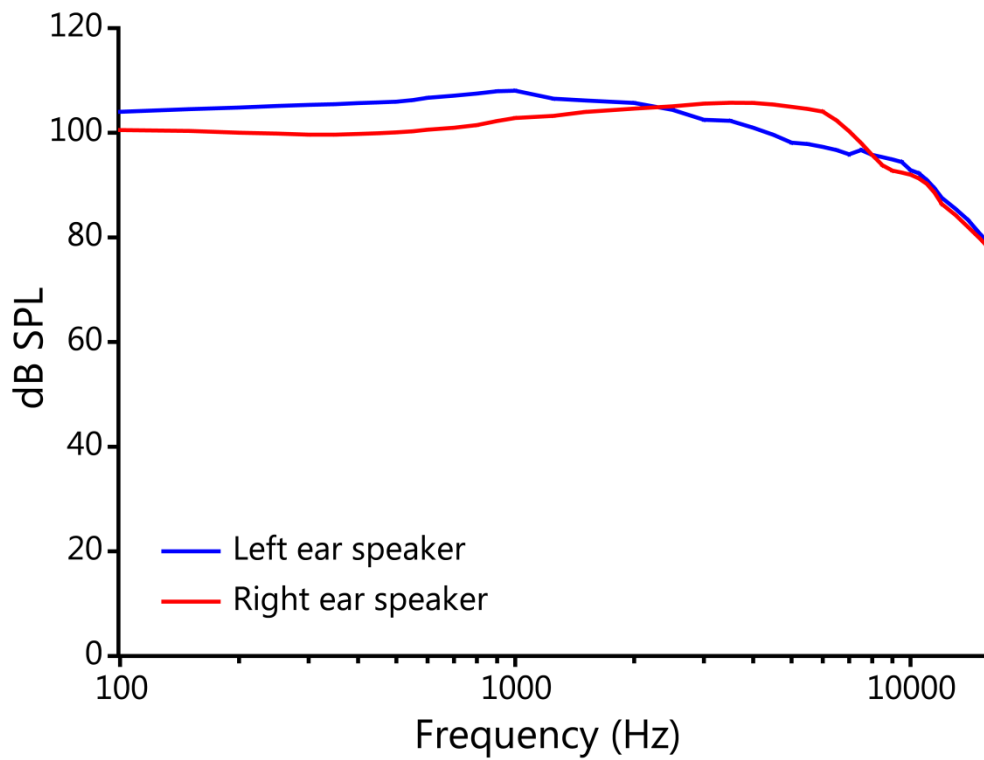


Figure 2.3 Calibration of the maximum output of the left and right ear speakers of the sound delivery system. The measurements for each ear were smoothed using a moving average filter (smooth function in Matlab). The output was approximately flat for both ears up to 9 kHz.

2.7 Electrodes

All recordings were obtained using borosilicate glass coated tungsten electrodes (Baldwin *et al.*, 1965; Merrill and Ainsworth, 1972). Electrode penetrations were made vertically through either the exposed left IC or through the cortex overlying the right IC. The electrode was lowered by hand until the electrode tip touched the surface of the brain. The electrode was then advanced and retracted by a stepper-motor microdrive activated by a remote control outside the sound attenuating room.

2.8 Electrophysiological Recordings

As the electrode tip entered the dorsal aspect of either IC, multi-unit spikes were 'driven' by the sound stimuli. Responses matched the classically defined dorso-ventral tonotopic organisation of the IC (Rose *et al.*, 1963; Clopton and Winfield, 1973; Popelar and Syka, 1982).

Extracellular action potentials and local field potentials were amplified (X 10,000) and band pass filtered (second order Butterworth, 0.1–3 kHz) by an amplifier (Dam-80; World Precision Instruments, UK). Spikes were further high pass filtered (300 Hz) via TDT2 hardware before being discriminated, converted to logic pulses, and time stamped to an accuracy of 10 μ s. In some cases spike waveforms were collected and stored using a PC Lab System (AD Instruments) running Scope software.

On isolation of a single unit, the CF and minimum threshold to tones presented to the ear contralateral to the recorded IC were estimated to establish the settings for data collection. The parameters of the stimuli used to test each neuron were defined relative to this initial estimate.

Neurons were characterised by first recording responses to a FRA paradigm (Evans, 1979; LeBeau *et al.*, 2001). FRAs were generated from the pseudorandom

presentation of pure tones to monaural contralateral ear, or binaural diotic stimuli (75 ms duration, 5 Hz repetition rate, 5 ms cosine² ramped rise/fall time) from two octaves above to three octaves below the estimated CF in 1/10th octave intervals. The level of the standard stimulus ranged from 10 to 90 dB attenuation from the maximum output of the system (~100 dB SPL) in 5 dB steps. As the threshold of some neurons was higher than others, the resolution of these units' responses was poor using these ranges. In those cases the range of levels and the size of the increments were reduced. The number of spikes produced in response to each stimulus was counted and displayed at the appropriate position in a plot of tone frequency versus attenuation level, according to a colour scale.

Units were also recorded in response to multiple repetitions of a CF pure tone (repetition rate of 4 Hz) played at 20 dB above threshold. Peri-stimulus time histograms (PSTHs) were constructed with bin widths of 1 ms from the 10 ms immediately preceding stimulus onset to 65 ms post stimulus offset. Some neurons in the IC exhibit long recovery times following auditory stimulation. To avoid the next stimulus occurring within the recovery phase of a units' response, there was always a minimum period of 160 ms between consecutive stimuli.

Field potentials were recorded by low pass filtering the output of the preamplifier at 1 kHz before averaging the response online using the PC Lab System. All field potential responses were recorded in response to transient 10 kHz pulses of 1-ms duration with 0.01 ms rise/fall time.

2.9 Termination of Experiments

At the conclusion of each experiment, an i.p. injection of sodium pentobarbitone was given. The pedal withdrawal and blink reflexes were assessed to ensure a sufficient plane of anaesthesia had been reached for the animal to be perfused transcardially. The heart was exposed ventrally,

the pericardium was removed and a stainless steel cannula was inserted into the left ventricle and clamped in place. The heart was then perfused by gravity with 300 mls of a wash solution comprised of 0.1 M phosphate buffered saline (PBS) and 2 mls of heparin (1,000 I.U. per ml) at a pH of 7.4 (± 0.1). This was followed by perfusion of 200 mls of a fixative solution (4 % paraformaldehyde in 0.1 M PBS).

2.10 Histological Processing and Analysis

After perfusion the skull was opened and the brain removed and placed in 4 % paraformaldehyde, for at least 24 hours at 4 °C to ensure thorough fixation of all proteins in the tissue. For cryoprotection, the brain was transferred to a 30% sucrose solution in 0.1 M PBS and left until it sank (normally 2-4 days). The brain was then embedded in Tissue-Tek O.C.T, frozen and sectioned in the coronal plane using a cryostat (HM 560, Microm). Sections were mounted on slides, stained with cresyl violet and coverslipped.

In most cases the tissue was not processed to verify recording location. All recordings were made from within the IC from neurons with response properties that are similar to previous recordings made within the CNIC (Rees *et al.*, 1997; LeBeau *et al.*, 2001) or DCIC. The approximate location of recorded neurons could be evaluated according to their CF but no claims are made as to the exact location of individual recordings.

2.11 Data Analysis

Details relevant to the methods employed to analyse neurons according to their FRA responses are presented in Chapter 4 and 5. Methods specific to temporal response properties are provided in the methods section of Chapters 6.

2.12 Statistical Analyses

Normality tests were performed on all data using the D'Agostino-Pearson K^2 test in Matlab. This test was chosen over the Shapiro-Wilk test because most cells fired with the same number of spikes to multiple repetitions of PSTH stimuli. If multiple replications of the same value are present in a data set it reduces the accuracy of the Shapiro-Wilk test. The D'Agostino-Pearson omnibus test first calculates the skewedness and kurtosis of the distribution and then determines the distance that each value differs from that of a hypothetical Gaussian distribution and does not suffer from the drawbacks of the Shapiro-Wilk test. A P value is then returned from the sum of the squares of the discrepancies of the actual values from the expected values. If P was < 0.05 the data were considered to be non-normally distributed.

A large proportion of data sets were found to be non-normally distributed so non-parametric tests have been used throughout all Chapters. While this did lead to some loss of statistical power for a few normally distributed groups, in many cases these tests still returned significant differences. The Wilcoxon matched pairs test was used to compare paired samples, and the Mann-Whitney test was used for unpaired samples. All statistical analyses other than normality tests were performed in SigmaPlot 11.

Friedman's test was used for comparison of three or more groups, such as the control, cool and recovery groups of spikes per stimulus with repeated measures. Following each Friedman test, multiple Wilcoxon matched pairs tests were employed to test for statistical significance between each possible pairing between the groups. The null hypothesis (that no difference existed between groups) was rejected if $P < 0.05$ for the Friedman's test or $0.05/n$ (n = number of groups tested) for the Wilcoxon test with Bonferroni correction (e.g. $P = 0.017$ for each Wilcoxon matched pairs test following a statistically significant difference between 3 groups using a Friedman test). For multiple groups without repeated measures the Kruskal-Wallis ANOVA on ranks was used. *Post*

hoc analyses were performed using multiple pairwise Mann Whitney tests with Bonferroni correction.

Chapter 3. Temperature change and electrophysiological deactivation with cryoloop cooling

3.1 Introduction

The major problem that has been encountered by researchers attempting to investigate the role of the CoIC in auditory processing has been the development of a suitable methodology. Prior studies have either transected the CoIC in behavioural experiments (Moore *et al.*, 1974) or blocked glutamatergic transmission using pressure injection of kynurenic acid into one IC while recording single units in the contralateral IC (Malmierca *et al.*, 2003; Malmierca *et al.*, 2005). The first method is limited due to the technical challenge of the surgery, the uncertainty as to how complete and accurately placed the lesion until the tissue has been processed histologically, and the lack of reversibility of the experimental manipulation. The second method was informative but yielded a low number of tested units owing to the difficulty, because of mechanical disturbances, of holding a single unit during the injection of the drug (Malmierca *et al.*, 2005).

To assess the role of the CoIC in auditory processing a new method was required. This Chapter will report a series of experiments which tested the feasibility of using cryoloop cooling to induce deactivation of neural activity in one IC. The application of cooling for this purpose has been in use for over a century (see Brooks (1983)) and has been applied extensively in both electrophysiological and behavioural studies (Schiller and Malpeli, 1977; Sherk, 1978; Girard and Bullier, 1989; Michalski *et al.*, 1993; Lomber *et al.*, 1999; Antunes and Malmierca, 2011; Coomber *et al.*, 2011). This method has numerous advantages over drug injection, including rapid onset and recovery and no mechanical effects on the preparation.

An important question about the utility of the technique is the extent to which the cooling effect spreads through neural tissue, both from the perspective of ensuring that the tissue targeted for cooling has been fully deactivated, and that the distal recording site has not been functionally affected by spreading cold.

These issues have been addressed in earlier investigations in cat and primate models, but never in IC. Cooling has been applied to midbrain sites in only a few studies (Keating and Gooley, 1988; Lomber and Payne, 1996; Lomber *et al.*, 2001). In smaller animals such as guinea pig (Villa *et al.*, 1999; Nakamoto *et al.*, 2008; Coomber *et al.*, 2011) and rat (Kayama *et al.*, 1984; Yuan *et al.*, 1986; Villa *et al.*, 1999; Antunes and Malmierca, 2011) cooling has only been used to deactivate cortex. Because several factors determine the efficacy of cooling (the geometry of the tissue, the surface area to which the cryoloop is applied, the blood flow in the tissue, and the distance between the sites of cooling and recording) it is problematic to extrapolate the effects of cooling from one brain structure to another. The verification of the technique is therefore imperative.

In this Chapter, the hypothesis that cooling induced deactivation in guinea pig offers an effective means of deactivating one IC while leaving the other auditory nuclei uncooled was tested. Cryoloop cooling was hypothesised to produce temporary, spatially selective reversible deactivation of one IC. Experiments in this Chapter aimed to record the temperature changes imparted to the ascending auditory system by cooling one IC. This was hypothesised to reduce the temperature in that IC below that required to deactivate neural activity. The responses of single units were hypothesised to be reversibly suppressed by cooling. The cooling paradigm was hypothesised not to damage the cooled tissue. Finally, the contralateral IC and the ipsilateral AN, CN and cochlea were hypothesised to be unperturbed by the experimental manipulation.

3.2 Methods

The general methods, including the surgical preparation of the animal, and cooling deactivation are as described in Chapter 2. The details pertaining to the measurement of temperature in the IC and other structures, and the electrophysiological recordings presented in this Chapter are as follows:

3.2.1 Thermocouple measurements

To record temperature changes in the brain during cooling, both the temperature of the cryoloop and the temperature at a fixed point within the brain needed to be measured concurrently. To achieve this, a mini-hypodermic type-T thermocouple (outer diameter 0.2 mm) was secured to a microdrive in a dorso-ventral orientation and connected to a digital thermometer. The thermocouple tip attached to the cryoloop allowed constant monitoring of the external temperature imparted to the left IC. The needle thermocouple tip was then positioned at the desired location using the stereotaxic manipulator. All thermocouple penetrations were made in a dorso-ventral direction through the tissue. Temperature was measured once per second throughout all phases of a cooling cycle, each of which lasted approximately 20 minutes. Measurements were made in: 1) the left IC in contact with the cryoloop; 2) the contralateral (right) IC; 3) the left CN and left cochlea.

3.2.2 Electrophysiological recordings and analyses

Electrophysiological recordings were made from the left IC of 13 adult guinea pigs (\bar{x} weight = 765 g; IQR = 595 to 888 g). The first electrode penetration was made 10.5 mm posterior of bregma and 2.5 mm lateral of the midline. In most experiments, multiple electrode penetrations were made around this position. Single units and multi-unit clusters were classified using both FRA and PSTH analyses as described in Chapter 2. Single units were discriminated online by visualising the spike waveforms and setting a level discriminator.

Some units were recorded as the temperature was reduced in steps of 2 to 4 °C until the cryoloop temperature reached 5 ± 3 °C. Recordings were made at each cooling step until the responses of the unit decreased substantially from control, at which point cooling was stopped. This maximised the chances of achieving recovery responses from each unit.

Averaged local field potentials (LFPs) were also recorded in the IC contralateral to the cryoloop (Fig. 3.12) by low-pass filtering the recorded neural activity at 1 kHz and averaging 80 sweeps of the response.

3.3 Results

3.3.1 Cooling produced a thermal gradient around the cryoloop

Temperature measurements were first made in the IC in contact with the cryoloop to assess the extent of temperature change in the target nucleus of the cooling paradigm.

Temperature readings were taken from the IC in contact with the cryoloop and the ipsilateral DNLL. These measurements were made 10.8 mm posterior of bregma and 3.0 mm lateral of the midline at a depth of 4 mm from the dorsal surface of the IC. The location of the thermocouple tip within the DNLL was verified histologically by staining 50 μm coronal sections with Cresyl Violet.

With the cryoloop placed on the IC the cryoloop temperature was typically 33 to 34 $^{\circ}\text{C}$, a few degrees below the maintained core physiological temperature of 38 $^{\circ}\text{C}$. With the thermocouple tip in the DNLL, cooling was initiated and the cryoloop held at 5 ± 3 $^{\circ}\text{C}$. The temperature in the DNLL dropped from 35.0 $^{\circ}\text{C}$ to 30.4 $^{\circ}\text{C}$. The thermocouple was then drawn 2 mm up the track to a point midway along the dorso-ventral axis; the temperature in this position during cooling was 27.3 $^{\circ}\text{C}$. The thermocouple was then moved to the surface of the IC, approximately 1 mm caudal of the loop where the temperature was measured as 11.3 $^{\circ}\text{C}$. To determine the temperature change between the surface and 2 mm into the IC, the thermocouple was then placed 1 mm down the same track, where the temperature was 15.1 $^{\circ}\text{C}$.

A schematic coronal section showing these measurements is shown in figure 3.1A. Plotting tissue temperature during cooling as a function of depth from the surface of the IC showed a steep gradient of temperature change (Fig. 3.1B; dashed line, filled circles). The position along this track where the tissue was 20 $^{\circ}\text{C}$, the temperature at which cooling begins to deactivate neural responses (Brooks, 1983; Lomber *et al.*, 1999), was estimated to be 1.4 mm from the

surface and is indicated by the dashed lines either side of the thermocouple track (Fig. 3.1A).

This procedure was repeated in another experiment with the addition of a further thermocouple penetration 3.75 mm left of the midline. In both of these penetrations, measurements were made in 1 mm increments from the surface along the dorso-ventral axis to a depth of 4 mm. These measurements showed a shallower gradient of temperature change with depth from the surface (Fig. 3.1B; solid line, filled circles).

For comparison, the data plotted with solid lines and open circles show temperature measurements made in guinea pig auditory cortex replotted from Coomber *et al.* (2011). Temperature measurements in the IC distal to the cryoloop tip were higher than in cortex at both 1 and 2 mm from the surface in the first experiment but the data from the second experiment showed a high degree of overlap with the cortical values.

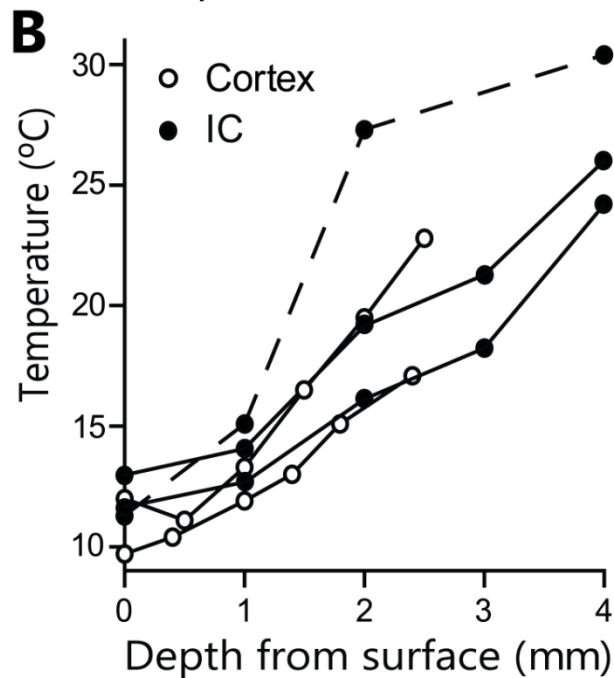
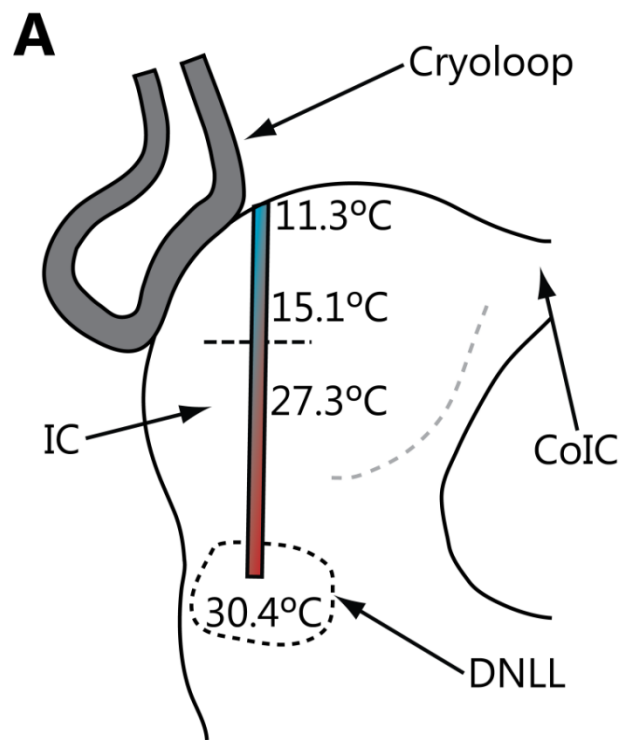


Figure 3.1 (A) Schematic coronal section through the IC showing placement of the cryoloop and temperatures measured in the IC with a needle thermocouple during cooling. A steep gradient was measured between depths of 1 and 2 mm. (B) Temperature measured in (A) (filled circles, dashed line) and the two other cases (filled circles, solid lines). Values plotted by open circles, and solid lines show equivalent temperature measurements made in guinea pig auditory cortex (replotted from Coomber *et al.* (2011) for comparison).

3.3.2 Cooling caused small temperature changes in the contralateral IC

The temperature in the IC contralateral to the cryoloop was assessed in four experiments. The thermocouple was placed in a mirror opposite position to that used the IC in contact with the cryoloop and 1 mm from the dorsal surface of the IC. The first experiment showed that when the cryoloop was cooled, the temperature in this location within the contralateral IC decreased from 34.9 °C to 30.7 °C. The second experiment found a decrease from 33.0 °C to 28.1 °C. The third of these experiments examined if there was an effect of cooling duration in this position within the contralateral IC to the cryoloop. Five cooling cycles of varying durations from 3 to 30 minutes were performed (Fig. 3.2A). Temperature drops ranged from a minimum of 3.7 °C after 3 minutes to 5.4 °C after 30 minutes of cooling. In a further experiment, measurements were made 1.5 mm and 3.0 mm lateral of the midline with reductions from 33 °C to 27.9 °C and 28.2 °C respectively. The minimum temperatures plotted against cooling cycle duration from all four experiments were best fit by a one phase exponential decay ($r^2 = 0.96$) as shown in Figure 3.2B.

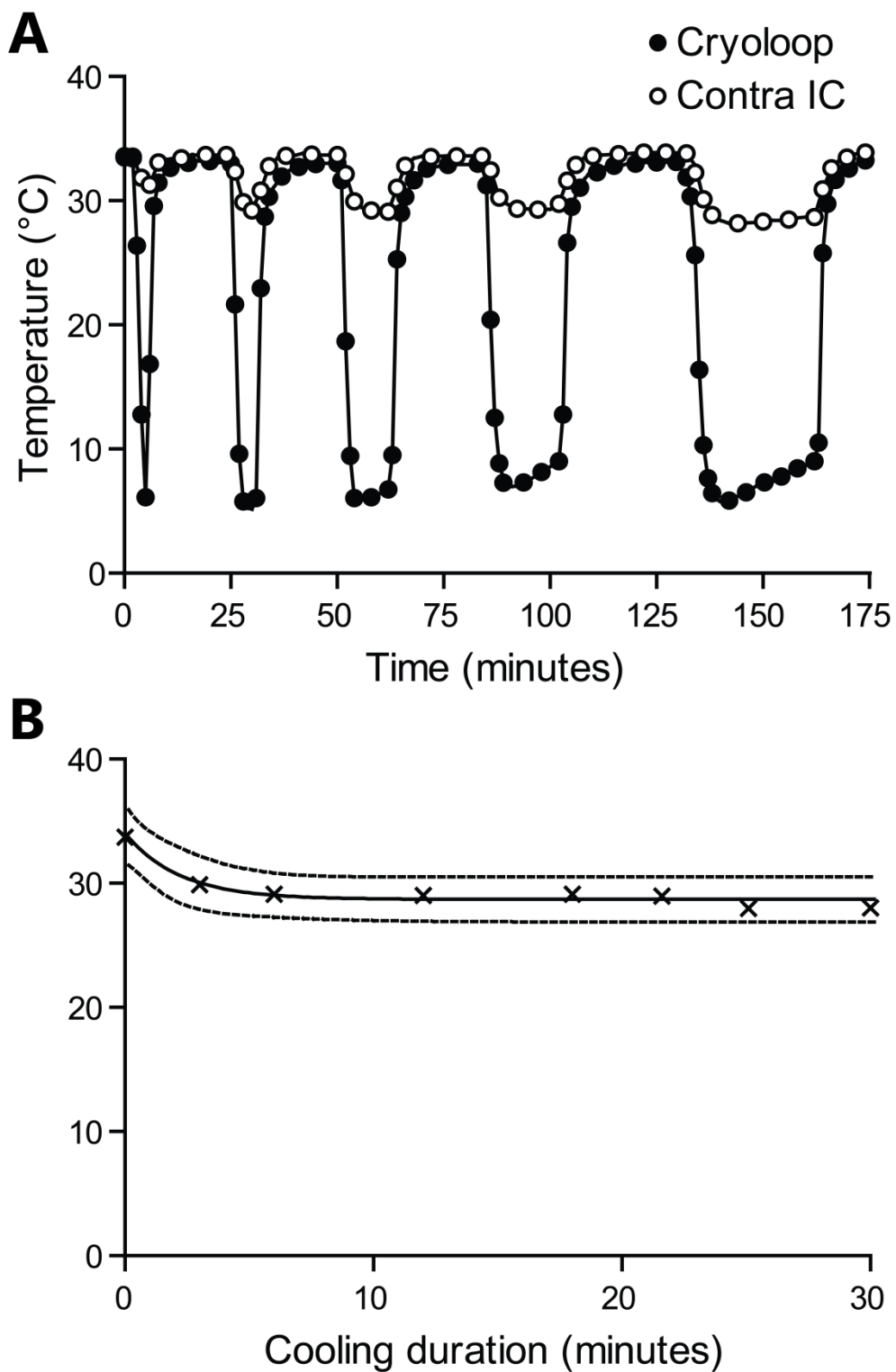


Figure 3.2 (A) Temperature of the cryoloop (filled circles) and at 1 mm into the contralateral IC (open circles) during repeated cycles of cooling of varying durations. Temperature in the contralateral IC fell a few degrees below control. (B) Temperature in the contralateral IC as a function of duration of cooling was stable for durations up to 30 minutes. A one phase exponential decay ($r^2 = 0.96$) and 95 % confidence limits show the plateau of temperature change.

3.3.3 Temperature changes across both ICs in the coronal plane

In a further experiment seven thermocouple penetrations were made through both ICs in the same coronal plane. Five penetrations were made in 0.75 mm steps from the midline through the IC contacted by the cryoloop. Two penetrations through the opposite IC were made at 1.5 and 3 mm from the midline. All penetrations were made during one cooling cycle. Four measurements were made at 1 mm increments up to 4 mm from the dorsal surface of the IC in each location. The thermocouple was given 30 seconds to equilibrate before it was moved to the next position in the each track. The average temperature change across three experiments with the needle thermocouple in similar positions are summarised in figure 3.3.

The effect of cooling was greatest in tracks adjacent to the cryoloop. In the IC contralateral to the cryoloop, the surface temperature was 27 and 28 °C at 1.5 and 3.0 mm from the midline respectively (Fig. 3.3). The dorso-ventral temperature gradient was also reduced in these tracks, with the temperature at the ventral-most points being 31 and 33 °C respectively.

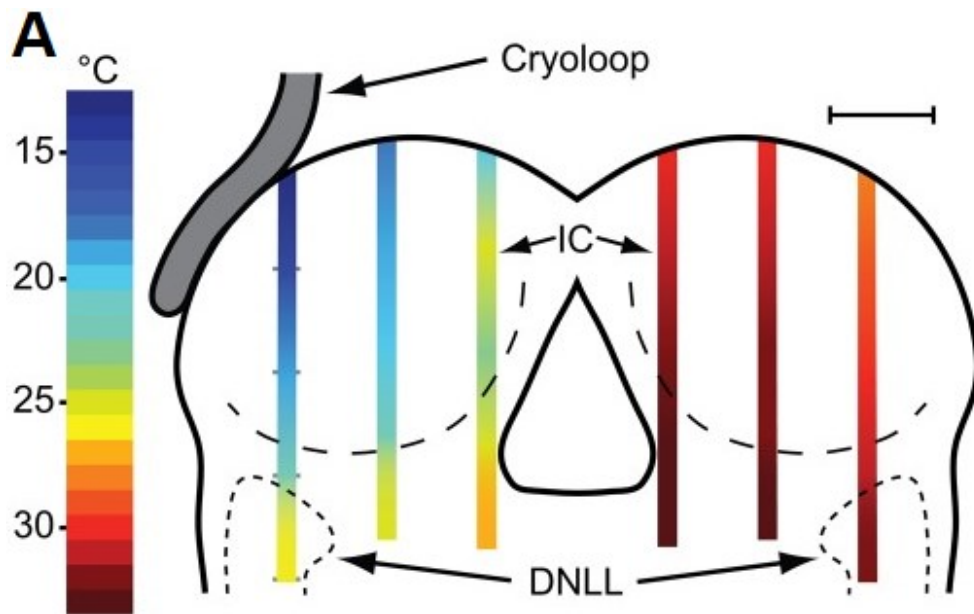


Figure 3.3 Schematic coronal section through the ICs showing placement of the cryoloop. Temperature measurements from thermocouple penetrations made with a needle thermocouple during a cooling cycle. Four points are plotted in each track at 1 mm increments. Each point is the mean temperature from 3 experiments in that location. Temperatures sufficient to deactivate neuronal firing *in vivo* were restricted to the area in the cooled IC adjacent to the cryoloop. Scale bar = 1mm.

3.3.4 The ipsilateral cochlea and cochlear nuclei were not cooled

In one experiment the temperature was measured in the CN during cooling of the ipsilateral IC to determine if cooling the IC lead to cooling of the CN – a source of both direct and indirect afferent input to the contralateral IC. The location of the CN was first identified by recording ipsilaterally driven auditory responses and the thermocouple was then positioned in the CN at the same location as the electrode. During 20 minutes of cooling the temperature of the CN never fell more than 2 °C below control (Fig. 3.4A).

Temperature was also measured throughout the course of a cooling cycle in the cochlea ipsilateral to cooling. These measurements were made from three different locations. In the first of these measurements (Fig. 3.4B) the thermocouple tip was placed in contact with the round window. A second set of measurements were made with the thermocouple tip in contact with the exterior surface of the first turn of the cochlea. A final set of measurements were made with the thermocouple tip placed inside the cochlea through a hole in the wall of the bony labyrinth. In all cases the maximum change in temperature recorded was 2.0 °C or less after 30 minutes of cooling.

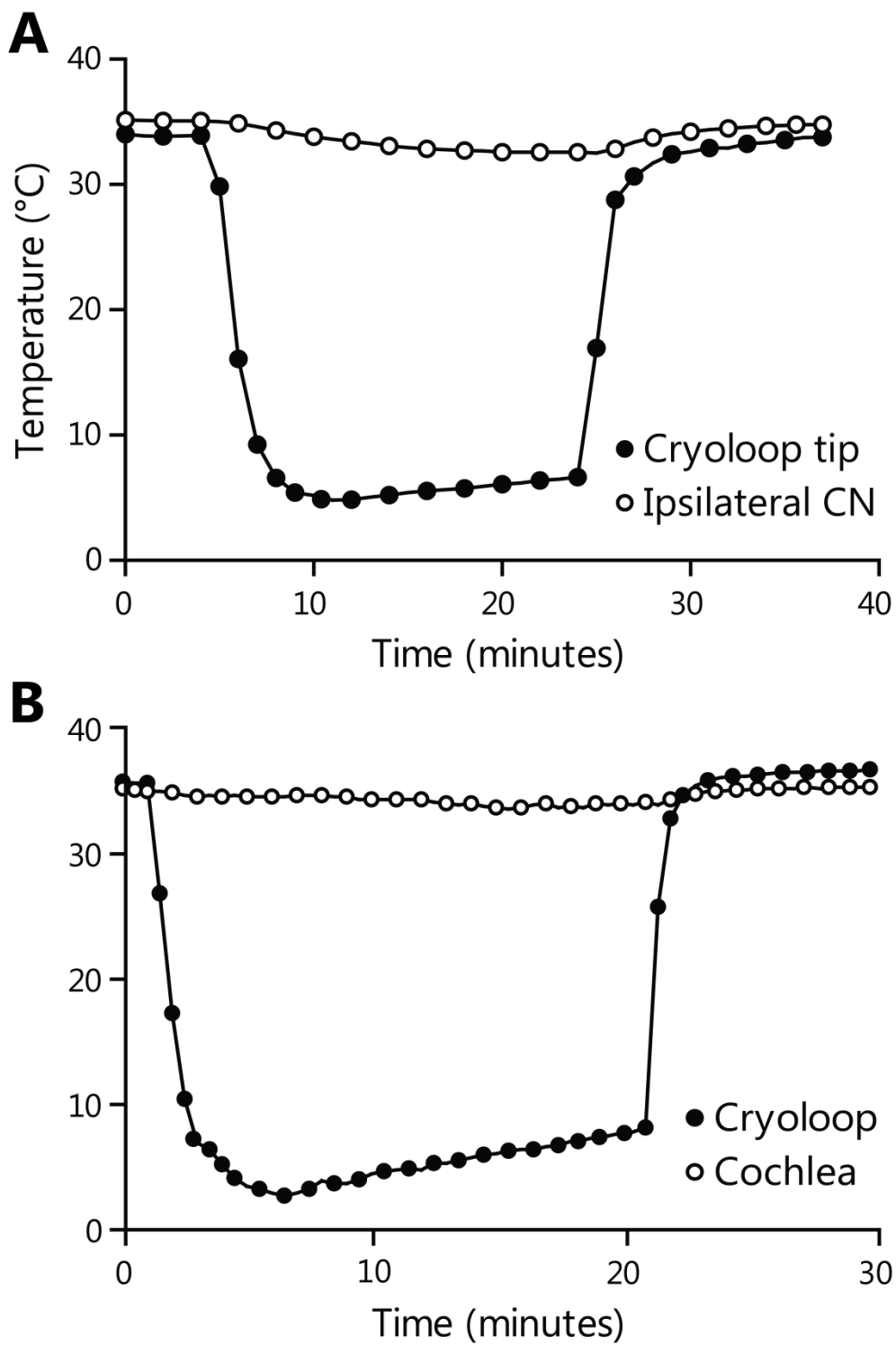


Figure 3.4 (A) Cooling resulted in a less than a 2 °C reduction in temperature in the CN ipsilateral to the cryoloop, and (B) the cochlea.

3.3.5 Neuronal deactivation in the cooled IC

The effect of cooling on sound driven neural activity in the cooled IC was assessed by recording single units and multi-unit clusters at different depths in the cooled IC across 11 experiments.

Recordings were completed from 33 single units and 9 multi-unit clusters. The responses to multiple repetitions of a pure tone 20 dB above threshold at CF were collected in each condition. To test for any significant change in firing rate the number of spikes evoked per stimulus in each condition was assessed with a Friedman omnibus test. Multiple *post hoc* Wilcoxon signed ranks tests were used to determine differences between pairs of conditions. In order to be included in these analyses control and recovery data had to show no significant difference ($P > 0.017$, following Bonferroni correction) in firing rate and the PSTH had to recover a similar pattern to that in the control condition. Of the single units 21 passed this criterion and are included here. The recovery firing rate of these single units ranged from 72.0 to 127.6 % of control ($\bar{x} = 95.2$ %; IQR = 88.8 to 100.6 %). Of the 9 multi-unit clusters, 7 passed the criteria for inclusion. Recovery firing rates of multi-unit clusters ranged from 71.5 to 121.3 % of control ($\bar{x} = 98.7$ %; IQR = 85.0 to 106.6 %).

To maximise the chances of achieving recovery recordings, some cooling cycles were terminated before reaching 5 ± 3 °C if a large decrease in firing rate was observed. This produced a range of minimum temperatures which were applied to the population of units included in the dataset. The lowest cryoloop tip temperature was 2 °C while the warmest maximal cooling temperature applied was 20.3 °C ($\bar{x} = 8.1$ °C).

3.3.6 Complete deactivation of a unit in the dorsal CNIC

Spiking was reduced by cryoloop cooling in the majority of units. Figure 3.5 shows the On-sustained responses (classified according to Rees et al., 1997) of a unit which was characterised as having a CF of 229 Hz. The neuron fired 338 times to 100 presentations of the stimulus (Fig. 3.5A – black line) producing a distribution of spikes per stimulus with a median of 4 with an IQR from 3 to 4 (Fig. 3.5B – left). Cooling the cryoloop resulted in the unit firing just 1 spike in response to 100 stimuli (Fig. 3.5A – blue line). During cooling the median, 25th and 75th quartiles of the distribution of firing rates were all 0 (Fig. 3.5B – middle). After cooling was stopped, the cryoloop recovered to control temperature (32.8 °C). On recovery the unit fired 325 times and the response regained an On-sustained morphology (Fig. 3.5A – grey line). The distribution of spikes per stimulus following recovery had a median of 4 with an IQR from 2 to 4 (Fig. 3.5B – right).

There was a significant difference in firing rates between conditions ($\chi^2(2) = 124.79, P < 0.001$). *Post hoc* tests found significant differences between control and cool ($Z = -8.31, P < 0.001$) and cool and recovery firing rates ($Z = -8.04, P < 0.001$). There was no significant difference between control and recovery firing rates ($Z = -0.24, P = 0.81$).

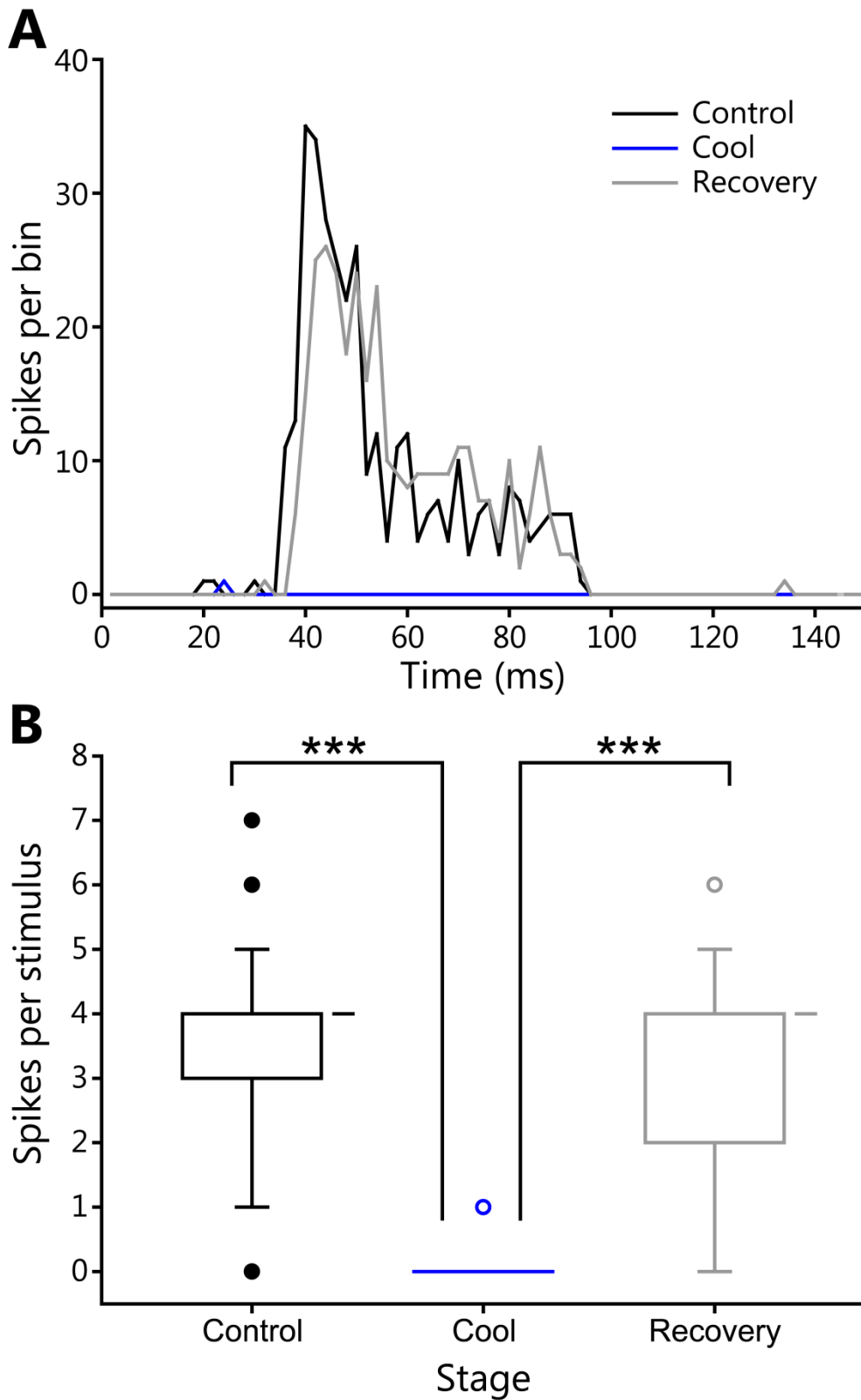


Figure 3.5 (A) PSTHs of a unit in the dorsal CNIC throughout a cooling cycle. Cryoloop cooling reversibly deactivated spiking. The unit recovered in both firing rate and PSTH morphology. (B) Cooling produced a significant decrease in firing rate. On recovery, the unit fired the same median spikes per stimulus as in the control condition.

3.3.7 Neuronal deactivation halfway down the tonotopic axis of the IC

The neuron in figure 3.6A was characterised in the control condition as having an On-sustained response morphology (fig. 3.6B) with a V shaped FRA (Fig. 3.6E). This neuron fired 753 times during in response to 100 presentations of the PSTH stimulus ($\bar{x} = 8$, IQR = 6 to 8). Cooling resulted in the number of spikes dropping to 103 ($\bar{x} = 1$, IQR = 0 to 2) with onset spikes accounting for the majority of these (Fig. 3.6C). Cooling was stopped at a cryoloop temperature of 14.3 °C as a large decrease in firing rate was observed. Cessation of cooling produced an immediate increase in spiking activity. When the temperature measured at the cryoloop tip returned to the control value (33.6 °C) the neuron produced 757 spikes in response to PSTH stimulation with the exact same median and IQR as in the control condition (Fig. 3.6D). In addition to the recovery of firing rate, the shape of the PSTH returned to an On-sustained morphology.

There was a statistically significant difference between the firing rates across the control, cool and recovery conditions ($\chi^2(2) = 150.34$, $P < 0.001$). *Post hoc* analysis found no significant difference between control and recovery firing rates ($Z = -0.38$, $P = 0.71$). There was a statistically significant difference between firing rate in control and cool ($Z = -8.61$, $P < 0.001$) and cool and recovery conditions ($Z = -8.61$, $P < 0.001$). As determined from the FRA, the CF was 2.1 kHz and the threshold was 75 dB attenuation (Fig. 3.6E). The unit had a Q_{10} of 3.40 and a Q_{40} of 1.00. Auditory evoked spikes were fired to 173 frequency-level combinations of the 936 presented. Cooling reduced the number of frequency-level combinations which elicited spikes dropped to 87 bins (Fig. 3.6F) and increased the Q_{10} to 4.38 and the Q_{40} to 1.44. Throughout all stages of cooling the threshold and CF were unchanged. Following recovery, the neuron regained tuning measures similar to those in the control condition. The FRA area increased to 182 bins (Fig. 3.6G). Q_{10} and Q_{40} fell to 3.40 and 1.19 respectively.

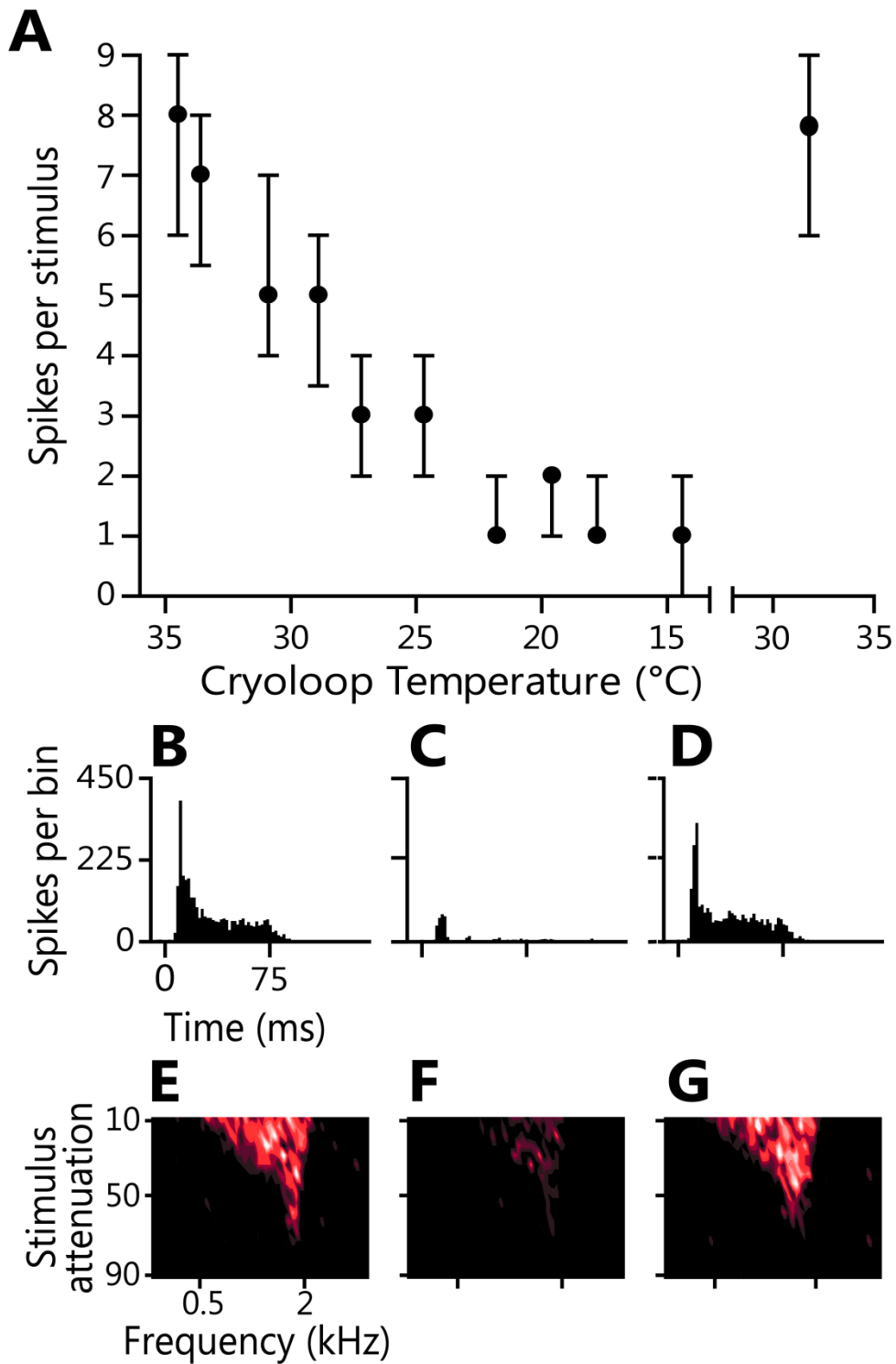


Figure 3.6 (A) Firing rate of a unit during stepwise cooling. The median number of spikes fired per stimulus decreased from 8 (IQR = 6 to 9) to 1 (IQR = 0 to 2). Following recovery median firing rate returned to 8 (IQR=6 to 9). The unit had an On-sustained PSTH (B) and a V-shaped FRA (E). During cooling only spikes near stimulus onset remained (C), but frequency tuning was retained (F). On recovery the unit regained its original PSTH shape (D) and firing rate across the FRA returned to control levels (G).

3.3.8 Cooling did not deactivate neurons in the ventral IC

The effect of cooling on the firing of units in the IC varied as a function of depth. Units located in the ventral regions of the IC (with CFs > 8 kHz) tended not to be deactivated as much by cooling. Figure 3.7 shows a unit which was characterised as having a CF of 13.8 kHz and an On-sustained PSTH response (Fig. 3.7A, black line). In the control condition the neuron fired 376 times to 60 presentations of a CF tone 20 dB above threshold ($\bar{x} = 6$; IQR = 4 to 8).

None of the PSTHs recorded throughout the 20 minute cooling cycle showed a significant deviation from control firing rate. The data in Fig. 3.7A, (blue line) are from the final PSTH before cooling was terminated during which the cryoloop was held at 3.4 °C. The unit fired 371 times to the stimulation paradigm during this recording. After the loop temperature recovered to 30.8 °C, the unit fired 354 spikes to the 60 presentations of the stimulus (Fig. 3.7A, grey trace). The median and IQR stayed the same through all three stages of the cooling cycle (Fig. 3.7B). There was no significant difference between firing rates in the three conditions ($\chi^2(2) = 1.82$, $P = 0.40$).

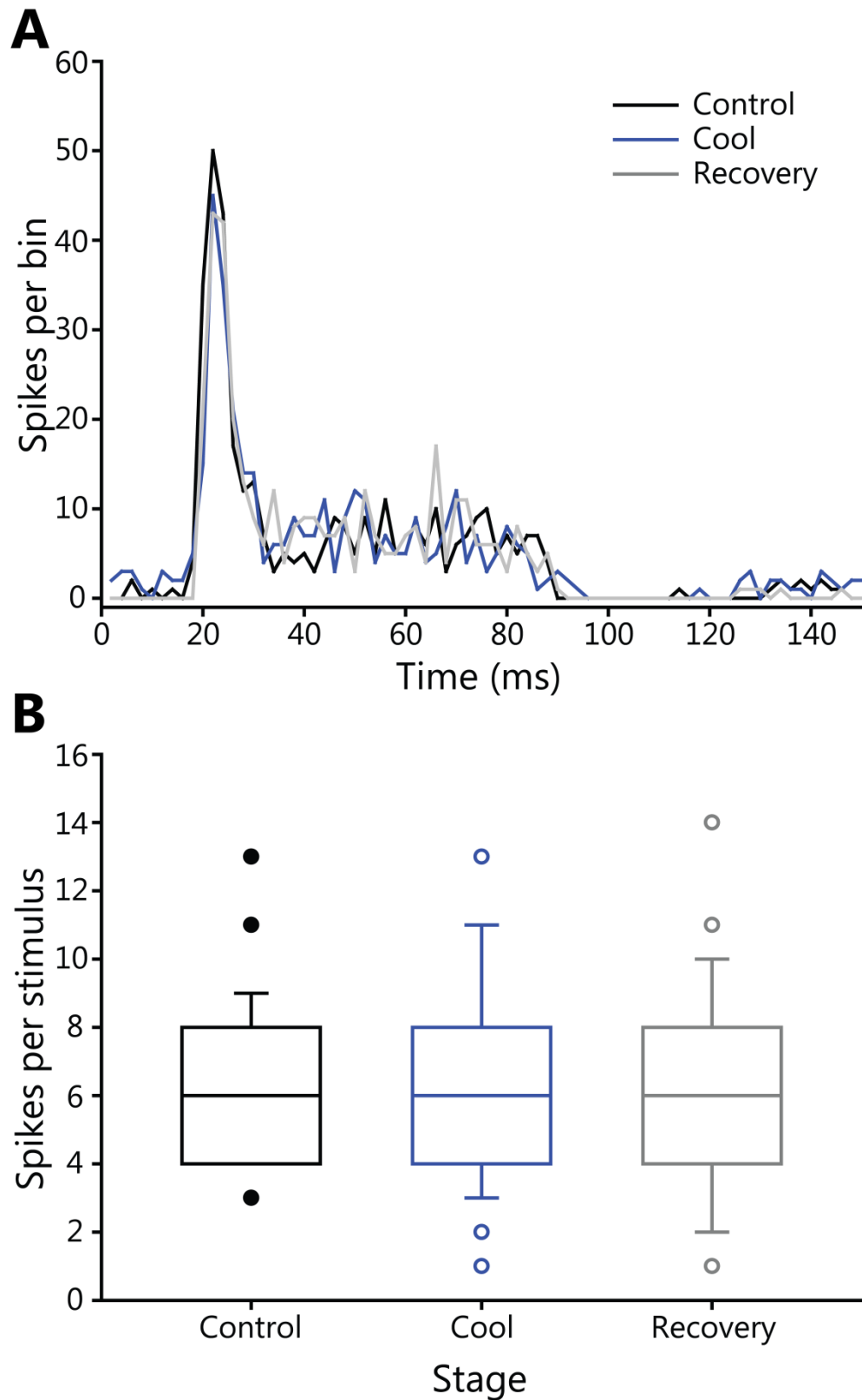


Figure 3.7 (A) PSTHs of a unit with a CF of 13.8 kHz. Spiking activity and PSTH shape were unchanged throughout all recordings. (B) The median and IQR were unchanged throughout all conditions. There was no significant difference between firing rates ($\chi^2(2) = 1.82$, $P = 0.40$).

3.3.9 Multi-unit responses to cooling matched those of single units

Multi-unit activity was recorded using the same procedure as for single unit recordings. The responses of multi-units were modulated by cooling in a similar manner to single units. Figure 3.8 shows four multi-unit clusters recorded at approximately 1 mm intervals along an electrode penetration through the IC. The deviations from 1 mm steps were to maximise the signal in each position.

All locations were recorded during cooling cycles with the cryoloop temperature held at 5 ± 3 °C. Cooling induced a gradient of neural deactivation along the track as measured by the response to contralateral stimulation (Fig. 3.8B). For the two most superficial positions firing rate was almost totally abolished by cooling. The recordings 2,210 μm from the surface reduced less in firing rate than the more superficial sites. At the ventral-most position there was a still smaller reduction in firing, although the morphology of the PSTH did change between the control and cooled conditions. There was a statistically significant difference in firing rate between conditions in the three dorsal-most positions (26 μm : $\chi^2(2) = 73.2$; 1,125 μm : $\chi^2(2) = 93.5$; 2,210 μm : $\chi^2(2) = 26.0$; all $P < 0.001$). *Post hoc* analysis in the dorsalmost position found a significant difference between control & cool ($Z = -8.04$, $P < 0.001$) and cool & recovery groups ($Z = -5.96$, $P < 0.001$), but not between control & recovery groups ($Z = -1.11$, $P = 0.27$). This pattern was repeated at 1,125 μm from the dorsal surface with significant differences between control & cool ($Z = -8.38$, $P < 0.001$) and cool & recovery groups ($Z = -7.53$, $P < 0.001$), but not between control & recovery groups ($Z = -1.74$, $P = 0.08$). In the third position the difference between control and cool firing rates was also significant ($Z = -5.02$, $P < 0.001$). The same was true of the cool and recovery groups ($Z = -5.12$, $P < 0.001$), with no significant difference between control and recovery responses ($Z = -1.91$, $P = 0.06$). There was no significant difference in firing rate between the three experimental conditions in the ventral-most position ($\chi^2(2) = 1.10$, $P = 0.58$).

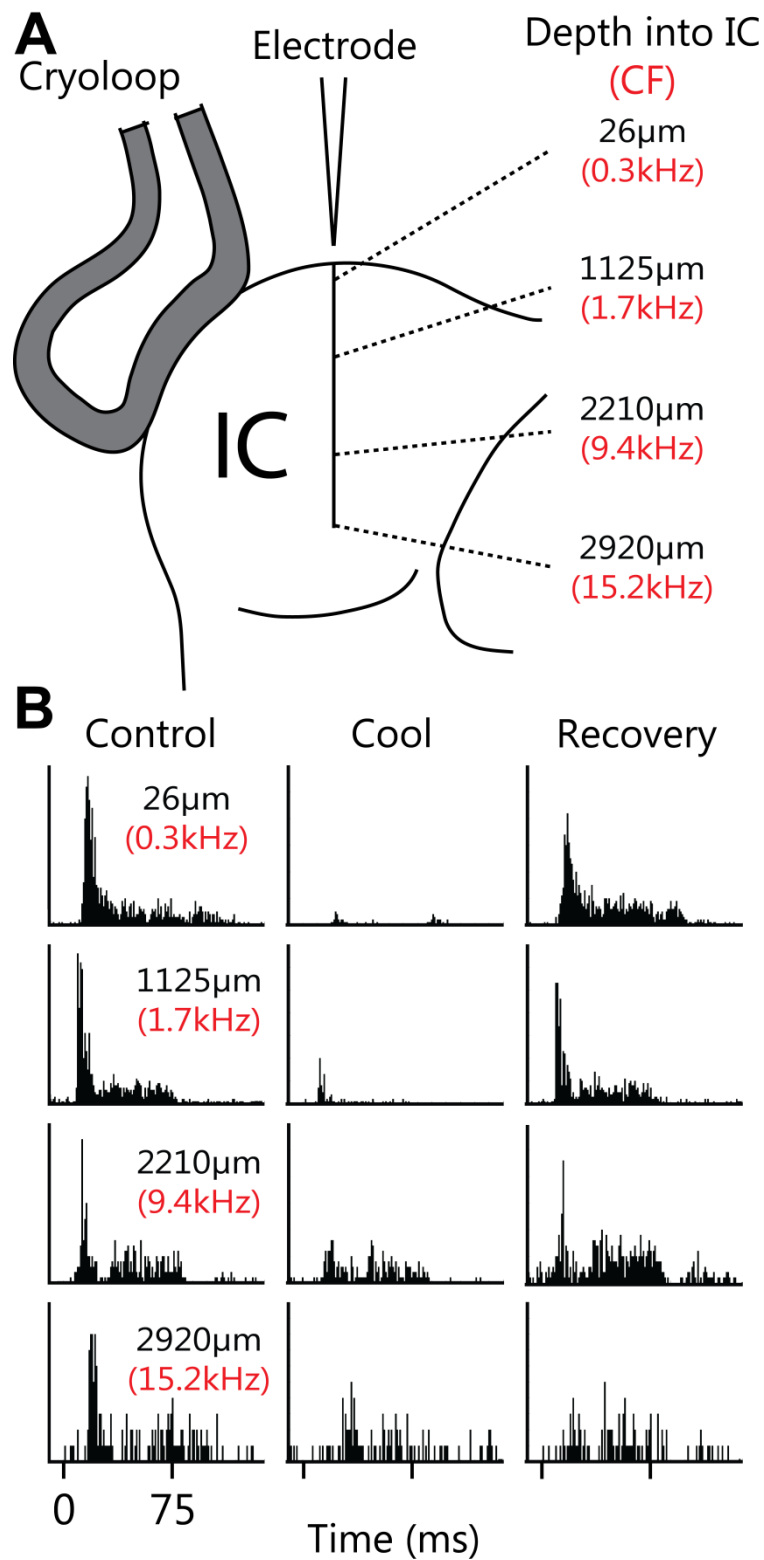


Figure 3.8 (A) Schematic representation of 4 multi-unit recordings made at ~ 1 mm steps along the dorso-ventral axis of the IC. (B) PSTHs recorded at the four locations shown in (A) during control, cool and recovery stages. Cooling resulted in a statistically significant reduction of spiking in the three most dorsal positions, but not in the deepest position.

3.3.10 Neural deactivation was restricted to the dorsal IC

Figure 3.9A shows the quotient of spikes fired in the cooled condition over the control condition plotted as a function of CF for all units which passed the criteria for inclusion. The quotient of change in firing rate during cooling was fit by a linear regression ($r^2 = 0.52$, $P < 0.001$). This fit indicates that cooling produced a 40 % or greater reduction in firing rate for locations representing CFs up to 8 kHz. No units with CFs higher than 8 kHz showed a reduction in firing rate greater than 60 %.

These data are summarised in figure 3.9B by binning the responses into groups spanning the CF range of the units. This plot confirms that cooling deactivated neural activity re control at CFs up to at least 8 kHz. For units with CFs above 8 kHz the reduction in firing rate during cooling was much lower. This graph also demonstrates the recovery of firing rate in those units included in these analyses.

FRAs were recorded in each stage for 14 of the single units which recovered from cooling. To assess if there was a change in the tuning of these units, CFs were compared across the population of cells between each condition. The median (control: 1.15; cool: 1.20; recovery; 1.30), and IQR (control: 0.53 to 2.00; cool: 0.55 to 2.00; recovery; 0.51 to 1.80). CFs of all units were similar in all conditions. No unit changed in CF by more than one bin in any stage for any unit. There was no significant difference in CFs between conditions ($\chi^2(2) = 0.88$, $P = 0.64$).

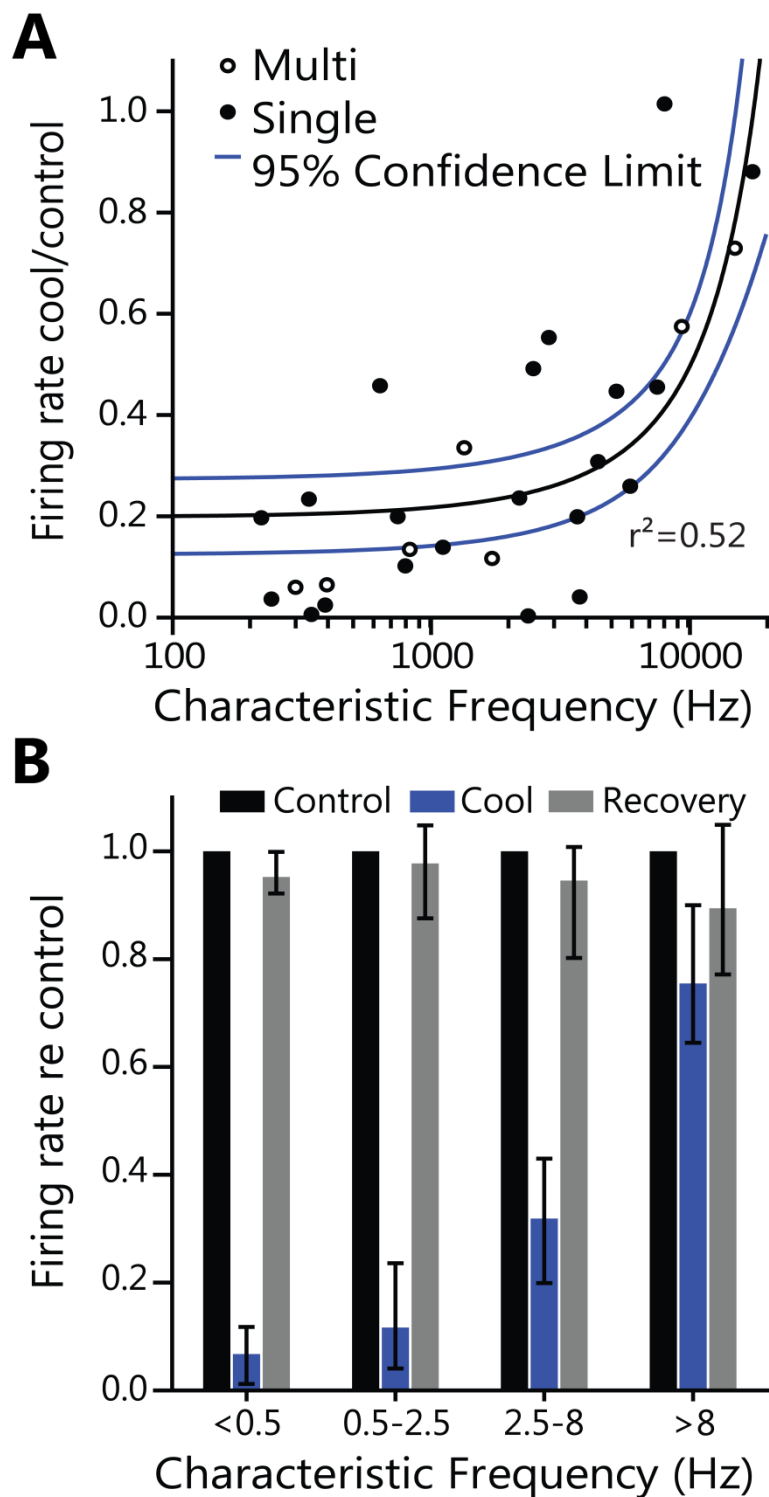


Figure 3.9 (A) Quotient of spikes fired in the cool and control conditions as a function of unit CF for all units. Reductions in firing were most evident in neurons with low CFs in the dorsal IC adjacent to the cryoloop. (B) Units with CFs < 8 kHz showed a statistically significant reductions in firing due to cooling. Units with CFs > 8 kHz showed no statistically significant reduction in firing during cooling. In all cases firing rates recovered close to control values on rewarming.

3.3.11 Histological analysis of cooled tissue

The integrity of the neural tissue was assessed by Nissl staining after repeated cooling cycles. Following six experiments in which one IC underwent multiple cooling cycles over the course of several hours and electrophysiological data were recorded, the animal was perfused, and 50 μm sections were cut through the midbrain and stained with cresyl violet to check for signs of cryogenic tissue damage. Figure 3.10A shows a coronal section midway through rostro-caudal axis of the IC. The cortex that normally overlies the left IC was aspirated during the initial preparation to allow placement of the cryoloop (top left). In this and all other cases, the shape and macro-structure of the IC appeared normal. There was some bleeding from the site of aspiration that formed small clots along the midline (black arrowhead) and at the ventro-lateral edges of the tectum lateral to each sagulum (red arrowheads). There were no blood clots on the surface of the IC at the point of contact with the cryoloop and no sign of vascular damage within the tissue.

A higher magnification (400X) image taken from the dorsal surface of the cooled IC in an area that was in contact with the cryoloop shows epithelial cells on the surface and neurons directly beneath (arrowheads) with normal morphology (Fig. 3.10B). Another 400X magnification image taken from the centre of the cooled IC (Fig. 3.10C) showed neurons with normal morphology and intact nucleoli (arrowheads). Comparison with sections from the uncooled IC showed no discernible qualitative differences between the macro- or micro-structure of the tissue.

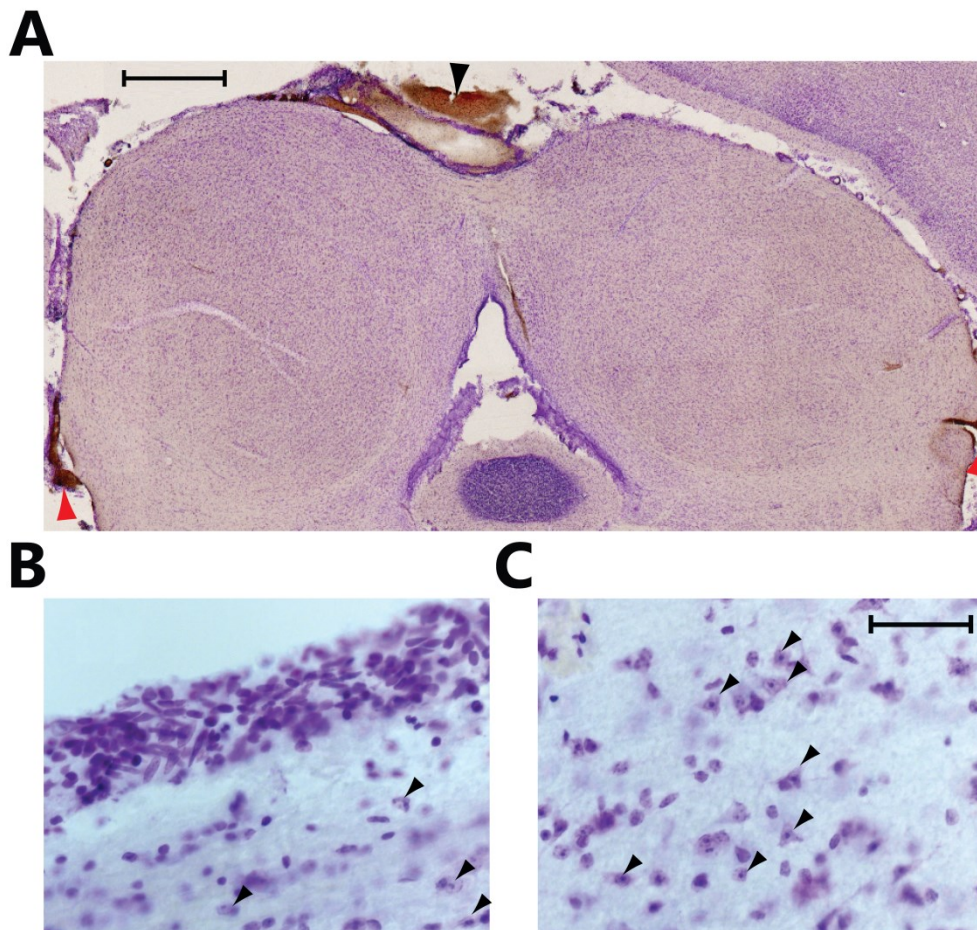


Figure 3.10 (A) Coronal section (10X objective photo-merge) through the IC following a cooling experiment in which the IC was cooled five times. Aspiration of the cortex overlying the left IC and placement of the cryoloop did not produce any noticeable trauma to the tissue. Blood clots at the midline (black arrowhead) and bilaterally at the ventro-lateral edges of the tectum (red arrowheads) resulted from aspiration of the cortex. Scale bar = 1 mm. (B) Neurons near the dorsal surface of the IC contacted by the cryoloop showed no sign of damage. (C) Neurons within the cooled IC had normal morphology and no signs of ischemic damage were present. 40X objective in B and C. Scale bar = 50 μ m (also applies to B).

3.3.12 Moderate cooling occasionally induced neuronal hyperactivity

While cooling produced a reliable and repeatable deactivation in neurons in the dorsal IC, it was observed that during initial stepwise cooling, some neurons showed an increase in firing rate before becoming deactivated as cooling progressed.

Figure 3.11A shows PSTHs of a unit which had a CF of 1.3 kHz and a Pauser response type. The unit was subjected to two cooling steps with the cryoloop held first at 16 °C and then 8 °C. PSTHs were recorded at each stage. There was a significant difference in firing rate across groups ($\chi^2(3) = 96.2, P < 0.001$). Cooling the cryoloop to 16 °C produced a significant ($Z = -4.8, P < 0.001$) increase in firing rate from 142 ($\tilde{x} = 1, \text{IQR} = 0 \text{ to } 2$) to 251 spikes ($\tilde{x} = 2, \text{IQR} = 2 \text{ to } 3$). Qualitative inspection of this change showed an increase in both onset and sustained components of the response (Fig. 3.11B).

As shown in figure 3.11C & E, cooling the cryoloop to 8 °C reduced firing to 64 spikes ($\tilde{x} = 0, \text{IQR} = 0 \text{ to } 1$) - a statistically significant reduction compared to both control firing rate ($Z = -4.9, P < 0.001$) and with the cryoloop held at 16 °C ($Z = -7.8, P < 0.001$). Cooling was discontinued at this point and the firing rate recovered to 156 spikes ($\tilde{x} = 1, \text{IQR} = 1 \text{ to } 2$) which was not significantly different from the control group ($Z = -5.7, P = 0.52$). Of the 18 single units which were cooled in a stepwise manner, five significantly increased in firing rate (all $P < 0.001$) at one point in the cooling cycle.

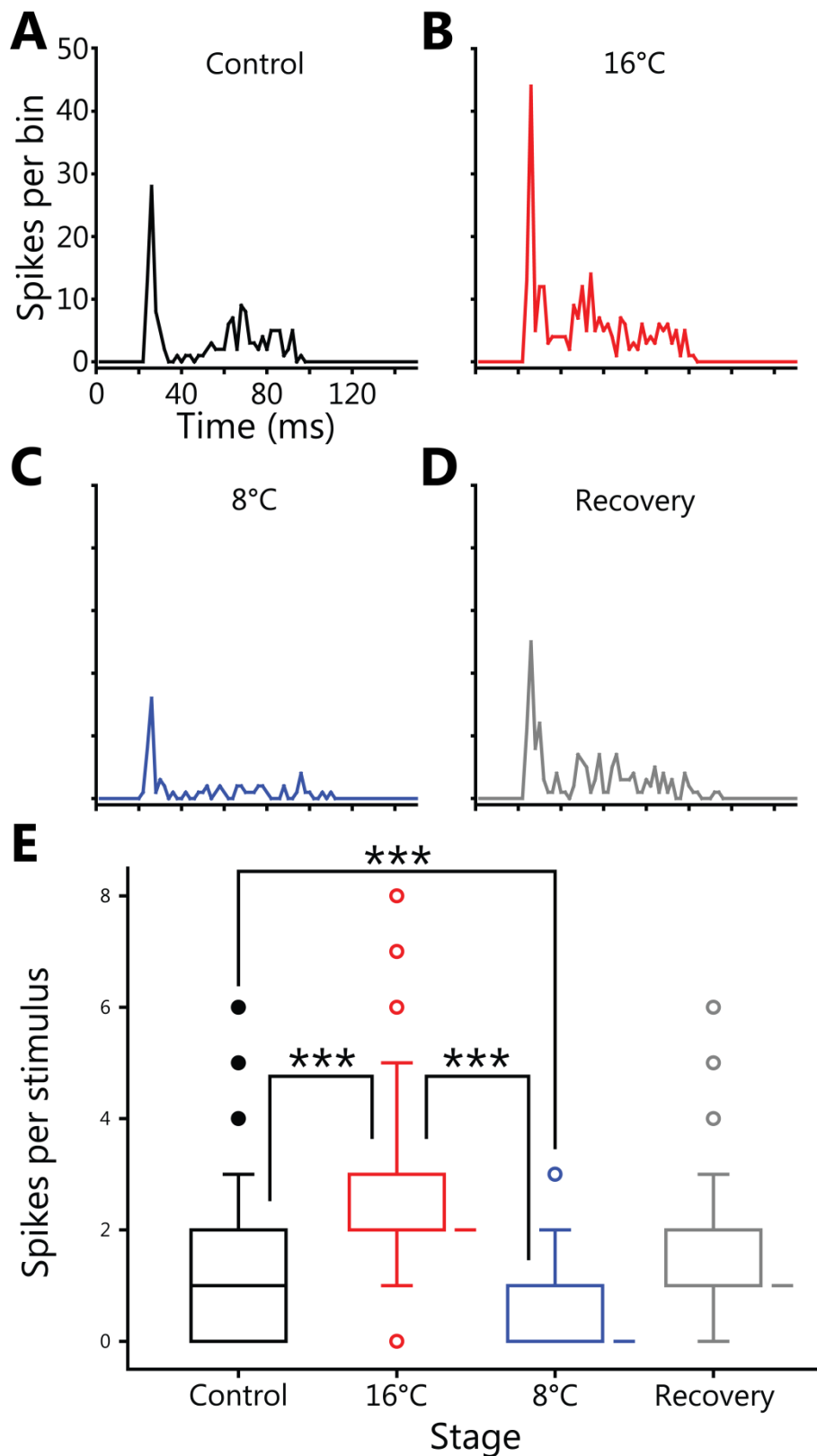


Figure 3.11 (A) Pauser PSTH of a unit with a CF of 1.3 kHz. (B) Firing rate increased when the loop was cooled to 16 °C. (C) Further cooling to 8 °C caused a decrease in firing rate (D) which recovered upon recovery. (E) Both changes during cooling were significantly different from control.

3.3.13 Differential modulation of LFP components in the IC contralateral to cooling

To produce a viable model by which intercollicular projections can be reversibly deactivated, cooling also had to leave afferent input to the contralateral IC unaffected. To this end, the impact of cooling the left IC on LFPs recorded in the right IC was investigated. Figure 3.12 shows examples of LFPs recorded from the right IC before, during and after cooling of the left IC in response to three stimulus conditions: contralateral stimulation; ipsilateral stimulation and binaural diotic stimulation (Fig. 3.12A, B, & C respectively). In the case of contralateral and binaural stimulation there was a pronounced negative component with a post stimulus latency of 6 ms that corresponded to the afferent volley. This was followed by a biphasic waveform that returned to baseline at around 30 ms post stimulus onset. The afferent volley was less pronounced in the case of the response to ipsilateral stimulation.

When the left IC was cooled, the magnitude and latency of the afferent volley was unchanged irrespective of stimulation source, but there were clear changes in the later potentials. The form and extent of the changes varied between the different stimulus conditions. In the case of contralateral stimulation the largest change occurred in the first negative-going potential whereas with diotic stimulation the largest difference between cool and control was in the positive-going potential at ~17 ms. With ipsilateral stimulation the single broad positive waveform reduced in height and became broader.

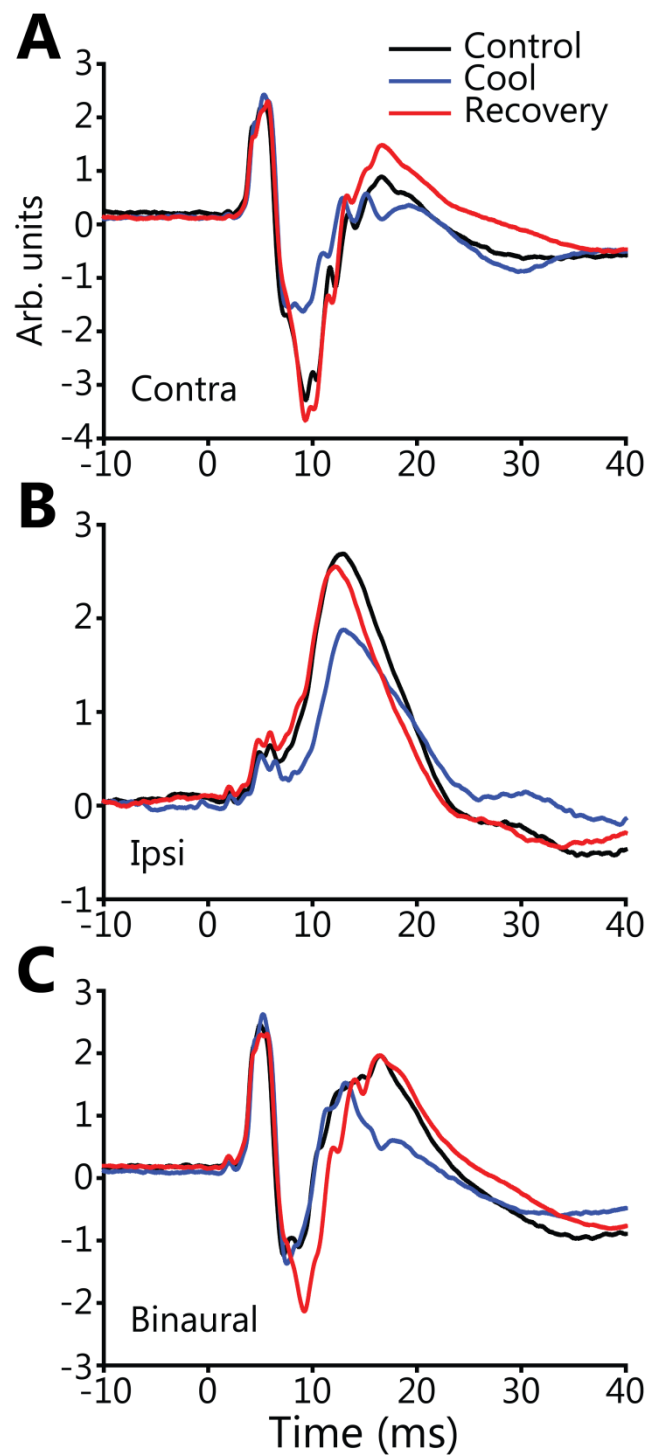


Figure 3.12 LFPs recorded in the IC contralateral to cooling in response to 1 ms duration, 10 kHz tone pulses presented to (A) the ear contralateral to the recorded IC, (B) the ipsilateral ear and (C) both ears. Responses are shown for control (black), cool (blue) and recovery (red) phases in the contralateral IC. Note that the initial peak in all panels was barely changed by contralateral IC cooling while the later peaks were reversibly modulated.

3.4 Discussion

Cooling has been demonstrated to be an effective means of deactivating areas of brain tissue in many studies utilising behavioural or electrophysiological means (Brooks, 1983; Lomber *et al.*, 1999; Antunes and Malmierca, 2011; Coomber *et al.*, 2011). It is essential that the application of the technique be validated in each situation to which it is applied. This is due to the potentially confounding effects of direct cooling spreading to other areas in the network and thus not providing a spatially selective deactivation of the target of cooling.

The most important considerations are first, that cooling deactivates the targeted area in a reversible manner, and second, that the cooling induced deactivation is restricted so that it does not impact on other nuclei. Only by establishing the selective and reversible deactivation of the targeted nucleus can strong inferences be made about the observed results imparted by the experimental paradigm. The aim of the experiments reported in this Chapter was to establish the utility of cooling as a method for discovering how one IC is influenced by the other. If the technique could be demonstrated to be viable in the anaesthetised guinea pig it would confer considerable advantages over the drug injection techniques used previously (Malmierca *et al.*, 2003; Malmierca *et al.*, 2005). The data presented show that cooling does fulfil all requirements to be used for this purpose.

Cooling deactivation has been applied to the AC of rat, cat and guinea pig to study its interactions with the medial geniculate body (MGB) and the IC (Villa *et al.*, 1991; Lomber *et al.*, 2007a; Nakamoto *et al.*, 2008; Nakamoto *et al.*, 2010; Coomber *et al.*, 2011). Cooling has not previously been applied directly to the IC. The only other reports of its application in the midbrain investigated the function of the superior colliculus in cat and macaque where brain size is larger than in guinea pig (Keating and Gooley, 1988; Lomber and Payne, 1996; Lomber *et al.*, 2007b). In these studies the effect of deactivation was tested in

behavioural assays rather than on measures of neuronal function. The paucity of directly applicable previous data led to the control experiments reported in this Chapter.

3.4.1 Restricted cooling efficacy matches previous data

The spread of cooling in the IC (Fig. 3.1 and Fig. 3.3) was similar to the 2 mm depth of deactivation reported when cryoloops were placed on the surface of the cerebral cortex in cat and guinea pig (Girard and Bullier, 1989; Lomber *et al.*, 1999; Girardin and Martin, 2009; Coomber *et al.*, 2011). Cooling was not homogenous throughout the IC. A temperature gradient extended along the dorsal to ventral axis of the IC (Fig. 3.3) corresponding to its well-established tonotopic gradient (Rose *et al.*, 1963; Merzenich and Reid, 1974; Semple and Aitkin, 1979; Malmierca *et al.*, 1995).

One might expect cooling to be more efficient in the IC since, in contrast to the flat surface of the cortex in guinea pig, the exposed IC protrudes from the surrounding brainstem tissue, making a large portion of its surface area accessible. A factor that might reduce the cooling effect in the IC is its high blood flow. The IC is highly vascular and demonstrates one of the highest blood flows of all brain regions (Reivich *et al.*, 1969; Gross *et al.*, 1987; Song *et al.*, 2011). High blood flow may warm the IC and so counteract the cooling effect. The vascularisation of the IC is known to be non-isotropic (Gross *et al.*, 1987; Dorr *et al.*, 2007; Song *et al.*, 2011), but to what extent that could exert an influence on the spread of cooling is beyond the scope of this thesis.

The different rates of temperature change along the dorso-ventral axis in figure 3.1B may be explained by the difference in animal size between experiments. Experiment 8032, which is summarised in figure 3.1A and shown as the dashed line in figure 3.1B was conducted with a 940 g guinea pig. Experiment 8056 shown in figure 3.1B as the filled circles with the solid connecting lines, was

conducted in an animal that weighed 765 g. While both animals were adult at the time of experimentation, the data from experiment 8056 appears to qualitatively correlate closely with the data from the guinea pig auditory cortex from Coomber *et al.* (2011). The two animals used to acquire those data weighed 708 g and 716 g. While the close match between these data may be coincidental, it is plausible that the change in weight with maturity of the guinea pig coincided with an increase in brain volume and/or vascularity which may account for this variability. However, there are numerous other factors which may have influenced the results such as the room temperature, the size and extent of contact of the cryoloop with the target nucleus. As such, these parallels are drawn with this reservation.

3.4.2 Cooling did not deactivate other nuclei in the auditory system

A second key factor in determining the utility of cooling for deactivating the IC is the extent to which deactivation is limited to the cooled IC. The DNLL lies immediately below the IC, but our temperature measurements suggest that the ventral part of the IC was not cooled sufficiently to affect neural function and nor was the DNLL below it (Fig. 3.3). The latter finding is important since the DNLL sends crossed connections to the contralateral DNLL and the IC. The measurements made in the DNLL are restricted to a few experiments in which the temperature was recorded throughout. Further repeats of these measurements may strengthen the claim that the DNLL was unchanged throughout cooling.

The data show that cooling the left IC did produce a small fall in temperature on the contralateral side (Fig. 3.2 and Fig. 3.3), but never more than 5 °C below control even after a prolonged cooling cycle of 30 minutes duration. Furthermore, these measurements probably overestimate the reduction in temperature. To place the thermocouple in the correct position for these measurements the overlying cortex was aspirated. This in itself produced a fall

in temperature of a few degrees. Even under these conditions the temperature of the contralateral IC during cooling was close to 30 °C. The cortex was always in place during single unit recordings in the contralateral IC (see Chapters 4, 5 and 6). Thus it is likely that the temperature of the contralateral IC would be a few degrees higher than measured when the overlying cortex was intact.

In a previous study where cooling was used to deactivate auditory cortex in guinea pig it was thought that perfusion of cooled blood from the cortex resulted in a temperature reduction of the cochlea by about 4 °C on the side ipsilateral to the cooled cortex (Coomber *et al.*, 2011). In contrast to these findings, cooling the IC lead to a minimal effect on the cochlea and CN, with the temperature reduced by 2 °C or less from control. This difference may be due to the different shapes and vasculature in IC and cortex leading to a reduction in cooled blood passing the vicinity of the cochlea, and the lower cooling temperatures (2 ± 1 °C) applied in the cortical study than employed in this study (5 ± 3 °C). The experiments undertaken in this study aimed to keep cooling cycles as brief as possible and most cooling cycles were less than 20 minutes in duration. This may be one possible difference between the experimental protocols employed here and by Coomber *et al.* (2011) and thus the data derived from each may not be directly comparable.

3.4.3 Cooling deactivated the dorsal IC

Spiking activity was reversibly deactivated in the dorsal half of the IC by cooling and returned to control values within a few minutes of its termination (Fig. 3.8). Cooling deactivated neurons with CFs up to ~8 kHz (Fig. 3.9). Although firing rates were significantly reduced by cooling, it was typical that neurons retained tuning characteristics similar to control, with CF unchanged (Fig. 3.6E-G). A similar reduction in firing or synaptic potential, with retention of stimulus selectivity has been observed for orientation tuning of neurons in visual cortex in cat (Michalski *et al.*, 1993; Ferster *et al.*, 1996; Girardin and Martin, 2009).

Biophysical studies of the effects of cooling on neuronal responses have mainly been performed *in vitro*. Temperature modulates the responsiveness of neurons *in vitro* in several ways, including reducing synaptic efficacy by reducing the probability of transmitter release, and by differential effects on the operation of sodium and potassium ion channels (Hardingham and Larkman, 1998; Volgushev *et al.*, 2000a; Volgushev *et al.*, 2000b; Trevelyan and Jack, 2002; Cao and Oertel, 2005). At temperatures where neurons become deactivated *in vitro* (~10 °C), firing may still occur if the stimulus is sufficiently strong (Volgushev *et al.*, 2000b). Such effects are consistent with the observation that spikes can occur even at very low temperature and the frequency selectivity of afferent input to IC neurons was unchanged. While *in vitro* studies have proved useful in elucidating the effects of cooling on the responses of channels and conductances, such studies do not necessarily reflect all the changes that occur in an intact animal since these preparations do not maintain the natural blood, oxygen and nutrient flow of the *in vivo* preparation. Cooling most likely causes dramatic changes in the blood flow to neurons and this may account for why neurons which have been observed to spike in a bath temperature of 7 °C *in vitro* (Volgushev *et al.*, 2000b) have not been reported *in vivo*.

3.4.4 Cooling did not damage tissue

As reported by others, there was no anatomical evidence of damage to the brain by cooling (Keating and Gooley, 1988; Lomber *et al.*, 1999; Yang *et al.*, 2006; Girardin and Martin, 2009), even after the IC had been exposed to multiple cooling cycles (Fig. 3.10). Cells were intact after histological processing, and there was no qualitative difference between ICs. It has been shown in cat, dog and cow that even brief cooling to 0 °C produces a permanent lesion (Miyazaki *et al.*, 1963). In the current experiments, the cryoloop temperature was never allowed to fall below 2 °C and the majority of cooling cycles did not drop below 5 °C.

It is remarkable that the brain has such resistance to temperatures that are far below those to which it would be exposed in any physiological situation. In the periphery the wide range of temperatures to which mammals have been exposed throughout evolution would have selected for the exquisite array of compensatory mechanisms found in the skin. Due to the demand for homeostatic maintenance of temperature in the brain, it is not surprising that changes of temperature can also be compensated for. That focal reductions in temperature of ~30 °C below control did not cause any noticeable ischemia or cell death is remarkable. Quite how this is achieved is not clear, but it is highly fortuitous for neurophysiologists.

3.4.5 Moderate cooling induced increases in firing rate

Due to the stepwise cooling paradigm employed in the recording of many neurons, it was possible to observe dramatic changes in firing rates in response to moderate changes in temperature. It was observed that 10 units which were subjected to stepwise cooling increased in firing rate during one of the first stages of cooling; 5 of which were statistically significantly higher than controls. Three of the 7 units which decreased during moderate cooling were statistically significantly lower than controls.

Raised neuronal firing rates due to moderate cooling have been noted previously both *in vivo* and *in vitro* and in many nuclei (Brooks, 1983; Volgushev *et al.*, 2000b). These authors differ in their reports of the temperatures at which this phenomenon occurs, with Brooks claiming a range of 30 to 25 °C in the spinal cord of cat, while Volgushev *et al.*, reported an enhancement of repetitive firing in a subpopulation of their sample (7/32) in the visual cortex of the rat in the range of 24 to 18 °C. Volgushev *et al.* showed that this hyperexcitability was caused by a decrease in K⁺ conductance which increased the input resistance and depolarised neuronal membranes which in turn lead to neurons being closer to threshold. In an elegant study, Cao and Oertel (2005) investigated the

effect of changing bath temperature from 33 to 23 °C on the amplitude and kinetics of the low-voltage-activated K⁺ current (I_{KL}) and the DTX-insensitive, high-voltage-activated K⁺ current (I_{KH}) in Octopus cells of the CN in rat. The lower temperature did not alter the amplitude of I_{KH} but did reduce the amplitude of I_{KL} , suggesting that this temperature sensitive current might be the cause of cooling induced hyperexcitability. While these studies were conducted in different model species and different nuclei, the ubiquity with which these channels are expressed support the notion that these biophysical changes may be conserved in IC.

Evidence in support of the temperature range of 30 to 25 °C being the temperature range at which hyperexcitability occurs comes from intracellular recordings in the pericruciate cortex of the cat (Reynolds Jr *et al.*, 1975). Cooling the cortex to 30 °C using a Peltier device produced increases in membrane resistance, the duration of action potentials and spontaneous firing. While these factors all peaked at 27 °C, the authors did not cool to lower temperatures so direct comparison with the Volgushev *et al.* or Cao and Oertel data is not possible. The discovery that spikes are broader at 23 °C than at 27 °C, coupled with the decrease in I_{KL} from 27 °C to 23 °C discovered by Cao and Oertel (2005), suggests that the lower of the two postulated temperature ranges may be more accurate.

One further observation in the present study was the presence of three neurons which were strongly deactivated at cryoloop temperatures of 22, 23 and 25 °C. Being unaware of any reports of neuronal deactivation at these temperatures, this finding appears to be novel. This finding also seems to be contrary to all previously reported investigations into the nature of cooling. As there appears to be no plausible biophysical explanation for this effect, it is possible that these neurons may be involved in an intracollicular circuit in which they received an inhibitory input from one or more neurons that became hyperactive during

moderate cooling which in turn led to a reduction in their firing. An alternative possibility is that these channels may have expressed a channel which is temperature sensitive and shut down at moderate temperature reductions.

3.4.6 Changes in LFPs in the IC contralateral to cooling suggest a commissural selective deactivation

Given the extensive commissural fibres that interconnect the two ICs, blockade of these connections seems the most likely explanation for the changes we observed in the contralateral IC during cooling of the other IC. However, an alternative mode of influence that could, at least in part, account for the effects induced by IC cooling on the responses of single units in the contralateral IC (reported in Chapters 4, 5 & 6) is the modulation of descending activity from the IC since the neurons giving rise to these fibres will also be deactivated by cooling. In guinea pig, the IC sends descending projections to several brainstem centres, both ipsi- and contra-laterally (Malmierca *et al.*, 1996; Schofield, 2001; Schofield, 2010). Could the removal of descending input to these centres by cooling one IC lead to the changes in neural activity observed in the contralateral IC? Although this cannot be ruled out, evidence from LFPs suggests otherwise (Fig. 3.12). The first prominent peak in the LFP (particularly evident in responses to diotic stimuli or to stimuli applied to the ear contralateral to the recorded colliculus) had a latency of 6 ms. This latency also corresponds to previous measurements of P5 latency in the auditory brainstem response of guinea pig, and to responses recorded intracollicularly (Dum *et al.*, 1981; Harrison and Palmer, 1984). The first peak in the LFP corresponds to the latency of the incoming afferent volley to the IC or to the synaptic potentials that it generates (Szczepaniak and Møller, 1993). This short latency peak was minimally changed by cooling the contralateral IC, both in terms of its amplitude and its latency. In contrast, the later waves in the LFP, which reflect the activity of intracollicular processing (Szczepaniak and Møller, 1993), showed

marked changes in morphology and latency with cooling. These changes could therefore represent the modulation of a commissurally-mediated influence over processing within the IC. It could be argued that the LFP is not sufficiently sensitive to reflect the effect of descending control mediated by the IC, so the conservative position is to assume that the effects of cooling one IC on the other are mediated by more than one pathway. This limitation applies to any method of deactivating the IC. It seems likely that different populations of neurons in the IC give rise to descending and commissural projections (Okoyama *et al.*, 2006), so techniques such as optogenetics could be developed to enable selective deactivation of the descending and commissural systems and sidestep this issue.

A further route whereby deactivation of one IC could affect the other is via a cortico-thalamic loop. Tracer studies show that the commissure contains some fibres that project from the IC to the contralateral auditory thalamus (Aitkin and Phillips, 1984) and there are descending connections from the contralateral cortex to the IC that probably involve the commissure (Winer *et al.*, 2002; Bajo and Moore, 2005; Bajo *et al.*, 2007). Deactivation of the IC would partially remove the drive to these centres and could, therefore, reduce the influence of their descending input to the contralateral IC. The contribution of these components to the commissure is, however, relatively small. Furthermore, these fibres terminate almost exclusively in the DCIC and LCIC and are therefore unlikely to exert a direct effect on the CNIC.

3.5 Conclusion

Cryoloop cooling is a viable means of producing deactivation in the IC and of studying interactions between the two ICs. The rapid onset and reversibility of cooling combined with the absence of any need for interference with the preparation during the cooling process offer major advantages over drug injection methods. Like all methods that do not allow for selective deactivation of different neuron types, there is no way of isolating the contribution of commissural input from effects of descending or ascending connections to other nuclei, but evidence suggests the modulation of commissural input is the major effect of cooling deactivation. Cryoloop cooling does have drawbacks compared to other methods, such as the lack of deactivation along the entire tonotopic axis of the IC and the lack of pharmacological specificity of the deactivation. With these caveats, cryoloop cooling is the best model presented to date to tackle this issue. The establishment of this model allows for strong arguments to be made that the modulations in spiking activity in the IC contralateral to cooling shown in Chapters 4, 5 and 6 were caused by the removal of the contralateral ICs' contribution to auditory processing.

Chapter 4. Modulation of Frequency Response Areas by Deactivation of the Contralateral IC

4.1 Introduction

One way by which neurons in the IC can be distinguished is based on their frequency-level receptive fields (Aitkin *et al.*, 1975; Ehret and Merzenich, 1988; Ramachandran *et al.*, 1999; LeBeau *et al.*, 2001; Hernández *et al.*, 2005; Palmer *et al.*, 2013). While a large proportion of neurons in the CNIC have V-shaped frequency tuning (Rose *et al.*, 1963; Aitkin *et al.*, 1975; Ehret and Moffat, 1985; LeBeau *et al.*, 2001; Palmer *et al.*, 2013), several other frequency response types have been identified (Vater *et al.*, 1979; Ehret and Moffat, 1985; Ehret and Merzenich, 1988; Ramachandran *et al.*, 1999; LeBeau *et al.*, 2001; Hernández *et al.*, 2005; Wallace *et al.*, 2012; Palmer *et al.*, 2013) such as Narrow responses with a limited bandwidth across all levels (also known as 'level tolerant' or 'I-type'), or Closed responses which have a circumscribed island of excitatory response around which firing decays to zero (also known as 'O-type' or 'non-monotonic').

This range of frequency response characteristics in the IC is in arrant contrast with the AN where all fibres have V-shaped tuning (Kiang, 1965; Evans, 1972). While the IC receives ascending afferent input from a multitude of auditory brainstem nuclei, the CN is the only obligatory nucleus between AN and IC. The CN has more frequency response types than the AN and fewer than the IC (Evans and Nelson, 1973; Rhode and Greenberg, 1992) suggesting that frequency analysis becomes progressively more complex at higher levels in the auditory system.

Evidence suggests that the non-V-shaped frequency responses of IC neurons are formed by local inhibition. The strongest support for this hypothesis comes from studies where bicuculline, an antagonist of GABA_A receptors, was applied iontophoretically to single neurons in the IC. In these studies the tuning of

Narrow and Closed FRAs became more V-shaped (Vater *et al.*, 1992; Yang *et al.*, 1992; LeBeau *et al.*, 2001; Lu and Jen, 2003).

An alternative hypothesis is that IC neurons inherit their frequency response characteristics from the afferent projections they receive from lower nuclei (Ramachandran *et al.*, 1999; Davis, 2002). The evidence for this hypothesis comes from data collected in decerebrate cat. This hypothesis asserts that there are just three response types in IC: V-shaped, O-type, and I-type. To date these data have not been replicated in an intact preparation, anaesthetised or awake. A study in the pentobarbitone anaesthetised Chinchilla by Palombi and Caspary (1996) provides some additional support for this hypothesis. This paper reported 'isointensity frequency contours' from the responses of IC neurons and found that the disinhibitory effects of bicuculline were mediated within the excitatory region that was defined before the drug was applied. However the drawback of presenting stimuli at one level is that the interplay between inhibition and excitation across the entire FRA of the neuron is not observed. Furthermore, pentobarbitone anaesthesia is known to modulate the frequency responses of auditory neurons (Gaese and Ostwald, 2001).

This Chapter has tested the hypothesis that commissural inputs to the IC influence the frequency response areas of IC neurons. As non-V-shaped FRAs in the intact preparation form a heterogeneous population (Palmer *et al.*, 2013), some of which have not been reported in lower auditory centres, some of these types are hypothesised to be formed at the level of the IC. If true, the formation of new response types may be influenced by CoIC input. As the vast majority of CoIC projections originate within the IC, if deactivation of one IC were to produce tuning changes in non-V-shaped FRAs, it would be compelling evidence that these FRA types are not merely inherited from lower brainstem nuclei.

The only study to date which has investigated the functional role of the CoIC in frequency analysis was conducted by Malmierca *et al.* (2003). They recorded single IC neurons in the IC before and after pressure injection of kynurenic acid (a non-selective antagonist of glutamate receptors) in a tonotopically matched region in the contralateral IC. This study found that the frequency receptive fields of 83% of neurons tested changed after drug injection. However, these experiments produced a yield of 12 cells from 38 experiments. The low unit count did not permit any systematic evaluation of the influence of the CoIC on different frequency response types, but does suggest that the CoIC has an effect on the frequency analysis undertaken by many IC neurons.

Hernández *et al.* (2006) reported that in rat approximately 20% of commissurally projecting IC neurons are GABAergic, with the remainder presumed to be glutamatergic. This finding is consistent with both the increases and decreases in FRA area observed by Malmierca *et al.* (2003), which may have been mediated by either monosynaptic or polysynaptic connections (Smith, 1992; Moore *et al.*, 1998).

To date there have been no detailed studies into how one IC influences the frequency responses of a sizeable number of neurons in the other IC. The aim of the experiments in this Chapter was to record a representative sample of the FRA types reported in the guinea pig IC (LeBeau *et al.*, 2001; Palmer *et al.*, 2013), and to identify any changes in the FRAs of these neurons produced by deactivating the contralateral IC using the cooling paradigm described in Chapter 3. In this Chapter only changes in FRA shape and area are considered, but the data collected in these experiments were also used as the basis for the analysis of additional measures derived from the FRAs such as CF, threshold and bandwidth; the data from the analyses of these measures are presented in Chapter 5.

The experiments reported here aimed to record FRAs from a large number of IC neurons before, during and following recovery from a cooling cycle. The effects of cooling were hypothesised to mimic those of local iontophoretic application of GABA_A receptor agonists or antagonists. Specifically the areas of complex FRA shapes were thought to be influenced by CoIC input and deactivating the contralateral IC was hypothesised to change the shape of these FRAs. Those FRA types which resemble the V-shaped responses seen in AN and CN were hypothesised to change in shape to a lesser degree as inhibition which may be influenced by the CoIC was hypothesised to not have as much effect of the shape of these responses as on more complex FRAs. While inhibition in IC can originate from ascending afferent input or via interactions within the IC, the CoIC provides a large source of GABAergic inhibition to each IC. If removing CoIC input to IC neurons caused changes in FRAs similar to those observed by iontophoretic application of GABA_A channel blockers, it would support the hypothesis that inhibition from the CoIC helps to form FRAs in the IC.

4.2 Methods

The general procedures applied to acquire the results outlined in this Chapter are described in Chapter 2. Methods specific to this Chapter are described below. All recordings reported here were made from the IC contralateral to the cryoloop.

4.2.1 Experimental procedure

FRA's were measured in response to contralateral monaural and binaural diotic stimuli after isolation of a single unit. For a small subsection of units, only binaural FRA's were measured. Initial recordings were used as 'control' FRA's to which FRA's measured during and after contralateral IC cooling were compared. In this regard, each neuron served as its own control. FRA's recorded during cooling were completed (along with other analyses, which will be described in Chapter 6) with cooling cycles lasting less than 25 minutes. Units were given up to an hour to recover, although the majority of those that recovered did so within 20 minutes of termination of cooling. To minimize the duration of recordings throughout cooling, FRA's were only recorded to contralateral monaural or binaural diotic stimuli, but not ipsilateral monaural stimuli.

4.2.2 Measurement of changes induced by cooling

Changes to FRA's in this Chapter are described only in relation to excitatory sound driven responses. FRA's were formed from a matrix of frequency and level combinations, each presented once to the unit. The firing rate of the unit to each stimulus was then plotted by interpolating between the integer values of spikes per stimulus, and plotted. All measures were derived from the original values, not the interpolated graphical representation of the FRA. The excitatory area of each FRA was measured as the total number of bins in which driven responses occurred. Owing to the variable spontaneous firing rate of neurons in the sample, the mean spontaneous firing rate was calculated for each FRA. This

was done by averaging the number of spikes elicited to the array of maximally attenuated stimuli in each FRA, i.e. the bottom row of values. Responses in which the firing rate exceeded two standard deviations above the mean were deemed to be part of the excitatory FRA and were counted. For this reason the area of each FRA is given in the arbitrary unit 'bins', with each bin representing one frequency-level combination. The percentage change in area in the contralateral IC cooled condition relative to the control condition was then calculated.

4.2.3 Analyses of FRAs

Because the time to acquire each FRA was ~5 minutes, and time was required to present other stimulus types, multiple repetitions of the FRA stimuli were not possible. For this reason statistical comparisons for individual units between conditions were not possible. One FRA was analysed in each condition and a criterion of 20 % change was applied to indicate a significant change in FRA area. Each stimulus used to generate the FRA is only presented once, but because each FRA is made up of several hundred stimuli there is a strong basis to support the contention that each FRA shows a reliable and repeatable representation of that units' frequency response type (see Fig. 4.2).

4.3 Results

The results presented in this Chapter are from single unit recordings in the right IC of guinea pig made before, during and after a cooling cycle of the left IC. The classification and stability over time of FRAs in the sample will be presented and examples of changes in FRA area induced by cooling the contralateral IC will be shown. Population analyses comparing the changes that occurred in different FRA types and changes in relation to contralaterally and binaurally driven stimuli will be presented.

The findings of these analyses will be discussed in the context of this study and how they might relate to commissurally mediated, intercollicular processing of stimulus frequency.

All electrophysiological recordings described in this Chapter were made from single units in the right IC of 21 adult guinea pigs (\bar{x} weight = 824 g; IQR = 747 to 940 g; Range = 460 to 1,093). Electrode penetrations were made from 10.3 to 12.5 mm posterior of bregma and from 2.0 to 3.1 mm lateral of the midline. In most experiments, multiple electrode penetrations were made within these ranges.

4.3.1 Classification of FRAs

FRAs to contralateral and binaural stimulation were recorded from 76 units; a further 8 units were presented with binaural stimuli only.

The majority of units in this Chapter were categorised using the criteria set out by LeBeau *et al.* (2001). Examples of each type of unit observed in this sample are shown in figure 4.1; observable similarities amongst all units in each type were as follows:

- i) *V-shaped monotonic* FRAs (Fig. 4.1A) fired spikes to an increasing range of frequencies either side of CF as stimulation level increased. At high levels of stimulation these units sometimes fired spikes up to 3 octaves below CF, forming a 'low frequency tail'. When plotted on a logarithmic frequency axis, most of these FRAs were non-symmetrical about CF - a trend more pronounced in units with higher CFs. As stimulation level increased at CF, firing rate also increased and sometimes plateaued.
- ii) *V-shaped non-monotonic* FRAs (Fig. 4.1B) were similar to V-shaped monotonic FRAs except that as stimulation level was increased at CF there was an initial increase in firing rate which then decreased at higher levels. Due to the non-monotonic nature of these responses at CF, they were classified separately from V-shaped monotonic FRAs. For example, the unit in figure 4.1B fired 50% more spikes at 60 dB attenuation than at 10 dB attenuation at CF.
- iii) *Low Tilt FRAs* (Fig. 4.1C) also had a non-monotonic spike rate at CF, but also elicited no driven activity at frequencies higher than CF. These FRAs has excitatory responses that were tilted towards lower frequencies as level increased.
- iv) *Narrow* FRAs (Fig. 4.1D) were V-shaped and fired monotonically to increases in stimulus level at CF, but as level was increased the range

of frequencies which elicited spikes did not increase. These FRAs tended to be near symmetrical and did not have a low frequency tail.

- v) *Closed* FRAs (Fig. 4.1E) had an excitatory response to specific frequency-level combinations that were circumscribed by bins with no driven activity. These units exhibited a restricted response to sound stimuli. These FRAs were always inhibited from firing at high levels of stimulation.
- vi) *Multi-peaked* FRAs (Fig. 4.1F) had multiple peaks which were separated by a discernible gap in which no driven activity was recorded. These FRAs tended to have monotonic increases in firing rate and a large increase in bandwidth between 10 and 40 dB above threshold.
- vii) *Broad* FRAs (Fig. 4.1G) had a very wide bandwidth across the excitatory response area. These units typically showed an excitatory response at levels below ~30 dB attenuation (generally lower) which spanned at least 1.5 octaves above and 2.5 octaves below CF. These FRAs had the widest bandwidths of any FRA class at 40 dB above threshold. Near threshold there could be one broad peak or multiple peaks.

Numerous other FRA subtypes have been reported in the mammalian IC (such as High Tilt, Inhibitory and Complex/Mosaic types), but none of these were found during the course of these experiments and therefore they will not be discussed further.

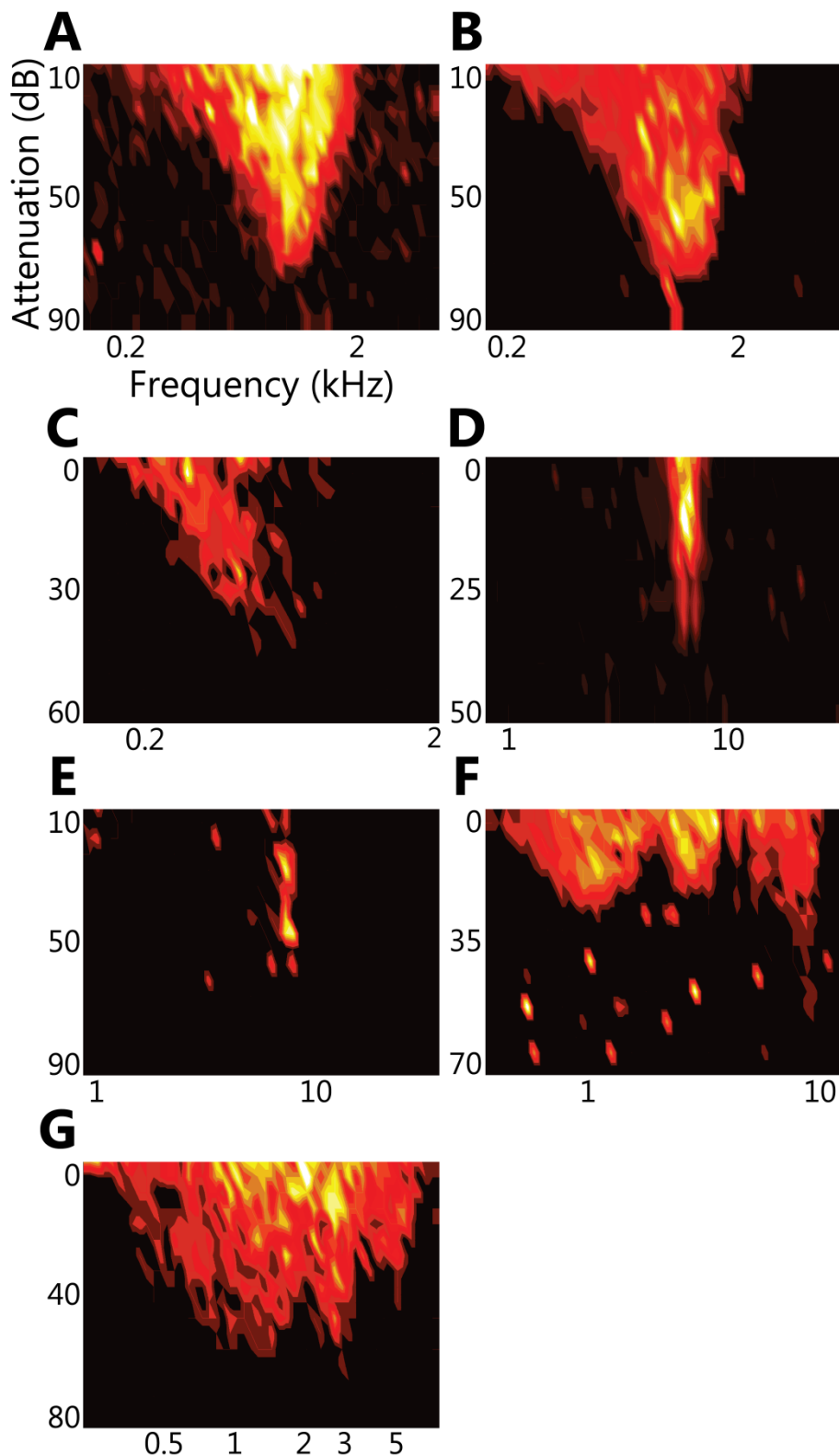


Figure 4.1 Examples of each of the FRA types found in this dataset. Most FRA types fell within the inclusion criteria set out previously for neurons in guinea pig IC by LeBeau et al., (2001): (A) V-shaped monotonic; (B) V-shaped non-monotonic; (C) Low Tilt; (D) Narrow; (E) Closed; (F) Multi-peaked. (G) Broad FRAs were also found in this sample.

4.3.2 Stability of FRAs over time

As discussed above, owing to the time required to acquire each FRA the analyses in this Chapter involve comparisons of one FRA taken at each stage of a cooling cycle. To assess whether changes in FRA area induced by the paradigm reflect changes due to contralateral IC cooling rather than inherent variability in the neuronal response, the stability of FRAs over time was assessed.

Figure 4.2A shows the binaural FRA of a Narrow unit. Stimuli spanned 2 octaves above and 3 octaves below 8.5 kHz with 10 frequency steps per octave. Stimulus levels ranged from 0 to 48 dB attenuation in 4 dB steps. This unit had a CF of 8.75 kHz, a threshold at 40 dB attenuation and an area of 122 bins. This unit was recorded for over an hour and multiple binaural FRAs were collected spanning 5 to 57 minutes after the initial categorisation (Fig. 4.2B-H). Qualitative analysis showed that the unit retained its Narrow tuning, maximum firing rate and a similar rate of spontaneous firing throughout the duration of the recordings. Quantitative analysis of the CF, threshold, area and spikes within each FRA showed that no measure changed by more than 18 % while CF, threshold and spike measurements changed less than 10 % (Table 4.1). That this was found with a Narrow unit which had a small area, composed of relatively few bins, and thus more likely to reach the 20 % criterion, indicates the repeatability with low variance of the responses and therefore the applicability of the 20 % criterion of change.

Two other units were studied in this manner and showed similar stability. This indicates that single FRAs are stable over the duration of recordings made in this Chapter.

Analysis	Time since characterisation (mins)	CF (kHz)	Threshold (dB attenuation)	Area (bins)
4005	0	8.75	40	122
4007	5	8.75	40	104
4011	11	8.75	44	102
4013	17	8.26	36	110
4015	28	8.75	40	100
4017	34	8.26	40	112
4019	40	8.75	40	106
4021	57	8.75	36	118

Table 4.1 The stability of measures derived from multiple repetitions of a binaural FRA analysis applied to a single neuron over the course of approximately one hour. The maximum change in area re control was 18%.

This analysis supports the use of a 20 % criterion as a sufficient parameter by which changes in FRA area during cooling of the contralateral IC can be inferred to be due to the experimental paradigm and not neuronal response variability. This criterion is the same as has been used previously where similar problems with implementing statistical analyses occurred (Li and Kelly, 1992; Burger and Pollak, 2001; LeBeau *et al.*, 2001; Malmierca *et al.*, 2005; Park *et al.*, 2008).

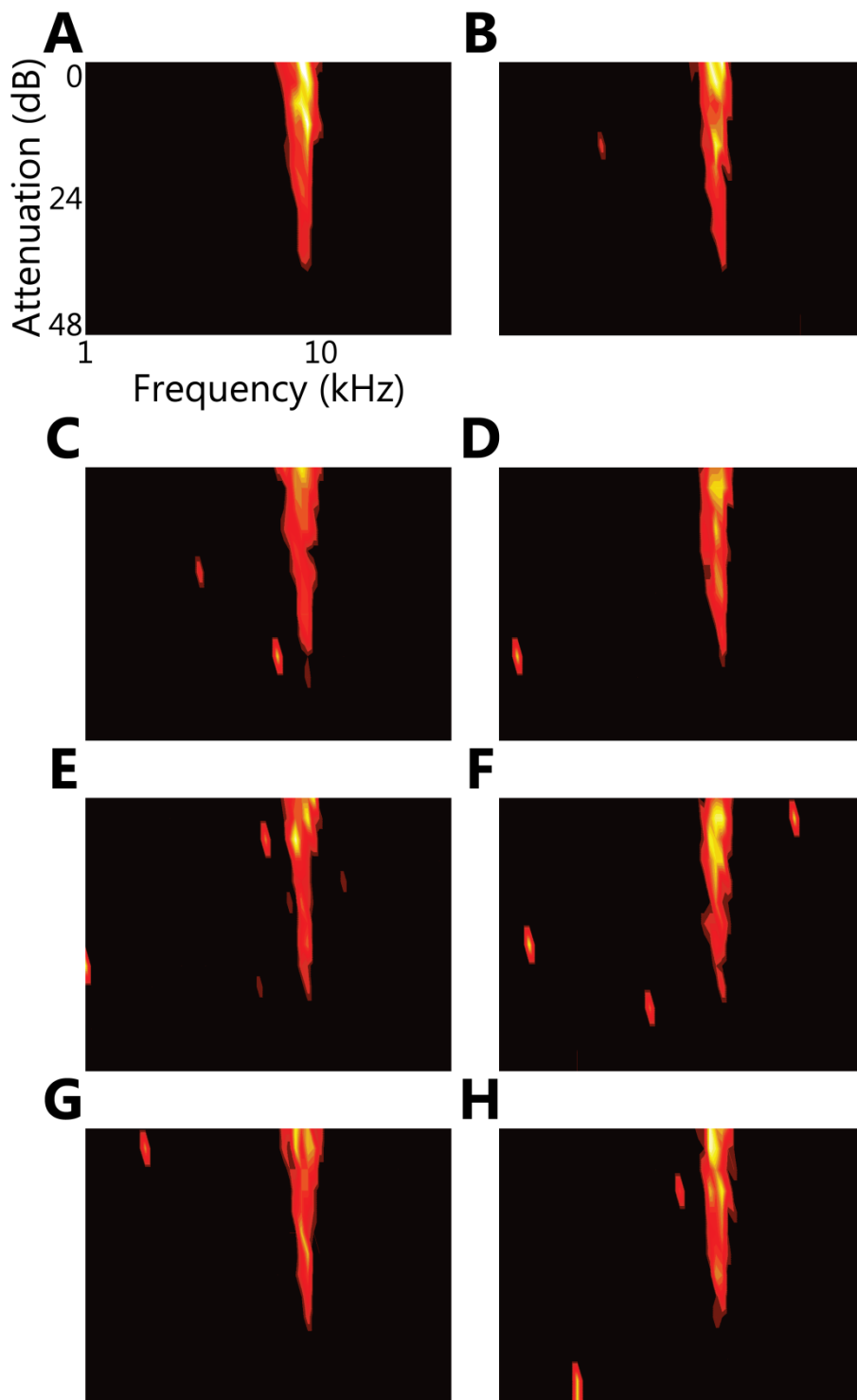


Figure 4.2 Binaural FRAs of a Narrow unit at various time points relative to when the unit was first classified: (A) 0 mins; (B) 5 mins; (C) 11 mins; (D) 17 mins; (E) 28 mins; (F) 34 mins; (G) 40 mins; (H) 57 mins. Note the similarity of the CF, threshold, bandwidth, excitatory response area, and spontaneous firing rate in all cases.

4.3.3 Classification of FRA types in this dataset

All units included in this Chapter were deemed to have recovered if their FRA area was within 20 % of the control area after termination of cooling. The heterogeneity of FRA types in the guinea pig IC makes defining the specific numbers and relative proportions of each FRA type in the sample imperative. At present there is no statistical method by which FRAs can be objectively classified as a specific type (Palmer *et al.*, 2013). Therefore FRAs in this Chapter were classified qualitatively, using the criteria set out earlier in section 4.3.1.

V-shaped monotonic units comprised the largest number of neurons (41 of 84; 48.8 %). These formed almost the entire population of V-shaped units as only 3 non-monotonic V-shaped units were found. Combined, V-shaped units formed more than half of the sample (44 of 84; 52.4 %). The number and percentage of each of the seven FRA types found in this dataset are summarised in table 4.2.

FRA type	# to contralateral stimulation	# to binaural stimulation
V-shaped monotonic	36	41
V-shaped non-monotonic	3	3
Low Tilt	2	2
Narrow	10	10
Closed	2	4
Multi-peaked	17	18
Broad	5	6

Table 4.2 the distribution of each type of FRA in the dataset. All neurons were recorded in response to binaural diotic stimulation and most were also recorded in response to contralateral ear monaural stimuli.

4.3.4 Frequency distribution of units

The distribution of CFs was skewed to the low frequency end of the audiogram with 73 of 84 (86.9 %) units having CFs below 10 kHz. When binned according to the logarithmic representation of frequency in the auditory system (Fig. 4.3), the number of units with CFs less than 2 kHz was 38 (45.2%) while those greater than 2 kHz totalled 46 (54.8 %; Fig. 4.3A).

When FRA type was factored into the distribution of CFs there was a differential representation of FRA class with frequency. V-shaped monotonic FRAs had a two peaked distribution (Fig. 4.3B, black bars) with 17 units having CFs between 1 and 2 kHz and 10 units with CFs between 8 and 16 kHz. By contrast, Multi-peaked units, had a broad unimodal distribution that peaked in the high frequency regions between 8 and 16 kHz. Narrow units also had a unimodal distribution which peaked in the higher frequency range, but in contrast to Multi-peaked units the peak fell between 4 and 8 kHz. All 3 V-shaped non-monotonic, both Low Tilt and 3 of 4 Closed units had CFs between 0.5 and 2 kHz. The other Closed unit had a CF of 6.5 kHz. The low number of these latter 3 FRA types made it difficult to draw out any clear pattern of CF distribution. The 6 Broad FRAs were found in low frequency areas, with a range of CFs from 0.6 kHz to 3.1 kHz.

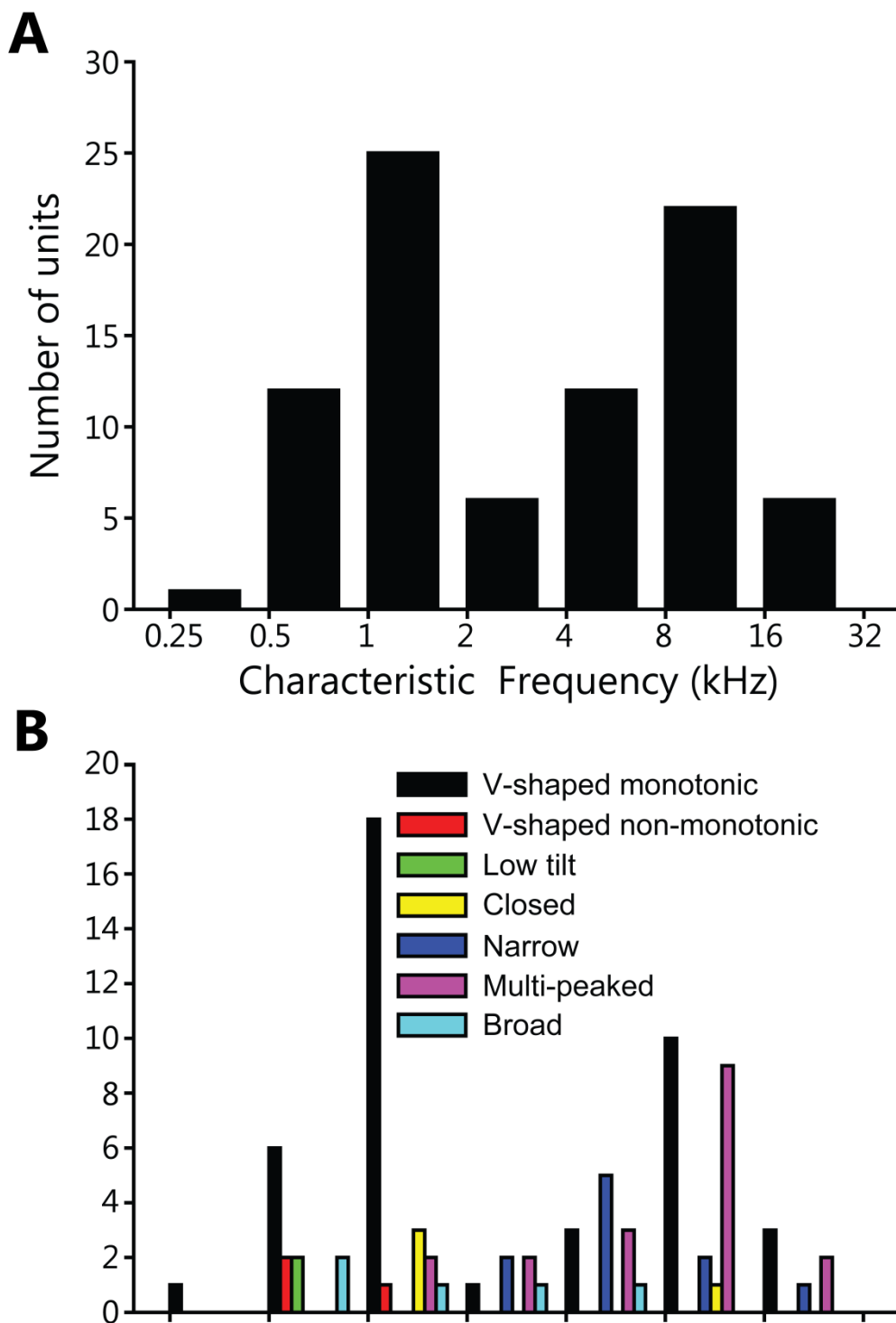


Figure 4.3 (A) CFs of all units in this dataset. There was an approximately even division of units with CFs above (46; 54.8%) and below (38; 45.2%) 2 kHz. Plotted on a logarithmic abscissa the distribution appears bimodal with one peak between 1 & 2 kHz and another between 8 & 16 kHz. (B) V-shaped monotonic FRAs formed the majority of units with CFs lower than 2 kHz. Multi-peaked FRAs had a broad CF distribution which peaked between 8 and 16 kHz. No Narrow or Closed FRAs had CFs lower than 2 kHz.

4.3.5 Increases in area of V-shaped monotonic FRAs

Of the 41 V-shaped monotonic units in this dataset, 37 were tested with both contralateral and binaural stimulation. The remaining 4 were presented with binaural stimulation only. Therefore there were 78 FRAs which were recorded throughout contralateral IC cooling which passed the criterion for inclusion. A range of changes in the area of these FRAs was seen during contralateral IC cooling.

Of the 78 V-shaped monotonic FRAs, 27 increased in area during cooling, 10 of which increased by more than 20 % (comprised of 8 units: 5 contralaterally stimulated and 5 binaurally stimulated). An example of one unit for which the binaurally driven FRA increased in area is shown in figure 4.4. This unit was characterised as having a CF of 1.1 kHz, a threshold of 54 dB attenuation, and an area of 299 bins (Fig. 4.4A). During contralateral IC cooling the CF was unchanged and threshold rose by just 1 db to 53 dB. The area of the FRA increased to 362 bins, with increases in bandwidth along both its low and high frequency edges (Fig. 4.4B). The recovery FRA was taken 22 minutes after cooling was stopped (Fig. 4.4C). The CF was marginally reduced to 1.03 kHz, the threshold rose slightly to 47.0 dB, and the area reduced back to 260 bins. The contralateral FRAs of this unit were unchanged by cooling with an area of 298 bins in the cool condition compared to 309 bins in the control condition.

There was also a change in firing rate within the FRA. Changes in firing rate will be analysed in detail in Chapter 6.

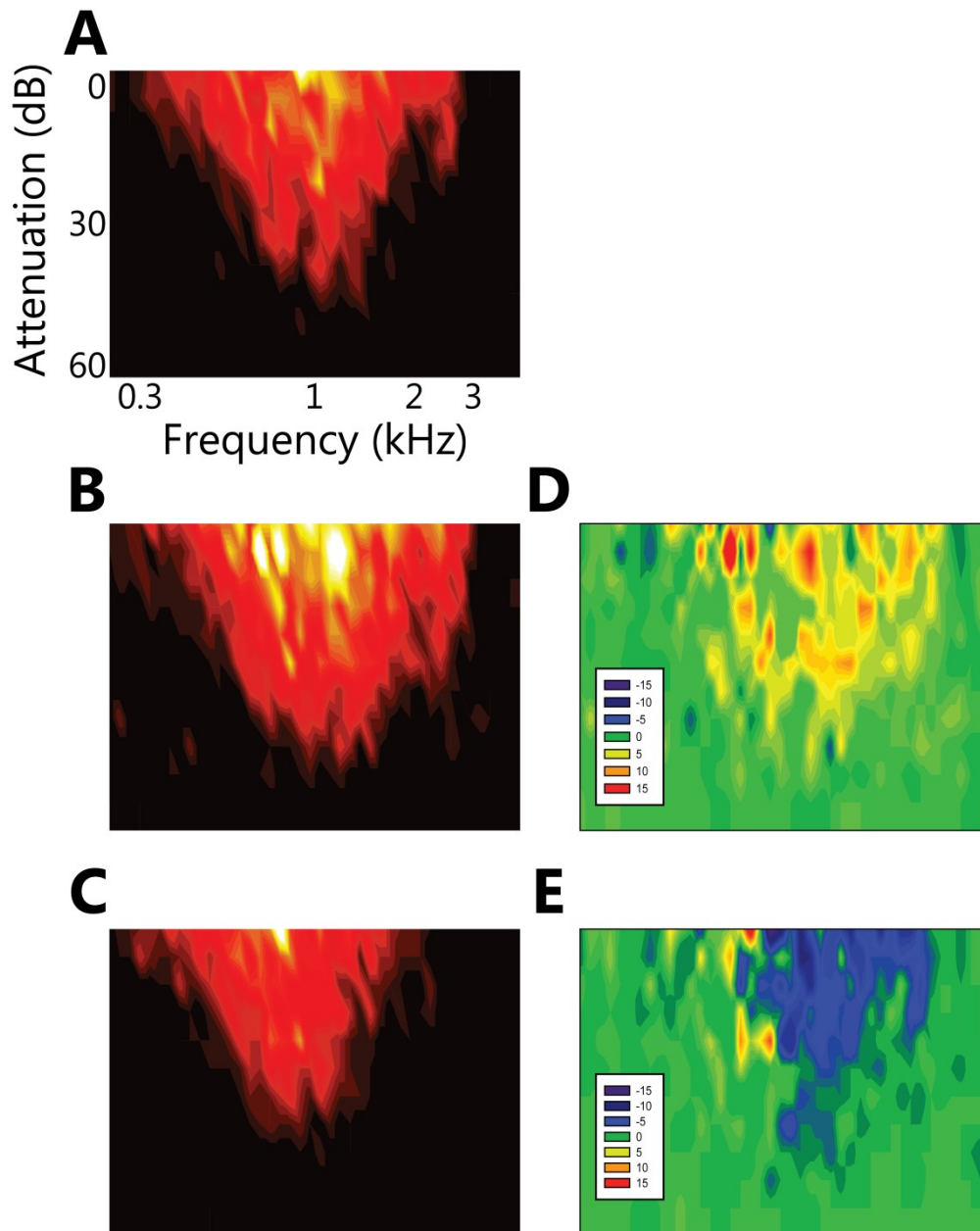


Figure 4.4 FRAs of a V-shaped monotonic unit to binaural stimulation throughout (A) control, (B) contralateral IC cool and (C) recovery phases of a cooling cycle. The CF and threshold were almost unchanged throughout all three phases. During contralateral IC cooling, FRA area increased due to an expansion in bandwidth at both edges of the response area. A difference plot (B-A) showed these changes (D). These changes reversed after cooling was stopped. A difference plot (C-A) showed the reversal and undershoot of firing on recovery (E).

4.3.6 Decreases in area of V-shaped monotonic FRAs

Forty nine of the remaining 51 FRAs decreased relative to control, 14 of which reached criterion (comprised of 12 units: 7 contralaterally stimulated and 7 binaurally stimulated). The remaining 2 FRAs were unchanged during contralateral cooling.

One FRA which decreased in area is shown in figure 4.5 in response to contralateral stimulation. The CF of the unit in the control FRA was 0.20 kHz, the threshold was 54.5 dB, and the FRA had an area of 280 bins (Fig. 4.5A). Cooling the contralateral IC reduced the area of the FRA to 203 bins (Fig. 4.5B). The CF was unchanged throughout all stages but the threshold rose to 46.2 dB. Following recovery, the changes observed during contralateral IC cooling were reversed (Fig. 4.5C). The binaural FRAs of this unit decreased from 225 to 193 bins, a decrease of 14.2 %. Changes were not exclusively found at the edges of tuning.

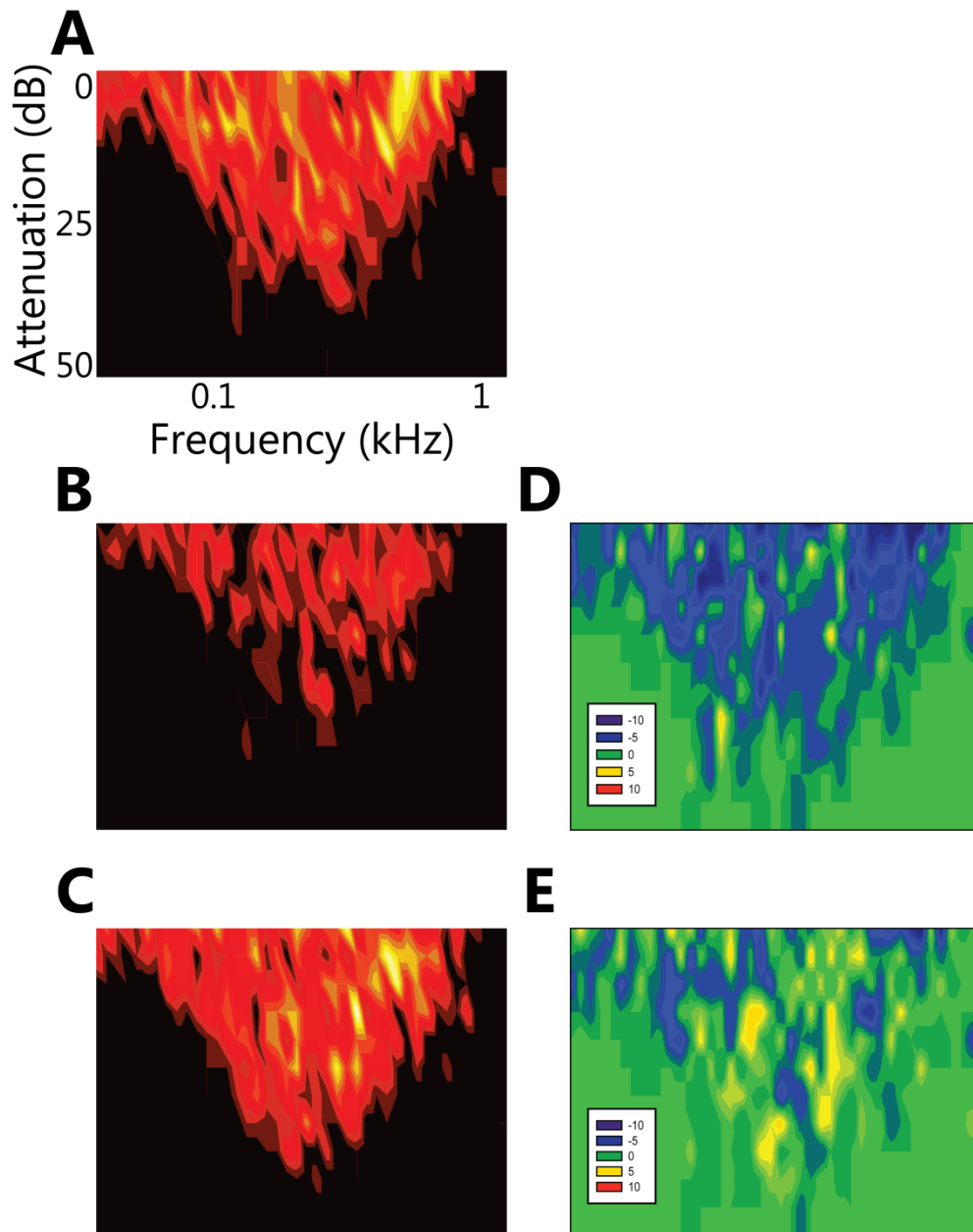


Figure 4.5 V-shaped monotonic FRAs of one unit in response to contralateral stimulation throughout (A) control, (B) contralateral IC cool, and (C) recovery phases of a cooling cycle. The CF and threshold were unaffected by cooling but the area decreased by 27.5 % during contralateral IC cooling. (D) The decrease across the FRA was highlighted by a difference plot (B-A) which appeared to show a drop in responsiveness. (E) These changes reversed after cooling was stopped and a difference plot (C-A) showed small differences between control and recovery.

4.3.7 Lack of change in area of V-shaped monotonic FRAs

While more V-shaped monotonic FRAs decreased in area than increased during contralateral IC cooling, the majority (54/78) did not reach criterion. Figure 4.6 shows a unit which was unchanged during contralateral IC cooling. The area of the FRA was 171 bins in the control condition, the CF was 1.09 kHz and the threshold was 50 dB attenuation (Fig. 4.6A). During contralateral IC cooling the area reduced marginally to 165 bins, the threshold rose to 46 dB, while the CF was still 1.09 kHz (Fig. 4.6B). Following recovery the area of the FRA was 162 bins, the threshold was 49 dB attenuation and the CF was 1.02 kHz (Fig. 4.6C). No measure changed to criterion. This example is typical of the response of the majority of V-shaped monotonic FRAs to contralateral IC cooling found in this study.

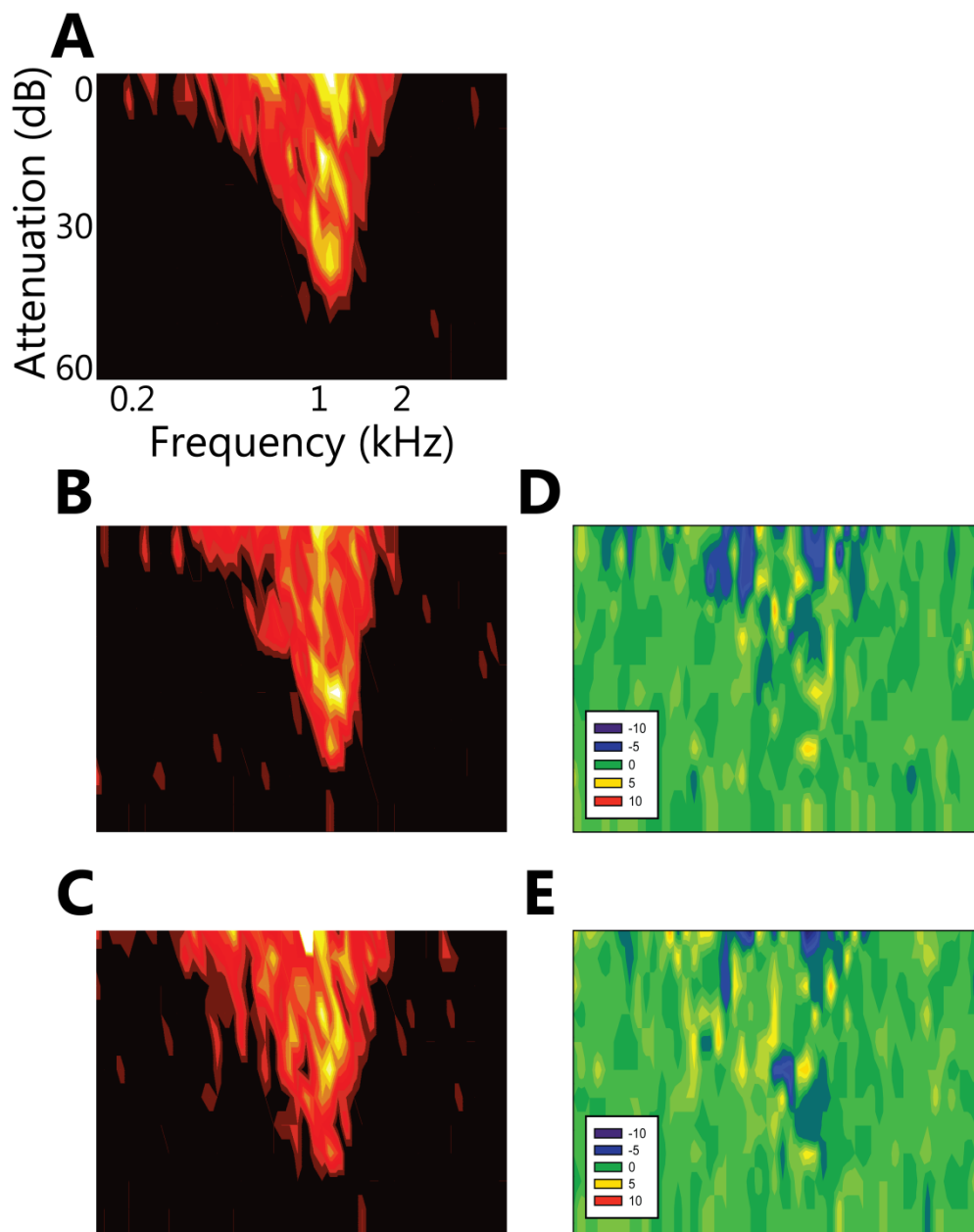


Figure 4.6 FRAs of a unit with a V-shaped monotonic response area to contralateral stimulation throughout (A) control, (B) contralateral IC cool, (C) and recovery phases of a cooling cycle. No measure derived from the FRA changed in either direction to meet the 20 % criterion for significant change. Due to response variability, some bins changed in the (D) cool and (E) recovery conditions compared to control but there was no pattern across the FRA. This type of response was typical of the majority of V-shaped monotonic FRAs.

4.3.8 The population of V-shaped monotonic FRA areas were unchanged by cooling of the contralateral IC

When analysed as a population, the change in area of V-shaped FRAs during contralateral IC cooling was approximately Gaussian (Fig. 4.7). The median change was 0.95 (IQR = 0.83 to 1.08) – this was due to the higher tendency of FRAs to decrease in area during contralateral IC cooling (Fig. 4.7A). Though a few FRAs did change more than 20 %, the vast majority did not. When compared to a hypothetical distribution with a median of 1 there was no significant difference in the observed distribution ($Z = -1.42$; $P = 0.16$). When the relative contributions of the contralaterally and binaurally driven FRAs were plotted (Fig. 4.7B), both had a similar distribution. One sample ranks tests found no significant difference for either contralateral ($Z = -0.46$; $P = 0.65$) or binaural ($Z = -1.49$; $P = 0.14$) groups compared to a hypothetical distribution with a median of 1.

Comparing the entire distribution of V-shaped FRA areas during contralateral IC cooling to that in the control condition found no significant difference ($Z = -0.92$; $P = 0.36$). This was also true for the sub-groups of contralaterally ($Z = -1.50$; $P = 0.13$) and binaurally ($Z = -1.36$; $P = 0.17$) stimulated FRAs.

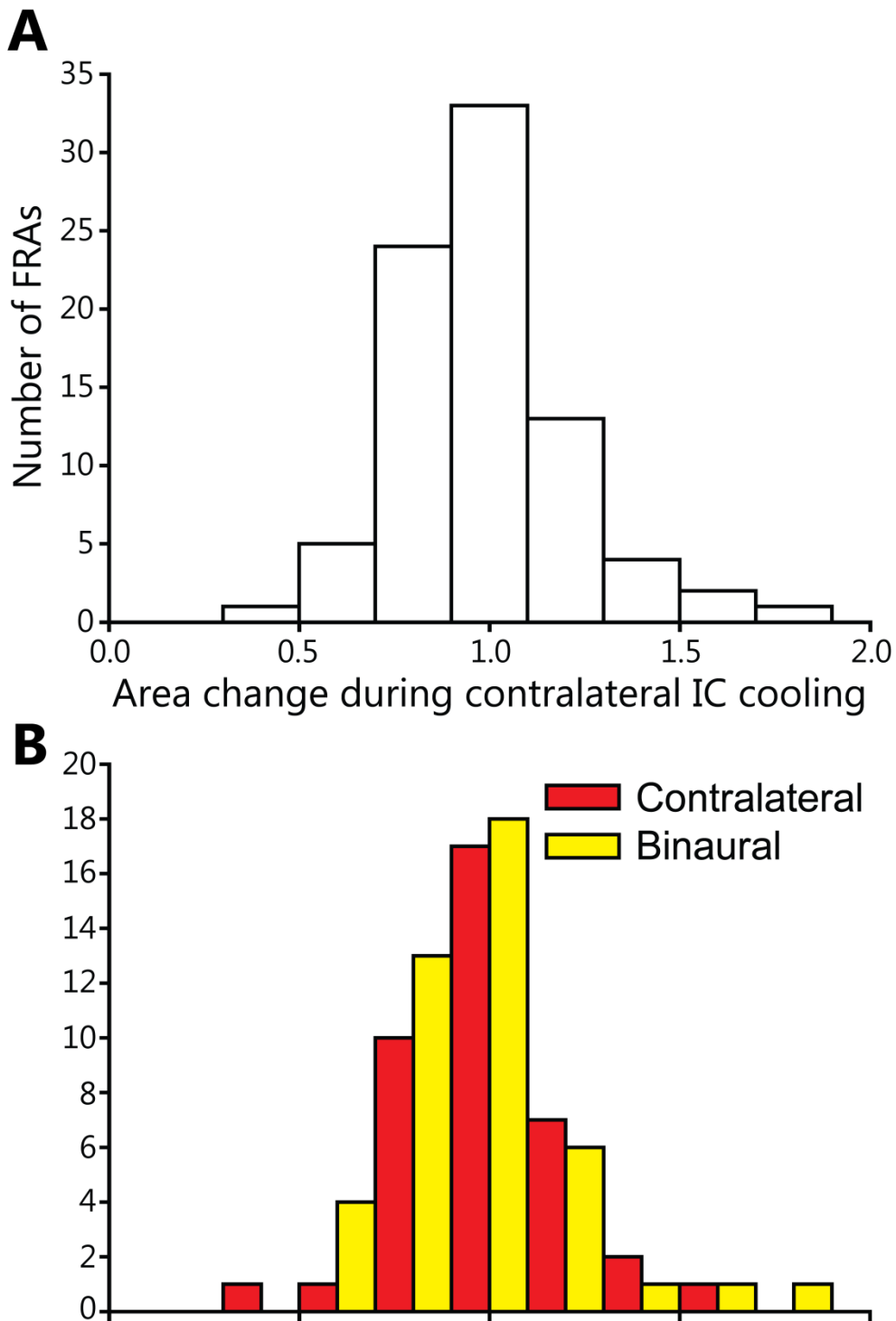


Figure 4.7 The ratio of FRA area change (contralateral IC cool FRA area/control FRA area) for (A) all V-shaped monotonic FRAs and (B) for the relative contribution of contralaterally (red) and binaurally (yellow) driven V-shaped monotonic FRAs. Contralateral IC cooling did not produce a significant change in the population of FRA areas for the contralateral ($Z = -0.46$, $P = 0.65$), binaural ($Z = -1.49$, $P = 0.14$) or combined ($Z = -1.42$, $P = 0.16$) populations.

4.3.9 Cooling did not change the area of non-V-shaped non-monotonic FRAs

Only 3 V-shaped non-monotonic units were found which passed the inclusion criteria following recovery from contralateral IC cooling. Contralateral and binaural FRAs were generated from all 3 of these units at each stage of the cooling paradigm.

Cooling failed to modulate the area of any of the six V-shaped non-monotonic FRAs. One example of this class of FRA is shown in figure 4.8. This unit was found in the dorsal region of the IC, had a CF of 0.38 kHz and a threshold of 70 dB attenuation in the control condition. The maximum firing rate was tilted along the low frequency edge of tuning which produced a non-monotonic rate-level function at CF. The FRAs in this figure were recorded in response to binaural stimulation and produced a control area of 424 bins (Fig. 4.8A). Contralateral IC cooling produced little change in the response of the unit. During cooling of the contralateral IC the FRA had an area of 427 bins and similar bandwidth and threshold to the control condition (Fig. 4.8B). After a recovery period of 22 minutes the binaural FRA had an area of 388 bins and while the firing rate reduced relative to that during contralateral IC cooling, the shape of the FRA was similar to control (Fig. 4.8C). A rate-level function (RLF) at CF found that the peak firing rate of the non-monotonic function was at 60 dB attenuation in all stages (not shown).

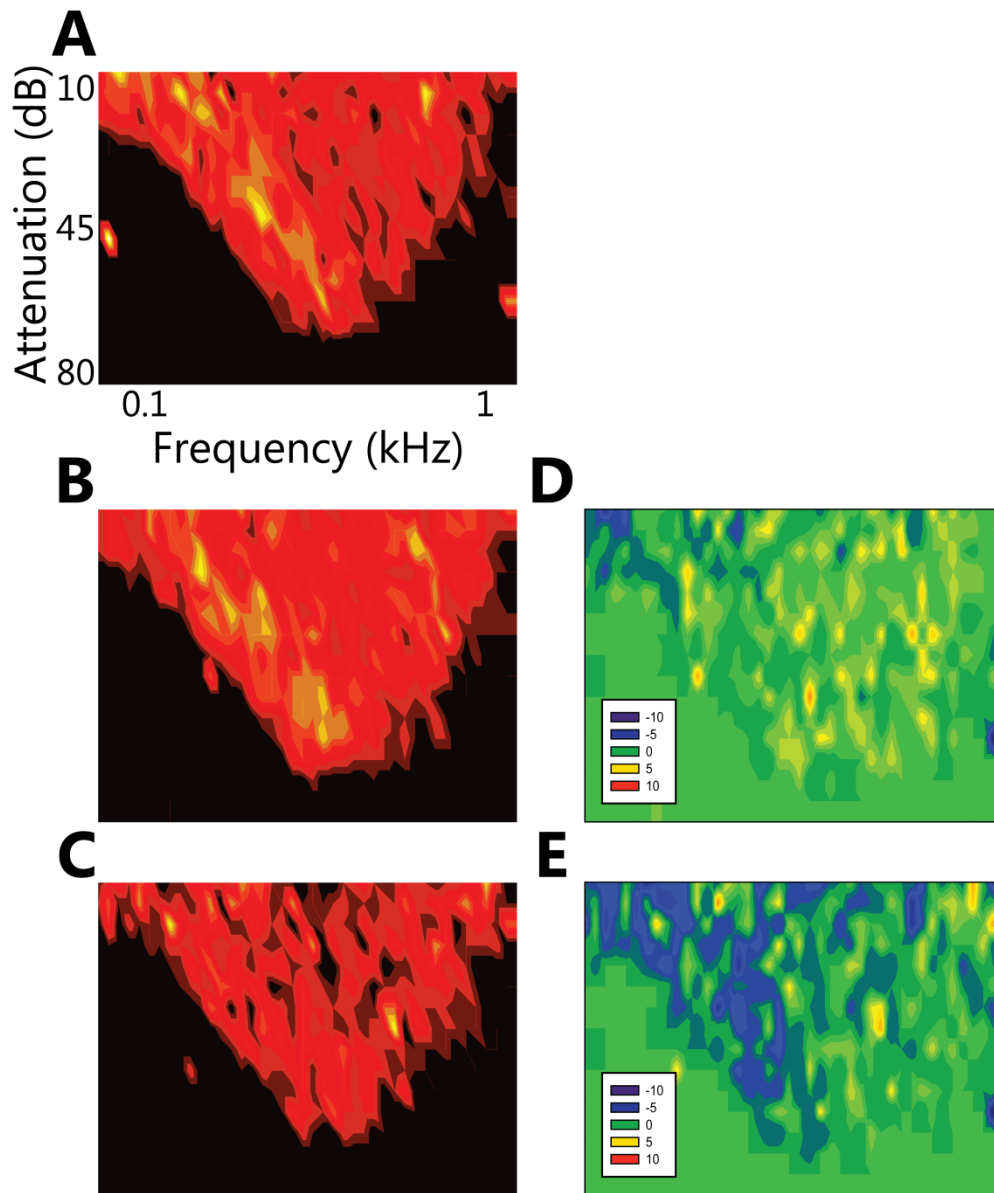


Figure 4.8 Binaural FRAs from a V-shaped non-monotonic unit (A-C) showed little change in area or tuning during contralateral IC cooling. A slight increase in maximal firing rate was seen during contralateral IC cooling from 6 to 8 spikes. The majority of bins within the excitatory area which did not elicit spikes in (A) the control condition did so (B) during contralateral IC cooling; a trend which reversed (C) after cooling was stopped. The non-monotonic nature of the response at CF was similar in all conditions.

4.3.10 One of two Low Tilt units reached criterion

Only 2 neurons with Low Tilt FRAs were found which recovered to the inclusion criterion; contralateral and binaural FRAs were recorded from both of these units.

Both Low Tilt units were found during the same experiment and in the same electrode track. The binaural and contralateral FRAs of one unit reached the criterion of significant change while the FRAs of the other unit did not. The binaural FRAs of the unit which did not change to criterion are shown in figure 4.9. This unit had a CF of 0.48 kHz which was unchanged at all stages of the cooling paradigm. The threshold of the FRA was virtually unchanged throughout all stages, being 46 dB attenuation in the control phase, 47 dB attenuation in the contralateral IC cool phase, and 47 dB attenuation in the recovery phase. The area increased to 430 bins during cooling from 381 bins in the control phase, an increase of 12.9 %. The area of the FRA decreased during recovery to 320 bins.

The other Low Tilt FRA which reached criterion did so by reducing in area. This FRA had a very high spontaneous firing rate which decreased during contralateral IC cooling. The reduction in spontaneous firing rate was matched by a 55 % decrease in area to contralateral and a 57 % decrease to binaural stimulation. However, due to the high spontaneous firing rate these changes are not easily visualised and have not been presented as an exemplar.

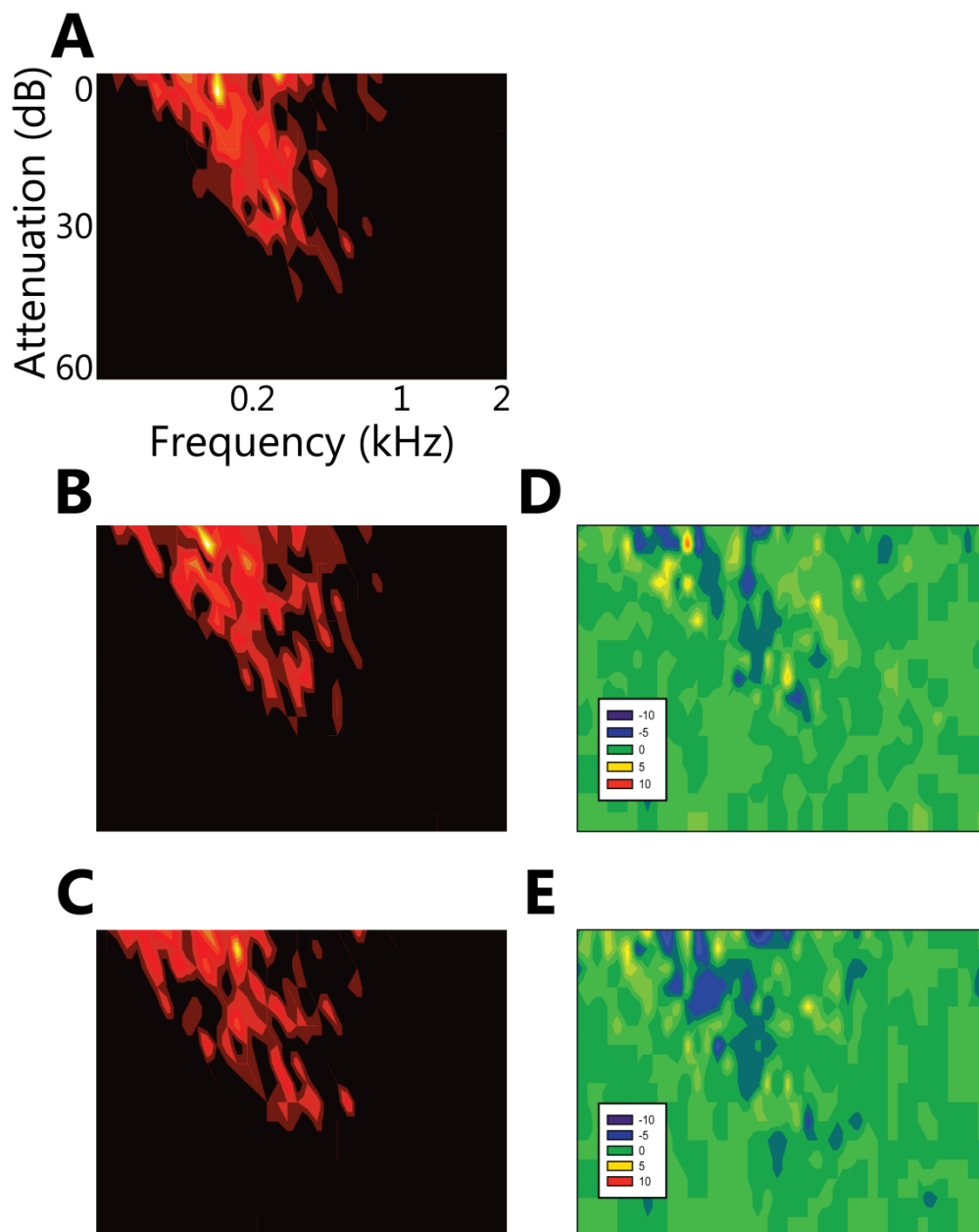


Figure 4.9 Binaural FRAs of a Low Tilt unit in the (A) control, (B) contralateral IC cool, and (C) recovery stages of a cooling cycle. Contralateral IC cooling increased the area of the FRA by 13%. (D) Difference plot (B-A) showing there was an increase in area at both edges of the response area, that reversed on recovery (C and E). Cooling induced changes recovered following cessation of cooling suggesting that the moderate changes observed were caused by the paradigm.

4.3.11 Cooling reduced the area of most Narrow FRAs

A total of 10 Narrow units were found. These formed the second largest non-V-shaped group of units in this dataset. All Narrow units were presented with both contralateral and binaural stimulation.

Of the 20 Narrow FRAs in this dataset, the area change of 10 FRAs reached criterion. Nine of these decreased in area during contralateral IC cooling while the other increased in area.

An example of one Narrow unit whose FRA decreased in area to both contralateral and binaural stimulation during contralateral cooling is shown in figure 4.10. In response to contralateral stimulation, this unit had a CF of 3.1 kHz, a threshold of 31 dB attenuation, and an area of 64 bins (Fig. 4.10A). The lack of a low frequency tail, and the steep near symmetrical slopes of the high and low frequency edges of the FRA led to this unit to be classified as Narrow. During contralateral IC cooling the CF of the unit was unchanged but the threshold increased to 18 dB attenuation (Fig. 4.10B). The rise in threshold was accompanied by a concomitant reduction in area to 32 bins – half that of control. Following recovery, the CF was again unchanged, but the threshold decreased back to 29 dB attenuation, and the area increased to 69 bins (Fig. 4.10C). In the control condition the unit had almost no spontaneous activity.

During cooling the unit began to fire spontaneously in bursts which ranged from 2 to 5 spikes, at a mean rate of 6.1 Hz. Following recovery, the spontaneous rate decreased to 0.7 Hz and when the unit did fire spontaneously, it was in single spikes as opposed to bursts.

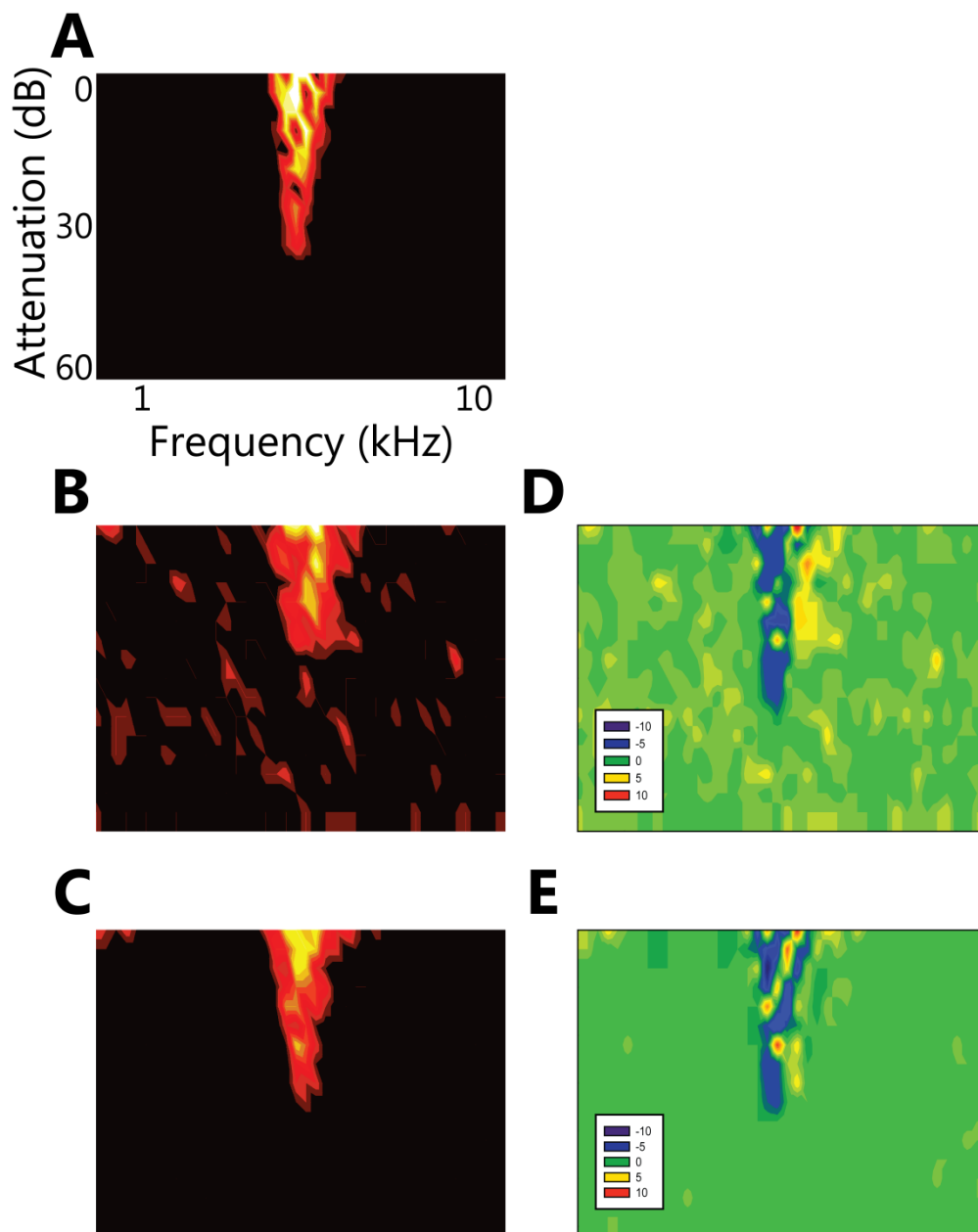


Figure 4.10 Contralaterally driven Narrow FRAs from a unit in the IC contralateral to cooling. (A) The FRA was classified as having a CF of 3.1 kHz, a threshold of 31 dB attenuation, and an area of 64 bins. (B) Cooling increased the threshold to 18 dB attenuation, and decreased the area to 32 bins. The unit also developed a high rate of spontaneous burst firing. (C) The threshold and area recovered to 29 dB attenuation and 69 bins respectively after cooling was stopped. Difference plot (B-A) showed there was a reduction in response at CF but an increase in response on the high frequency edge (D). This change disappeared on recovery as shown in a difference plot of recovery-control (E).

4.3.12 Contralateral IC cooling increased the area of all Closed FRAs

Only 4 units were classified as Closed. Two of these units were studied with contralateral and binaural stimulation while the other two received binaural stimulation only. This produced a total of six Closed FRAs which were subjected to all three stages of the paradigm.

Closed FRA responses were distinct from any other class of FRAs in this dataset for two reasons. Firstly, every FRA in the group increased in area during cooling of the contralateral IC relative to control. Secondly, the change in area of all FRAs was large enough to reach criterion. The area changes relative to control ranged from 130 % to 247 %.

An example of one such change in the area of a Closed FRA is shown in figure 4.11. This unit was studied in response to binaural stimulation only. In the control condition the CF was 6.5 kHz, and the threshold was 64 dB attenuation. The small number of stimuli which evoked driven activity, resulted in an area of 70 bins (Fig. 4.11A). Contralateral IC cooling induced an increase in area to 173 bins and a reduction of threshold to 70 dB attenuation. The cooling paradigm also caused a change in the shape of the FRA to a morphology which was more V-shaped. Sound driven spikes were elicited to a wider range of frequencies either side of CF as level increased, including a low frequency tail (Fig. 4.11B). Furthermore, the RLF at CF switched from being non-monotonic to monotonic during contralateral IC cooling. Cessation of cooling led to recovery of the Closed shape which strongly resembled the control condition (Fig. 4.11C). The area recovered back to 85 bins, the threshold increased to 66 dB attenuation, the RLF became non-monotonic again, the low frequency tail disappeared and the selective tuning was regained.

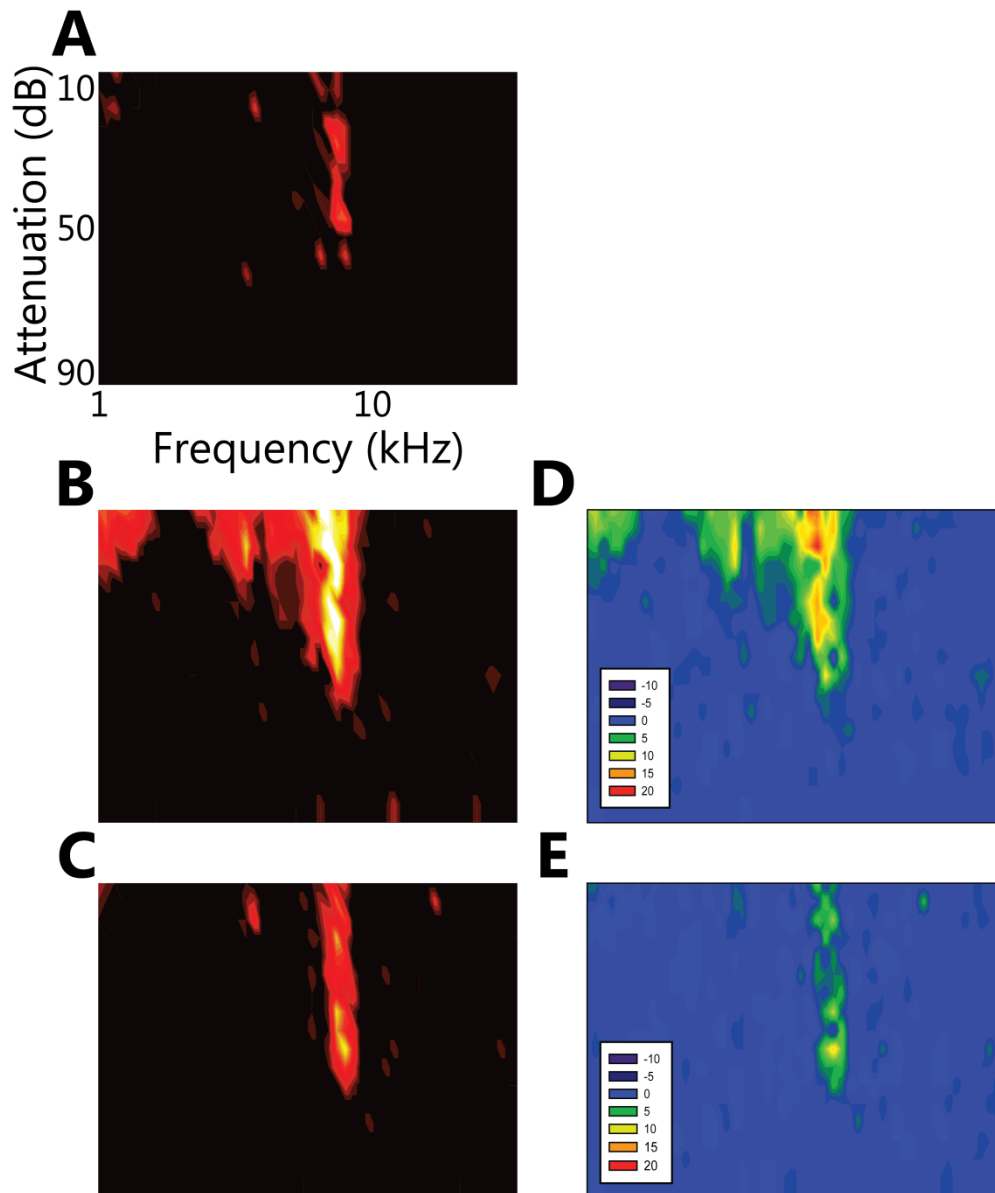


Figure 4.11 (A) Binaural FRAs from a Closed unit which had a CF of 6.5 kHz, a threshold at 64 dB attenuation, and an area of 70 bins in the control condition. (B) Contralateral IC cooling produced a decrease in threshold to 70 dB attenuation and an increase in area to 173 bins. The morphology became V-shaped. (C) Following recovery, the unit regained similar tuning to the control condition with a reduction in maximum firing rate, a non-monotonic RLF at CF and narrow, near symmetrical edges of tuning. The area reduced to 85 bins and the threshold increased to 66 dB attenuation. (D) Comparison of the change during cooling obtained by subtracting B from A showed a substantial expansion in FRA area. A difference plot of recovery-control showed that the response returned to being non-monotonic with a similar tuning to control (E).

4.3.13 A high proportion of Multi-peaked FRAs changed to criterion

Multi-peaked FRAs formed the second most populous FRA type with 18 units studied. FRAs were recorded from each unit to both contralateral and binaural stimuli save for one unit which was presented with binaural stimuli only. This produced a population of 35 Multi-peaked FRAs.

The population of Multi-peaked FRAs showed a high proportion of area change during contralateral IC cooling with 20 of the 35 FRAs reaching the 20 % criterion of change. Of the FRAs which reached criterion, 9 decreased while 11 increased in area.

The contralateral FRAs of one unit which decreased in area are shown in figure 4.12. This unit had three discernible regions of excitatory response to contralateral stimulation. Each of these regions had a clear peak, and the threshold of each peak was within 10 dB of the other two. The lowest frequency peak had a CF of 1.2 kHz and a threshold at 35 dB attenuation, the middle peak had a CF of 3.1 kHz and a threshold of 30 dB attenuation, and the highest frequency peak had a CF of 7.2 kHz and a threshold of 40 dB attenuation. Each of these peaks was separated by more than one octave from its adjacent peaks. Each peak had an increase in threshold of 25 dB between the peaks in which no spikes were fired (Fig. 4.12A).

Cooling the contralateral IC produced a reduction in the area of the FRA from 213 bins to 131 bins, a decrease of 38.5 % (Fig. 4.12B). Interestingly, this change was not a homogenous decrease in the response of the entire area of the FRA, but rather the lower two frequency peaks increased in threshold and decreased in area while the high frequency peak was unchanged. The threshold of the lowest frequency peak increased to 20 dB attenuation and the middle frequency peak increased in threshold to 10 dB attenuation. Even with these changes in area, the CFs of all three peaks remained unchanged. Following termination of

contralateral IC cooling, the FRA regained an area and morphology similar to that in the control condition, although maximal firing rate did increase relative to control (Fig. 4.12C). The threshold of the two lower peaks also recovered back to control.

Differential changes in area across the FRA were observed in six of the twenty Multi-peaked FRAs which changed in area more than 20 %. Of these, five were due to differential decreases in the lower frequency peaks of the FRA. In four of these cases the area of the high frequency peak was almost unchanged while the low frequency peaks were greatly reduced (3) or increased (1) in area (Fig. 4.12). The other 14 Multi-peaked FRAs had changes across the entire FRA.

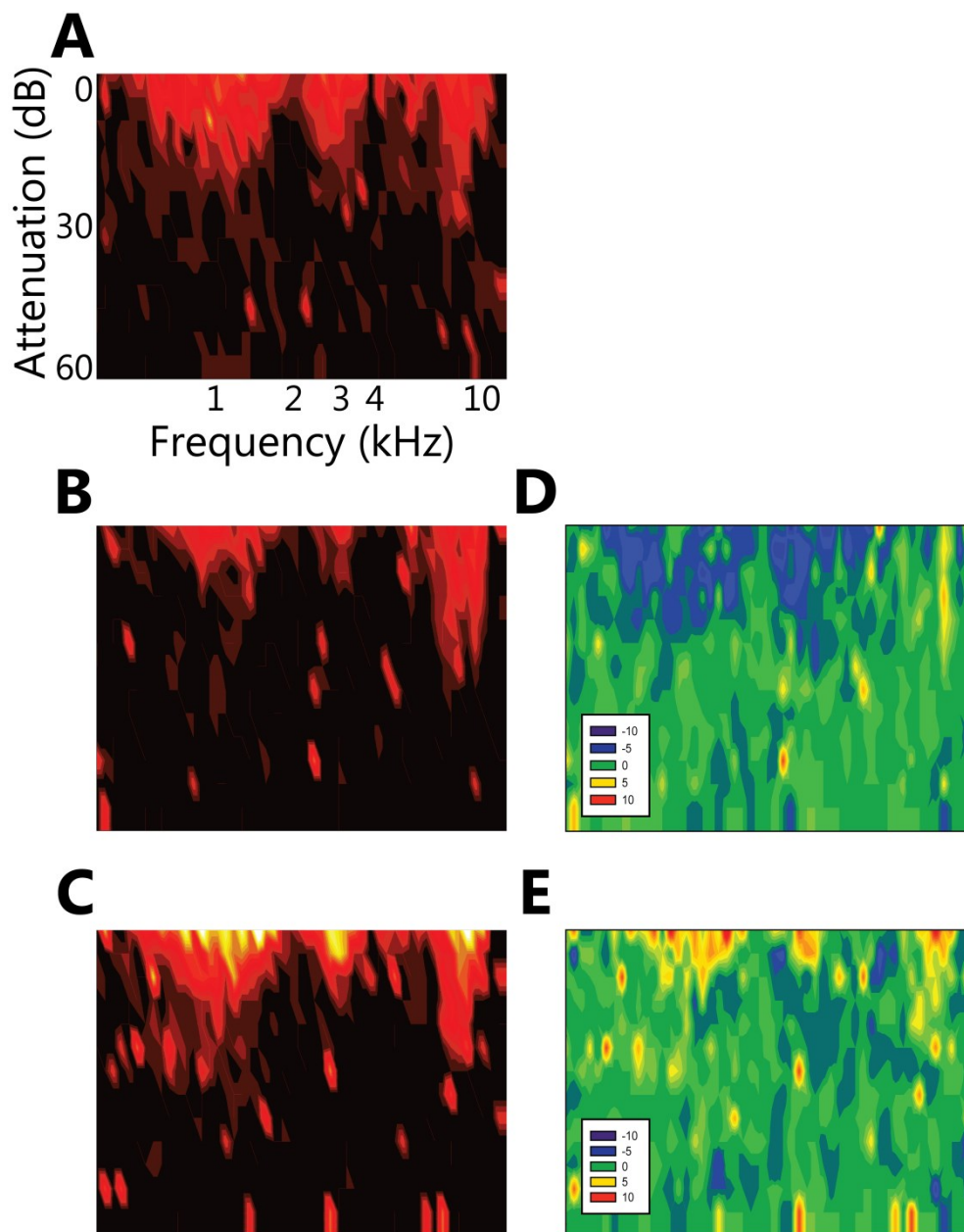


Figure 4.12 (A) Contralateral FRAs of a Multi-peaked unit with three distinct peaks of excitatory response with CFs of 1.2, 3.1 and 7.2 kHz. These peaks were not harmonically related. The threshold of the peaks was (in ascending frequency order): 35, 30 and 40 dB. (B) Contralateral IC cooling induced a reduction in area of 38.5 %. The threshold of the low and middle frequency peaks increased to 20 and 10 dB respectively, while the threshold of the high frequency peak remained unchanged. (C) Recovery of FRA area was complete within 10 minutes of stopping cooling. A difference plot (B-A) showed a reduction in the two lower frequency peaks during cooling (D). There was a rebound in firing rate on recovery as shown by a difference plot of recovery-control (E).

4.3.14 Broad FRAs had the largest areas of any FRA type and reduced in area

Five Broad units were studied in response to both contralateral and binaural stimulation while one was recorded in response to binaural stimulation only, producing a total of 11 FRAs. Broad FRAs had the largest areas of any FRA type. The median area of all other FRAs was 172 bins; the median of Broad FRAs was 328 bins. The area of Broad FRAs was significantly larger than the pooled areas of all other FRAs in this sample ($U = 465, P < 0.001$).

Of the 11 Broad FRAs, the area of 9 was reversibly reduced during contralateral IC cooling. One FRA increased in area and one had the same area as control throughout. Four of the FRAs which decreased in area reached criterion. The one Broad FRA which increased in area did so by 39.9 %. As well as being the only increase in area, it was also the largest change in area of any Broad FRA. The unit shown in figure 4.13 is an example of a Broad FRA which reduced in area during contralateral IC cooling and recovered similar tuning to the control condition following termination of cooling. Contralateral stimulation produced a FRA which had an area of 479 bins. The CF was 3.1 kHz about which the FRA was approximately symmetrical when plotted on a logarithmic frequency axis. The unit had a peak at the most sensitive point of the FRA with a threshold of 70 dB attenuation. At the highest level of stimulation (10 dB attenuation) the bandwidth spanned from 0.5 kHz to 14.4 kHz (Fig. 4.13A).

Contralateral cooling decreased the area of the FRA to 378 bins, a decrease of 20.3 %. At CF the threshold was raised to 54 dB attenuation. A similar change in threshold was seen across the entire FRA (Fig. 4.13B). The morphology of the FRA was unchanged by cooling. Recovery was rapid with a restoration of the shape and threshold seen in the control condition occurring within 10 minutes of cooling being stopped. The area of the FRA returned to 498 bins and the threshold at CF was the same as control.

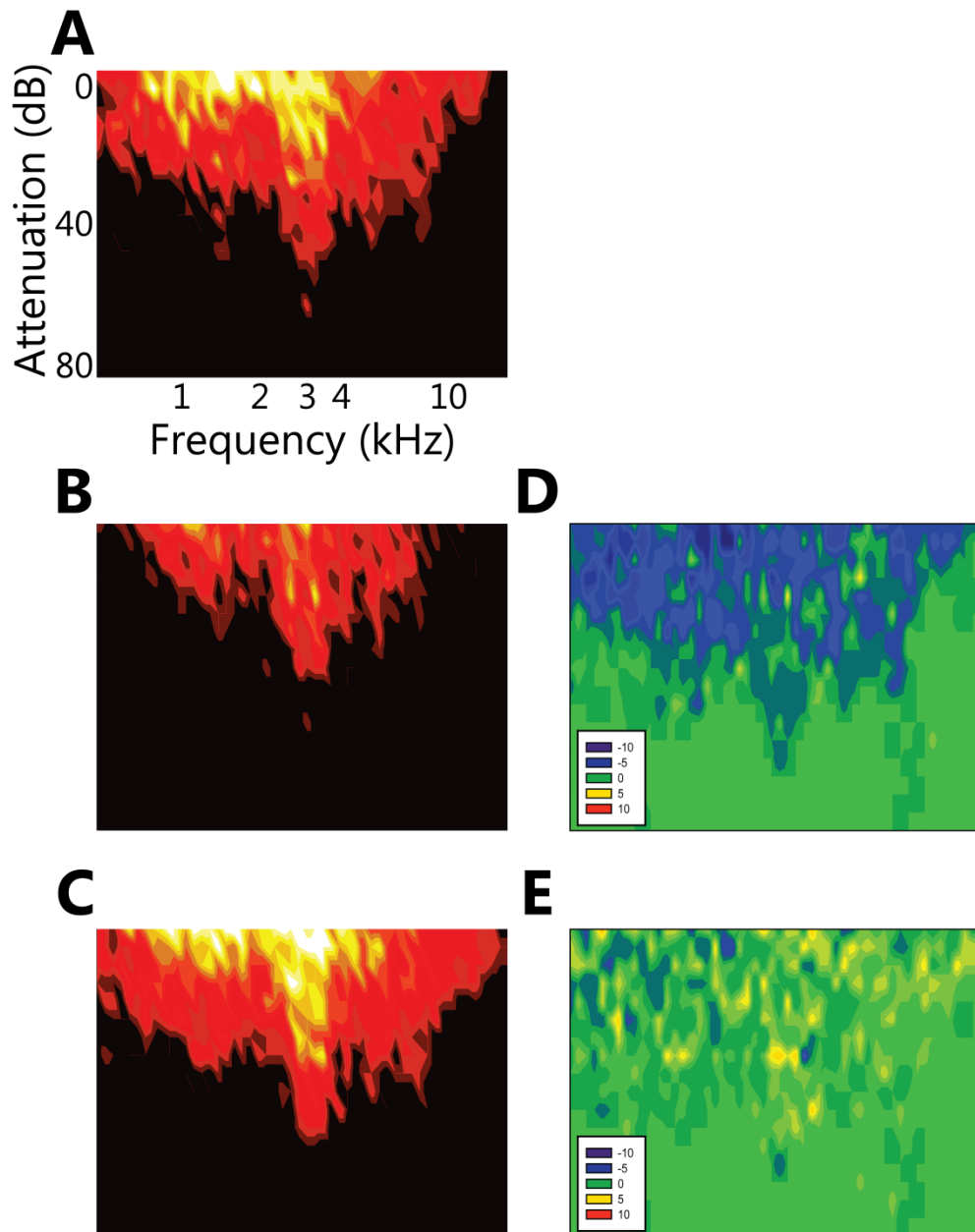


Figure 4.13 (A) Contralaterally driven FRAs of a Broad unit with a CF of 3.1 kHz and a threshold of 70 dB attenuation. Note the broad frequency tuning from 15 dB above threshold upwards. (B) Contralateral IC cooling caused a large reduction in the excitatory area across the FRA and an increase in threshold. (C) Recovery of the original area and shape occurred within 10 minutes of cooling being stopped. (D and E) Subtraction plots B-A and C-B respectively show changes during cooling occurred uniformly across the FRA and that recovery responses were similar to control.

4.3.15 Area changes of non-V-Shaped FRAs were bidirectional

Population analyses of non-V-shaped FRA types were not feasible due to the low numbers of each type in the dataset. In order to form a large enough group of FRAs where trends were discernible, non-V-shaped FRAs were pooled (Fig. 4.14). The change in FRA area during contralateral IC cooling was approximately Gaussian with a median of 1.01 (IQR = 0.77 to 1.32). Of the 82 FRAs in the non-V-shaped population, 37 decreased in area, 42 increased in area and three were unchanged during contralateral IC cooling. As shown in figure 4.14A, when compared to a hypothetical distribution with a median of 1, the population was not significantly different ($Z = -0.57$; $P = 0.57$). Examining the relative contribution of binaurally and contralaterally driven FRAs in the population showed little difference between the two (Fig 4.14B). The median of the contralaterally driven FRAs was 1.01 (IQR = 0.77 to 1.19) and that of binaurally driven FRAs was 0.97 (IQR = 0.72 to 1.50). The population of both contralaterally driven FRAs ($Z = 0.22$; $P = 0.83$) and binaurally driven FRAs ($Z = -0.63$; $P = 0.53$) showed no significant difference from a distribution with a hypothetical median of 1.

Comparing the distributions of FRA areas in the control and contralateral IC cool conditions found no significant differences for the population of contralateral ($Z = -0.07$, $P = 0.95$), binaural ($Z = -0.70$, $P = 0.48$) and pooled ($Z = -0.44$, $P = 0.66$) FRAs.

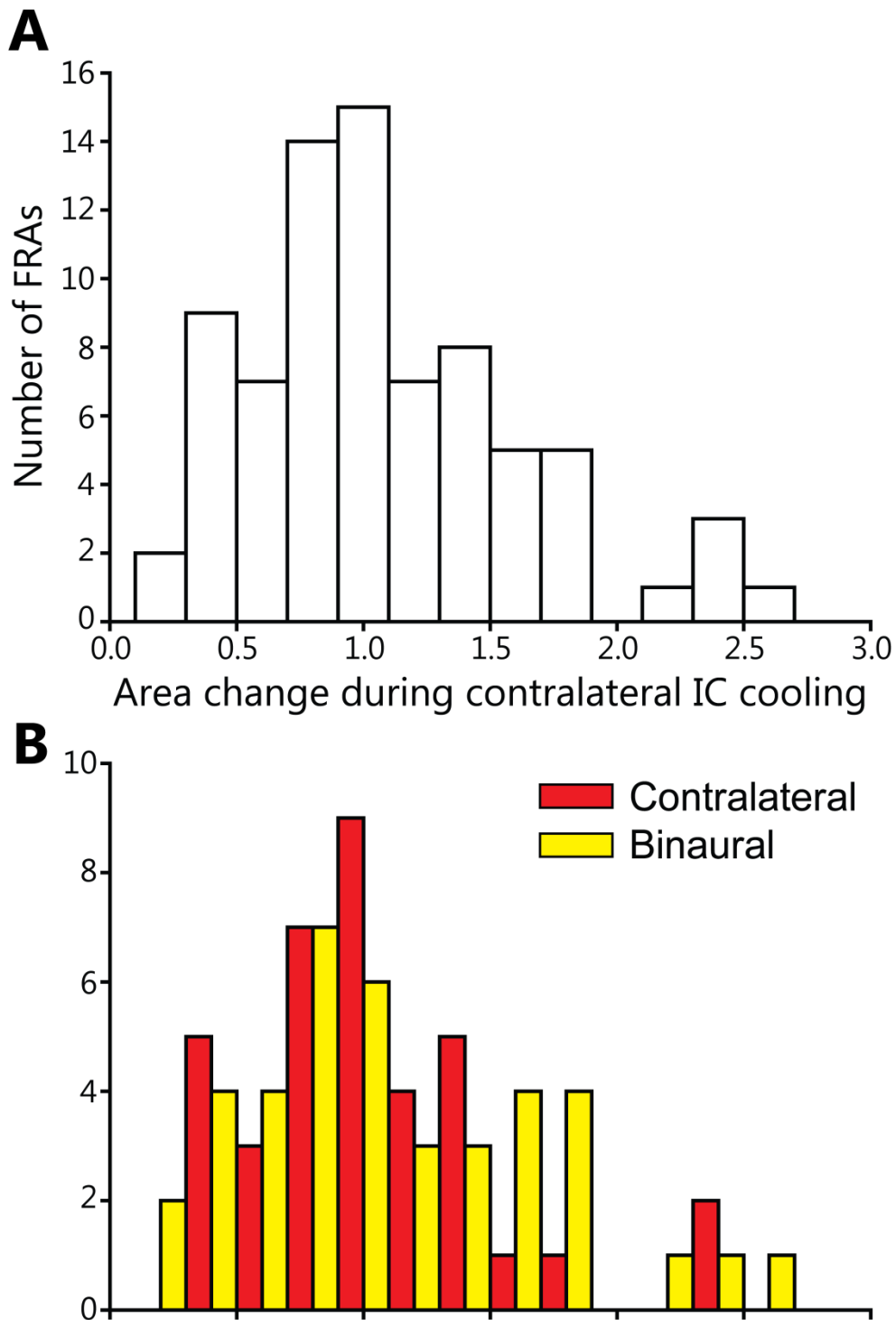


Figure 4.14 (A) The ratio of FRA area (contralateral IC cool/control condition) for all non-V-shaped FRAs. The distribution was asymmetrical due those FRAs which more than doubled in size. (B) The ratio of area change for contralaterally and binaurally driven FRAs. Contralateral IC cooling did not produce a significant change in the population of FRA areas for contralateral ($Z = -0.07$, $P = 0.95$), binaural ($Z = -0.70$, $P = 0.48$) or pooled ($Z = -0.44$, $P = 0.66$) groups.

4.3.16 V-shaped and non-V-shaped FRAs had similar distributions of control FRA areas

The similar number of FRAs in each group (78 V-shaped, 82 non-V-shaped) allowed for comparisons to be made between the distributions of area change observed in each.

The areas of V-shaped FRAs ($P = 0.004$) or non-V-shaped FRAs ($P < 0.001$) were not normally distributed in the control condition. There was no significant difference between the area of V-shaped and non-V-shaped FRAs in the control condition when both contralateral and binaural FRAs were pooled ($U = 2654$, $P = 0.064$) although the range of non-V-shaped FRAs was larger (Table 4.3 – top two rows). This was also true for comparisons between the contralateral FRAs (Table 4.3 – middle two rows; $U = 553$, $P = 0.81$), and binaural FRAs of both groups (Table 4.3 – bottom two rows; $U = 779$, $P = 0.36$).

Group	Min	25 %	Median	75 %	Max	Range
V-shaped	69	121	164	220	356	287
Non-V-shaped	29	101	212	342	570	541
Contra V-shaped	71	119	165	244	356	285
Contra non-V-shaped	45	115	222	356	570	525
Binaural V-shaped	69	129	163	214	343	274
Binaural non-V-shaped	29	88	208	327	547	518

Table 4.3 The distributions of V-shaped and non-V-shaped FRAs had similar medians and IQRs in the control condition (top two rows). This was also true for contralaterally (middle two rows) and binaurally (bottom two rows) driven FRAs. There was no significant difference between the groups due to the large overlap in the centre of the distributions.

4.3.17 Area changes of non-V-shaped FRAs were larger than V-shaped

Contralateral IC cooling expanded the range of FRA areas of both groups; V-shaped to 350 bins from 287, and non-V-shaped to 680 from 541. The median area of V-shaped FRAs was unchanged by cooling, while that of non-V-shaped FRAs reduced by 4 bins to 208 bins. During cooling there was still no significant difference between the area of both groups ($U = 2699$, $P = 0.09$). There was no significant difference between the area of contralateral FRAs ($U = 597$, $P = 0.20$) and binaural FRAs ($U = 755$, $P = 0.26$) either.

The differences in area between the two groups in the control condition are apparent in that the V-shaped FRAs (Fig. 4.15A; filled circles) comprised approximately half of the range of the non-V-shaped FRAs (Fig. 4.15A; open circles). The range of changes in the population of non-V-shaped FRAs was more than V-shaped FRAs (Fig. 4.15B). The range of area change of V-shaped FRAs was 1.20 (0.58 to 1.78), almost half the range of non-V-shaped FRA area changes which was 2.35 (0.20 to 2.54). The IQR of V-shaped FRAs was 0.25 (0.83 to 1.08) while the IQR of non-V-shaped FRAs was 0.55 (0.77 to 1.32). The median change of V-shaped FRAs was 0.95 while that of non-V FRAs was 1.01. There was no significant difference between the groups ($U = 2945$, $P = 0.39$).

These different ranges of change between the two groups were not due to a bias of the inherent wider range of non-V-shaped FRAs in the control stage. There were 56 non-V-shaped FRAs with areas within the range of the V-shaped FRAs in the control condition. The range of area change of these non-V-shaped FRAs was the same as that of the full population (0.20 to 2.54). The effect was not due to a single outlier on each edge of the distribution as the IQR was 0.64 (0.69 to 1.33) - wider than the full population. The median change of this subset of non-V-shaped FRAs was unchanged (1.00) and there was still no significant difference between the distributions of these non-V-shaped FRAs and the entire population of V-shaped FRAs ($U = 2083$, $P = 0.65$). As the distributions

overlapped but were spread over different ranges, an analysis of the skewness and kurtosis of each distribution was performed. The skew of the change in V-shaped (1.14) and non-V-shaped FRAs (1.09) was similar. The kurtosis of the change in V-shaped FRAs was much higher (2.69) than that of non-V-shaped FRAs (1.89). This was due to the much wider range of the latter distribution. To assess if there was a difference in the shape of the distributions, a two sample Kolmogorov-Smirnov test was performed. This found a significant difference between the change in V-shaped and non-V-shaped FRAs ($D = 0.24$; $P < 0.0001$).

4.3.18 Changes in absolute area were significantly different between V-shaped and non-V-shaped FRAs

To determine if the wider range of area changes of non-V-shaped FRAs was significantly larger than those seen in V-shaped FRAs the absolute change in area was calculated. This was done in an attempt to compare the extent of changes in FRA area irrespective of the direction of change. Comparison between the absolute change in V-shaped and non-V-shaped FRAs showed that the two distributions were different (Fig 4.15C). Absolute change in V-shaped FRAs (binned in intervals of 10 % change) had a sigmoidal shape with 67 of 78 FRAs falling in the first two bins. Non-V-shaped FRAs had a broader distribution with a peak shifted to the right of the V-shaped distribution.

The maximum absolute change of V-shaped FRAs was 0.78. The maximum of non-V-shaped FRAs was 1.54. The IQR of V-shaped FRAs was 0.18 (0.06 to 0.24). The IQR of non-V-shaped FRAs was 0.44 and shifted to the right of V-shaped FRAs (0.11 to 0.55). The median of V-shaped FRAs was 0.14, while that of non-V-shaped FRAs 0.30. There was a significant difference between the groups ($U = 2085$, $P < 0.001$). The absolute change in V-shaped data was best fit with a 3 parameter sigmoidal function (Fig. 4.15C - green line; $r^2 = 0.99$, $P < 0.0001$),

while that of non-V-shaped FRAs was fit best by a 4 parameter Weibull function (Fig. 4.15C - orange line; $r^2 = 0.98$, $P < 0.0001$).

To assess if these changes were due to the wider range of control non-V-shaped FRAs, only those non-V-shaped FRAs with areas within the bounds of the V-shaped distribution were compared. This analysis found that the maximum absolute non-V-shaped FRA change was the same as for the full distribution. The IQR shifted further to the right and increased to 0.45 (0.13 to 0.60). The median also shifted to the right, being 0.32, and the difference between this subset of non-V-shaped FRAs and the entire V-shaped FRA population was still significant ($U = 1262$, $P < 0.001$).

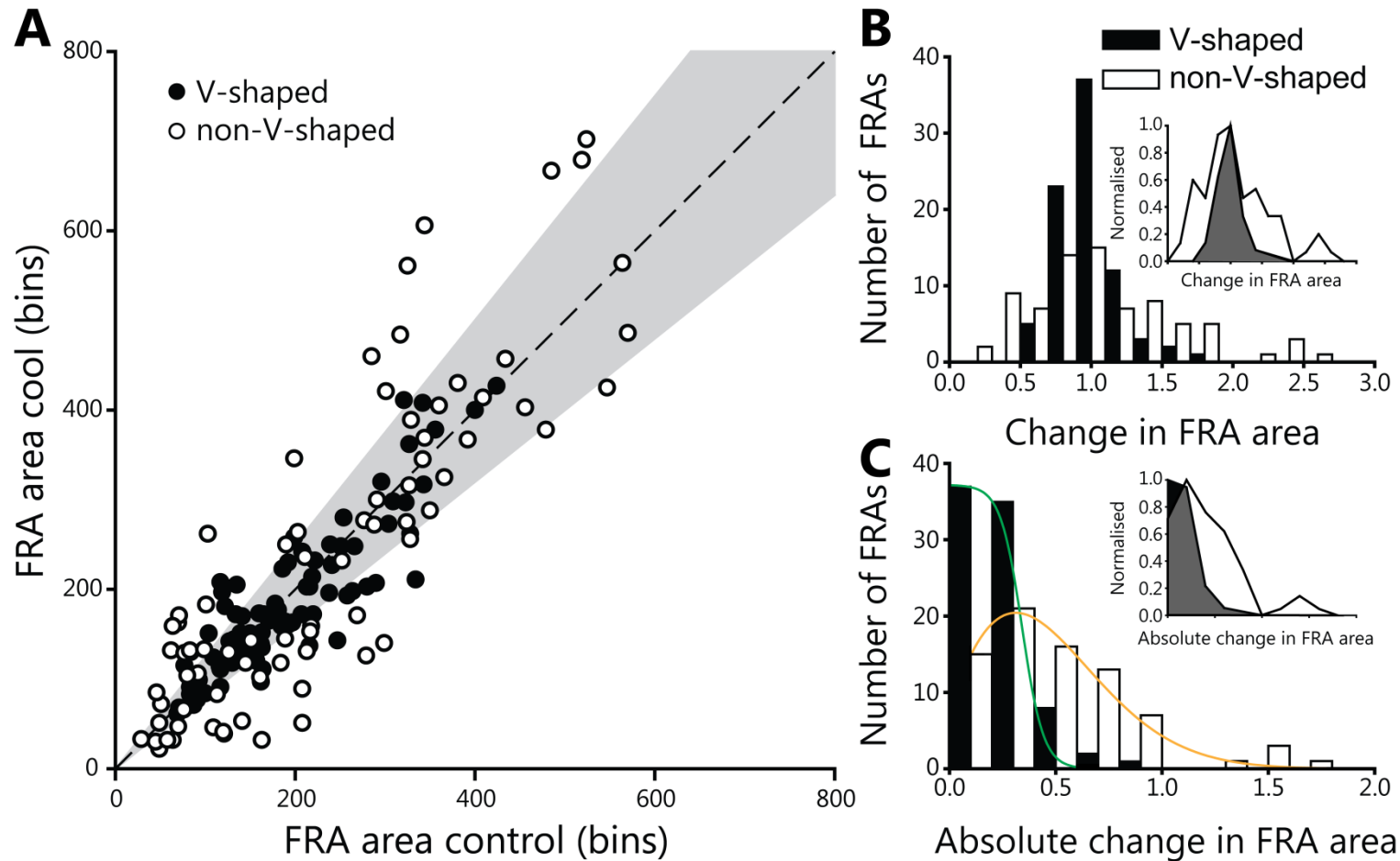


Figure 4.15 (A) Distribution of changes in FRA area of all units. Units were grouped into either V-shaped or non-V-shaped FRAs. The range of changes in non-V-shaped FRAs was wider than V-shaped FRAs, even for those non-V-shaped FRAs which had a control area within that of the V-shaped population. (B) The change in non-V-shaped FRAs was greater than V-shaped but both distributions overlapped around their medians. Inset shows the wider range of changes observed in non-V-shaped FRAs when the groups were normalised. (C) The difference in the absolute ratio of contralateral IC cool to control area between V-shaped and non-V-shaped FRAs was statistically significant ($U = 2085$, $P < 0.001$). Inset shows the different shapes of the population of changes in the two groups after normalisation.

Having found a significant difference between the absolute changes in area between V-shaped and non-V-shaped FRAs, the breakdown for each FRA type which contributed to this analyses is shown in table 4.4. The percentage of FRAs which had an absolute change greater than 0.5 showed a difference between the groups. Almost all V-shaped FRAs changed by less than 0.5. This was also true for Broad FRAs - possibly due to their larger control FRA areas compared to other FRA types. Of the other four non-V-shaped FRA types 40 % (26 of 65) of these groups (Low Tilt, Narrow, Closed, Multi-peaked) changed by more than 0.5 in absolute area.

Group	# FRAs	#FRAs absolute area change > 0.5	% FRAs absolute area change > 0.5
V monotonic	78	3	3.8
V non-monotonic	6	0	0
Low Tilt	4	2	50
Narrow	20	9	45
Closed	6	3	50
Multi-peaked	35	12	34
Broad	11	0	0
Total V-shaped	84	3	3.6
Total non-V-shaped	76	26	31.7
Total non-V-shaped (excluding Broad)	65	26	40

Table 4.4 The number of each FRA type that showed an absolute change in area of > 0.5 showed a clear difference between V-shaped and non-V-shaped FRAs. A large percentage of non-V-shaped FRAs (with the exception of Broad FRAs) changed by > 0.5.

More neurons tended to change in the same direction to both contralateral and binaural stimulation. Of the 76 units which received both stimuli sources, 46 changed in the same direction during CoIC cooling, while 30 changed in opposite directions. For 26 units both decreased in area and for 20 both increased in area. Eleven neurons decreased to contralateral stimulation and increased to binaural stimulation. The other 19 units increased to contralateral stimuli and decreased to binaural stimuli. There was no clear trend in the direction or magnitude of changes to each stimulation source across the population.

4.4 Discussion

This Chapter has examined the effects of unilateral IC deactivation by cryoloop cooling on the FRAs of single units in the IC contralateral to cooling. The main finding is that the FRAs of neurons in the IC can be influenced by activity from the contralateral IC. This finding has confirmed the findings of Malmierca *et al.* (2003) in a much larger sample of neurons and with a different but comparable technique. Further to which it has been found that there are differential extents to which the areas of FRAs are modulated, with non-V-shaped FRAs changing significantly more than V-shaped FRAs (Fig. 4.15).

The distribution of FRA types in this sample had a near equal number of V-shaped (44) and non-V-shaped (40) FRAs. Previous studies where frequency responses of IC neurons in anaesthetised or awake mammals were recorded have also tended to have a higher proportion of V-shaped responses than non-V-shaped (Ehret and Moffat, 1985; Casseday and Covey, 1992; Yang *et al.*, 1992; Egorova *et al.*, 2001; LeBeau *et al.*, 2001; Hernández *et al.*, 2005; Alkhatib *et al.*, 2006).

As in all other previous studies of FRA changes, statistical comparisons were not used and a criterion of change was implemented. As the comparisons during contralateral IC cooling were made re initial control values, recordings from three neurons were made without experimental manipulation to evaluate if area measures were stable over time. Over the course of an hour, even a Narrow unit, which was more likely to change above criterion than FRAs with a large control area due to chance, did not change in area by more than 18 % (Fig. 4.2). Similar confirmations of FRA stability over time have been reported previously (LeBeau *et al.*, 2001; Malmierca *et al.*, 2005).

4.4.1 FRA classification in the IC

In all auditory nuclei, spectral processing is dependent upon the frequency analysis of the cochlea which is first encoded by AN fibres (Kitzes and Semple, 1985; Malmierca and Hackett, 2010). That there are increasing numbers of FRA types between the AN, the CN and the IC (AN: Kiang (1965); Evans (1972); CN: Evans and Nelson (1973); IC: LeBeau *et al.* (2001); Hernández *et al.* (2005)) suggests a growing complexity of spectral analysis at the single unit level along the ascending auditory pathway.

At the level of the IC, these divergent receptive fields form an assortment of up to nine different morphologies (Hernández *et al.*, 2005) of which seven were found in the course of this study (Fig. 4.1). The extremes of each morphological type are clearly distinguishable from one another, yet there are a number of examples in this sample and others which to some degree or another, fall between the definitions of two FRA types (Palmer *et al.*, 2013). Consequently, no objective classification protocol to date has found a method by which 100 % of FRAs can be classified into discrete groups (Sutter, 2000; Hernández *et al.*, 2005; Palmer *et al.*, 2013). As a result of this, qualitative classification, while not ideal, is as valid as any other current method of classifying FRAs. Evidence for this comes from the slight variation between qualitative and quantitative methods used by Sutter (2000) in cat A1. One consequence of this classification method is that the criteria which need to be applied are broad so as to encompass a large proportion of the sample with some similar features. As all these classifications segment the total distribution into discrete categories, the data are perhaps best described as points on a continuum (Palmer *et al.*, 2013). However, as clear distinctions can be made between many FRAs, it is helpful to compare the differences between distinct FRA morphologies.

The majority of FRAs in this dataset were described by the criteria set out by LeBeau *et al.* (2001). Units which were classified as being 'Double-peaked' in

that study were renamed in this analysis as 'Multi-peaked'. This broader phrasing allowed for the inclusion of all FRAs which had two discernible peaks while also including FRAs which had more than two distinct excitatory peaks (e.g. Fig. 4.1F and Fig. 4.12). There were six units which had FRAs that were unclassifiable using the criteria of LeBeau *et al.* (2001). These FRAs resembled the broadly tuned FRAs described by Kelly *et al.* (1991) and the U-shaped FRAs described by Hernández *et al.* (2005) in the rat. Broad FRAs in the guinea pig had one or more small peaks at threshold, each of which protruded out from the main body of the excitatory FRA by 5 to 10 dB. Thus, despite the wide range of frequencies to which the unit responded, some frequency selectivity could occur near threshold in Broad FRAs.

4.4.2 FRA formation in the IC

That the frequency receptive fields of neurons increase in complexity between AN and CN, and between CN and IC, suggests that the receptive fields of neurons are transformed at each stage of the sub-thalamic ascending auditory pathway. Iontophoretic blockade of GABAergic inhibition in the IC has shown that for V-shaped neurons the excitatory response increased primarily within the existing response area (Palombi and Caspary, 1996; LeBeau *et al.*, 2001; Xie *et al.*, 2005). This suggests that the V-shaped FRA morphology is inherited from a lower stage in the ascending auditory system, while local or afferent inhibition scales the firing rate of the FRA. Further recent support has been provided by comparisons of the tuning of IC V-shaped FRAs in guinea pig with those recorded in CN and AN, which found similar bandwidths at 10 re threshold at all three stages of the auditory pathway (Palmer *et al.*, 2013). Comparisons between AN and IC V-shaped responses in decerebrate cat also found similarities (Ramachandran *et al.*, 1999).

While similarities were found between V-shaped IC responses in both guinea pig and cat, there are points of disagreement between the study of

Ramachandran *et al.* (1999) and the majority of the literature. This study found a much lower number of V-shaped units than their type 'I' (Narrow) and type 'O' (Closed) than those reported in the intact preparation (Egorova *et al.*, 2001; LeBeau *et al.*, 2001; Hernández *et al.*, 2005; Alkhatib *et al.*, 2006; Palmer *et al.*, 2013). Furthermore, all V-shaped responses were found in low frequency regions, a finding which is incongruous to the majority of the literature using anaesthetised or awake recordings. The one study which found a similar distribution of V-shaped responses was interestingly also performed in the decerebrate cat (Chase and Young, 2005). This suggests that a possible species or preparation difference may be the reason for these contrasting findings. Another important difference between the results of Ramachandran *et al.* (1999) is the long (200 ms) duration stimuli employed, which is different to the short tones (50 to 75 ms) used by most other studies. Due to the long duration of their stimuli, Ramachandran *et al.* (1999) decided to discard the initial 50 ms of their response and only analyse the remaining 150 ms. As such, their data are not directly comparable with the majority of the literature. These differences mean that the claims of strong correlations between frequency response types and sound localisation cues (Ramachandran *et al.*, 1999; Davis, 2002), and therefore possible inheritance of response type from lower brainstem nuclei in the IC, must be discussed in light of this. Another explanation could be that in the decerebrate preparation the axotomisation of the brachium of the IC lead to death or malfunction of IC neurons. This may have led to a recalibration of the balance of intra-collicular processing and a higher level of neuronal inheritance from lower centres.

The area of a large proportion of non-V-shaped FRAs which could be classified as Closed or Narrow using the criteria of LeBeau *et al.* (2001), have been found to expand when local GABAergic inhibition in the IC was blocked by iontophoresis of bicuculline (Yang *et al.*, 1992; Wang *et al.*, 1996; Hall, 1999; LeBeau *et al.*, 2001; Xie *et al.*, 2005). A similar finding has also been observed in

MGB (Suga *et al.*, 1997). These data are suggestive that local inhibition at each stage in the ascending auditory pathway contributes to the creation of *de novo* FRA types and varying degrees of inhibition form different shaped responses.

4.4.3 Comparison of V-shaped and non-V-shaped FRA area changes

The main finding of this Chapter is that neurons in one IC can modulate the spectral processing undertaken by the contralateral IC. The data confirm and expand upon the findings of Malmierca *et al.* (2003) which showed that commissural projections influence the response properties of neurons in the IC and that these influences can mediate expansion or contraction of FRA areas. Furthermore, the proportion and magnitude of the change in FRA area was much larger in neurons with non-V-shaped FRAs than in those with V-shaped FRAs.

4.4.4 Changes in V-shaped FRAs

The responses of V-shaped FRAs to contralateral IC cooling fit with previous data in which disinhibition was manifest as firing rate changes within the existing FRA and not changes in area (Vater *et al.*, 1992; Yang *et al.*, 1992; Palombi and Caspary, 1996; LeBeau *et al.*, 2001; Xie *et al.*, 2005). The observed changes in V-shaped FRAs could be explained by a change in general excitability of the neuron (Figs. 4.4 and 4.5). Excitatory drive is near threshold at the edges of tuning and a slight up or down regulation of either excitation or inhibition could cause the unit to fire in response to more or fewer frequencies and hence expand or contract. Some V-shaped responses contained bins within their FTC which did not contain spikes (see control in Figs. 4.4, 4.5 & 4.6). This was likely due to the stochastic nature of the response of the unit to one presentation of each frequency-level combination within the FRA. For units where the excitatory drive was near threshold this may have produced a distribution of responses which, when rescaled by contralateral IC cooling, may

have become more homogenous, and appear to have changed in area while the edges of tuning were largely unchanged.

Due to the spontaneous rate in the vast majority of units being low, any inhibitory sidebands which were present in the FRA were not observable. As such, whether those V-shaped FRAs which changed beyond criterion did so due to a modulation of flanking or more general inhibition is unknown.

4.4.5 Changes in non-V-shaped FRAs

As all non-V-shaped FRAs reflect to varying extents a transformation from the V-shaped responses of the AN, they were grouped. (Although that is not to deny that V-shaped FRAs in IC are processing the spectral characteristics of auditory stimuli in a more complex or integrative manner than at level of the AN.)

Previous studies have justified grouping non-V-shaped FRAs on the basis that they represent a continuum of inhibitory effects (LeBeau *et al.*, 2001; Hernández *et al.*, 2005). However, the broad tuning of Multi-peaked FRAs at 40 dB above threshold and Broad FRAs at most levels above threshold makes it hard to justify such a classification here. These FRA types are consistent with a continuum of both excitatory and inhibitory integration along the ascending auditory pathway.

The non-V-shaped FRAs found in this distribution show a high similarity to those described previously in guinea pig (LeBeau *et al.*, 2001) as well as other species such as cat (Ehret and Merzenich, 1988), horseshoe bat (Vater *et al.*, 1992), moustache bat (Yang *et al.*, 1992), mouse (Egorova *et al.*, 2001), rat (Hernández *et al.*, 2005) and chinchilla (Alkhatib *et al.*, 2006). These data give strong indication that there is a high level of similarity in the morphology of FRAs in mammalian IC, though any cross species generalisations are made with caution. Even with this caveat, the many conserved FRA types, in spite of the

differing audiograms and ecological niches occupied by these various species, implies that FRA IC morphologies are likely formed by similar interactions between excitation and inhibition.

Non-V-shaped FRAs are a heterogeneous distribution of morphologies (Fig. 4.1), each of which is distinct from the next due to the differential confluence of excitation and inhibition involved in their formation. Ideally one would compare differences between each FRA morphology, however, the small numbers of some types do not allow for such comparisons to be made.

The expansion of Closed FRAs observed here has been noted previously following iontophoretic block of inhibitory receptors in the IC (Yang *et al.*, 1992; Wang *et al.*, 1996; Hall, 1999; LeBeau *et al.*, 2001; Xie *et al.*, 2005) and MGB (Suga *et al.*, 1997). This indicates that the CoIC inputs to Closed units may be exclusively inhibitory or they modulate the local inhibition that forms them. With local iontophoretic application of bicuculline Narrow FRAs also expanded. The opposite was found here in that Narrow FRAs decreased in area. The implication of this is that innervation of Narrow FRAs is in opposition to that of Closed FRAs supporting the idea that intercollicular projections can mediate inhibitory and excitatory effects in a selective manner. However, low numbers in both groups mean that these claims can only be speculative.

The finding that non-V-shaped FRAs were modulated in area more than V-shaped FRAs is of importance as it is the first time it has been demonstrated that the CoIC exerts a differential modulatory effect on the frequency selectivity of neurons in the IC. This again supports the idea that the effects of intercollicular projections are selective for their targets.

4.4.6 Changes in Multi-peaked FRAs were more than opposite

There has been little discussion in the literature about Multi-peaked FRAs in the IC. Multi-peaked FRAs had clearly distinguishable, though heterogeneous

morphologies. As with previous descriptions of Multi-peaked FRAs in IC (Casseday and Covey, 1992; Hernández *et al.*, 2005) and A1 (Sutter and Schreiner, 1991), for the vast majority of units, peaks were not harmonically related.

Multi-peaked FRAs are topographically located in the dorsal region of Cat A1 (Sutter and Schreiner, 1991). In rat IC the majority of Multi-peaked FRAs have a CF in the mid-range of frequencies from 6 to 12 kHz (Hernández *et al.*, 2005). Multi-peaked FRAs in this sample peaked in the middle range of frequencies in the guinea pig audiogram (8 to 16 kHz), showing a degree of similarity to those of Hernandez and colleagues. In the only other description of the tonotopy of Multi-peaked responses, the number of this type was found to increase with CF (Portfors and Wenstrup, 2002). However, this study only sampled up to 60 kHz, while the species examined, the moustached bat, is known to have responses over 110 kHz (Kössl and Vater, 1985). It is therefore possible that the Multi-peaked responses were in fact highest in the middle of the audiogram of that species too.

These findings support the contention of Hernández *et al.* (2005) that Multi-peaked FRAs may be a functionally specialised class of IC neurons that are involved in the processing of complex sounds, which represent a specific range of frequencies within the audiogram. Both guinea pig 'scream' and 'whistle' calls are formed from upward frequency modulations that span up to approximately 18 kHz. If the hypothesis of Casseday *et al.* (1994) that IC neurons are tuned to biologically relevant ranges holds true for guinea pig, then these units may be able to convey more information about such calls than other FRA types.

The high number of Multi-peaked FRAs which reached criterion (57 %) suggests that they too are different from V-shaped FRAs and that their spectral responses are strongly influenced by the contralateral IC. As there are multiple areas of excitatory response, these FRAs are likely formed from a complex interplay of

different sources of excitation across a broad spectral range. As such, the approximately even number of those which increased (11) or decreased (9) to criterion likely reflects changes in multiple parameters of CoIC mediated input during CoIC deactivation.

It is interesting to note that most Multi-peaked FRAs which increased in area expanded across the entire range of their excitatory response while more than half of those that decreased in area showed a differential change in the responses around their peaks. This suggests a differential role for the CoIC in scaling the responses of Multi-peaked FRAs. One methodological consideration is that only responses up to around 8 kHz were deactivated in the contralateral IC. Five of the six FRAs which changed differentially did so for peaks at frequencies below 8 kHz, while the peaks with CFs above 8 kHz were unchanged. This is consistent with the deactivation of equivalent frequency inputs from the contralateral IC.

Multi-peaked FRAs are not typically associated with responses in the CNIC, and it may be possible that these FRAs were sampled from the DCIC. Commissural projections originating in the DCIC appear to have a more diffuse pattern of inputs to the contralateral DCIC compared to the more tonotopic projections originating from CNIC neurons (Malmierca *et al.*, 2009). The different patterns of projections from DCIC and CNIC via the CoIC allow for speculation as to the different roles in auditory processing that these pathways may underlie.

The DCIC may be involved in a global scaling of responses in contralateral IC across a wide frequency range, while tonotopic projections, which are known to innervate the matching contralateral lamina, may have frequency selective inputs that operate only within the spectral range of their lamina. While the population of responses recorded here is too low to provide compelling evidence for this assertion at this stage and the exact location of the recorded

neurons are also unknown, future investigations may illuminate the differential functional roles of the CoIC in influencing Multi-peaked FRAs.

4.4.7 Broad FRAs are a distinct FRA type which were modulated differently than other FRA types

Broad FRAs have been barely discussed in the literature to date. Broadly tuned frequency responses were first contrasted with the narrow frequency tuning of the CNIC by Erulkar (1959). It has since been reported that units in the DCIC and LNIC are more broadly tuned than the CNIC (Aitkin *et al.*, 1972; Merzenich and Reid, 1974; Aitkin *et al.*, 1975; Syka *et al.*, 2000). Aitkin *et al.* (1975) characterised the responses of single neurons in the external nucleus (anatomically defined from an atlas of the cat brainstem as defined by Berman (1968)) as 'broad' in the anaesthetised rabbit. Broadly tuned FRAs have also been reported in other studies (Hernández *et al.*, 2005; Palmer *et al.*, 2013). Without histological verification, it is hard to know where the Broad FRAs recorded in this study were located.

The changes observed in Broad FRAs were surprisingly most similar to the changes seen to Narrow FRAs. As 83 % of Broad FRAs reduced in area while only one increased, the CoIC appears to be providing excitation to these units. The reduction in area tended to be across the range of the FRA, indicating a change in non-selective excitatory or inhibitory drive, rather than the removal of spectrally selective inhibition. Broad FRAs most likely receive afferent projections from a wide range of sources. In order to calibrate these multiple inputs, the CoIC could be increasing the dynamic range of the neuron in order that small perturbations in the drive to the unit do not drive the cell as easily as they may if the threshold were lower. This would require the summation of numerous different inputs in order to cause the neuron to fire and give the cell more integrative space in its neural output. Iontophoretic application of GABA

receptor agonists and antagonists to Broad FRAs may elucidate more of the nature of these response types.

It is not surprising that Broad FRAs, which fire across a large proportion of the audiogram, reduced in FRA area rather than increased. It may be argued that their initial FRA area may be a limiting factor prohibiting expansion. However, one Broad unit did expand by ~40 %, which argues against this position. Furthermore, if the direction of change is discounted, the fact that Broad FRAs tended to change indicates a CoIC influence on their FRAs which is stronger than V-shaped Monotonic FRAs.

4.4.8 No commissural selectivity for monaural or binaural stimuli

The findings of this study contrast with those of Malmierca *et al.* (2003) who found changes in FRA area to be 'more dramatic' in response to binaural than monaural stimulation. As with that study, a range of changes were seen in response to either stimulation type. There were changes in FRA area in the same direction to both stimulation types for 46/76 units (61 %) while the remaining 30/76 (39 %) changed in opposite directions to each stimulus type. While these differences may be borne out of species or methodological differences, a major factor may be the small sample size in that study. Indeed, examples of changes similar to each of those described by Malmierca *et al.* (2003) were found in the course of this study, suggesting that greater sampling may have helped clarify this issue, something which was also reported by the same group in a later paper (Malmierca *et al.*, 2005).

4.5 Conclusion

Commissural fibres are known to project from one IC to the other in a tonotopic manner (Beyerl, 1978; Adams, 1980; Brunso-Bechtold *et al.*, 1981; Aitkin and Phillips, 1984; González-Hernández *et al.*, 1986; Coleman and Clerici, 1987; Saldaña and Merchán, 1992; Malmierca *et al.*, 1995). CoIC fibres which emanate from the CNIC have been shown to project in a point to point manner as well as diffusely innervating the contralateral frequency band lamina and DCIC (Malmierca *et al.*, 2009). The large proportion of units that changed in FRA area during contralateral IC cooling supports the hypothesis that commissural projections are extensive and integral to auditory processing. In the IC there are many spectrally distinct neuronal responses. The CoIC selectively and differentially innervates these different response types, supporting a view of specific and complex processing occurring between the ICs. The commissural influence on the FRA area of IC neurons was much stronger on non-V-shaped FRAs than V-shaped FRAs. The CoIC is therefore an essential component of the frequency analysis performed by neurons in the IC and the increased complexity of FRA shapes observed in IC compared to CN and AN is influenced by CoIC input.

Chapter 5. Changes in Parameters of Tuning and Selectivity Derived from FRAs Induced by Contralateral IC Deactivation

5.1 Introduction

The findings presented in the previous Chapter showed differential changes in FRA area depending on whether a unit had a V-shaped or non-V-shaped response. These data suggest a distinction between how differing FRA types in the IC are influenced by the CoIC. These data alone do not however, allow for comparison between FRAs of the many additional parameters which can be derived from each FRA and how these parameters were modulated by the cooling paradigm.

FRAs contain a wealth of information in addition to the area of the excitatory response. These measures include the CF, threshold, and tuning bandwidth of each unit and they provide important information about different aspects of each neuron's frequency response characteristics in response to tonal stimuli. As each of these measures requires thorough and detailed consideration in their own right, they have been separated from the FRA area data presented in Chapter 4.

5.1.1 Characteristic frequencies of IC neurons and tonotopy

Tonotopy is one of the fundamental organising principles of all mammalian auditory nuclei (Tasaki, 1954; Tunturi, 1955; Rose *et al.*, 1963; Bourk *et al.*, 1981). Tonotopy has even been observed in several nuclei which are outside what is classically regarded as the 'auditory pathway' - for example the amygdala (Chen *et al.*, 2012). The tonotopic organisation of the IC was one of the earliest noted characteristics of auditory responses observed within the IC (Katsuki *et al.*, 1958; Rose *et al.*, 1963; Merzenich and Reid, 1974). Functional measurements of IC tonotopy have been made using numerous experimental methods such as

single unit recording (Rose *et al.*, 1963; Aitkin *et al.*, 1970; Clopton and Winfield, 1973; Malmierca *et al.*, 2008), c-FOS immunohistochemistry (Ehret and Fischer, 1991), 2-deoxyglucose autoradiography (Webster *et al.*, 1983; Huang and Fex, 1986) and fMRI (Baumann *et al.*, 2011).

The development of tonotopy in the IC occurs in the early post-natal weeks (Aitkin and Moore, 1975; Romand and Ehret, 1990; Rübtsamen, 1992; Romand, 1997), and once formed it persists throughout life (Willott *et al.*, 1991; Keithley *et al.*, 1994). The frequency representation of IC neurons can be shifted in response to auditory stimuli when paired with electrical stimulation (Gao and Suga, 1998; Yan and Suga, 1998; Gao and Suga, 2000). These transient shifts in CF are thought to involve dynamic modulation of IC neurons via the corticofugal system. As each AC projects to the contralateral IC via the CoIC (Winer *et al.*, 2002; Bajo and Moore, 2005; Bajo *et al.*, 2007), it may be hypothesised that removing these inputs may shift the frequency representation in the contralateral IC. The cooling paradigm which was established in Chapter 3, allows for investigation into whether the CF of IC neurons can be modulated by deactivation of the contralateral IC.

5.1.2 Threshold as a measure of IC neuron sensitivity to sound

Whether an auditory neuron fires spikes in response to a pure tone depends of both the level and frequency of the stimulus. For all neurons which respond to pure tones, the frequency range over which sound driven spikes are elicited reduces with level until only a single frequency evokes firing; this is defined as the CF. The threshold of a unit is defined as the minimum stimulus level which elicits at least one driven spike at any frequency. For the vast majority of IC neurons this occurs at one frequency, although some units (Multi-peaked) have more than one peak in their excitatory response and therefore have multiple thresholds at differing frequencies.

Thresholds of single units can span a wide range of levels throughout the auditory system from AN (Tasaki, 1954; Kiang, 1965; Evans, 1972) upwards, including IC (Harnischfeger, 1978). By definition the threshold of a unit provides a measure of how sensitive that unit is to pure tone stimulation. Due to the combination of inhibitory and excitatory fibres which project via the CoIC (González-Hernández *et al.*, 1996; Hernández *et al.*, 2006), and the modulation of local IC neurons by the CoIC (Moore *et al.*, 1998), deactivating the contralateral IC may alter the balance of inhibition and excitation and thus the sensitivity of neuronal responses in the IC. No detailed descriptions of the effects of contralateral IC deactivation on the threshold of IC neurons have been reported to date.

5.1.3 Bandwidth as a measure of frequency selectivity in IC neurons

The objective measure “Q” was first adapted for use as a measure of the sharpness of tuning curves in the AN of cat by Kiang (1965). This measure was derived from the quality factor which has been used by engineers to describe the damping of an oscillator. In its engineering implementation it is derived from the bandwidth of the tuning function (measured 3 dB down from the peak) divided by its centre frequency. At the level of the AN, the Q_{10} of a tuning curve is given by dividing CF by the bandwidth 10 dB above threshold because the bandwidth at 3 dB is difficult to assess. This measure was taken up as a useful measure of auditory neuronal bandwidth by numerous investigations in nuclei such as DCN (Goldberg and Brownell, 1973), IC (Aitkin and Moore, 1975; Aitkin *et al.*, 1975; Palmer *et al.*, 2013), MGB (Symmes *et al.*, 1980; Calford and Webster, 1981), A1 (Phillips and Irvine, 1981), and belt regions of auditory cortex (Phillips and Irvine, 1982). This measure increases with frequency in a linear manner – a fact that has complicated comparisons of bandwidth in auditory nuclei across their tonotopic axes. Due to the high variability in bandwidth of auditory neurons at high levels re threshold (c.f. Closed and Narrow FRAs with Broad

FRAs at high stimulation levels in Chapter 4), measures of bandwidth at higher levels re threshold may provide more information than Q_{10} (Palmer *et al.*, 2013).

Whitfield (1968) first proposed the square root transformation as means to remove the dependency of Q_{10} on CF. Recordings made from the MGB of the freely moving cat appeared to show that this transformation did indeed remove the frequency dependence of Q_{10} measurements (Whitfield and Purser, 1972). Calford *et al.* (1983) supported this assertion based on recordings at multiple levels of the auditory system in the pentobarbitone and ketamine anaesthetised cat. Data from adult (Semple and Kitzes, 1985) and neonatal (Kitzes and Semple, 1985) gerbil IC using the same anaesthesia as (Calford *et al.*, 1983) appeared to verify the frequency independence of this measure.

However, Moore *et al.* (1983) found that in the pentobarbitone anaesthetised ferret IC that the square root transform did not remove the positive correlation of bandwidth with CF. As such, the use of the square root transform as a means to eliminate this confounding relationship with frequency has dwindled. The only paper since this finding to have implemented the square root transform, did so in concert with both raw bandwidth and Q_{10} analyses of the same data (Rutkowski *et al.*, 2003). At present there is no compelling evidence to displace Q_{10} as the principal measurement of auditory neuronal bandwidth and it is still used in the current literature (Sumner and Palmer, 2012; Palmer *et al.*, 2013).

Given that differential changes in area were found in Chapter 4 between different FRA morphologies, it would seem obvious that changes will also be found in parameters derived from these FRAs. The experiments described in this Chapter sought to quantify and compare these changes. Measures of CF, threshold and bandwidth were taken from each FRA in each condition and then compared at both single neuron and population levels.

The aim of this Chapter was to analyse objectively several parameters which can be derived from the FRA of an IC neuron in each condition and examine if any patterns of change occurred. The CF of each neuron was hypothesised to be formed by the cumulative selective afferent input it receives from each projecting afferent nucleus. If this were so, removal of the CoIC input would not alter the CF as the selective deactivation would not modify the ascending afferent input to the neuron. As threshold has been shown previously to be modulated by contralateral IC deactivation (Malmierca *et al.*, 2003), it was hypothesised that the thresholds of many IC neurons would be influenced by CoIC input and when removed, a change in threshold would be observed. The bandwidth was hypothesised to be unchanged by CoIC removal near threshold, due to similarity of IC neuron bandwidths near threshold, irrespective of their shape (Palmer *et al.*, 2013). At higher levels the possible influence of CoIC of inhibition helping to form complex responses such as Narrow and Closed types allowed for the hypothesis that there would be differential changes between FRA types at high levels re threshold.

5.2 Methods

The surgical and recording procedures used to acquire these data are as described in Chapter 2. The data which were used to derive the results presented here are the same as which were presented in Chapter 4.

The measurements which were made from each FRA were: CF, threshold, and bandwidth at 10 (BW₁₀) and 40 dB (BW₄₀) above threshold. These measures were derived using the method of Ingham *et al.* (2006). Responses to the lowest level of stimulation across all frequencies within the FRA were used to define the mean spontaneous firing rate. Those bins within each FRA which contained values greater than two standard deviations of the mean spontaneous rate were then determined. For each frequency the lowest stimulus level at which the spike rate exceeded the mean spontaneous rate plus two standard deviations was deemed to be the excitatory threshold for that frequency. The array of excitatory thresholds was then fitted with a 10th order polynomial which produced the excitatory frequency tuning curve (FTC) of the FRA. For more complex FRA shapes, a 10th order polynomial was not always accurate in reflecting the response of a neuron. A reduction in the number of interpolation points of the polynomial often resolved this issue.

The minimum point of the FTC was used to define the CF and threshold of the unit (Fig 5.1). The bandwidth of the FTC at 10 dB and 40 dB were then measured relative to this point. For Multi-peaked units the most sensitive peak was used to make these measures.

This method was highly accurate at estimating each measure for V-shaped, Low Tilt, Multi-peaked and Broad units, but for Narrow and Closed units the fit of the polynomial tended to be poor. For most Narrow and Closed units, reducing the order of the polynomial did not produce a satisfactory estimate of the CF and threshold. In these cases, the minimum point of the excitatory threshold array

was used to define CF and threshold and linear interpolations along the low and high frequency slopes were used to measure the BW_{10} and BW_{40} .

The Q_{10} and Q_{40} of each FRA were derived using the method described by Kiang (1965):

$$"Qx \text{ dB}" = \frac{CF}{\text{Bandwidth at } x \text{ dB re threshold}}$$

The square root transform (Whitfield, 1968; Whitfield and Purser, 1972; Calford *et al.*, 1983) was calculated from the same data:

$$\text{SqRT} = \sqrt{H} - \sqrt{L}$$

Where H is the value of the high frequency slope of the FTC at x dB above threshold, and L is the value of the low frequency slope at the same point re threshold.

The cube root transform was also calculated using the same method as above with cube root substituted for the square root.

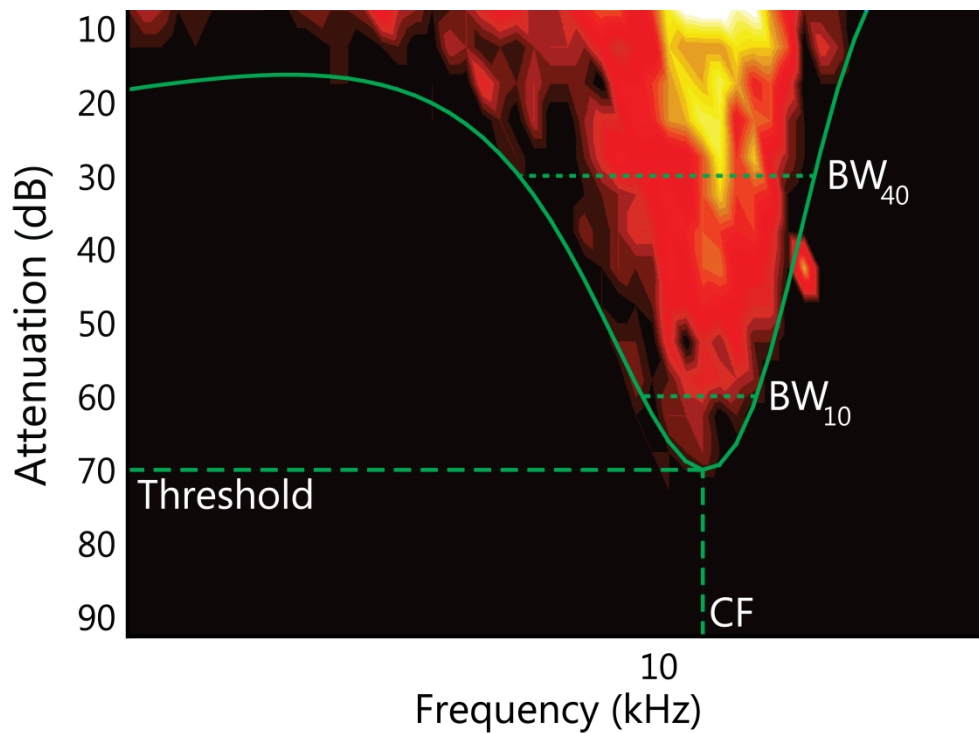


Figure 5.1 The frequency threshold curve derived by calculating, at each frequency presented, the bin representing the lowest sound level in which firing exceeded the mean spontaneous firing rate by more than 2 standard deviations. A 10th order polynomial was fitted to this array to define the frequency tuning curve (FTC) of each FRA. This was calculated from the raw data, not the interpolated points used to display the data. Measurements were derived from the minimum of the polynomial to determine the CF and threshold of the unit (long dashed lines). Bandwidths at 10 dB (BW_{10}) and 40 dB (BW_{40}) above threshold were also derived from the polynomial by measuring the intercept with the high and low frequency slopes at 10 and 40 dB above threshold respectively (short dashed lines).

5.2 Results

All results presented here were derived from measurements taken from the 84 units presented in Chapter 4.

5.2.1 Contralateral cooling did not change the CF of IC neurons

The CF of almost all FRAs was unchanged by contralateral IC deactivation (Fig. 5.2A). Combining contralateral and binaural FRAs, there were 160 FRAs in the population. The CF of 5 FRAs increased more than 20 %, while 2 FRAs decreased by more than 20 %. The CF of 114 (71.3 %) changed by less than a tenth of an octave (Fig 5.2B). One FRA did clearly shift in CF; this was caused by disinhibition of the unit which produced a 15 dB reduction in threshold and an increase in CF. All other FRAs which reached the 20 % criterion did so with minor changes in the shape and area of their FRA and as such, these changes were attributed to variability of the response.

The change in CF of contralaterally driven FRAs was not significantly different from a hypothetical distribution with a median of 1 ($Z = -0.14$, $P = 0.84$), nor was that of the binaurally driven FRAs ($Z = -1.53$, $P = 0.13$). This was also true for all FRAs with both types of stimulation pooled ($Z = -1.34$, $P = 0.18$). There was also no significant difference between the change in CF of contralaterally and binaurally driven FRAs ($U = 3009$, $P = 0.52$).

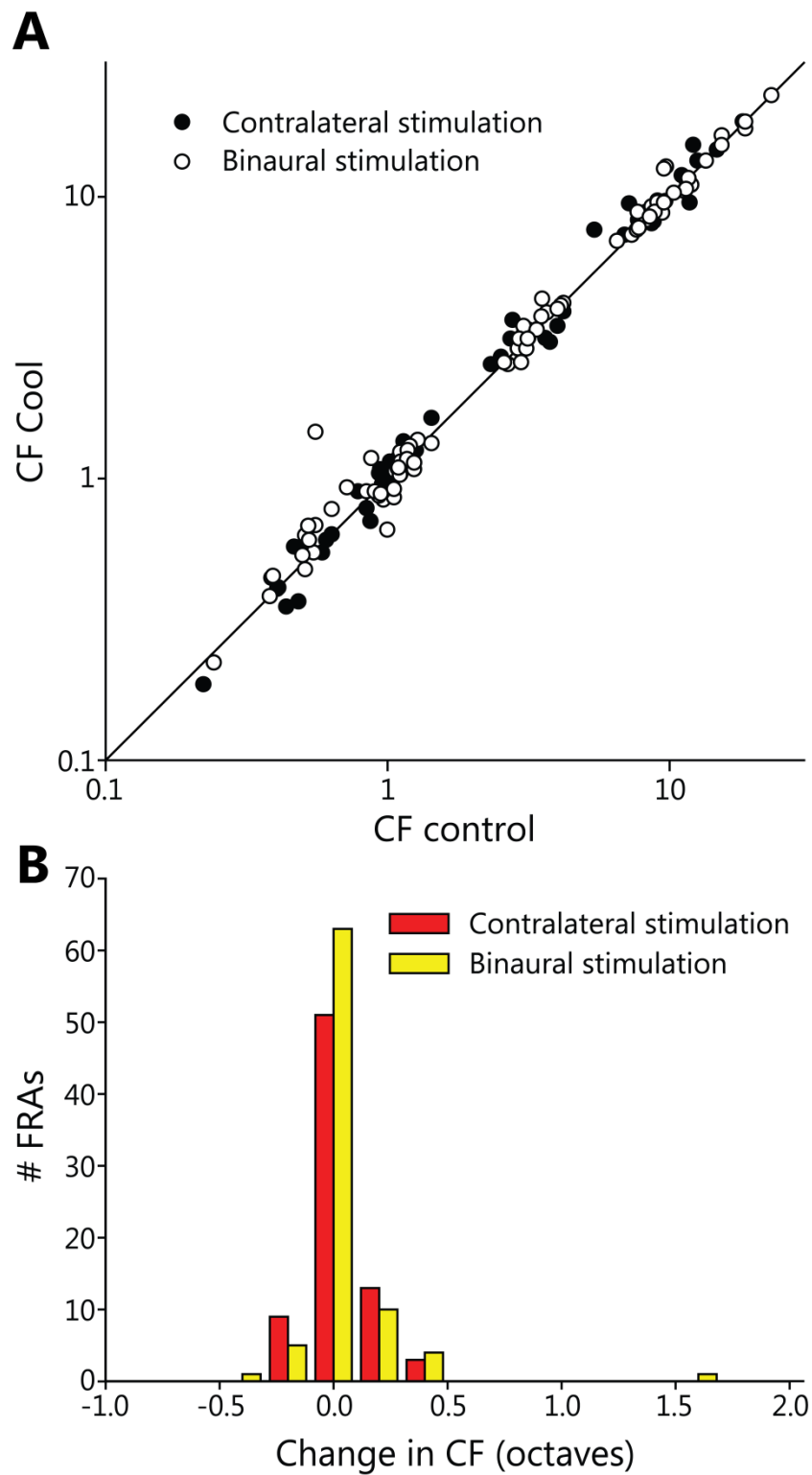


Figure 5.2 (A) Contralateral IC cooling did not significantly change the CF of FRAs ($Z = -1.34$, $P = 0.18$). (B) Of the 160 FRAs, the CF of 159 (99.4 %) changed by less than half an octave and 114 (71.3 %) changed by less than a tenth. There was no significant difference between the change in CF of contralateral and binaurally driven FRAs ($U = 3009$, $P = 0.52$).

5.2.2 Threshold was modulated by contralateral IC deactivation

Figure 5.3 shows the minimum threshold of all FRAs in this dataset in the control condition. The most sensitive FRAs had thresholds close to but above the behavioural audiogram of the guinea pig up (Heffner *et al.*, 1971; Evans, 1972). The most sensitive FRAs with CFs above ~6 kHz were at least 10 dB above the audiogram.

The thresholds of Narrow units were raised relative to other groups in the sample; while this may be due to the sample size, other groups with fewer FRAs in the dataset, such as Broad and Closed FRAs, had units with lower thresholds. Narrow units with thresholds near the behavioural audiogram have been described using the same preparation and protocols (LeBeau *et al.*, 2001), supporting the case for low sampling being the possible cause.

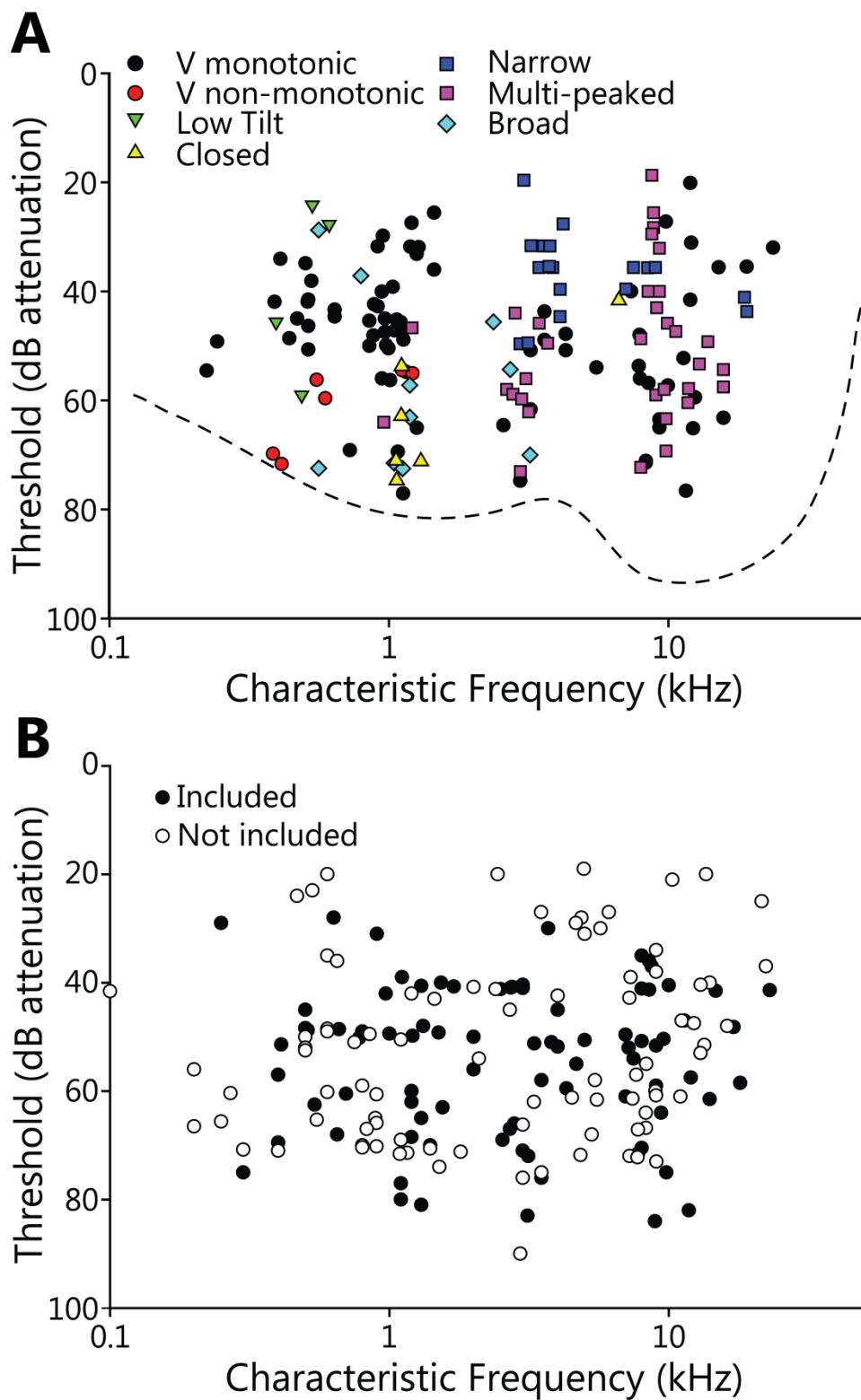


Figure 5.3 (A) The minimum threshold and CF (measured as in figure 5.1) of FRAs, reported here as studied with the cooling paradigm, plotted as a function of CF. (B) As (A) but with the initial estimate of threshold and CF, including the additional units recorded but which did not fulfil the recovery criterion (filled circles). This shows there was no bias in the sample to cause the distribution observed in (A).

Thresholds of a high proportion of units were changed by contralateral IC deactivation (Table 5.1). More FRAs increased than decreased (Fig. 5.4); of the 160 FRAs, 97 showed an increase in threshold, 35 by more than 20 %; 58 decreased in threshold, 25 by more than 20 %; 5 were unchanged. During contralateral IC cooling, both bounds of the IQR raised from 37 - 58 dB to 36 - 53 dB. The median threshold was raised from 48 dB to 44 dB. This increase in the distribution of thresholds was statistically significant ($Z = -3.4$, $P = 0.001$).

Group	Min	Max	25%	75%	Median	Significant? (Wilcoxon sign rank test)
V monotonic control	20.2	77.1	40.0	55.9	47.7	Yes
V monotonic cool	17.5	74.4	37.1	52.7	44.9	$Z=-2.1, P=0.03$
V non-monotonic control	54.5	71.7	55.1	69.8	57.9	No
V non-monotonic control	51.2	67.7	52.7	67.7	55.7	$Z=-1.8, P=0.08$
Low tilt control	24.2	59.0	26.0	52.3	36.7	No
Low tilt cool	15.0	50.0	15.0	48.4	30.9	$Z=-1.5, P=0.14$
Narrow control	20.0	50.1	32.0	40.7	36.0	No
Narrow cool	10.0	48.0	31.0	42	36.0	$Z=-0.1, P=0.93$
Closed control	41.3	74.4	53.5	70.9	66.7	No
Closed cool	46.7	79.9	46.7	77.1	60.1	$Z=-0.94, P=0.35$
Multi-peaked control	18.7	73.1	44.5	59.5	54.4	Yes
Multi-peaked cool	18.4	75	36.0	56.2	43.0	$Z=-2.21, P=0.03$
Broad control	28.7	72.5	47.8	71.1	63.1	Yes
Broad cool	34.0	62.6	42.7	58.8	53.3	$Z=-2.4, P=0.02$
Total control	18.7	77.1	38.6	58.4	48.4	Yes
Total cool	10.0	79.9	36.0	53.7	44.2	$Z=-3.4, P<0.001$

Table 5.1 Threshold changes by FRA classification. Contralateral IC deactivation produced a median 4 dB increase in threshold across the population of 160 FRAs. The median threshold of every FRA type increased, except Narrow FRAs, which were unchanged.

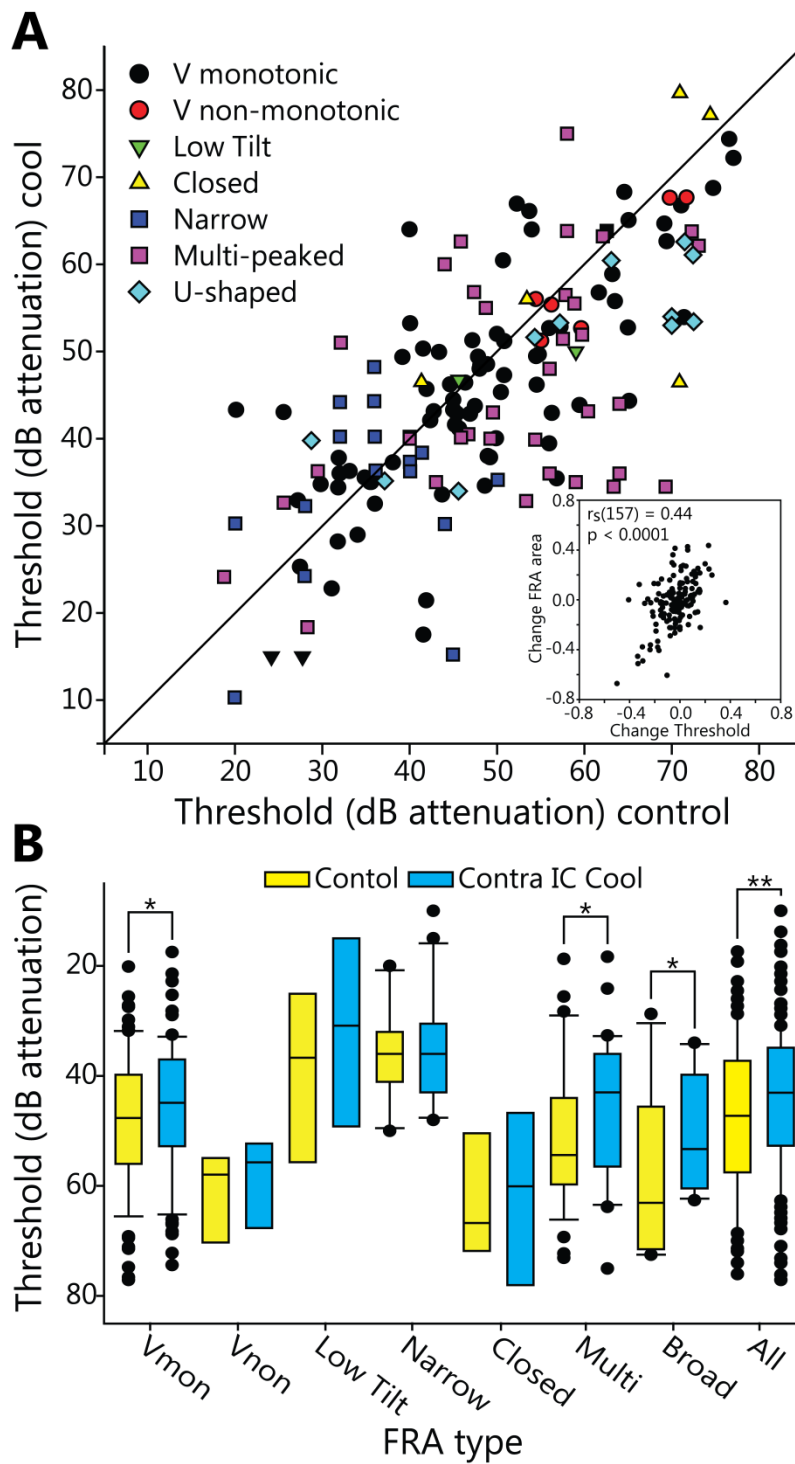


Figure 5.4 (A) Changes in threshold during contralateral IC cooling. The majority of FRAs increased in threshold. Inset: Change in threshold and change in FRA area had a significant positive correlation, showing these measures may be derived from shared mechanisms. (B) Contralateral IC cooling significantly raised threshold across all units (paired Wilcoxon sign rank test: $Z = -3.4$, $P = 0.001$). The distributions of V-shaped monotonic, Multi-peaked and Broad FRAs were raised significantly. The median threshold of all classes of FRA (other than Narrow), were raised during contralateral IC cooling.

The median threshold of six of the seven FRA classes was increased by deactivation of the contralateral IC (Fig. 5.4B). The median threshold of Narrow FRAs was unchanged. The increases in threshold were significant for V-shaped monotonic, Multi-peaked and Broad FRAs. It is interesting to note that for V-shaped non-monotonic and Low Tilt FRAs the median and IQR were also raised during contralateral IC cooling, though the small sample sizes precluded any patterns from emerging.

A more general comparison of the change in threshold of V-shaped and non-V-shaped FRAs showed similar medians in each distribution in the V-shaped ($\tilde{x} = 0.96$; IQR = 0.90 to 1.05; Range = 0.42 to 2.15) and non-V-shaped ($\tilde{x} = 0.92$; IQR = 0.74 to 1.13; Range = 1.59 to 0.33) groups, but the IQR was much broader in the latter. There was no significant difference between these groups ($U = 2850$; $P = 0.24$). However, due to the much broader range of changes in the non-V-shaped FRA group, the absolute change in threshold was significantly larger than in the V-shaped group ($U = 2169$; $P < 0.001$). As this finding matched the significant difference between the absolute change in V-shaped and non-V-shaped FRA areas, a correlation analysis was performed to assess if the change in threshold and change in area were related. A significant positive correlation was found between the change in threshold and the change in FRA area of all FRAs recorded ($r_s(157) = 0.44$; $P < 0.001$).

To determine if the threshold changes observed were uniform across all FRAs or differentially distributed, two further analyses were performed. The first was a test to investigate if there was any variability in the change of threshold relative to the initial sensitivity of the FRA.

Figure 5.5A is a box plot of the change in threshold seen in four bands of FRA sensitivity under control conditions. Thresholds in the control population ranged from 19 to 77 dB attenuation. Responses were grouped based into one of four equally sized groups (19 to 33, 33. to 48, 48 to 63, 63 to 77 dB attenuation).

There were 27 FRAs in the highest threshold group, 8 increased in threshold (5 to criterion), while 19 decreased (12 to criterion), producing a median quotient of change of 1.17 and an IQR of 0.90 to 1.35. This distribution was not significantly different from a distribution with a hypothetical median of 1 ($Z = -1.91$, $P = 0.06$). Thresholds were not significantly different during cooling than in control ($Z = -1.99$, $P = 0.46$).

The second highest threshold group contained 51 FRAs. The median threshold of the group was unchanged and contralateral IC cooling did not induce a significant difference in threshold ($Z = -0.22$, $P = 0.83$). The median change was 0.99 with an IQR from 0.91 to 1.11. The threshold of twenty six of these FRAs increased (6 to criterion), 22 decreased (10 to criterion) and 3 were unchanged. This group was also not significantly different from a hypothetical distribution with a median of 1 ($Z = -0.16$, $P = 0.87$).

The second lowest threshold group was also made up of 51 FRAs, of which 37 increased in threshold (14 to criterion), while only 13 decreased (3 to criterion) while one was unchanged. The median threshold was raised from 55 to 50 dB attenuation by contralateral IC deactivation - a significant increase ($Z = -3.62$, $P < 0.001$). This group had a median change of 0.91, an IQR of 0.77 to 1.01. This group was significantly different from a hypothetical distribution with a median of 1 ($Z = -3.67$, $P < 0.001$).

The remaining 31 FRAs formed the group with the lowest threshold responses. Of these, 26 increased in threshold (10 to criterion), 4 decreased (0 to criterion) and 1 was unchanged. The median threshold increased from 70 to 62 dB attenuation. This was a significant increase in threshold ($Z = -4.19$, $P < 0.001$). The median change of this group was 0.88, with an IQR of 0.76 to 0.96, and this group was also significantly different from a hypothetical distribution with a median of 1 ($Z = -4.19$, $P < 0.001$).

A Kruskal-Wallis one way ANOVA found a significant difference between the change in threshold of these groups ($H(3) = 22.75, P < 0.001$). Dunn's multiple pairwise comparisons found three significant differences in threshold between groups. Two of these were between the highest threshold group and the two lowest threshold groups. The other was between the second highest threshold group and the lowest threshold group (Fig. 5.5A). These significant differences emphasise the opposite directions of change in threshold amongst units with different control thresholds. Lower sensitivity FRAs increased in threshold while FRAs with high control sensitivity reduced during contralateral IC cooling (Fig. 5.5A).

A second analysis investigated if there was a CF dependent change in threshold in the sample. Much like the previous analysis, the population was divided into near equal groups. The population was split into those with CFs lower than 1, between 1 & 2, 2 & 4, 4 & 8, and those with a CF greater than 8 kHz. The change in threshold within these groups is shown in figure 5.5B.

All groups had a range which spanned either side of 1. Unlike grouping by control threshold, there was no obvious pattern of change in the median, IQR or range as CF increased. The IQR and range tended to increase as CF increased, with the 1 to 2 kHz group bucking this trend. None of the groups were significantly different from a distribution with a hypothetical median of 1 (<1 kHz: $Z = -1.82, P = 0.069$; 1-2 kHz: $Z = -1.08, P = 0.28$; 2-4 kHz: $Z = -0.85, P = 0.39$; 4-8 kHz: $Z = -1.83, P = 0.61$; > 8: $Z = -1.31, P = 0.19$). There was no significant difference between the change in these groups ($H(4) = 2.58, P = 0.63$).

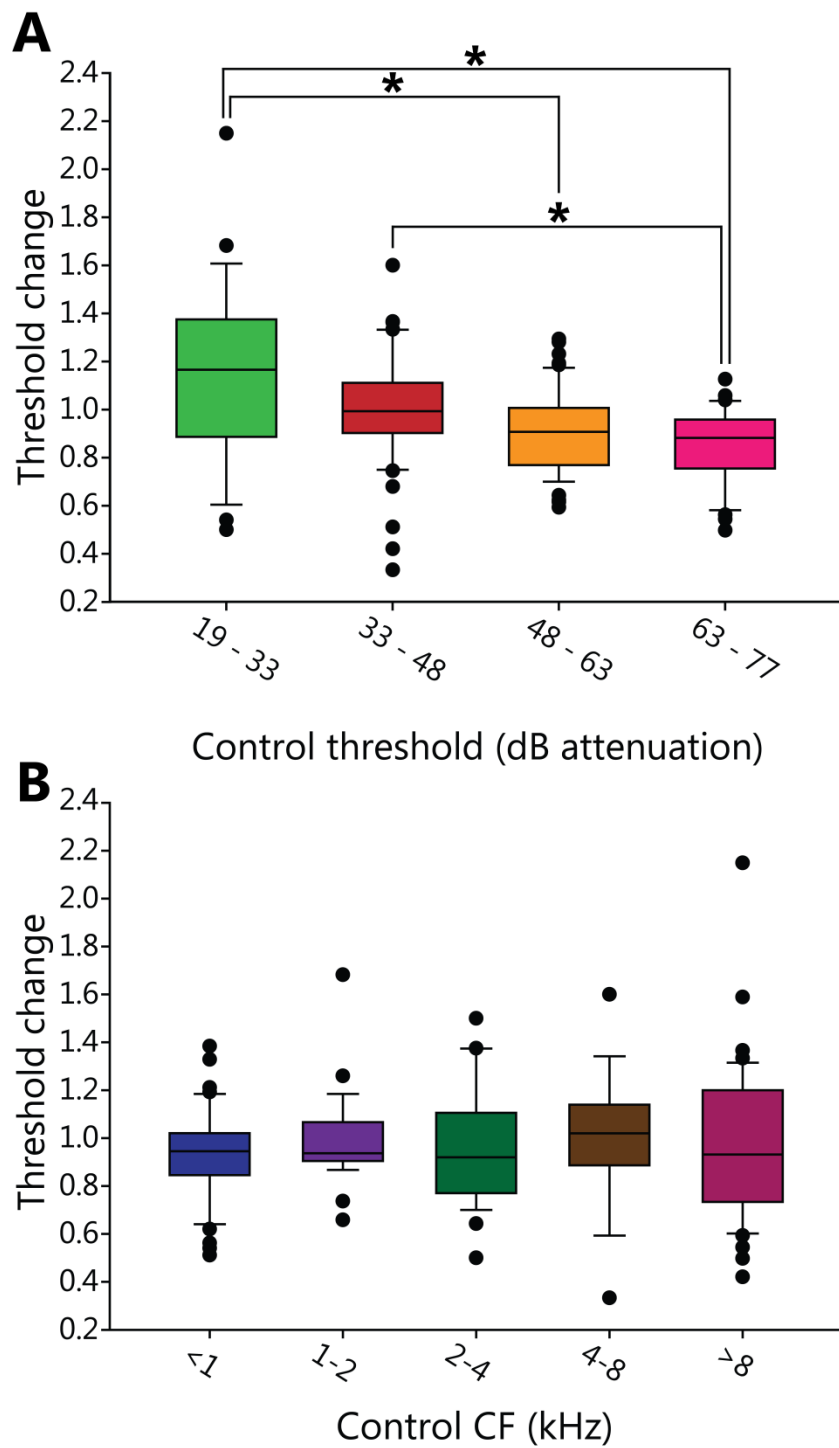


Figure 5.5 (A) Threshold change was dependent on control threshold. FRAs which had a lower threshold in the control condition tended to increase in threshold during contralateral cooling. Threshold in the two lowest threshold groups increased significantly. (B) There was no significant difference in threshold change as a function of control CF.

5.2.3 Threshold changes were similar to monaural or binaural stimulation

Changes in threshold were not dependent on whether stimulation was monaural or binaural (Fig. 5.6). Thresholds in the control condition in response to contralateral stimulation had an IQR from 38 to 56 dB and a median of 47 dB (Fig. 5.6A – left). Contralateral IC cooling raised the IQR (36 to 54 dB), and the median also rose to 44 dB (Fig. 5.6A – left middle). This change was statistically significant ($Z = -2.3$, $P = 0.02$). Control thresholds to binaural stimulation had an IQR from 39.1 to 62.3 dB, and the median was 49 dB (Fig. 5.6A – right middle). Contralateral IC cooling raised the IQR (36 to 53 dB), and the median to 47 dB (Fig. 5.6A – right). This was also a significant change ($Z = -2.5$, $P = 0.01$).

The changes in threshold induced by contralateral IC deactivation measured in response to contralateral and binaural FRAs are shown in figure 5.6B. Because cooling raised threshold irrespective of stimulation type the median of both groups was less than 1, (0.94 for both contralateral and binaural stimulation). The IQR for contralateral FRAs was 0.85 to 1.07, while for binaural FRAs the IQR was 0.81 to 1.10. There was no significant difference between the change in contralaterally and binaurally driven thresholds ($U = 3131$, $P = 0.84$).

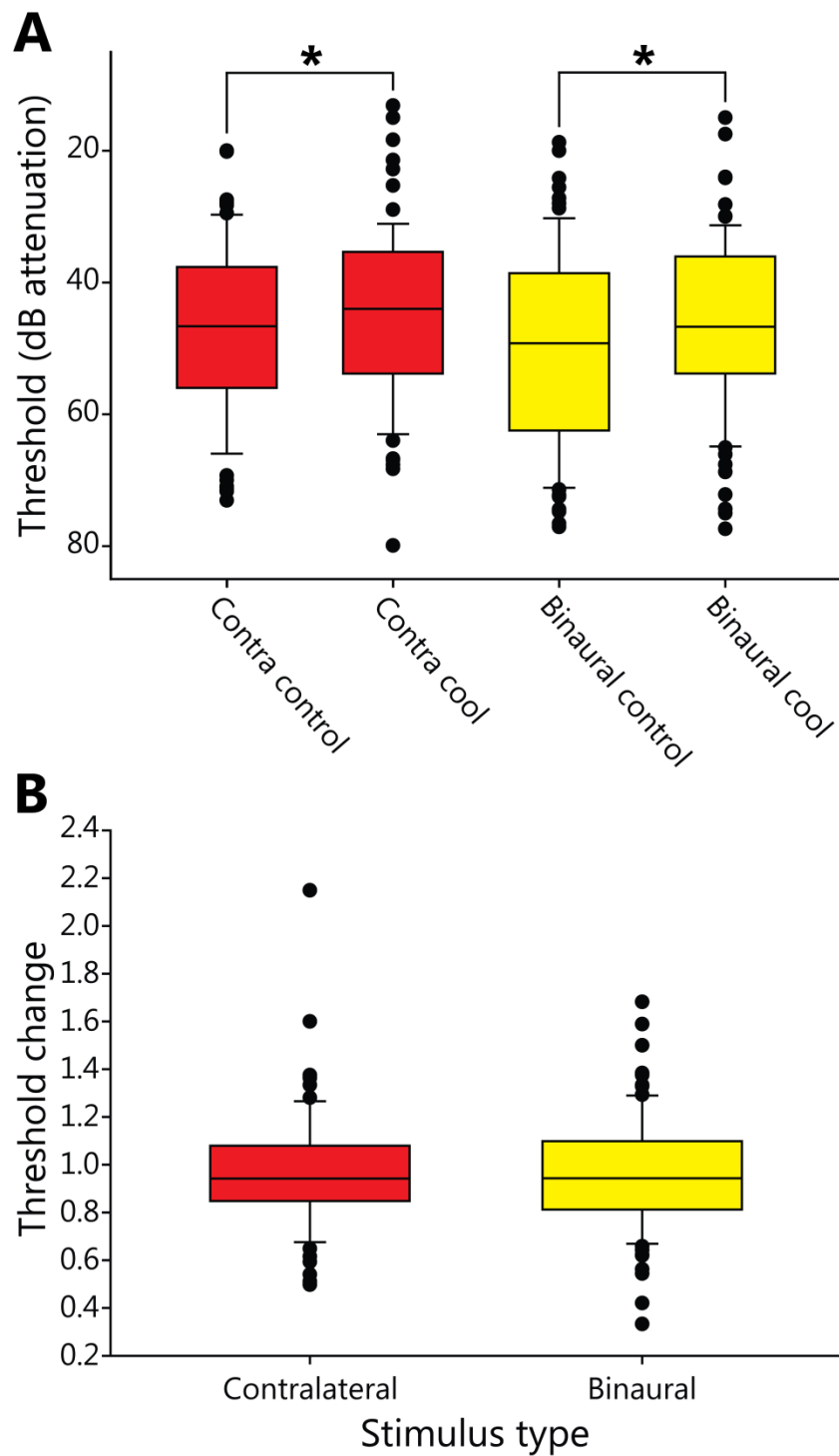


Figure 5.6 (A) Thresholds were significantly raised to both contralateral ($Z = -2.3$, $P = 0.02$) and binaural ($Z = -2.5$, $P = 0.01$) stimulation. (B) There was no significant difference between the change in threshold to contralateral and binaural stimulation ($U = 3131$, $P = 0.84$).

5.2.4 Control tuning bandwidths of FRAs 10 dB above threshold

The range of Q_{10} values of all FRAs in the population in the control condition is plotted in figure 5.7A. The dashed line shows the range of 286 units described by Syka *et al.* (2000) in the anaesthetised guinea pig. Q_{10} values tended to increase in a linear manner with CF in the data reported here, a finding matching similar reports (Syka *et al.*, 2000; Hernández *et al.*, 2005; Palmer *et al.*, 2013). A Spearman's rank order correlation was performed to determine if there was a relationship between CF and Q_{10} . There was a strong positive correlation, and this was statistically significant ($r_s(157) = 0.67, P < 0.0001$). Broad FRAs had the lowest median Q_{10} (0.73), and Narrow FRAs the highest (3.25). Due to the variability in CF between FRA groups, direct statistical comparisons were not possible. $Root_{10}$ values for all FRAs in this sample are plotted as a function of CF in figure 5.7B. The range of values was similar for all FRAs with CFs greater than 1 kHz. A Spearman's rank order correlation found a weak positive correlation between CF and $root_{10}$, and this was statistically significant ($r_s(157) = 0.28, P = 0.0003$).

Broad FRAs had the largest median $root_{10}$ (0.72), again reflecting their broad tuning. Low Tilt FRAs had the smallest median $root_{10}$ (0.29), while Narrow FRAs had the third smallest $root_{10}$ (0.35). The differences between the different measures with regard to FRA class with narrowest tuning shows the effect of measuring Q_{10} using CF as a parameter in the calculation (see section 5.2). While Narrow FRAs did not have the narrowest bandwidth at 10 dB above threshold they were distributed at mid to high CFs they had the highest Q_{10} of any FRA type.

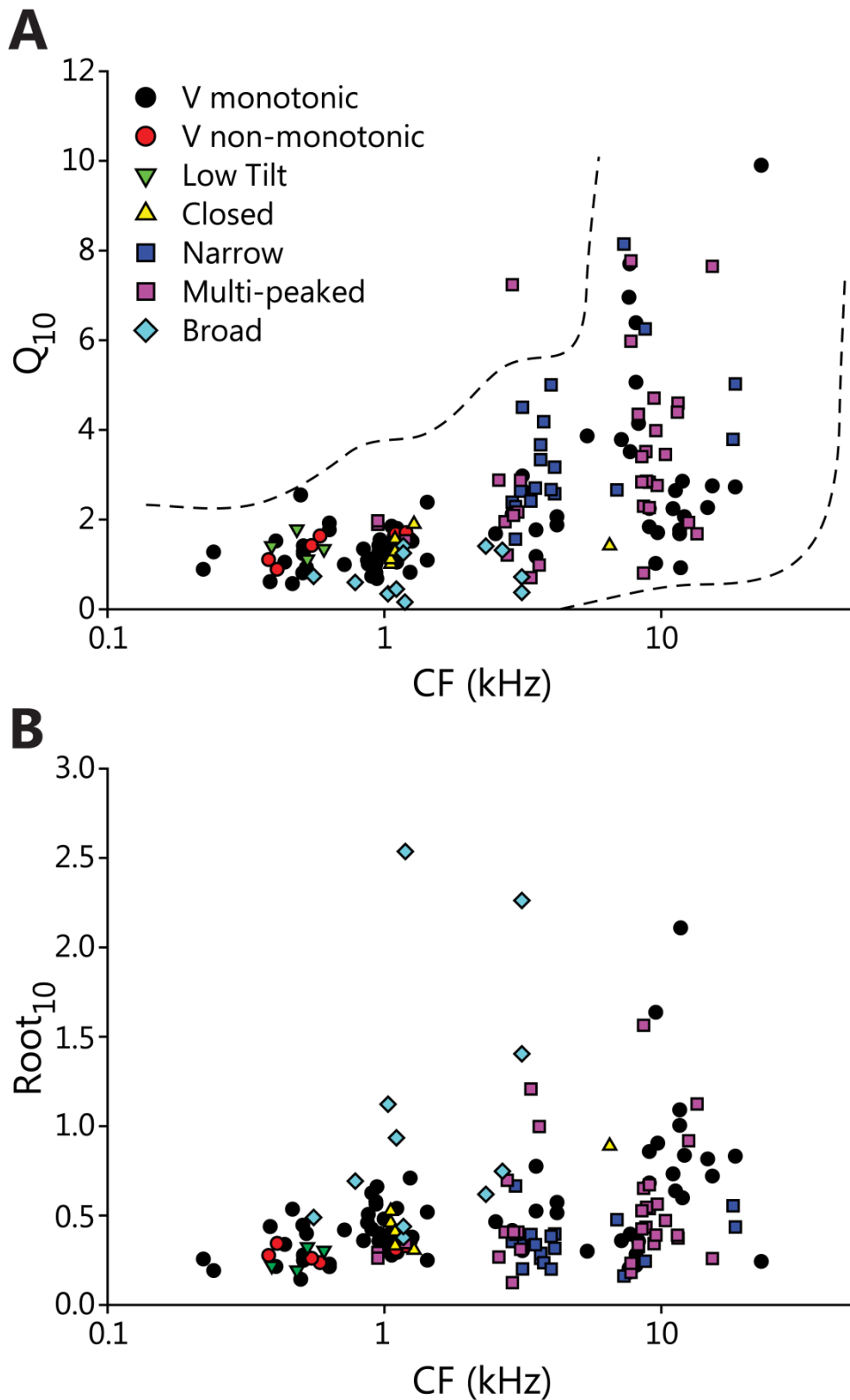


Figure 5.7 (A) Q_{10} values for all FRAs in the control condition. Note the increase in Q_{10} with CF. Dashed lines indicate the range of Q_{10} s found in 286 CNIC units by Syka *et al.* (2000). (B) Root_{10} values for all FRAs in the dataset. Note that the median and IQR range increased with CF. Both Q_{10} ($r_s(157) = 0.67$, $P < 0.0001$) and root_{10} ($r_s(157) = 0.28$, $P = 0.0003$) significantly correlated with CF.

5.2.5 Control tuning bandwidths of FRAs 40 dB above threshold

To determine if any changes in FRA bandwidth due to the paradigm were level dependent, the Q_{40} and $root_{40}$ were also calculated. There were 113 FRAs which had sufficiently low thresholds throughout all three stages of the cooling paradigm for these measures to be calculated.

The Q_{40} values of all FRAs in this sample are plotted in figure 5.8A. The values for all units in the sample fell within the range of values reported by Palmer *et al.* (2013). Much like the Q_{10} values described above, Q_{40} values increased with CF in a linear manner. There was a positive correlation between Q_{40} and CF which was significant ($r_s(111) = 0.71, P < 0.0001$). As would be expected, the population of Q_{40} values was lower than the Q_{10} values for the 113 FRAs which had both measures taken. Broad FRAs had the lowest median Q_{40} - 0.31, and Narrow FRAs had the highest - 1.25.

The $root_{40}$ of all 113 FRAs are shown in figure 5.8B. Much like $root_{10}$, the range of the $root_{40}$ values was approximately the same above 1 kHz. $Root_{40}$ and CF were significantly correlated ($r_s(111) = 0.42, P < 0.0001$). Broad FRAs' median $root_{40}$ was 1.78 – the lowest of any FRA type.

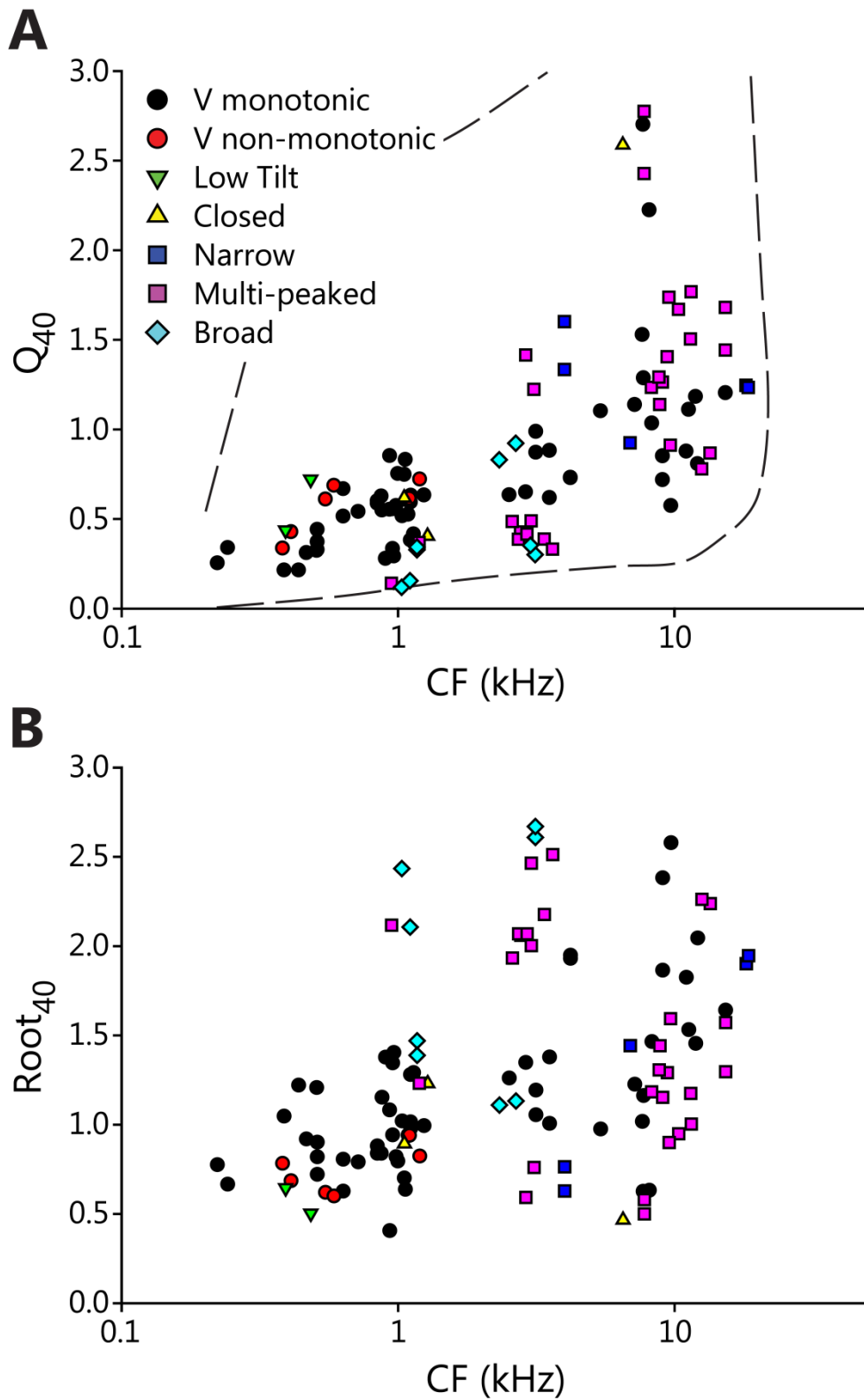


Figure 5.8 (A) Q_{40} values for all 113 FRAs in the control condition which qualified for this analysis. Q_{40} correlated significantly with CF ($r_s(111) = 0.71$, $P < 0.0001$). Dashed line indicates the range of the 2,826 FRAs reported by Palmer *et al.* (2013). (B) Root_{40} values for all 113 control FRAs. Root_{40} was significantly correlated with CF ($r_s(111) = 0.42$, $P < 0.0001$).

5.2.6 Cube root transformation made bandwidth independent of CF

As the square root transformation did not eliminate the correlation between bandwidth and CF at 10 or 40 dB above threshold, another method was sought to assess the bandwidths of FRA types in the population.

It was hypothesised that as the square root transformation reduced the amount of variance that could be accounted for by the correlation at 40 dB above threshold, the cube root transformation might remove this association with CF. To test this, the same methods used above to derive the root_{10} and root_{40} values were implemented with the modification that a cube root transform was used. The results of these analyses are plotted in figure 5.9.

The cube root transform at both 10 dB and 40 dB above threshold dramatically modified the distribution of the data. As shown in figure 5.9A, the cube root_{10} of all FRAs was found to not have a significant correlation with CF ($r_s(157) = -0.08$, $P = 0.34$). The cube root_{40} was also not significantly correlated with CF (Fig. 5.9B; $r_s(111) = 0.011$, $P = 0.91$). The cube root transform removed any dependence of this measure of tuning bandwidth on CF in this sample of IC units.

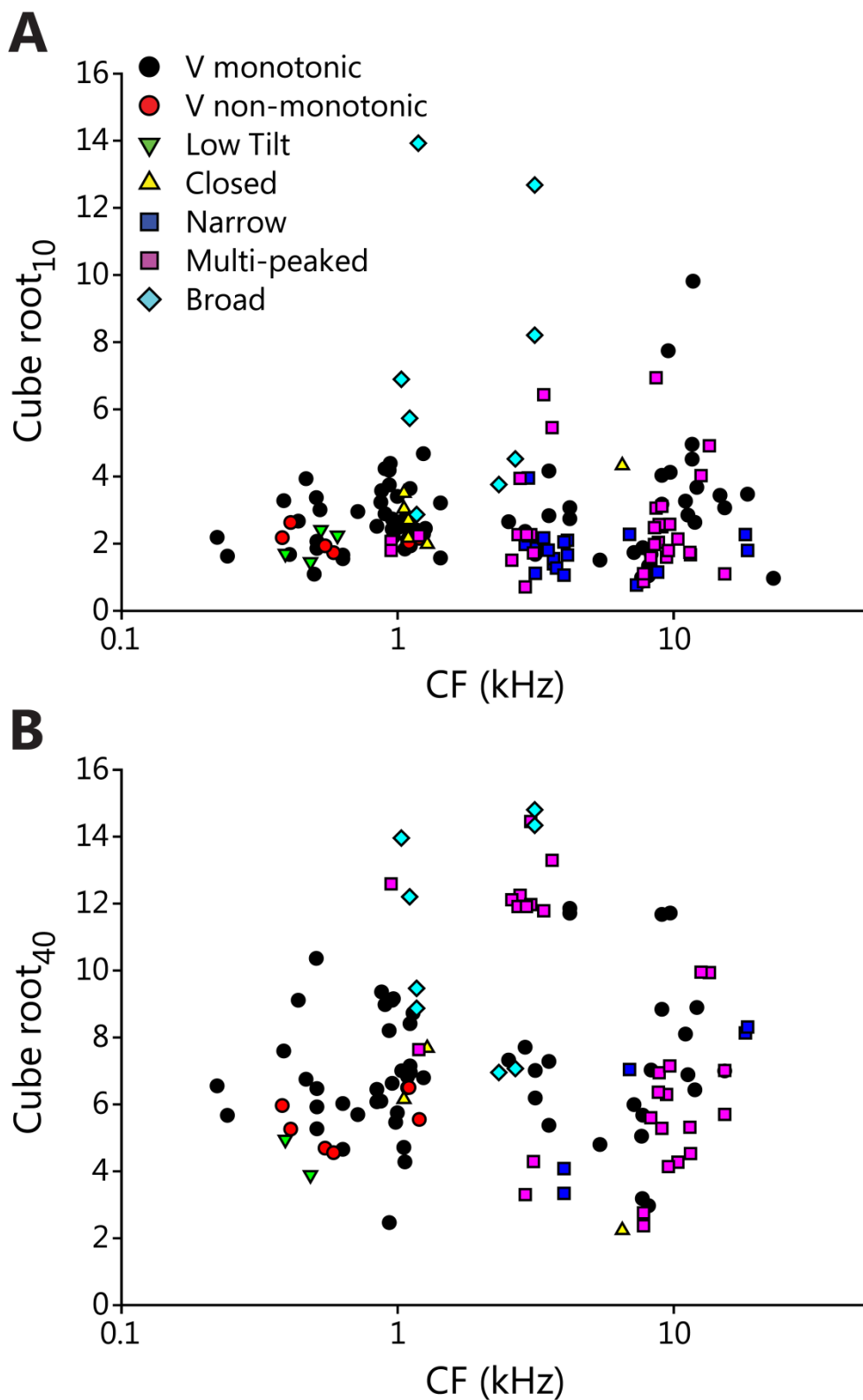


Figure 5.9 (A) Cube root transformation of all FRAs 10 dB above threshold. This transform removed any interdependence of the bandwidth measure on CF as the cube root₁₀ and CF were uncorrelated ($r_s(157) = -0.08$, $P = 0.34$). (B) The cube root transform also produced a measure of tuning sharpness uncorrelated with CF at 40 dB above threshold ($r_s(111) = 0.011$, $P = 0.91$).

5.2.7 Some FRA types had significantly different bandwidths at 40 dB above threshold

As the cube root transform allowed for objective measures of FRA bandwidth independent of CF, the sharpness of tuning by FRA classification was compared. Owing to the low numbers of FRAs in their respective samples, V-shaped non-monotonic, Low Tilt and Closed FRAs were not included in this analysis.

A Kruskal Wallis test found a significant difference between the four remaining FRA groups ($H(3) = 29.67, P < 0.0001$). *Post hoc* analysis for 6 multiple comparisons ($\alpha = 0.0083$) found that the tuning of V-shaped monotonic FRAs was significantly broader than Narrow FRAs ($Z = -3.79, P < 0.0001$), and narrower than Broad FRAs ($Z = -3.51, P < 0.0001$). While the median and IQR of Multi-peaked FRAs was narrower than V-shaped monotonic FRAs, this was not significant ($Z = -1.99, P = 0.05$). The tuning of Multi-peaked FRAs was also significantly narrower than Broad FRAs ($Z = -3.61, P < 0.0001$). Multi-peaked FRAs were broader at the median and IQR level than Narrow FRAs but not significantly so ($Z = -1.84, P = 0.07$). The largest disparity between groups was found between Narrow and Broad FRAs, with a significant difference between the distributions ($Z = -4.22, P < 0.0001$).

Because of the raised thresholds of Narrow FRAs in this sample, only 5 could be compared at 40 dB above threshold. Narrow FRAs formed too small a population to compare to other types at this level. There was a significant difference in the distributions across all three remaining groups ($H(2) = 9.93, P = 0.007$). *Post hoc* analysis found no significant difference ($\alpha = 0.0167$) between V-shaped monotonic and Multi-peaked FRAs ($Z = -0.70, P = 0.48$). V-shaped monotonic FRAs did have significantly narrower tuning than Broad FRAs ($Z = -3.34, P = 0.001$). Despite the median and IQR of Multi-peaked FRAs being narrower than Broad FRAs, the difference was not significant ($Z = -2.15, P = 0.03$).

5.2.8 Changes in tuning bandwidth induced by contralateral IC deactivation

To assess if IC deactivation modulated the bandwidth of contralateral IC neurons, the $Q_{10/40}$ and $\text{cube root}_{10/40}$ were compared before and during cooling. As shown above, and as outlined previously by Moore *et al.* (1983), the square root transform did not produce a bandwidth measure of IC neurons which is independent of CF and as such will not be used in these analyses. Q has been used so widely in the literature that using these measures allows for comparison to previous studies.

As illustrated in section 5.2.2, contralateral IC cooling produced changes in the threshold of many units. The bandwidth measures used in this analysis were taken using threshold as a reference point. As such, matched comparisons in the control and cool conditions could only be made for FRAs where there was little change in threshold between them. If units with large changes in threshold were included, the bandwidth measure re threshold would be unchanged, but the measure would be taken at a different stimulation level, and as such the measure would vary between conditions. The 20 % criterion of change was used to exclude FRAs whose threshold was deemed to have changed.

5.2.9 Changes in Q_{10} during contralateral IC cooling

There were 99 FRAs which were included for analysis at 10 dB above threshold. These comprised 56 V-shaped monotonic, 6 V-shaped non-monotonic, 2 Low Tilt, 5 Closed, 8 Narrow, 17 Multi-peaked and, 5 Broad FRAs. The ratio of changes in Q_{10} ranged from 0.35 to 2.30, with an IQR of 0.82 to 1.24, and a median of 1.00. Within this population, 48 decreased in Q_{10} during contralateral IC cooling, 44 increased, while 7 were unchanged (Fig. 5.10A). Of the 48 which decreased in Q_{10} , 20 did so by more than 20 %. Of the 44 which increased in Q_{10} , 28 reached the 20 % criterion. This asymmetry was largely due to a skew in

the change of V-shaped monotonic FRAs. There were 24 V-shaped monotonic FRAs which reduced in Q_{10} , while 28 increased, with the remaining 4 unchanged. This asymmetry was much greater at the extremes of the distribution, with 7 (13 %) decreasing to criterion, while 17 (30 %) increased to criterion.

While the number of V-shaped non-monotonic FRAs was much lower, all six decreased in Q_{10} during contralateral IC cooling, 4 by 20 % or more. Closed FRAs also followed this trend - of the 5 included in this analysis, 4 decreased in Q_{10} , with 2 reaching criterion. Only 2 Low Tilt FRAs were included, these both increased in Q_{10} by 3 % and 7 % respectively. Both Narrow and Multi-peaked FRAs had an almost equal number of Q_{10} changes, but with different relative distributions. Of 8 Narrow FRAs, 1 increased by 16 % and did not reach criterion, 4 reduced in Q_{10} by more than 20 %, and 3 increased by more than 20 %. A lower percentage of Multi-peaked FRAs changed in Q_{10} to reach criterion. Six (35 %) of the 17 Multi-peaked FRAs increased to criterion; 4 (24 %) decreased to criterion. Of the remaining 7 (42 %) Multi-peaked FRAs, 4 decreased in Q_{10} , 1 increased and 2 were unchanged, though none reached criterion.

The only FRA type other than V-shaped monotonic FRAs which had a bias towards an increase in Q_{10} were Broad FRAs. Of the 5 Broad FRAs, 2 (40 %) increased by more than 20 %. The other 3 (60 %) were almost unchanged - the maximum change in Q_{10} seen in this subgroup was an 8 % reduction from control. The full range of changes is plotted in figure 5.10A. As shown in the rightmost column of figure 5.10B, the median Q_{10} of the population of FRAs in the control condition was 1.64 (IQR = 1.28 to 2.65). This was unchanged during contralateral IC cooling, with the median being 1.64 (IRQ = 1.17 to 2.67). There was no significant difference between Q_{10} of all units in the control and contralateral IC cool conditions ($Z = 0.35$, $P = 0.73$). A Kruskal-Wallis one way ANOVA of the change in Q_{10} during contralateral IC cooling found no significant difference across groups ($H(6) = 8.80$, $P = 0.19$).

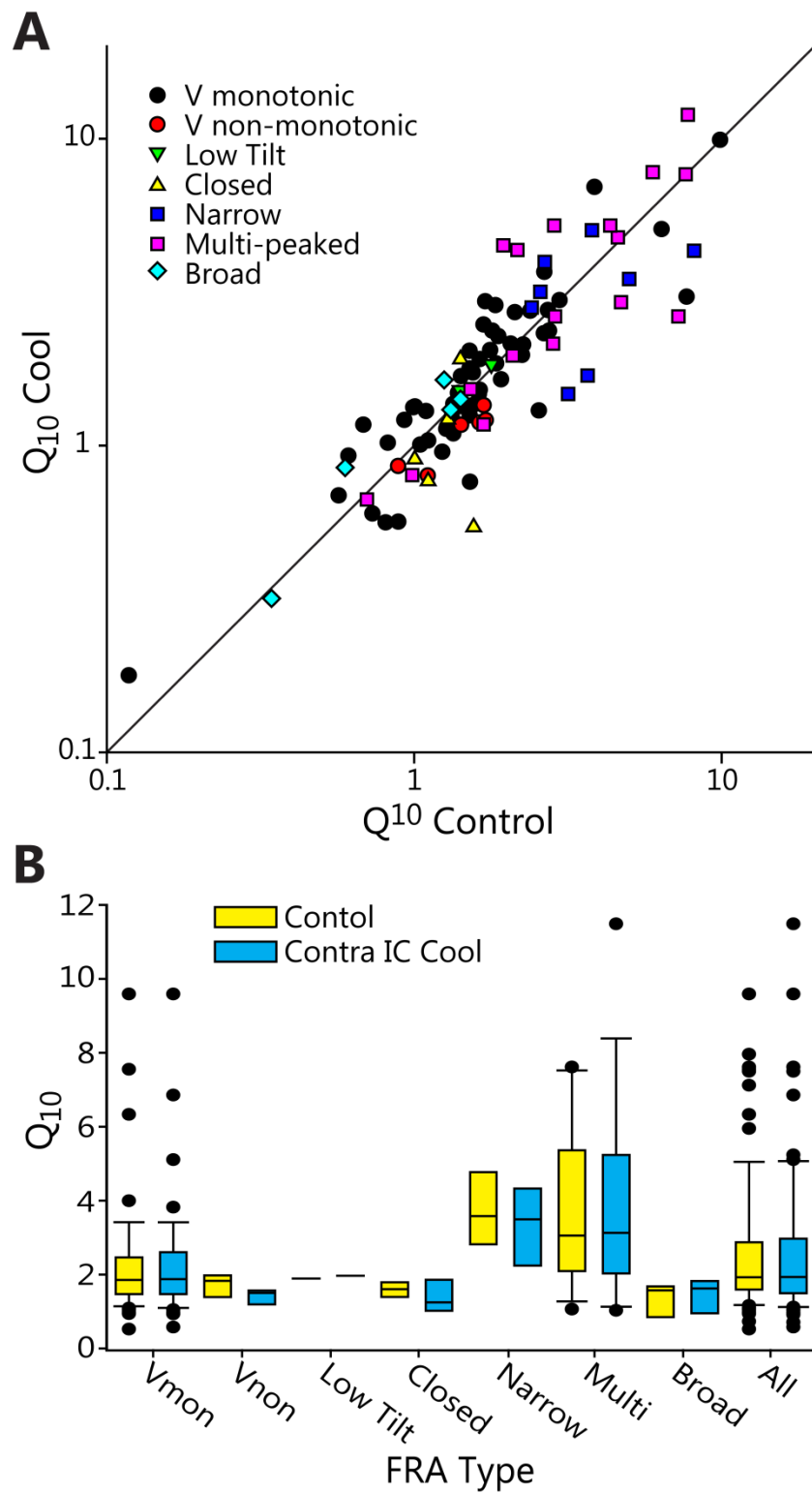


Figure 5.10 (A) Changes in Q_{10} during contralateral IC cooling. The range of Q_{10} changes were small as shown by the dense clustering around the line of identity. (B) Contralateral IC cooling did not significantly change Q_{10} for all FRAs ($Z = 0.35$, $P = 0.73$). No FRA type changed significantly relative to the others ($H(6) = 8.80$, $P = 0.19$).

5.2.10 Changes in cube root₁₀ during contralateral IC cooling

The median cube root₁₀ in the control condition was 1.28 (IQR = 1.72 to 3.04). Cooling the contralateral IC caused a small change in the population, which had a median of 1.45 (IQR = 1.26 to 1.77). There was no significant difference between the distributions ($Z = 0.45$, $P = 0.65$). The cube root₁₀ of 22 FRAs decreased to criterion, while 24 FRAs increased more than 20 % (Fig. 5.11A).

Of the 56 V-shaped monotonic FRAs, 29 decreased in cube root₁₀ (13 to criterion), and 22 increased in cube root₁₀ (10 to criterion). The change in cube root₁₀ of both Low Tilt FRAs was below criterion, much like their Q₁₀s. One FRA only changed by 3 % but the other increased by 18 %. Closed FRAs, much like V-shaped non-monotonic FRAs, followed the same pattern as Q₁₀ measures, with 4 increasing in cube root₁₀, 2 to criterion, and 1 decreasing to criterion.

The change in Narrow cube root₁₀ had a slight difference compared to the change in Q₁₀. As with Q₁₀, the cube root₁₀ of 4 FRAs increased by more than 20 %. There were 4 FRAs which decreased, but unlike with Q₁₀, only 2 reached the 20 % criterion of change using cube root₁₀. Interestingly, assessment of change in bandwidth with cube root₁₀ found a change in the Multi-peaked FRAs which reached criterion. The number which reduced in bandwidth was still 7 of 17, but only 5 reached the 20 % criterion. The number of those which increased in bandwidth was again 8, and as with Q₁₀, 4 reached criterion. Two other Multi-peaked FRAs were again unchanged using cube root₁₀. As with Q₁₀, Broad FRAs had a trend towards a reduction in bandwidth, but only one FRA reached the 20 % criterion with a reduction in cube root₁₀ of 24 %. The second FRA, which reached criterion using Q₁₀ as a measure of bandwidth, showed a reduction of 18 % when measured using cube root₁₀. As with Q₁₀, the remaining 3 Broad FRAs were minimally changed. There was no significant difference in the change of cube root₁₀ across groups between control and contralateral IC cool conditions ($H(6) = 10.03$, $P = 0.12$).

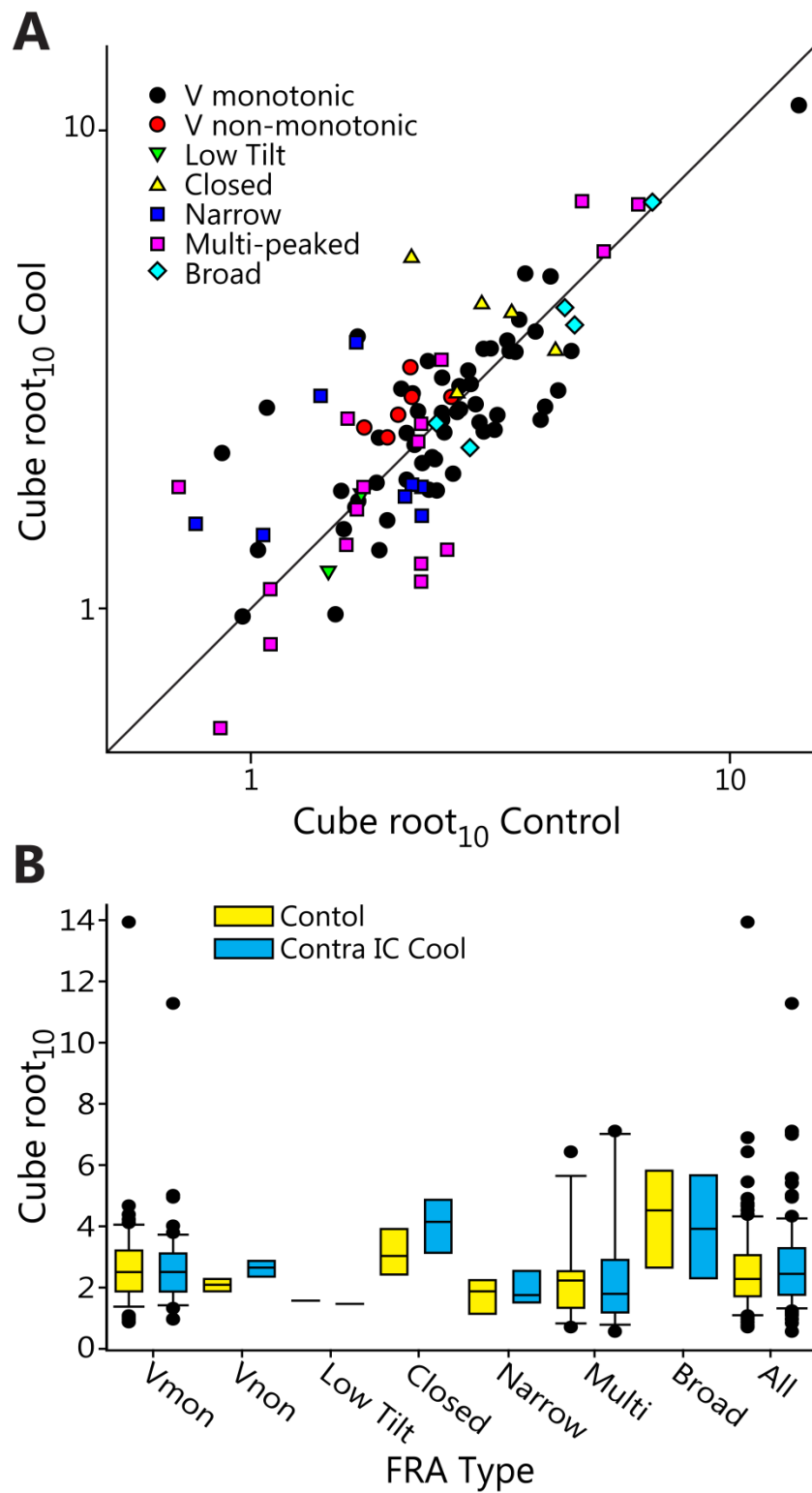


Figure 5.11 (A) Changes in cube root₁₀ during contralateral IC cooling. Note how the range of changes decreased in FRAs with larger cube root₁₀. (B) There was no significant difference between cube root₁₀ in the control and cool conditions ($Z = 0.45$, $P = 0.65$). Comparing the change of each FRA type also found no significant difference between groups ($H(6) = 10.03$, $P = 0.12$).

5.2.11 Changes in Q_{40} during contralateral IC cooling

To assess bandwidth changes at 40 dB above threshold, it was implicit that FRAs in all conditions have a threshold lower than 40 dB attenuation. This requirement was applied in addition to the inclusion criteria used in the bandwidth measures at 10 dB above threshold. There were 74 FRAs which passed these criteria and were analysed. These comprised 42 V-shaped monotonic, 6 V-shaped non-monotonic, 2 Low Tilt, 3 Closed, 1 Narrow, 16 Multi-peaked and, 4 Broad FRAs. In the control condition Q_{40} ranged from 0.12 to 2.77, with an IQR of 0.42 to 0.87 and a median of 0.62. Cooling the contralateral IC produced an increase at both extremes, with the minimum Q_{40} being 0.15 and the maximum being 3.11. The IQR broadened, with the 25th quartile reducing to 0.40 and the 75th quartile increasing to 0.87, while the median reduced slightly to 0.60. A Wilcoxon Signed Ranks test found no significant difference between Q_{40} in the control and contralateral IC cool conditions ($Z = -0.89$, $P = 0.38$).

Within the population, 42 FRAs decreased in Q_{40} , 30 increased, and 2 were unchanged (Fig. 5.12A). Only 13 of the 42 FRAs which decreased did so by more than 20 %, while 16 increased by more than 20 %. Therefore, while there was a trend for a greater number of FRAs to increase in bandwidth at 40 dB above threshold, the FRAs which changed to criterion in either direction were approximately even.

The 42 V-shaped monotonic FRAs all changed in Q_{40} during contralateral deactivation, with 21 increasing and 21 decreasing. Eleven increased by more than 20 %, 8 decreased by more than 20 %. V-shaped non-monotonic FRAs had a similar pattern to that found in Q_{10} , with all 6 FRAs reducing relative to control during contralateral cooling. The extent of reduction in percentage terms was reduced however, with only 2 reaching the 20 % criterion.

Of the 2 Low Tilt FRAs which were included, one decreased in Q_{40} by 10 % while the other increased by 51 %. All 3 Closed FRAs reduced in Q_{40} by more than 20 % with changes of 25 %, 55 %, and 72 % observed for these FRAs. Only one Narrow FRA was included in these analyses – this FRA was unchanged in Q_{40} during contralateral cooling.

The only FRAs which reached criterion for both Multi-peaked and Broad FRAs did so by increasing in Q_{40} . Nine of the 16 Multi-peaked FRAs decreased in Q_{40} , 2 were unchanged, and the remaining 5 increased. Three of these 5 FRAs which increased reached criterion. Of the 4 Broad FRAs, 2 decreased in Q_{40} , neither to criterion, one FRA increased by 1 % and another did so by 30 %.

Comparing the change in Q_{40} of each FRA type found a significant difference across groups ($H(4) = 12.78$, $P = 0.012$). Narrow and Low Tilt FRAs were excluded due to the low numbers in these groups (Fig. 5.12B). Due to the 10 pairwise comparisons in the *post hoc* analyses ($\alpha = 0.005$) with Dunn's method determined statistically significant differences between the change in V-shaped monotonic & Closed FRAs Q_{40} ($Z = -2.55$, $P = 0.004$), and Multi-peaked & Closed FRAs Q_{40} ($Z = -2.68$, $P = 0.002$).

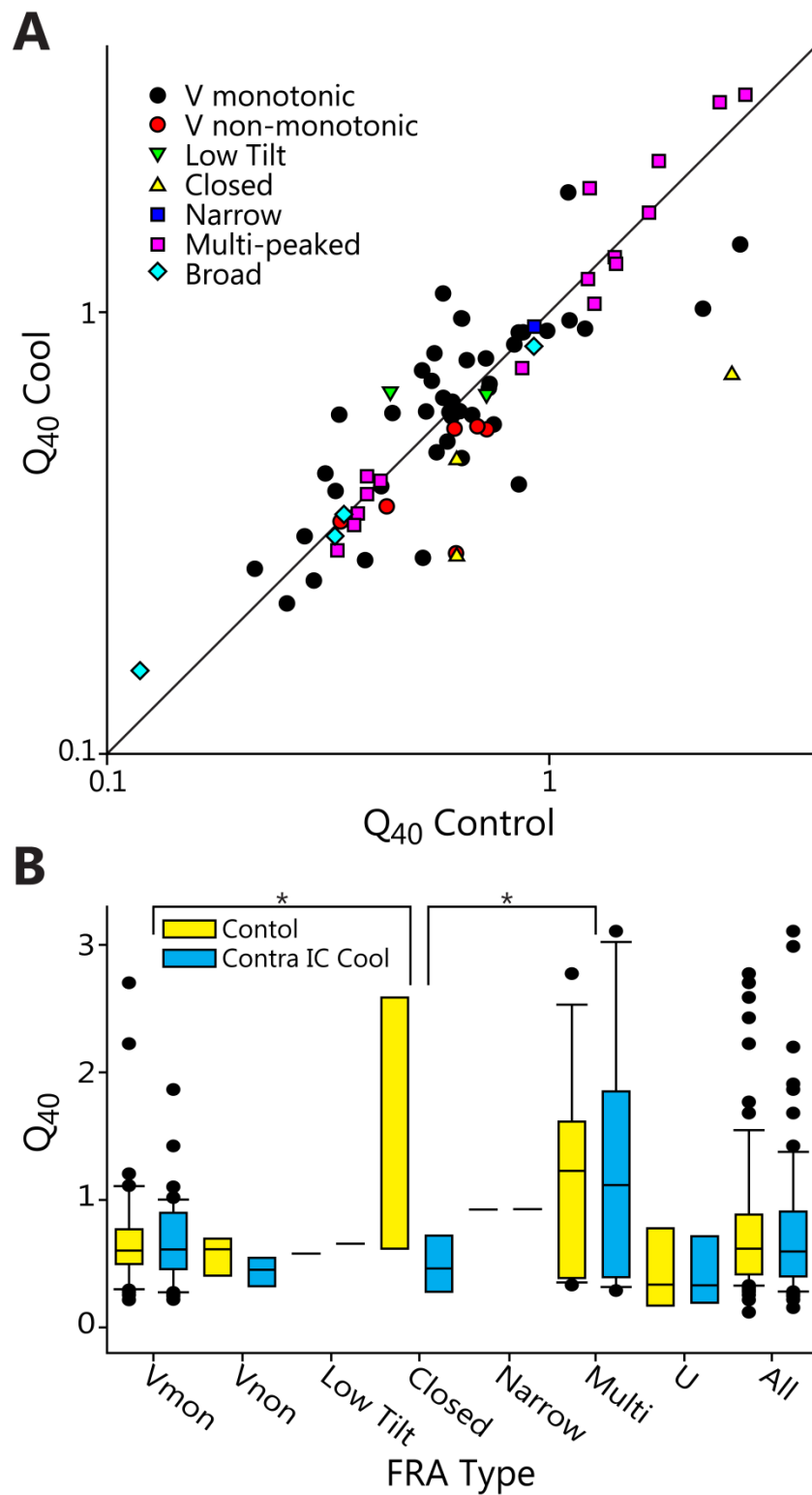


Figure 5.12 (A) The population of V-shaped non-monotonic & Closed FRAs both reduced in Q_{40} . The only changes $> 20\%$ for Multi-peaked and Broad FRAs were increases. (B) There was no significant difference between the control and cool Q_{40} of all FRAs ($Z = -0.89$, $P = 0.38$), but there were significant differences between the change in Closed vs. the change in V-shaped monotonic ($Z = -2.55$, $P = 0.004$), and vs. Multi-peaked FRA Q_{40} ($Z = -2.68$, $P = 0.002$).

5.2.12 Changes in cube root₄₀ during contralateral IC cooling

The median cube root₄₀ of the 74 FRAs in the control condition was 6.52 (IQR = 5.27 to 8.72). Contralateral IC deactivation induced an expansion in the cube root₄₀ of the population - the median increased to 6.87 and the IQR broadened (5.15 to 9.12). These changes were not significantly different to control ($Z = 1.34$, $P = 0.18$).

The cube root₄₀ of 8 FRAs decreased to criterion, while 12 FRAs increased to criterion (Fig. 5.13A). Cube root₄₀ produced a much wider range of responses than Q_{40} . As with Q_{40} , 21 of the 42 V-shaped monotonic FRAs decreased in cube root₄₀, the other 21 increased. There were fewer changes which reached criterion, with 6 increasing and 6 decreasing by more than 20 %. The 6 V-shaped non-monotonic FRAs all increased in bandwidth and therefore cube root₄₀ during contralateral IC cooling. As found for Q_{40} , 2 of the 6 V-shaped non-monotonic FRAs reached criterion.

Both Low Tilt FRAs reduced in bandwidth but not to criterion, decreasing in cube root₄₀ by 11 % and 19 % respectively. All 3 Closed FRAs increased to criterion, expanding by 71 %, 98 %, and 324 %. The only Narrow FRA was almost unchanged, increasing by 2 % in cube root₄₀ during contralateral IC cooling. The cube root₄₀ of 3 Multi-peaked FRAs was unchanged, 6 decreased and 7 increased. None of the Broad FRAs changed in cube root₄₀ by more than 12 %.

A significant difference was found between the change in cube root₄₀ of each FRA type ($H(4) = 12.84$, $P = 0.012$). As with Q_{40} there were significant differences between the change in cube root₄₀ of Closed & V-shaped monotonic FRAs ($Z = -2.73$, $P = 0.001$), and Closed & Multi-peaked FRAs ($Z = -2.69$, $P = 0.002$) as shown in figure 5.13B.

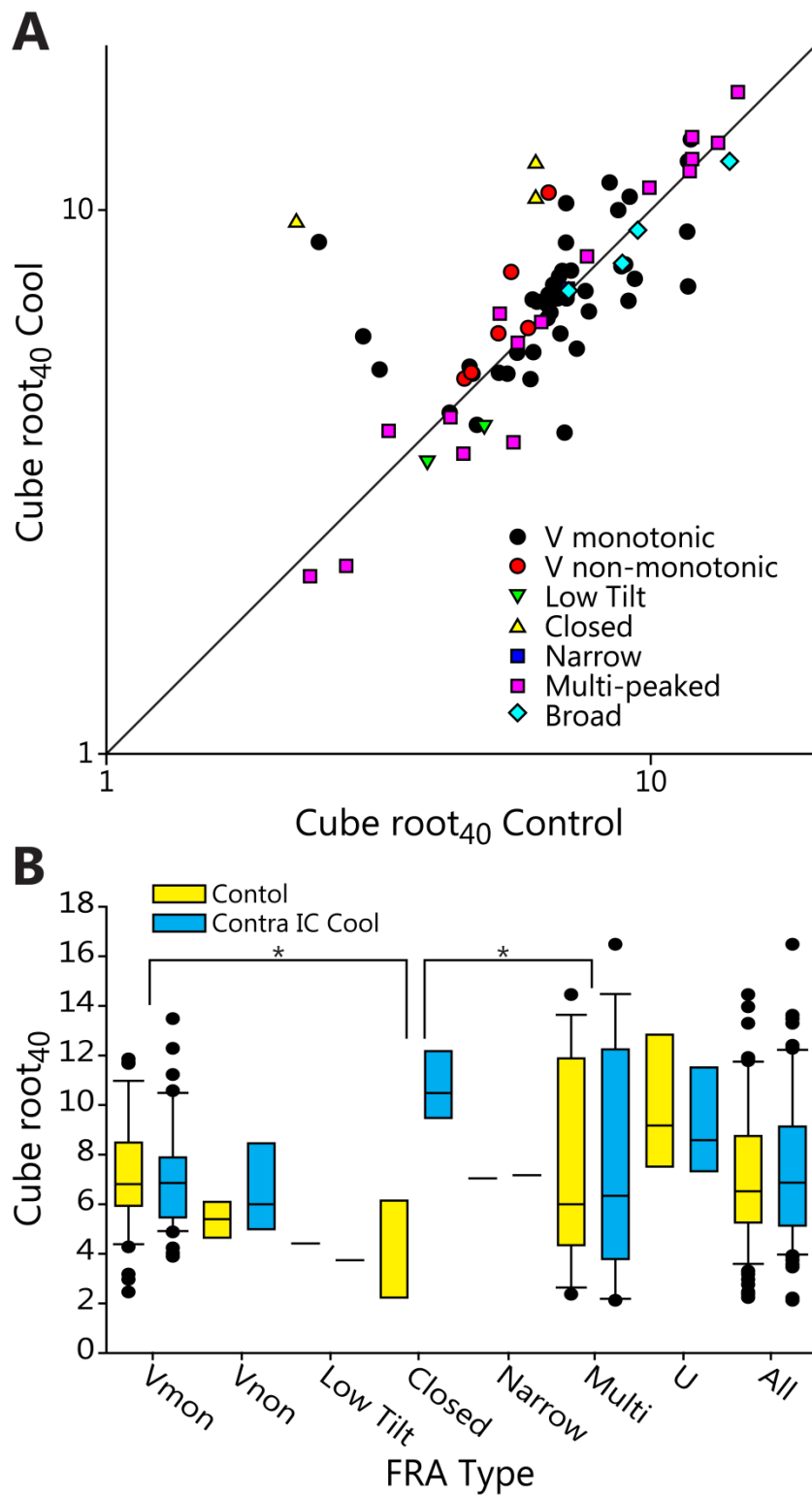


Figure 5.13 (A) As with Q_{40} , all V-shaped non-monotonic & Closed FRAs increased in bandwidth during the paradigm. (B) There was no significant difference between the control and contralateral IC cool cube root₄₀ of all FRAs ($Z = 1.34$, $P = 0.18$). There were significant differences between Closed & V-shaped monotonic ($Z = -2.73$, $P = 0.001$), and Closed & Multi-peaked FRA Q_{40} s ($Z = -2.69$, $P = 0.002$).

5.2.13 Initial bandwidth did not influence changes in bandwidth during cooling

To test if units with differing initial bandwidths tended to change during contralateral IC deactivation to a different extent or direction, analyses were performed which divided the control distributions into four equally sized groups (Fig. 5.14). The change in bandwidth of each at 10 and 40 dB above threshold were then compared.

For the two measures at 10 dB above threshold, the population size of 140 produced 4 groups of 35. For those measures at 40 dB above threshold, the division of the 74 FRAs resulted in two groups of 19 and two groups of 18. The changes in Q_{10} ($H(3) = 3.62$, $P = 0.31$), cube root_{10} ($H(3) = 1.80$, $P = 0.61$), Q_{40} ($H(3) = 3.06$, $P = 0.38$), and cube root_{40} ($H(3) = 0.79$, $P = 0.85$) during contralateral IC cooling were not significant between these groups.

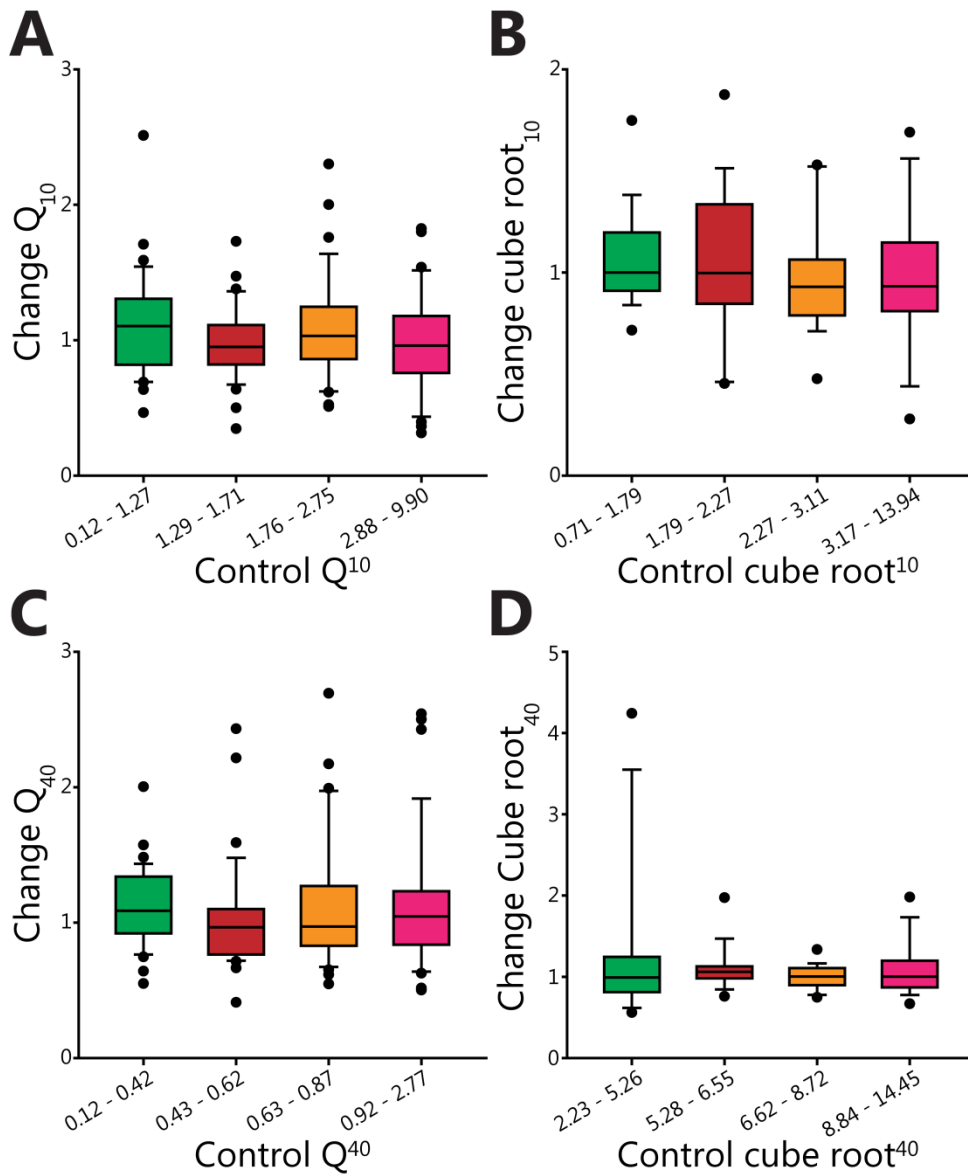


Figure 5.14 Analysis of the change in bandwidth at both 10 dB (A & B) and 40 dB (C & D) above threshold and using both Q (A & C) and cube root (B & D) measures. Statistical analysis with Kruskal Wallis ANOVAs on Ranks found no significant differences between the control and contralateral IC cool bandwidths between these groups using either $Q_{10/40}$ or cube root $_{10/40}$.

5.2.14 Bandwidth changes 10 and 40 dB re threshold were uncorrelated

A comparison of the measures $Q_{10/40}$ and $\text{cube root}_{10/40}$ and the changes in bandwidth at 10 dB and 40 dB re threshold during contralateral IC cooling was made. The relationship between Q and cube root measures of bandwidth is shown in figure 5.15A. The change in cube root_{10} and cube root_{40} for each unit is plotted as a function of the respective Q_{10} and Q_{40} for that bandwidth measure.

Changes seen at 10 and 40 dB above threshold largely overlapped. The range of changes at 10 dB was wider, save for two outliers, than at 40 dB. The data for measures at 10 and 40 dB were best fit by a modified three parameter exponential decay ($r^2 = 0.93$, $P < 0.001$).

An assessment of whether the changes observed in bandwidth at 10 and 40 dB above threshold were correlated is plotted in table 5.2. Of the 74 FRAs in each group, 54 Q and 50 cube root measures changed in the same direction at both 10 and 40 dB above threshold. For both measures, the number which increased (in bandwidth) in the same direction was higher than those which decreased in the same direction.

Plotting the change at 10 dB above threshold as a function of change at 40 dB above threshold (Fig. 5.15B) found no significant correlation at the population level between the change in Q ($r_s(74) = -0.04$, $P = 0.73$) or cube root ($r_s(74) = 0.002$, $P = 0.99$).

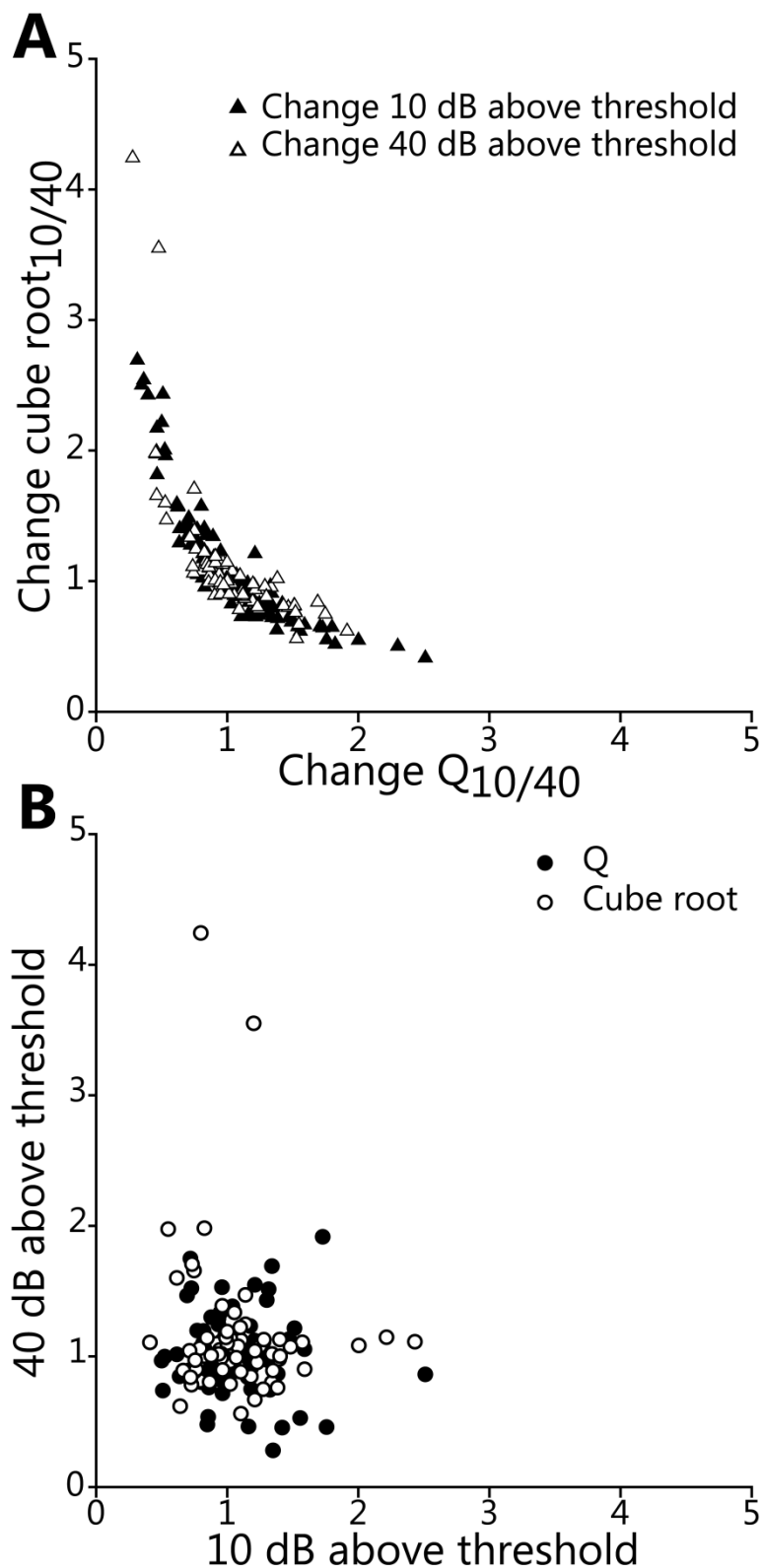


Figure 5.15 (A) The change in Q and cube root measures had a strong negative correlation at both 10 dB ($r_s(138) = -0.95$, $P < 0.0001$) and 40 dB above threshold ($r_s(72) = -0.86$, $P < 0.0001$). (B) There was no significant correlation between the change in either Q ($r_s(74) = -0.04$, $P = 0.73$) or cube root ($r_s(74) = 0.002$, $P = 0.99$) at 10 dB and 40 dB above threshold.

Bandwidth change 10 dB	Bandwidth change 40 dB	#
Q ₁₀ increase	Q ₄₀ increase	24
cube root ₁₀ increase	cube root ₄₀ increase	31
Q ₁₀ decrease	Q ₄₀ decrease	30
cube root ₁₀ decrease	cube root ₄₀ decrease	19
Q ₁₀ increase	Q ₄₀ decrease	12
cube root ₁₀ increase	cube root ₄₀ decrease	11
Q ₁₀ decrease	Q ₄₀ increase	8
cube root ₁₀ decrease	cube root ₄₀ increase	13

Table 5.2 Comparison of bandwidth changes at 10 and 40 dB above threshold. Seventy percent of bandwidth changes were in the same direction.

5.2.15 Bandwidth changes were unrelated to control CF

A comparison of the change in bandwidth at 10 and 40 dB above threshold is plotted in figure 5.16. The distribution of CFs observed in the control condition was split into 4 groups of 35 in the 10 dB group and 2 groups of 19 and 2 groups of 18 in the 40 dB group.

The median change in Q₁₀ was no more than 0.07 away from 1 for all 4 groups and there was no significant difference between the groups ($H(3) = 1.50$, $P = 0.68$). For cube root₁₀, the maximum deviation of the median from 1 was in the 8.24 – 22.97 kHz group which was only 1.07 (Fig. 5.16A). There was no significant difference between these groups either ($H(3) = 3.39$, $P = 0.34$).

The groups at 40 dB above threshold spanned different frequency ranges due to being formed of a subpopulation of the 10 dB group. The median of the 1.14 – 4.20 kHz group was 1.08, the largest deviation from 1 of any group in these analyses (Fig. 5.16B). There was no significant difference between any of the Q₄₀ groups ($H(3) = 3.15$, $P = 0.37$) or cube root₄₀ groups ($H(3) = 1.99$, $P = 0.58$).

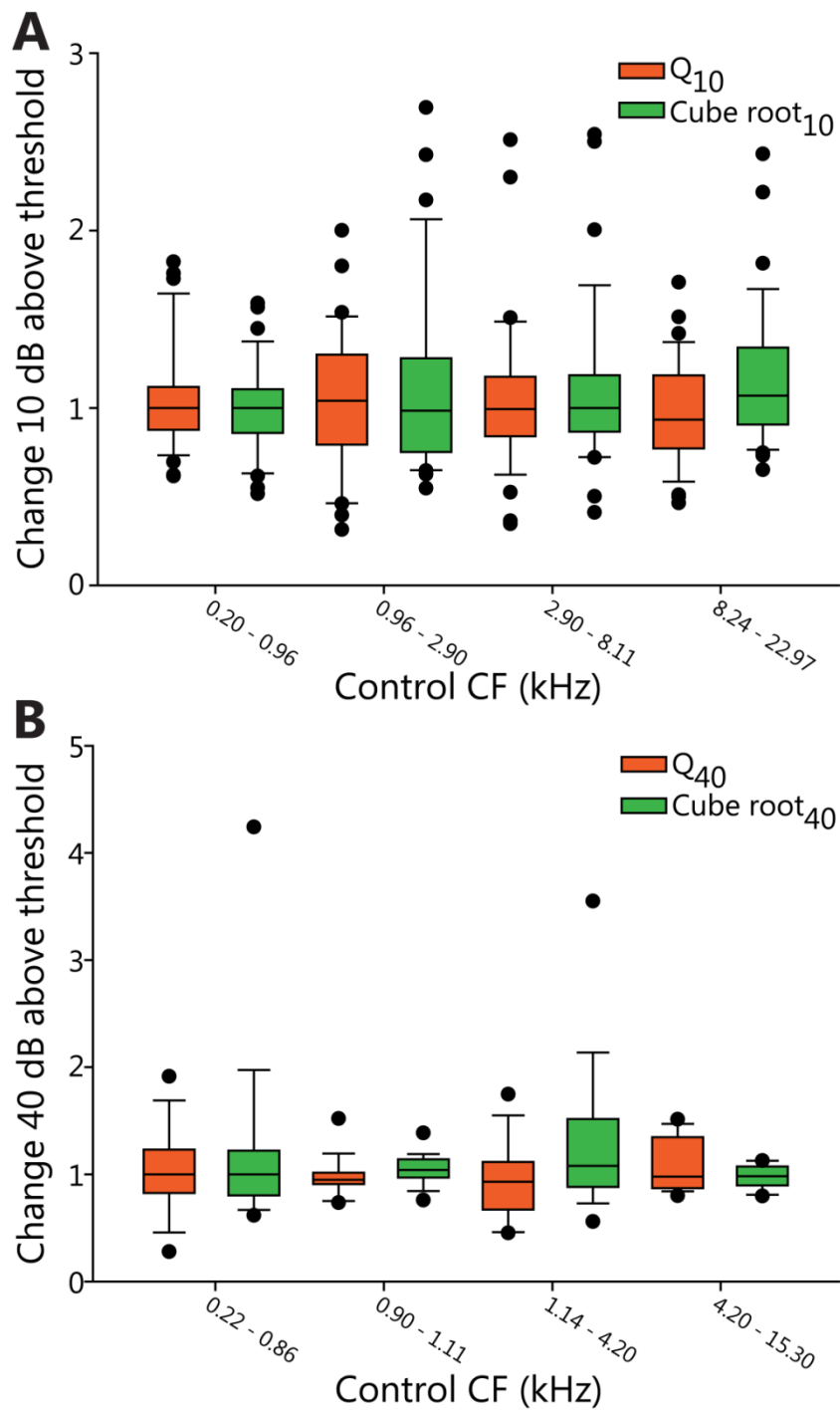


Figure 5.16 Changes in Q and cube root compared to control CF. (A) There were no significant difference in the range of changes in Q_{10} ($H(3) = 1.50$, $P = 0.68$), or cube root₁₀ ($H(3) = 3.39$, $P = 0.36$) during contralateral IC cooling based on control CF. (B) There was no significant difference in the change in Q_{40} ($H(3) = 3.15$, $P = 0.37$), or cube root₄₀ ($H(3) = 1.99$, $P = 0.58$) either.

5.2.16 Bandwidth changes were unrelated to control threshold

Figure 5.17 compares the bandwidth changes at both levels above threshold as a function of control threshold using both Q and cube root. The groupings were the same as were used in the previous section.

The change in Q_{10} was most in the 36 – 47 dB group, which had a median of 1.07 (Fig. 5.17A). There was no significant difference in the change of Q_{10} between any of the 4 groups ($H(3) = 3.89$, $P = 0.27$). The largest median difference from 1 in cube root₁₀ was in the 57 – 77 dB group which had a median of 1.05. As with Q_{10} , there was no significant difference across groups ($H(3) = 1.88$, $P = 0.60$).

As the inherent characteristic of the groups with changes at 40 dB above threshold was a minimum threshold of 40 dB attenuation at all stages of the cooling cycle, the groups analyses here ranged in control threshold from 40 to 77 dB (Fig. 5.15B). The 40 – 47 dB group had the largest change of the 4 groups, having a median of 1.11. This was the largest change of any group in this analysis. A Wilcoxon Signed Ranks test comparison to a hypothetical distribution with a median of 1 found no significant difference ($Z = -1.50$, $P = 0.13$). There was no significant difference between the changes in Q_{40} groups ($H(3) = 4.41$, $P = 0.22$). No significant difference was found between the change in cube root₄₀ either ($H(3) = 2.30$, $P = 0.51$).

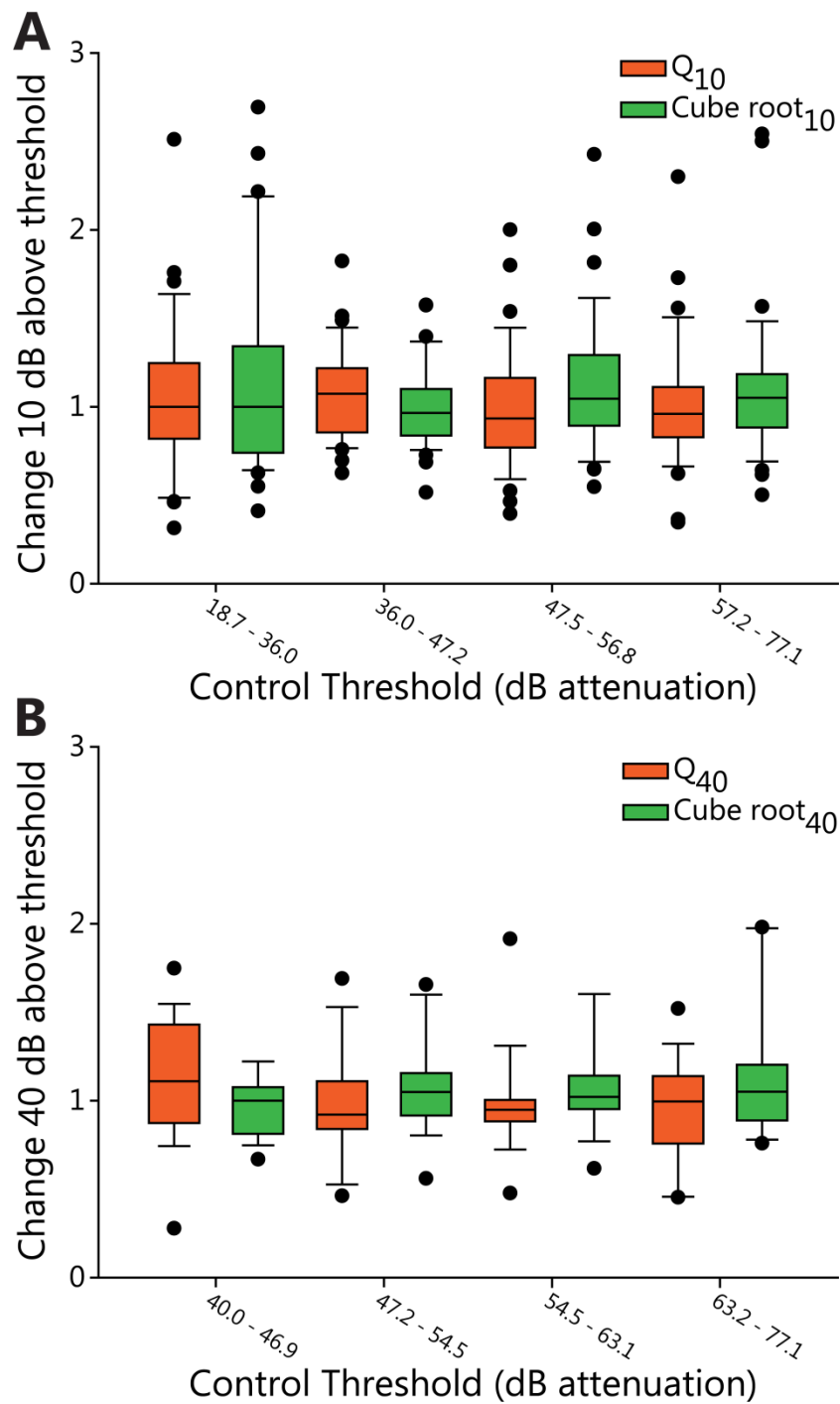


Figure 5.17 (A) There was no significant difference between the change in Q_{10} ($H(3) = 3.89$, $P = 0.27$), or cube root₁₀ ($H(3) = 1.88$, $P = 0.60$) during contralateral IC cooling based on control threshold. (B) This was also true at 40 dB re threshold for Q_{40} ($H(3) = 4.41$, $P = 0.22$), or cube root₄₀ ($H(3) = 2.30$, $P = 0.51$).

5.2.17 Bandwidth changes were not different in response to contralateral or binaural stimulation

In figure 5.18 the change during contralateral IC cooling in each bandwidth measure in response to contralateral and binaural stimulation are compared. The change in Q_{10} to contralateral stimuli had a median of 1.03 (IQR = 0.84 to 1.21), while the change to binaural stimuli had a median of 0.96 (IQR = 0.78 to 1.17). As shown in the left columns of figure 5.18A, there was no significant difference between these groups ($U = 2069$, $P = 0.11$). The median change of cube root $_{10}$ to contralateral stimuli was 0.98 (IQR = 0.78 to 1.19), while the binaural change had a median of 1.05 (IQR = 0.92 to 1.28). These groups were not significantly different ($U = 4395$, $P = 0.05$; Fig. 5.18A – right columns).

The change in Q_{40} to contralateral stimulation had a median of 0.95 (IQR = 0.86 to 1.21). The median change to binaural stimuli was 0.98 (IQR = 0.86 to 1.12). Due to the similarities between these distributions, as shown in the left columns of figure 5.18B, there was no significant difference between these groups ($U = 662$, $P = 0.82$). The median change in cube root $_{40}$ to contralateral stimuli was 1.02 (IQR = 0.89 to 1.13), while the median change to binaural stimuli was 1.01 (IQR = 0.90 to 1.13). As with the other groups tested, there was no significant difference between these groups ($U = 655$, $P = 0.76$).

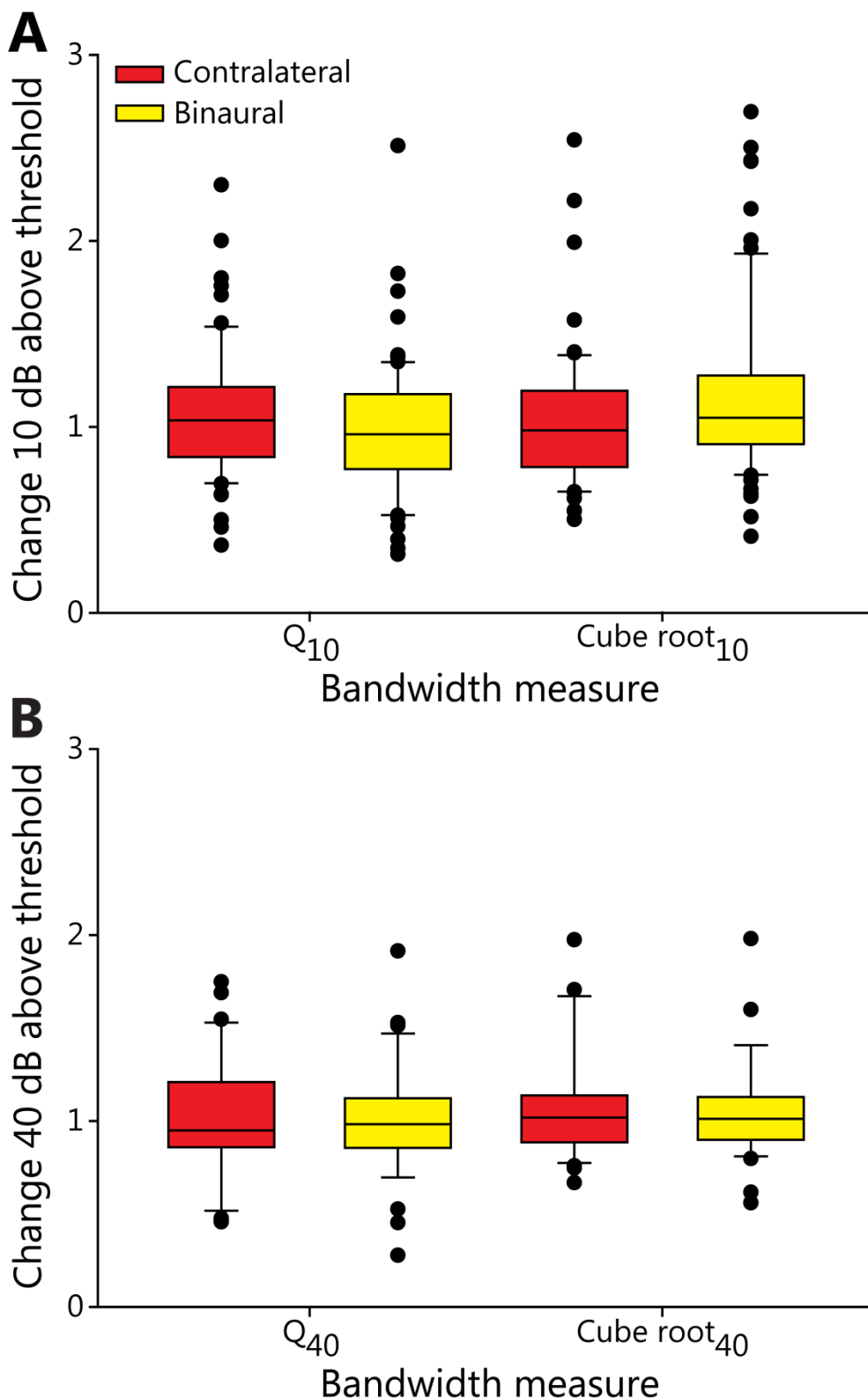


Figure 5.18 (A) Comparisons of the change in each bandwidth measure at 10 dB above threshold for contralateral and binaural stimulation. There was no significant difference between contralateral and binaural Q_{10} or cube root $_{10}$. (B) Contralaterally and binaurally driven changes were not significantly different for Q_{40} or cube root $_{40}$.

5.4 Discussion

The principle findings of the analyses reported in this Chapter are that several parameters of the FRA properties of IC neuron changed due to contralateral IC deactivation. The threshold of many units were modulated, with the population significantly increased (Fig. 5.4). The CF of the population was unchanged, with only one unit which showed a large CF shift following disinhibition of its FRA (Fig. 5.2). Bandwidth changes were more apparent at 40 dB (Fig. 5.12) re threshold than at 10 dB (Fig. 5.10).

5.4.1 Clustering of units with similar CF in this study

The clustering of units in the distribution (Fig. 5.3A) is worthy of note. The most likely explanation for this is the method used to find units in these experiments. When searching for single units there was a need for very high signal to noise ratio as a long time was needed to record cells throughout all stages of a cooling cycle. Due to the long duration of recordings from each cell, some drifted over the course of experimentation and the signal to noise ratio decreased. As such, units needed to be clearly discriminated from noise. When recordings were completed for a unit this meant that the electrode had to be moved so that the unit was not contaminating the following unit. Therefore the electrode was moved at least ~100 to 200 μm . As such, when moving down the tonotopic axis of the IC, the first cells encountered in a track had CFs up to ~2 kHz. Moving away from the first unit lead to a region of the IC being missed which lead to the lack sampled units with CFs between ~2 and ~4 kHz. Similarly, the lack of units between ~7 and ~9 kHz was caused by moving between the second and third units in each track. The data in figure 5.3B support this view as units which were initially characterised but not held to recovery filled the gaps in figure 5.3A, thus removing the clustering. An alternative possibility is that units with a large enough signal to noise ratio to be held to recovery were regularly

spaced in the IC. One possibility is that they are large stellate cells which are known to span the laminae (Oliver, 1984b).

5.4.2 Unchanged CF during contralateral IC cooling shows the influence of ascending afferent input to the IC

The lack of change in CF throughout any stage of contralateral IC deactivation was near universal (Fig. 5.2). Table 4.1 showed that even with near identical FRAs (i.e. those presented in figure 4.2), the CF changed by 1/10 of an octave in two of the eight FRAs. This variability indicates that the changes in CF by 1/10 of an octave could not be confirmed to be due to the experimental manipulation. Those FRAs which did change by more than 1/10 of an octave appeared to have a similar tuning and these changes were also likely due to variability in the response; save for one FRA which did shift in CF.

As the experiments presented here were performed in adult animals, tonotopy had developed into a mature representation of frequency in the IC (Romand and Ehret, 1990; Friauf, 1992). It is not surprising then, that a temporary removal of afferent input from the contralateral IC did not produce a shift in CF. Even with the removal of this source of input to the recorded neuron, the normal, frequency specific input from CN, and possibly from SOC and DNLL would have been maintained. The drive from these ascending afferents to the recorded neuron was not modified by eliminating activity from the contralateral IC and therefore the CF was unchanged. Furthermore, commissural projections from and to the CNIC are known to be tonotopic (Saldaña and Merchán, 1992; Malmierca *et al.*, 1995; Malmierca *et al.*, 2009), and removing this input would not modify the frequency representation of IC projections via the CoIC to the recorded neuron. This is consistent with experiments in which iontophoretic blockade of inhibition caused dramatic changes in Narrow and Closed frequency response shape of but no alteration in CF (Vater *et al.*, 1992; Yang *et al.*, 1992; LeBeau *et al.*, 2001; Lu and Jen, 2003). This finding also matches the

data of Malmierca *et al.* (2003) who found no change in CF with contralateral IC deactivation via drug injection of kynurenic acid.

These data seem to conflict with a recent report of CF shifts in one IC due to the pairing of auditory stimuli with electrical stimulation of the contralateral IC in mouse (Cheng *et al.*, 2013). Electrical stimulation of the fibres driving the recorded neuron may have provided afferent input from across the IC which would not normally be present in the unperturbed system. These additional, cross frequency inputs may have caused the reported CF shifts. The shifts in CF appear to be moderate and the change in CF of each unit in octaves may be more moderate than reported by Cheng *et al.* (2013). These shifts in CF may therefore be an artefact of the experimental paradigm and possibly unrepresentative of the actions of CoIC projections in auditory processing. Alternatively, the changes in CF observed may reflect plastic changes in the CoIC which are beyond the scope of the experiments performed in this study. For *in vitro* experiments of CoIC function, only artificial electrical stimulation is available and has provided useful information as to the nature of the inputs the CoIC provides to IC neurons (Smith, 1992; Moore *et al.*, 1998). The advantage of *in vivo* experiments is the opportunity to stimulate the intact system.

It is for these reasons that electrical stimulation is primarily used *in vivo* to test for sources of plasticity (Suga *et al.*, 1997; Yan and Suga, 1998; Suga *et al.*, 2002). Experiments which seek to infer the contribution of a nucleus to the normal physiological responses of another nucleus typically employ reversible deactivation (Brooks, 1983; Carrasco and Lomber, 2009b; Carrasco and Lomber, 2009a; Antunes and Malmierca, 2011; Anderson and Malmierca, 2013; Carrasco *et al.*, 2013).

Another possible mechanism, by which electrical stimulation could have produced shifts in CF, is by the unintentional stimulation of descending crossed projections from the ipsilateral AC to the contralateral IC. These projections are

known to terminate in the DCIC and CNIC (Winer *et al.*, 1998; Bajo and Moore, 2005; Bajo *et al.*, 2007), with the CoIC the likely candidate for the course of their contralaterally projecting axons. Stimulation of these fibres could possibly have caused the shifts in CF observed by Cheng *et al.* (2013) as the deep DCIC and CNIC are in one continuous lamina. This could have provided a substrate for intralaminar modulations of CF. Cooling is known to deactivate soma while fibres of passage are much more resistant to low temperatures (Brooks, 1983), and therefore the methods employed in this study did not cause such shifts in CF via this pathway. Considering these factors, it is not impossible that commissural projections can dynamically modify CF in the mature IC, but it appears unlikely.

5.4.3 Threshold shifts correlated with FRA area changes and were larger in non-V-shaped FRAs than V-shaped FRAs

In marked contrast to CF, threshold was influenced by cooling, with 60 of 160 (38 %) changing by more than 20 % during contralateral IC deactivation (Fig. 5.4). An interesting finding was that threshold increased significantly across all neurons with a median increase of 4 dB (Fig. 5.4B – right columns). This implicates intercollicular interactions in sensitising the responses of the population of IC neurons.

A recent study found that deactivating one primary auditory cortex (A1) and anterior auditory field in cat caused a similar significant increase in threshold in the contralateral A1 (Carrasco *et al.*, 2013). This suggests binaural interactions at multiple stages of the auditory pathway are essential to increase the sensitivity and specificity of single neuron responses.

The threshold of auditory neuronal responses in the brain is set at the cochlea. As such, there is a lower bound to which the threshold of FRAs could fall. No matter how much central processing modulated the threshold of IC neurons,

thresholds could not fall below this level. However, most neurons which had low thresholds in the control condition increased during contralateral IC cooling (Fig. 5.5). This finding supports the view that while the theoretical minimum threshold of IC neurons depends on the afferent drive from CN, in IC the threshold is determined by local processing as well.

Interestingly, this increase in threshold was not found in all neurons. Cells which increased in threshold during cooling of the contralateral IC were found to be restricted to those neurons with a low control threshold while those cells with a high control threshold decreased in threshold (Fig. 5.5.A). So while the neurons in the population which were most sensitive appear to garner some of this sensitivity due to commissural input, those IC neurons with low sensitivity appear to derive such high thresholds due to commissural inhibition. This suggests as Malmierca *et al.* (2005) found, that the CoIC is involved in controlling the gain of IC neurons and that the effect over the population appears to be level dependent. This gain may be manifest as an additive drive to low threshold units but to high threshold units, this gain control is subtractive near threshold. One function this may serve is to make the slopes of RLFs of different IC neurons, which allow the level of a sound to be discriminated due to changes in firing rate, to be spread across narrow ranges. Monotonic rate-level functions of many IC neurons do not extend over the entire range of audible levels, but rather saturate within 10 to 30 dB of threshold, while non-monotonic responses typically reach peak firing rates within the same range but do not peak at high levels (Irvine, 1986). Saturated responses over a wide range of levels of stimulation would lead to ambiguity in encoding the level of the stimulus. As such, neurons with sloping functions at high levels are essential if the IC is to encode changes in level across the full range of levels that occur physiologically. Commissural IC projections seem to 'pull apart' the dynamic ranges of IC neurons with thresholds at high and low levels. This may aid in creating sloping functions across different levels which may help disambiguate

level coding in the IC. That the effects observed were not dependent on CF or the type of stimulation indicates that this may be a non-specific mechanism.

Another interesting observation is that the range of changes in threshold of non-V-shaped FRAs was much greater than V-shaped FRAs, and the absolute change in non-V-shaped FRAs was also significantly larger than V-shaped. This matches the same finding for FRA area reported in Chapter 4 and suggests that the threshold and area of FRAs are closely linked - a postulate supported by the correlation between the change in FRA area and the change in threshold (Fig. 5.4). As these two measures are both important features of the spectral analysis performed by IC neurons, the link between the two is unsurprising and may indicate that the change in one was not independent of the other.

5.4.4 The cube root transform may be a useful measure of bandwidth in auditory neurons

The bandwidth of neurons found in this population (Fig. 5.7A and Fig. 5.8A) fit with those in previously published in guinea pig (Syka *et al.*, 2000; LeBeau *et al.*, 2001; Palmer *et al.*, 2013). As Moore *et al.* (1983) found in ferret IC, the square root transformation of bandwidths did not remove the correlation found between CF and Q_{10} (Fig. 5.7B and Fig. 5.8B), as purported by Calford *et al.* (1983). By transforming bandwidth by the cube root, the relationship with CF was removed in this sample of IC neurons. The claims of cube root transformation removing the dependence on CF are made purely on the sample of IC neurons found here. Whether this would hold true for other samples of IC, or indeed other auditory nuclei, it is not possible to say at present. For this sample of neurons, the cube root transformation of bandwidth did produce an measure independent of tuning bandwidth which provided an improvement in statistical power re Q. Only by comparing the responses from multiple nuclei as Calford *et al.* (1983) did, but with much larger numbers, can this measure be verified. Due to the development of multi-electrode recording systems, it may

now be possible to sample in sufficient numbers to test the viability of this method.

5.4.5 Bandwidth changes showed no pattern or difference with level

Irrespective of using either Q (Fig. 5.10) or cube root (Fig. 5.11), bandwidth at 10 dB re threshold was unchanged at the population level. The increases in V-shaped non-monotonic and Closed FRAs (Fig. 5.11) suggest there was an effect at 10 dB re threshold for those FRAs which expanded in area although this was not powered by enough units to be found to be statistically significant. There were some changes in other FRA types at 10 dB re threshold such as Multi-peaked and Narrow FRAs but there was no trend across the entire population.

At 40 dB re threshold there was a significant increase in Q_{40} (Fig. 5.12) and a significant decrease in cube root_{40} (Fig. 5.13) for Closed FRAs re V-shaped monotonic and Multi-peaked FRAs. Closed FRAs were different to all other FRAs in that their bandwidth at 40 dB re threshold expanded dramatically during CoIC cooling. The data here suggest that the shape of Closed FRAs is influenced by commissural input. The similarities between the expansion of Closed FRAs in IC found here and that reported previously by several authors following iontophoretic block of inhibition (Vater *et al.*, 1992; Yang *et al.*, 1992; LeBeau *et al.*, 2001; Lu and Jen, 2003) is interesting. These previous studies suggest that some Closed response types are formed *de novo* in the IC by local inhibition. Interestingly, the current findings suggest that this inhibition is influenced by the contralateral IC. Whether this effect is mediated via direct inhibition or modulation of local interneurons it is unknown at present as the methods used here do not allow for disambiguation of monosynaptic and polysynaptic circuits (Smith, 1992; Moore *et al.*, 1998). The low number of Closed responses found in this study mean that generalisations to the entire population must be made with caution, however, as all Closed FRAs found responded in a similar manner, it is a point of interest.

FRA classes are not discrete entities but points on a continuum of change and modification from simple V-shaped monotonic shapes (Yang *et al.*, 1992; LeBeau *et al.*, 2001; Hernández *et al.*, 2005; Palmer *et al.*, 2013). It is intriguing therefore, that as V-shaped non-monotonic FRAs were modulated similarly to Closed FRAs but to a lesser degree (Fig. 5.12). Inherent in their definition, V-shaped non-monotonic FRAs receive inhibition at high levels of stimulation that produces a non-monotonic RLF at CF. Unlike Closed FRAs, this inhibition is not enough to suppress firing at high levels completely or remove an expanding range of responsive frequencies with increasing level (Palmer *et al.*, 2013). That only this population of FRAs responded similarly to Closed FRAs in response to CoIC deactivation suggests a similar inhibition helps to form both or that these may be similar response types which receive differing strengths of inhibition, with a stronger influence on the formation of Closed than V-shaped non-monotonic FRAs. The similar changes in bandwidth at 40 dB re threshold for Closed and non-V-shaped monotonic FRAs, with Closed FRAs expanding more, suggests that these FRA types are formed by differing degrees of inhibition along the continuum of change from V-shaped monotonic. These findings also suggest a key commissural role in the formation of these response types.

There was no relationship between the change in bandwidth with CF, threshold, stimulation source, or control bandwidth, suggesting no simple pattern can explain the changes observed across the population. These effects may be mediated by local inhibition, but no obvious pattern emerged to support this possibility. The complexity of changes is supported by the lack of correlation between bandwidth changes observed 10 and 40 dB re threshold. It is well known that the CoIC is comprised of both excitatory and inhibitory fibres and there are likely multiple functions being sub served by different components. The combination of the likely multiple functional characteristics of the CoIC with the heterogeneous continua of FRA responses make the lack of clear pattern across the population unsurprising. One must stress that the lack of any pattern

found here does not obviate the possibility of specific changes in bandwidth of different response types - just that they were not found in this study.

5.5 Conclusion

The CF of IC neurons in the adult guinea pig was unchanged by short term deactivation of the contralateral IC. It is possible that tonotopy can be shifted over a long period of time due to a recalibration of the weighting of synaptic inputs to the IC, but it was not observed here. The afferent input which determines the CF of an IC neuron is not influenced by commissural block by any method tested to date. This implies that CF is largely inherited from the ascending afferent input. This was also found with direct cooling of neurons in Chapter 3. Conversely, threshold was highly modulated by CoIC input with the strongest effect being the reduction in threshold of the most sensitive neurons in the population, fitting with a commissural role in gain control. This is balanced by an inhibitory effect that reduces the excitatory frequency-level responses of high threshold units, and could thereby increase the discriminability of sloping rate-level functions between different units at different levels. The significant increase in threshold during contralateral IC deactivation matched a similar finding in the auditory cortex of cat – suggesting that commissural interactions via the CoIC and corpus callosum may act similarly with regards to contralateral neuron threshold sensitivity. The correlation between changes in threshold and FRA area shows that both these parameters are similar measures of IC response and both are strongly influenced by the contralateral IC. The bandwidth of Closed FRAs at high levels is strongly influenced by commissural input, be that mono or polysynaptic. Similar but lesser effects in V-shaped non-monotonic FRAs support the hypothesis that FRAs which are inhibited from V-shaped monotonic FRAs may represent points on a continuum of responses rather than discrete types and this FRA formation is dependent on the CoIC. Commissural input is therefore essential to auditory frequency analysis in the IC.

Chapter 6. Effects of Contralateral IC Deactivation on Temporal Response Properties of IC Neurons

6.1 Introduction

Neurons in the IC display a wide range of temporal response properties in response to pure tones within their excitatory FRA (Bock *et al.*, 1972; Willott and Urban, 1978; Kuwada *et al.*, 1984; Semple and Kitzes, 1985; Rees *et al.*, 1997; Tan *et al.*, 2007). Such responses can be grouped into one of three broad groups: (1) responses tuned to the onset of the stimulus; (2) responses which respond throughout the duration of the stimulus; (3) responses tuned to the end of the stimulus.

Neurons which respond throughout the duration of the stimulus are the most prominent type observed in the IC *in vivo*, with 70% having this response type in the pentobarbitone anaesthetised cat (Kuwada *et al.*, 1984), and 60 to 80 % of all neurons in the urethane or chloralose anaesthetised guinea pig (Rees *et al.*, 1997). This finding has also been replicated *in vitro*, with estimates of around 70 % of neurons in coronal slices taken from rat firing throughout the duration of supra-threshold depolarisations (Peruzzi *et al.*, 2000; Sivaramakrishnan and Oliver, 2001). Similarly, Li *et al.* (1999) made intracellular recordings in coronal IC slices from Sprague-Dawley rats and found 77 % of units exhibited responses that continued throughout the period of stimulation.

Temporal responses of IC neurons *in vivo* reflect the confluence of multiple factors such as the balance of afferent excitation and inhibition (Hind *et al.*, 1963; Rose *et al.*, 1963; Bock *et al.*, 1972; Ryan and Miller, 1978) and the channels expressed in the cell membrane (Sivaramakrishnan and Oliver, 2001). These factors can be modulated experimentally. For instance, it has been shown that the temporal structure of spike trains of neurons in sub-cortical auditory nuclei such as the CN (Rhode and Smith, 1986; Manis, 1990) and IC (Peruzzi *et*

al., 2000; Koch and Grothe, 2003; Tan *et al.*, 2007) can be modulated by hyperpolarisation. Application of bicuculline - a competitive antagonist of GABA_A receptors - found that local inhibition plays a significant role in forming the temporal response characteristics observed in the IC *in vivo* (Faingold *et al.*, 1989; Faingold *et al.*, 1991; Vater *et al.*, 1992; Park and Pollak, 1993; Casseday *et al.*, 1994; LeBeau *et al.*, 1996).

Malmierca *et al.* (2005) presented evidence that the CoIC can exert both inhibitory and excitatory effects on the firing rate of IC neurons, while Mei *et al.* (2012) found that electrical stimulation, presented in synchrony with auditory stimulation, suppressed almost all neuronal activity in the contralateral IC. The finding of the latter study is startling given that only 20 % of CoIC projecting CNIC neurons are inhibitory (González-Hernández *et al.*, 1996; Hernández *et al.*, 2006). Electrical stimulation is not normally used in investigations which attempt to imply the functional relationships between brain areas because electrical stimulation may disturb the natural current flow across post-synaptic membranes. Deactivation techniques confer the advantage of removing only physiological activity in the system which allows strong inferences to be made about causal links between brain areas (see Brooks (1983)).

To date there have been no investigations into the influence of the CoIC on temporal responses in IC. A systematic examination of the effects of the CoIC on a sizeable population of temporal responses of IC neurons using deactivation techniques is therefore essential if we are to determine the role of the CoIC in auditory processing in the IC. Whether CoIC projections can modulate the temporal pattern of IC responses is currently unknown. One previous study has shown that blocking the contralateral DNLL can change the firing rate of IC neurons (Faingold *et al.*, 1993) suggesting that tectal auditory nuclei can modulate firing rates in the IC, but effects on temporal structure were not investigated.

This Chapter will report the results of a series of experiments which used the cooling paradigm set out in Chapter 3 to determine the effects of IC cooling induced deactivation on the firing rate and temporal structure of contralateral IC neuronal responses to repetitive pure tone stimuli.

The experiments reported in this Chapter have sought to record PSTH responses from a large number of IC neurons in response to contralateral IC deactivation. Different PSTH morphologies were hypothesised to have different functional roles in the IC, and therefore they were hypothesised to receive selective CoIC input that contributes to the processing undertaken by each type. Due to the short latency and near ubiquitous nature of CoIC input to IC neurons (Smith, 1992; Moore *et al.*, 1998), it was hypothesised that changes in firing rate would be accompanied by changes in FSL, both of which are important in the neural output of IC neurons.

6.2 Methods

The methods used to record the data presented in this Chapter are broadly the same as outlined in Chapter 2. PSTHs were derived using the method set out Section 2.8. The parameters and the number of repetitions of the stimulus (always presented at 20 dB above control CF) were the same throughout the control, contralateral IC cool and recovery phases for each cell.

The number of stimulus repetitions used to record each PSTH varied across cells between 50, 100, 250 or 1,000. Units were recorded in response to a battery of stimuli which took 20 minutes to collect. To maximise the chance of holding the unit throughout recovery, only 50 repetitions of the PSTH stimulus were presented in the first few experiments. Over the course of the study the time to deliver the necessary stimuli without exceeding 20 minutes was optimised so that more repetitions were presented in each PSTH. This allowed for less variability and greater statistical power. To compensate for this change, comparisons between units were made by comparing the number of spikes fired per stimulus repetition. Comparisons within cells are made using the total number of presentations for that unit. Comparisons across populations of units were made between the responses to the first 50 repetitions of the stimulus. For a small proportion of units the first presentation in the series caused some multi-unit responses at response onset which were suppressed on further repetitions. To negate these artefacts, statistical comparisons between units were made using responses from the 2nd to the 50th presentation of the stimulus.

Because of the low firing rate of some units, and the dramatic suppression of firing rates during contralateral IC cooling of others, some responses were non-parametrically distributed. As a consequence non-parametric statistical tests have been implemented throughout. This may have led to an increase in type II errors due to the loss of power in the assessment of some parametrically

distributed responses. However, this did confer the advantage of decreasing the number of type I errors and therefore all statistically significant differences obtained can be strongly inferred to be the result of the experimental manipulation.

Statistical comparisons within a unit were performed using Friedman's repeated measures ANOVA. *Post hoc* comparisons were made using Dunnett's method: one test between the control response and the response during contralateral IC cooling; the other between the control response and the response after recovery from cooling. To be included in this dataset, each unit was required to have no significant difference between the control and recovery responses. Population analyses between multiple groups were made using a Kruskal-Wallis One Way ANOVA and unpaired group comparisons were performed with the Mann-Whitney rank sum test.

6.3 Results

Tone bursts to generate PSTHs were presented to 156 neurons over 17 experiments. Of these, 76 were held as single units throughout all three stages of a cooling cycle. There were 48 cells for which the control and recovery firing rates were not significantly different. Of the 28 units that were excluded at this stage, the firing rate of 24 did not recover back to within the range of the control firing rate. In most cases this was due to the cell dying or drifting so that it could no longer be discriminated.

There were 4 cells for which the firing rate changed significantly during contralateral IC cooling and on recovery the firing rate rebounded so that the control and recovery recordings were significantly different. Since these units were still well discriminated single units and the change in the recovery phase was a reversal from the change during contralateral IC cooling, the firing rate was deemed to have reversibly recovered with an over or under-shoot and these units were included in the dataset. This produced a total of 52 units.

6.3.1 Summary of the units included in this dataset

Almost all units could be classified into one of the types of PSTH responses set out by Rees *et al.* (1997). Examples of each of the eight types of PSTH found in this study are shown in Figure 6.1. Observable similarities amongst all units in each type were as follows:

- i) *Onset* (n = 6) types fired only at the onset of the stimulus (Fig. 6.1A).
- ii) *Build-up* types (n = 4) had a longer FSL than all types other than Offset units. The first spike in other PSTH types tended to be relatively constant with some jitter (less than 4 ms). Build-up units had a FSL with a high degree of jitter. The probability of spiking increased over time producing a ramped onset component in their PSTH. These units fired throughout the duration of the tone (Fig. 6.1B).

- iii) *Chopper* types (n = 5) were classified by their highly regular pattern of firing exhibited throughout the duration on the stimulus (Fig. 6.1C). Chopper PSTHs always had a minimum of three regularly spaced peaks. Owing to their regular firing, Choppers also had multiple discrete peaks in their inter-spike interval histogram (ISIH).
- iv) *Pauser* types (n = 5) had a short latency peak at the onset of the stimulus followed by a time window in which few or no spikes occurred. This was followed by firing throughout the duration of the stimulus (Fig. 6.1D).
- v) *On-sustained* types (n = 21) had a distinct onset peak and fired throughout the duration of the stimulus. (Fig. 6.1E).
- vi) *Sustained* types (n = 5) exhibited sustained firing throughout the duration of the stimulus but did not have a significantly higher firing rate in the first 10 ms of the response than at any other point during the response (Fig. 6.1F).
- vii) *Offset* types (n = 4) had a PSTH with a prominent peak following the end the stimulus (Fig. 6.1G) with little or no firing prior.
- viii) *Onset-offset* responses (n = 1) had a sharp onset peak and a broad offset peak with little spiking during the stimulus (Fig. 6.1H).

This sample contains examples of all reported PSTH types in the IC *in vivo* which have been reported to date.

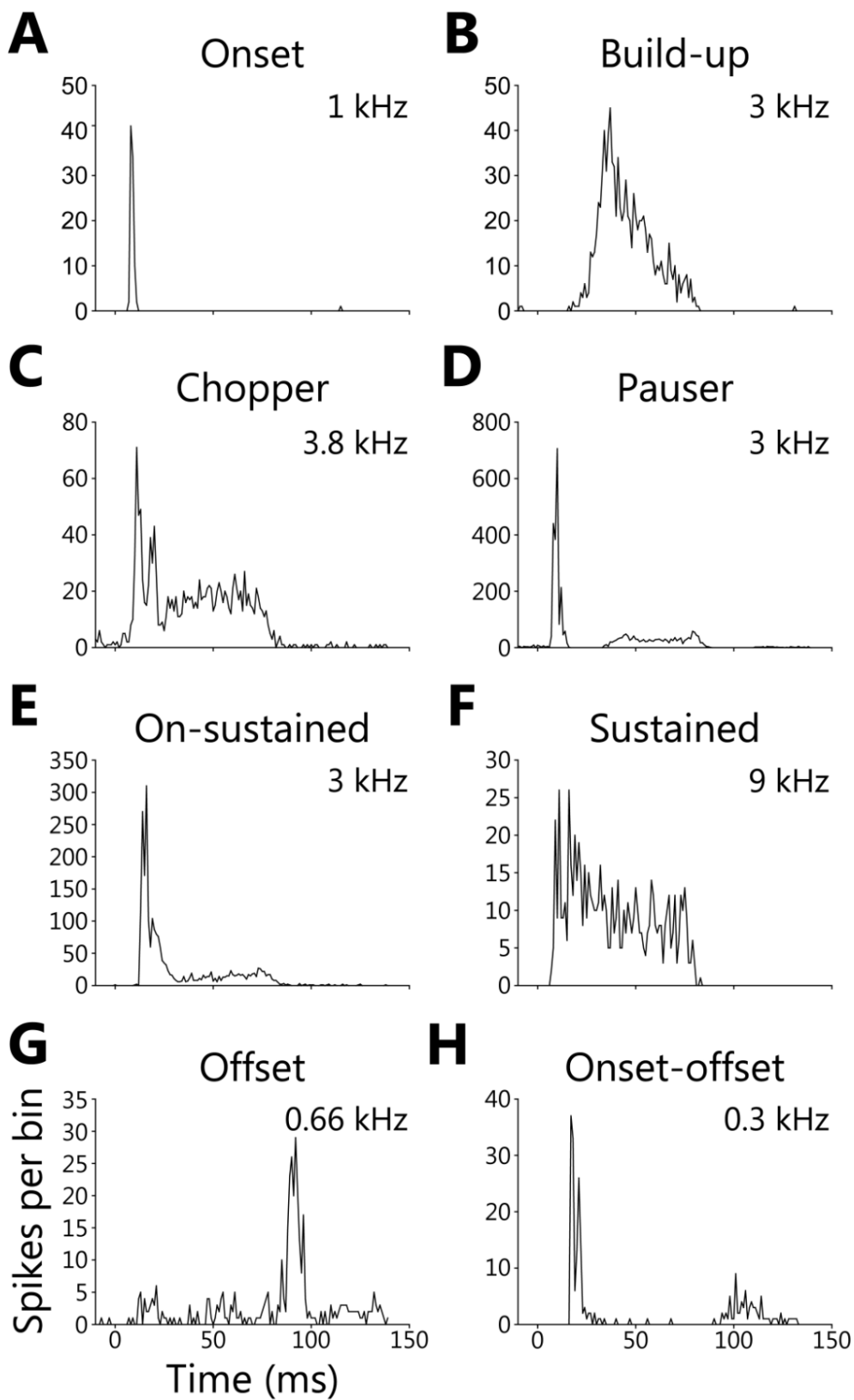


Figure 6.1 Examples of each PSTH morphology found in the course of these experiments: (A) Onset; (B) Build-up; (C) Chopper; (D) Pauser; (E) On-sustained; (F) Sustained; (G) Offset; (H) Onset-offset. The CF of each unit is shown inset on each panel.

6.3.2 The firing rate of Onset units increased during contralateral IC deactivation

Six Onset units were recorded across 5 experiments that had no significant difference between control and recovery firing rate. Three of these units recovered to both contralateral and binaural stimuli, 2 recovered to binaural stimulation only and 1 recovered to contralateral stimulation only. This produced 4 responses to contralateral stimulation and 5 to binaural stimulation.

Onset units could fire either one or two spikes at the onset of the stimulus. As the number of spikes fired to each stimulus was low, these distributions were not normally distributed. However, reporting the changes as median and IQR is not sensitive enough to show the changes that occurred to the responses of these units throughout cooling. Therefore the more sensitive mean and standard deviation will be presented in all cases.

Onset units to which both contralateral and binaural stimuli were presented were modulated in the same manner. Responses of 3 units were unchanged by contralateral IC cooling while the responses of the other 3 units significantly increased. An example of one Onset unit which significantly increased in firing rate is shown in figure 6.2. This unit was presented with 250 repetitions of a tone and elicited 109 (M = 0.44, SD = 0.52) and 50 (M = 0.20, SD = 0.41) spikes to contralateral (Fig. 6.2A) and binaural (Fig. 6.2D) stimulation respectively. Contralateral IC cooling caused an increase in spikes. The unit fired 144 spikes (M = 0.58, SD = 0.57) to contralateral (Fig. 6.2B) and 96 spikes (M = 0.38, SD = 0.54) to binaural (Fig. 6.2E) stimulation. Following recovery the number of spikes dropped to 97 (M = 0.39, SD = 0.59) in response to contralateral (Fig. 6.2C) and 62 spikes (M = 0.25, SD = 0.44) in response to binaural (Fig. 6.2F) stimulation. The unit fired with less jitter on recovery than in the control condition - this was more pronounced for binaurally driven spikes.

This change in firing rate was significant for both contralateral ($\chi^2(2) = 19.54$, $P < 0.001$) and binaural ($\chi^2(2) = 19.09$, $P < 0.001$) stimuli. *Post hoc* tests found significant differences between control and cool groups to both contralateral ($Z = 2.97$, $P = 0.003$) and binaural ($Z = 4.12$, $P < 0.001$) stimuli. There were no significant differences between the control and recovery spikes per stimulus for either contralateral ($Z = -1.2$, $P = 0.23$) or binaural ($Z = 1.23$, $P = 0.18$) stimulation.

This unit also produced a 34 % increase in FRA area to contralateral, and a 30 % increase to binaural stimulation. This was coupled with reductions in threshold of 23 % to contralateral, and 28 % to binaural stimuli. These associated changes suggest a general change in the gain of the neuron and an increase in excitability during contralateral IC deactivation.

The control firing rate of the population of Onset units was narrowly distributed ($M = 1.15$, $SD = 0.64$) as the mean firing rate of individual units ranged from 0.2 to 1.82 spikes per stimulus. During contralateral IC cooling the firing rate of Onset units increased ($M = 1.54$, $SD = 0.93$). Both the minimum (0.39) and maximum (3.42) mean firing rate increased, giving an increased range. This trend reversed following recovery both in terms of mean firing rate of the population ($M = 1.14$, $SD = 0.64$) and the range of responses ($\wedge = 0.25$, $v = 1.94$). There was a significant difference between population firing rates across conditions ($\chi^2(2) = 70.68$, $P < 0.001$) with the increase in firing rate during cooling of the contralateral IC being significantly higher than the control condition ($Z = 7.97$, $P < 0.001$).

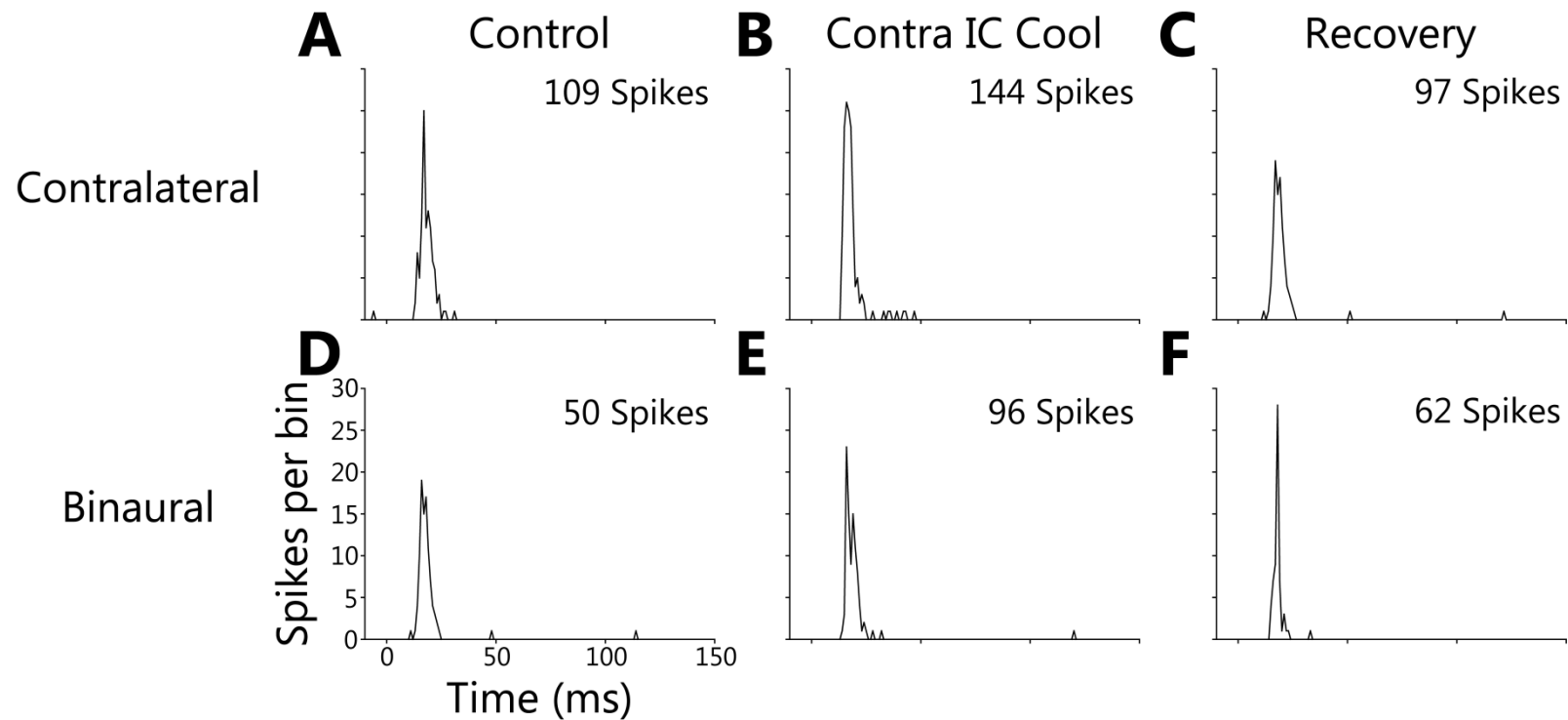


Figure 6.2 Example of the Onset responses (CF = 8.5 kHz) of an IC neuron in response to contralateral (top row) and binaural (bottom row) PSTH stimuli throughout control (left column), contralateral IC cool (middle column) and recovery (right column) phases of a cooling cycle. The unit had a sharp onset peak to both stimulation types. The firing rate was higher in response to contralateral (A) than to binaural (D) stimuli in the control condition. Firing rate increased significantly to both contralateral (B) and binaural (E) stimuli. These changes reversed on recovery with both contralateral (C) and binaural (F) stimulation.

6.3.3 The majority of Build-up responses were unchanged

The population of Build-up units was made up of 4 cells; 2 of these recovered to both contralateral and binaural stimulation, while one of each recovered with either contralateral or binaural stimulation. Each of the 4 cells was recorded in a different experiment. The responses of 2 units were unchanged by the paradigm. One cell increased in firing rate while another decreased to binaural stimuli but was unchanged to contralateral stimuli.

The responses of a Build-up unit throughout a cooling cycle are plotted in Figure 6.3. The unit fired with a similar temporal structure to both contralateral (Fig. 6.3A) and binaural (Fig. 6.3B) stimulation. The firing rate was similar in the control condition in response to contralateral ($M = 4.00$, $SD = 1.90$) and binaural ($M = 3.79$, $SD = 1.79$) stimulation. During contralateral IC cooling the number of spikes fired in response to contralateral ($M = 4.40$, $SD = 1.61$) and binaural ($M = 4.04$, $SD = 1.49$) stimulation firing increased slightly. Following recovery, the number of spikes dropped in response to contralateral ($M = 4.16$, $SD = 1.94$) and binaural ($M = 3.59$, $SD = 1.92$) stimulation. For this unit there was no significant difference in firing rates in response to either contralateral ($\chi^2(2) = 3.86$, $P = 0.15$) or binaural ($\chi^2(2) = 3.99$, $P = 0.14$) stimulation.

The population of Build-up units fired in the range of 3 to 5 spikes per stimulus in the control condition ($M = 4.17$, $SD = 0.57$; $\lambda = 3.70$, $\nu = 4.92$). Cooling the contralateral IC increased the firing rate of the population of Build-up units marginally ($M = 4.40$, $SD = 1.06$) while the range increased at both ends of the distribution ($\lambda = 2.35$, $\nu = 6.33$). After recovery the firing rate reduced to near control values ($M = 4.66$, $SD = 1.97$) and the range contracted ($\lambda = 3.59$, $\nu = 5.27$). There were no significant differences between the control, contralateral IC cool and recovery groups for the population of Build-up units ($\chi^2(2) = 0.23$, $P = 0.89$).

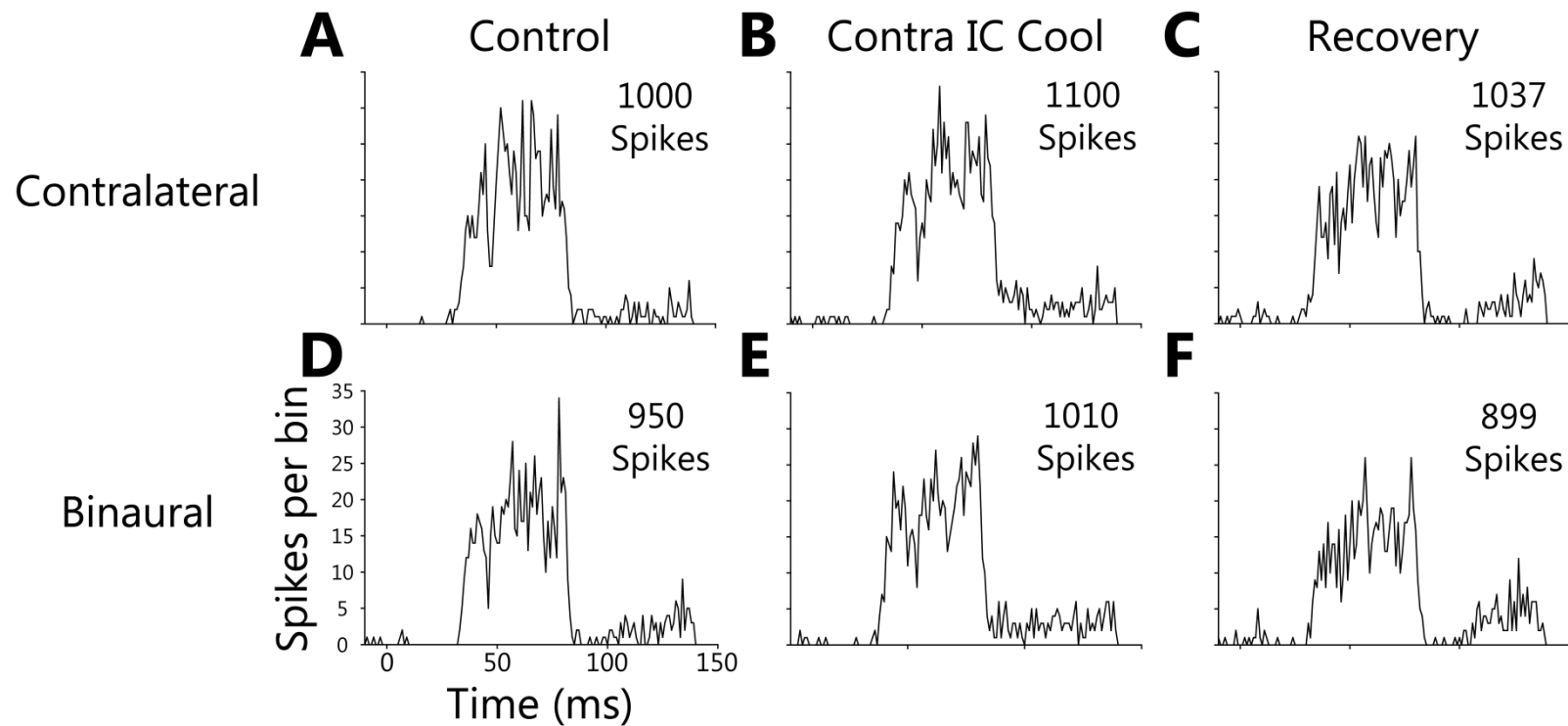


Figure 6.3 Responses of a Build-up unit (CF = 7.8 kHz) which was unchanged by the cooling paradigm. Firing rate was similar in response to contralateral (A) and binaural (D) stimulation in the control condition. Contralateral IC cooling did not modify the PSTH morphology or the firing rate significantly in either stimulus condition (B & E). This was also true on recovery (C & F).

6.3.4 The firing rate of Chopper units decreased while ISI increased

There were 5 Chopper units which were included in this dataset – all of which were studied with both binaural and contralateral stimulation and recovered after cooling.

All Chopper units reversibly decreased in firing rate during contralateral IC cooling to both stimulation conditions. The PSTHs of one such unit are shown in figure 6.4 to contralateral (Fig. 6.4A) and binaural stimulation (Fig. 6.4D). Each PSTH was constructed from the responses of the unit to 1,000 presentations of the stimulus. The unit fired between 3 and 5 spikes per stimulus to contralateral stimulation (M = 2.75, SD = 0.91) and fired between 4 and 5 spikes per stimulus to binaural stimulation (M = 3.21, SD = 1.20).

Contralateral IC cooling induced a reduction in firing rate to contralateral (Fig. 6.4B; M = 1.84, SD = 0.34) and binaural (Fig. 6.4E; M = 1.86, SD = 0.37) stimulation. The responses shifted from 3 and 4 sharp peaks in response to contralateral and binaural stimulation respectively, to 2 broad peaks irrespective of sound source. These reductions reversed upon cessation of cooling with both contralateral (Fig. 6.4C; M = 2.82, SD = 0.96) and binaural (Fig. 6.4F; M = 2.98, SD = 0.99) stimuli. The morphology of the PSTH also recovered to match the control condition.

These reductions in firing rate resulted in a significant difference between the contralateral ($\chi^2(2) = 116.51$, $P < 0.001$) and binaural ($\chi^2(2) = 122.14$, $P < 0.001$) responses. *Post hoc* analyses found that the firing rate during cooling of the contralateral IC was significantly lower than the control responses to contralateral ($Z = -6.64$; $P < 0.001$) and binaural ($Z = -7.98$; $P < 0.001$) stimulation. There was no significant difference between firing rates in the control and recovery groups for either contralateral ($Z = 1.36$; $P = 0.18$) or binaural ($Z = -2.07$; $P = 0.04$) stimuli.

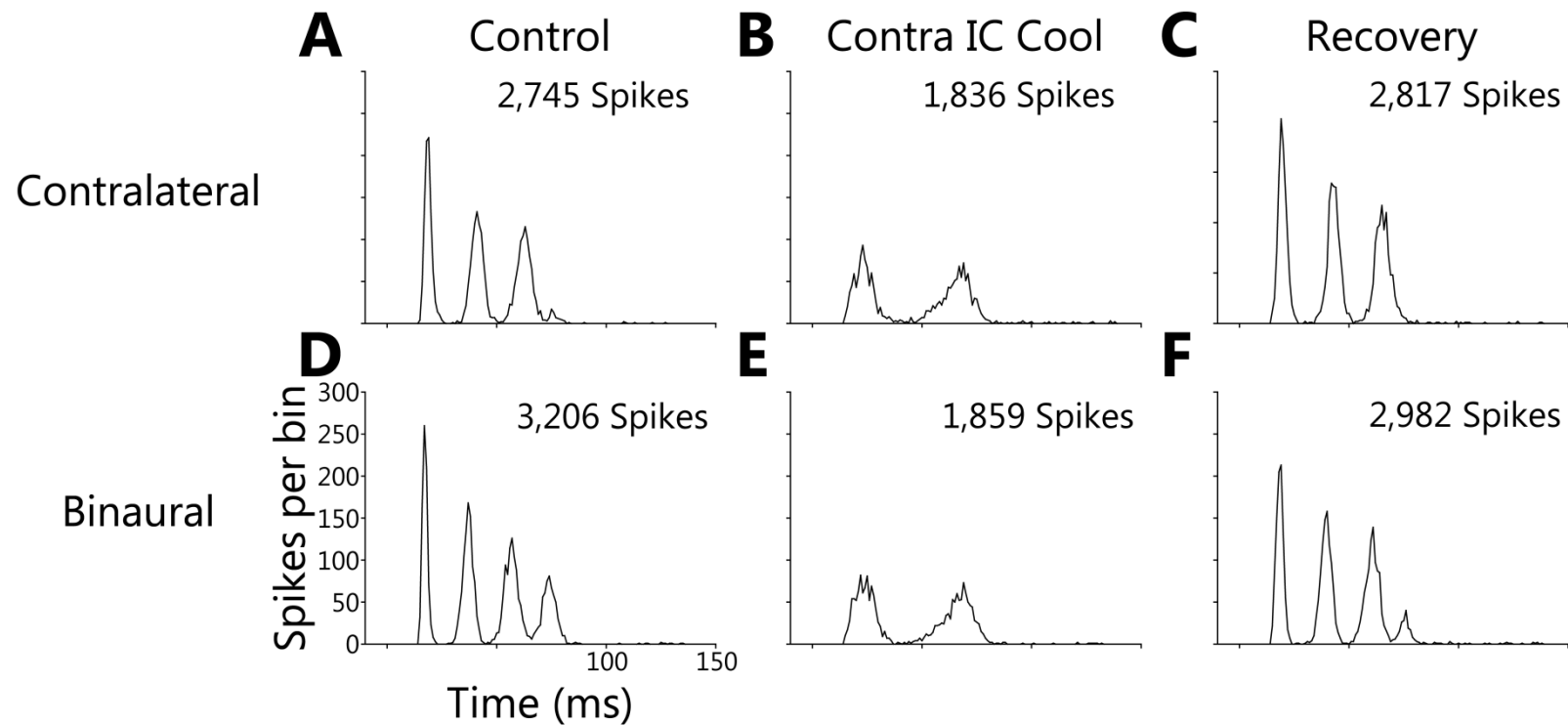


Figure 6.4 PSTHs for a Chopper unit (CF = 0.95 kHz) which decreased in firing rate during contralateral IC deactivation. The unit had three sharp peaks in response to (A) contralateral stimulation with an additional peak in response to (D) binaural stimulation. Contralateral IC deactivation caused a shift in the response to two broad peaks in response to both stimulus types (B & E). On recovery, the firing rate and PSTH morphology recovered to both stimulus types (C & F).

While the temporal response of this neuron was altered, the FRA area was unchanged to contralateral or binaural stimuli, with area changes of 0 % and 6 % respectively during contralateral IC deactivation. This finding implies a CoIC mediated selective contribution to the temporal response of this neuron, which was not a simple change in excitability.

Decreases in Chopper firing rates were accompanied by increases in inter-spike interval (ISI). Two examples of reversible increases in ISI are shown in figure 6.5. In the upper half of the figure (Fig. 6.5A-D) the ISIs of the unit shown in figure 6.4 are plotted in response to contralateral (Fig. 6.5A) and binaural (Fig. 6.5C) stimuli. The peak in ISI in the control condition was 21 ms to contralateral and 19 ms to binaural stimulation. During cooling the peak ISI increased to 42 ms in response to both stimulus types. On recovery, peak ISI reduced to 22 ms in response to contralateral stimuli and 20 ms to binaural stimuli. The similarities between these shifts in the peak ISI are highlighted by normalisation to the maximum ISI for contralateral (Fig. 6.5B) and binaural (Fig. 6.5D) stimulation.

A second example of a Chopper unit which increased in ISI during cooling is shown in panels E through H of figure 6.5. The unit produced a peak ISI of 14 ms to contralateral (Fig. 6.5E) and 11 ms to binaural (Fig. 6.5G) stimulation. Cooling the contralateral IC significantly reduced the firing rate to both types of stimulation. The peak ISI in response to contralateral stimulation changed to 21 ms and the peak ISI to binaural stimulation changed to 34 ms. The reduction in firing rate was greater to binaural stimulation which produced a broader and lower peak ISI (compare red traces in Fig. 6.5F & H). Recovery of firing rate shifted the peak ISI to 12 and 10 ms in response to contralateral and binaural stimulation respectively (Fig. 6.5E & G). Normalising to the maximum ISI in each stage shows the increased in ISI during contralateral IC cooling was greater for binaural (Fig. 6.5 H) than contralateral (Fig. 6.5F) stimulation.

This unit, while also increasing in peak ISI, showed a 34 % increase in FRA area to contralateral, and a 31 % increase to binaural stimulation. Coupled to this were a 9 dB decrease in threshold to contralateral, and a 4 dB decrease in threshold to binaural stimuli. These data support the earlier finding that changes in the temporal structure of Chopper units were independent of changes in FRA and general levels of excitability.

All 10 analyses of Chopper units significantly decreased during contralateral IC cooling. There was a significant difference between the control, contralateral IC cool and recovery groups of the population of Chopper firing rates ($\chi^2(2) = 299.21, P < 0.001$). *Post hoc* analyses found that the difference in firing rate between the control and contralateral IC cool groups was also strongly significant ($Z = -12.25; P < 0.001$).

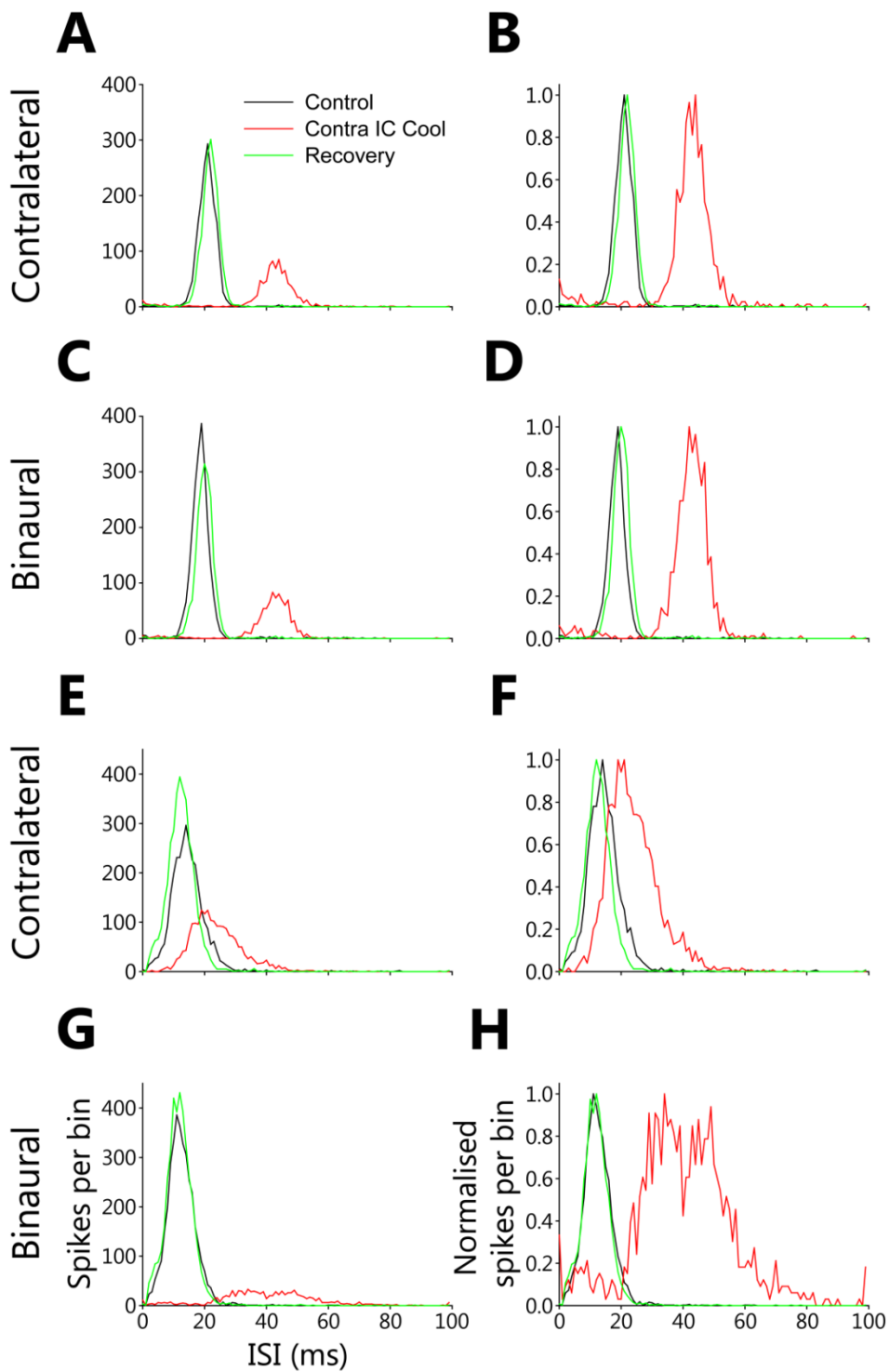


Figure 6.5 ISIs of two Chopper units which were reversibly modulated. Both had similar ISI to contralateral (black trace; A & E) and binaural (black trace; C & G) stimuli. Cooling the contralateral IC increased all ISI (red trace; A, C, E & G) which reversed on recovery (green trace; A, C, E & G). Normalised ISI of the unit in A-D shows the increase in ISI was similar to contralateral (B) and binaural (D) stimuli. The increase in ISI of the second unit (E-F) was much less to contralateral (F) than binaural (H) stimuli.

6.3.5 Most Pauser units decreased in firing rate

A total of 5 Pausers were included in this dataset. Three of these units recovered to both stimulation types while the other two recovered in response to contralateral stimulation only. One unit was unchanged to contralateral stimulation while the responses of all other units to both stimulation types reduced during contralateral IC cooling.

An example of a unit which reduced in firing rate during contralateral IC cooling is plotted in figure 6.6. In the control condition this unit had a sharp onset peak followed by silent period which was followed by a sustained response throughout the remainder of the stimulus (Fig. 6.6A & D). The unit fired with a slightly lower firing rate to contralateral (Fig. 6.6A; M = 3.25, SD = 1.54) than to binaural (Fig. 6.6D; M = 3.56, SD = 1.63) stimulation. Contralateral IC cooling reduced the number of spikes fired per stimulus in response to both contralateral (Fig. 6.6B; M = 2.59, SD = 1.12) and binaural (Fig. 6.6E; M = 2.13, SD = 1.04) stimuli. These reductions in firing rate recovered in response to contralateral (Fig. 6.6C; M = 2.93, SD = 1.66) and binaural (Fig. 6.6F; M = 3.66, SD = 1.87) stimulation after cooling was stopped.

There were significant differences between the responses of this unit in the three stages of the cooling cycle to contralateral ($\chi^2(2) = 25.31$, $P < 0.001$) and binaural ($\chi^2(2) = 46.92$, $P < 0.001$) stimulation. These significant differences were due to the reduction in firing rate during contralateral IC cooling (contralateral: $Z = -2.98$, $P = 0.003$; binaural: $Z = -5.00$, $P < 0.001$). There were no significant differences between the control and recovery groups (contralateral: $Z = 1.87$, $P = 0.06$; binaural: $Z = 1.47$, $P = 0.14$).

An additional effect was noted for this unit in that while firing rate decreased, the offset response increased during contralateral IC cooling. The offset response also shifted from ~80 ms post stimulus onset (Fig. 6.6A & D) to ~100

ms (Fig. 6.6B & E) and the peak at offset more than doubled in spike count – a trend which reversed following recovery (Fig. 6.6C & F).

The reduction in firing rate of this unit was accompanied by an increase in FRA area of 37 % to contralateral, and 61 % to binaural stimuli. These opposing changes between FRA area and temporal response indicate a CoIC selective influence on both rather than a general effect on the response of the neuron.

The mean firing rate of the 5 Pauser units varied between units ($M = 3.97$, $SD = 2.46$; $\lambda = 1.90$, $\nu = 7.87$). Cooling the contralateral IC caused a reduction in the mean firing rate and both limits of the distribution ($M = 3.09$, $SD = 1.86$; $\lambda = 1.32$, $\nu = 5.57$). Recovery from cooling reversed the reduction in mean, minimum and maximum firing rate ($M = 3.78$, $SD = 2.48$; $\lambda = 1.87$, $\nu = 7.70$).

There was a significant difference between the control, contralateral IC cool and recovery firing rates for the population of Pauser units ($\chi^2(2) = 101.52$, $P < 0.001$). The significant difference was due to the reduction in firing rate of the population during contralateral IC cooling ($Z = -8.53$, $P < 0.001$).

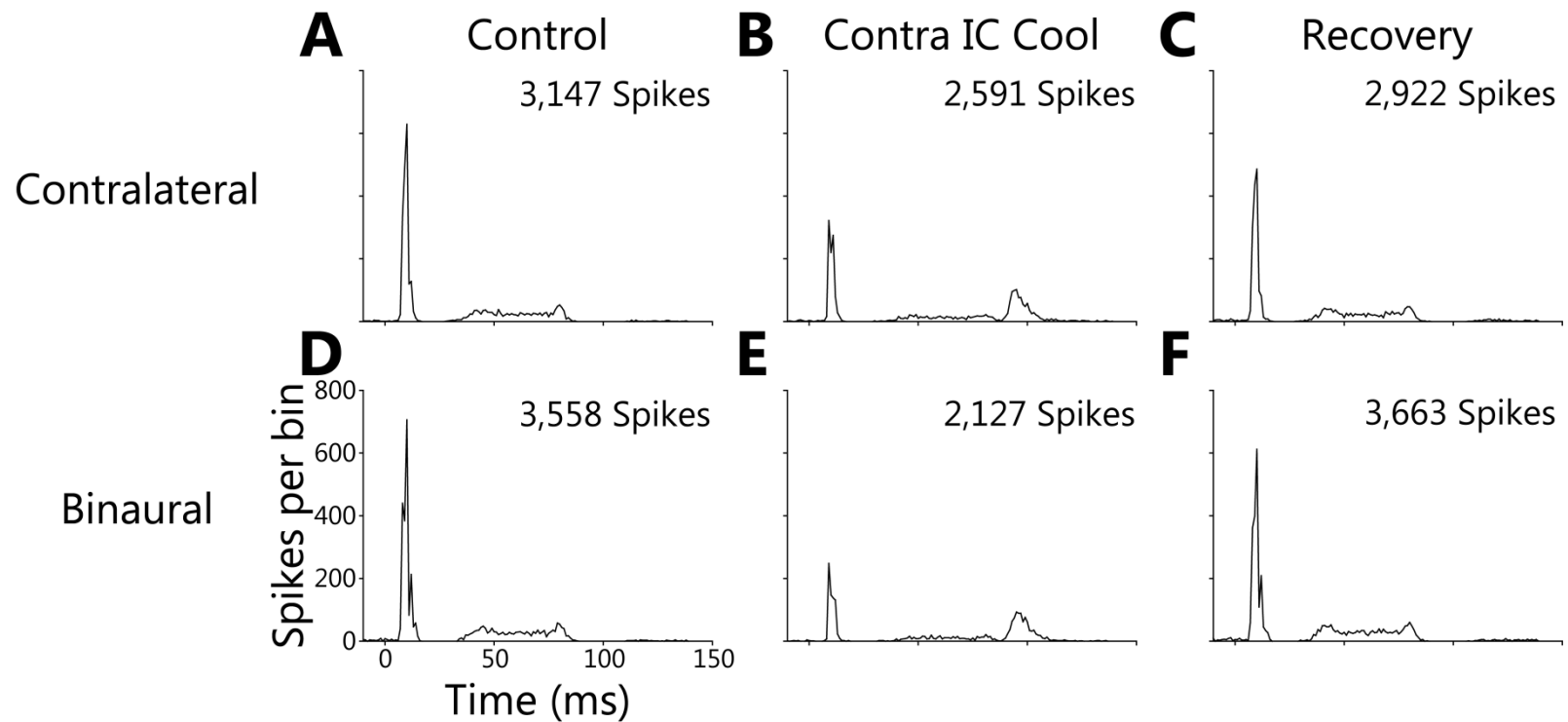


Figure 6.6 Responses of a Pauser unit (CF = 1.05 kHz) to contralateral (A) and binaural (D) stimulation. Deactivation of the contralateral IC caused a significant decrease in firing rate to both contralateral (B) and binaural (E) stimulation. The offset component of the response increased during contralateral IC deactivation to both stimulation sources. These changes reversed on recovery for both types of stimulation (C & F).

6.3.6 On-sustained units expressed a range of changes

On-sustained units were by far the largest PSTH class found in this dataset with 21 in total. Almost all of these units recovered with both contralateral and binaural stimulation. Two recovered only to binaural stimulation while one recovered to only contralateral stimulation. As well as being the most common morphology, On-sustained units had the broadest range of changes.

As there were a number of On-sustained units which increased, decreased or were unchanged in response to contralateral IC cooling, one example of each has been presented in figure 6.7. The top two rows of figure 6.7 show the response of one unit which increased in firing rate during cooling of the contralateral IC. The unit fired with a reliably timed first spike followed by a second spike which jittered over the course of about 10 ms giving a characteristic 'h' shape at the start of the PSTH response. These were followed by spikes that occurred with a high degree of variability during the remainder of the stimulus giving rise to the 'sustained' component of the PSTH. Such patterns were recorded in response to both contralateral (Fig. 6.7A) and binaural (Fig. 6.7D) stimulation. In the control condition the unit fired a high number of spikes in response to both contralateral (M = 7.47, SD = 2.03) and binaural (M = 6.27, SD = 1.92) stimulation. Cooling the contralateral IC increased the firing rate to contralateral (Fig. 6.7B; M = 10.04, SD = 2.19) and binaural (Fig. 6.7E; M = 8.98, SD = 1.87) stimuli. On recovery, the firing rate decreased to near control levels (contralateral: Fig. 6.7C; M = 7.41, SD = 1.96; binaural: Fig. 6.7F; M = 7.18, SD = 1.83). There were significant differences between the responses in the 3 stages of the cooling paradigm to contralateral ($\chi^2(2) = 38.76$, $P < 0.001$) and binaural ($\chi^2(2) = 38.34$, $P < 0.001$) stimulation. This was due to the increase in firing rate during contralateral IC cooling in response to contralateral ($Z = 4.87$; $P < 0.001$) and binaural ($Z = 5.01$; $P < 0.001$) stimuli. Firing rates in the control and recovery

conditions were not significantly different for either contralateral ($Z = -0.25$; $P = 0.81$) or binaural ($Z = 0.97$; $P = 0.34$) stimuli.

The two middle rows of figure 6.7 show data from another unit which had an On-sustained PSTH to contralateral (Fig. 6.7G; $M = 2.69$, $SD = 0.84$) and binaural (Fig. 6.7J; $M = 2.36$, $SD = 0.73$) stimulation. Cooling the contralateral IC reduced the firing rate to both contralateral (Fig. 6.7H; $M = 1.51$, $SD = 0.87$) and binaural (Fig. 6.7K; $M = 2.12$, $SD = 0.98$) stimuli. This reduction was mainly due to a reduction in the onset component of the response. Recovery from cooling saw the firing rate increase (contralateral: Fig. 6.7 I; $M = 2.43$, $SD = 1.59$; binaural: Fig. 6.7L; $M = 2.24$, $SD = 0.95$) to near control levels. There was a significant difference across groups to contralateral ($\chi^2(2) = 66.31$, $P < 0.001$) and binaural ($\chi^2(2) = 55.33$, $P < 0.001$) stimulation. This was due to a significant reduction from control firing rate during contralateral IC cooling to both contralateral ($Z = -6.6$, $P < 0.001$) and binaural ($Z = -6.6$, $P < 0.001$) stimuli. Recovery firing rates were not significantly different from control (contralateral: $Z = -0.70$, $P = 0.49$; binaural: $Z = -0.76$, $P = 0.45$).

The lower two rows of figure 6.7 feature an example of an On-sustained unit which was unchanged by contralateral IC cooling. The unit fired at a similar rate to either contralateral (Fig. 6.7M; $M = 4.73$, $SD = 1.88$) or binaural (Fig. 6.7P; $M = 4.95$, $SD = 1.67$) stimuli. During contralateral IC cooling the firing rate and PSTH morphology were unaffected in response to either contralateral (Fig. 6.7N; $M = 4.73$, $SD = 2.12$) or binaural (Fig. 6.7Q; $M = 4.70$, $SD = 1.83$) stimulation. After recovery the unit continued to fire in a similar manner to either contralateral (Fig. 6.7O; $M = 4.96$, $SD = 1.15$) or binaural (Fig. 6.7R; $M = 4.83$, $SD = 2.02$) stimuli. Statistical analysis of the response of the unit found no significant difference in firing rate at any stage, irrespective of stimulation type (contralateral: $\chi^2(2) = 0.96$, $P = 0.62$; binaural: $\chi^2(2) = 1.85$, $P = 0.40$).

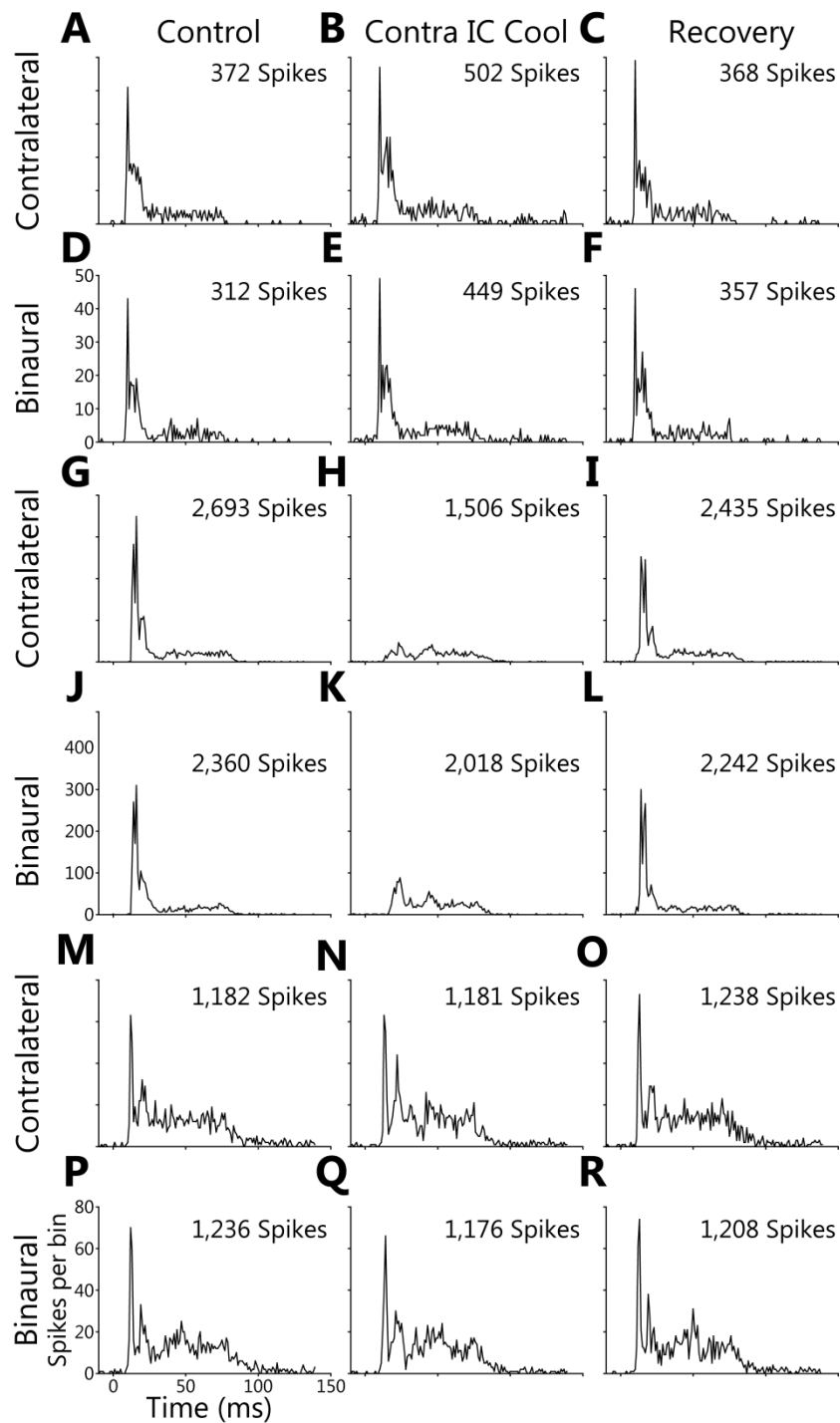


Figure 6.7 Examples of reversible changes in On-sustained responses. (A) Contralateral and (D) binaural responses (CF = 0.61 kHz) showed significant increases in firing rate (B & E) which reversed on recovery (C & F). Another On-sustained response to both contralateral (G) and binaural (J) stimuli (CF = 2.73 kHz) showed a significant reduction in firing rate to contralateral (H) and binaural (K) stimuli. Firing rate and PSTH morphology both recovered (I & L). An On-sustained unit (M & P; CF = 6.9 kHz) which showed no significant change in response to contralateral IC cooling (N & Q) or on recovery (O & R).

The population on 21 On-sustained units gave rise to a total of 39 analyses. There was an approximately even distribution of analyses which increased (n = 15), decreased (n = 10), or did not change (n = 14) during contralateral IC cooling. There were a wide range of firing rates in the On-sustained population in the control condition (M = 4.74, SD = 3.32; $\lambda = 0.43$, $v = 13.92$). Cooling the contralateral IC increased the range at each end of the distribution but average firing rate was unchanged (M = 4.74, SD = 3.63; $\lambda = 0.27$, $v = 17.47$). Recovery had little effect on firing rate (M = 4.66, SD = 3.33; $\lambda = 14.12$, $v = 0.29$). There was no significant difference in firing rate for the population between any of the three stages of the paradigm ($\chi^2(2) = 3.46$, P = 0.18).

There was an asymmetry in the changes observed which was dependent on control firing rate. More units with low control firing rates tended to increase during contralateral IC deactivation while units which fired more spikes in the control condition tended to decrease (Table 6.1). A Fisher's exact 3X2 permutation test (Freeman-Halton extension) between the distributions of significant increases, significant decreases or no change in firing rate options in the highest and lowest quartiles of On-sustained firing rates was performed. The probability of the observed distributions occurring was below the criterion for significance (P = 0.02).

Control Firing Rate	No Change	Increase	Decrease
Lowest Quartile	4	5	1
Lower Mid-Quartile	2	3	6
Upper Mid-Quartile	5	4	0
Upper Quartile	0	2	6

Table 6.1 The change in firing rate induced by cooling the contralateral IC varied depending on the control firing rate of the unit. The lower quarter of the distribution had a higher proportion of units which increased in firing rate or were unchanged than those that decreased. In the quartile of analyses with the highest control firing rates there were no units which were unchanged and more units decreased than increased their firing rate.

6.3.7 Sustained units changed firing rate during contralateral IC deactivation

There were a total of 6 Sustained units in the population. Three of these recovered in response to both contralateral and binaural stimulation sources, two recovered to contralateral stimuli only and one recovered to binaural stimuli only. This formed a population of nine analyses.

There was a tendency for Sustained units to change their firing rate during contralateral IC cooling, with 8 of the 9 analyses reversibly changing from control. Of these, the firing rates in five analyses increased and three decreased. The other analysis was unchanged at any stage of the paradigm.

It was interesting to note that units with Sustained PSTHs tended to have a lower firing rate than all other PSTH types which fired throughout the duration of the stimulus ($M = 2.56$, $SD = 1.66$; $\lambda = 0.92$, $\nu = 6.14$). During cooling of the contralateral IC the mean population firing rate was unchanged although the range did increase at both ends of the distribution ($M = 2.84$, $SD = 2.89$; $\lambda = 0.33$, $\nu = 10.04$). Following recovery the range returned to near control levels and the increase in mean firing rate reduced ($M = 2.47$, $SD = 1.78$; $\lambda = 0.73$, $\nu = 6.10$). This change in the population firing rate during cooling was not significantly different from either control or recovery ($\chi^2(2) = 0.89$, $P = 0.69$).

6.3.8 Offset and Onset-Offset PSTHs tended to change in firing rate

Four units had Offset responses. Two of these units recovered in response to contralateral and binaural stimulation, one unit only recovered to contralateral stimulation while one unit only recovered to binaural stimulation.

Two units increased in firing rate during cooling of the contralateral IC - one in response to contralateral stimulation only, the other to both stimulus types. The unit which recovered to only contralateral stimulation increased in firing rate. The other unit was unchanged to either stimulation source.

Offset units tended to fire several spikes per stimulus. They fired more than both Onset units and Sustained units ($M = 3.46$, $SD = 1.34$; $\lambda = 1.86$, $\nu = 5.35$) but less than all other PSTH types. The cooling paradigm caused an expansion at both extremes of the population and an increase in the average firing rate ($M = 3.88$, $SD = 2.07$; $\lambda = 1.76$, $\nu = 6.37$). These changes reversed following recovery ($M = 2.93$, $SD = 1.61$; $\lambda = 1.83$, $\nu = 5.90$). There was no difference at the population level between firing rates during the three stages of the paradigm ($\chi^2(2) = 0.33$, $P = 0.96$).

There was only one unit which had an Onset-offset PSTH morphology. This unit fired with a similar rate to contralateral ($M = 2.18$, $SD = 1.46$) and binaural ($M = 2.26$, $SD = 1.71$) stimuli. The unit's firing was unchanged to contralateral ($M = 2.34$, $SD = 1.69$) but reduced to binaural ($M = 1.66$, $SD = 1.33$) stimulation. The recovery responses to contralateral ($M = 1.93$, $SD = 1.59$) and binaural ($M = 2.02$, $SD = 1.90$) stimuli were similar to control. The responses to contralateral stimuli were not significantly different ($\chi^2(2) = 3.53$, $P = 0.17$) while those to binaural stimuli were ($\chi^2(2) = 10.94$, $P = 0.004$). This significant difference was due to the reduction in firing rate during contralateral IC cooling ($Z = -2.55$, $P = 0.01$) while recovery was not significantly different to control ($Z = -1.46$, $P = 0.15$).

6.3.9 Summary of changes in firing rate of all units by PSTH type

The changes observed in each PSTH class are summarised in figure 6.8.

The changes in Onset units (Fig. 6.8A) were distinct from those of any other PSTH type as they are the only group which increased in firing rate during contralateral IC cooling. This can be seen by the points to the right of equivalence in the ratio of spikes fired during contralateral IC deactivation to control in figure 6.8A.

The decreases in firing rate of Chopper (Fig. 6.8C) and Pauser (Fig. 6.8D) units are also of note. Build-up (Fig. 6.8B), On-sustained (Fig. 6.8E), Sustained (Fig. 6.8F), Offset (Fig. 6.8G), and Onset-offset (Fig. 6.8H) PSTHs all shared similarities in the range and direction of changes in firing rate of their respective populations.

It is interesting to note that of the PSTH types which fired throughout the duration of the stimulus, Chopper and Pauser types (the two types with temporally regular ISI responses) exhibited decreases in population firing rate. Build-up, On-sustained and Sustained types (those without regularly spaced spikes) could either increase or decrease in firing rate and had no significant change in their respective population firing rates during cooling of the contralateral IC.

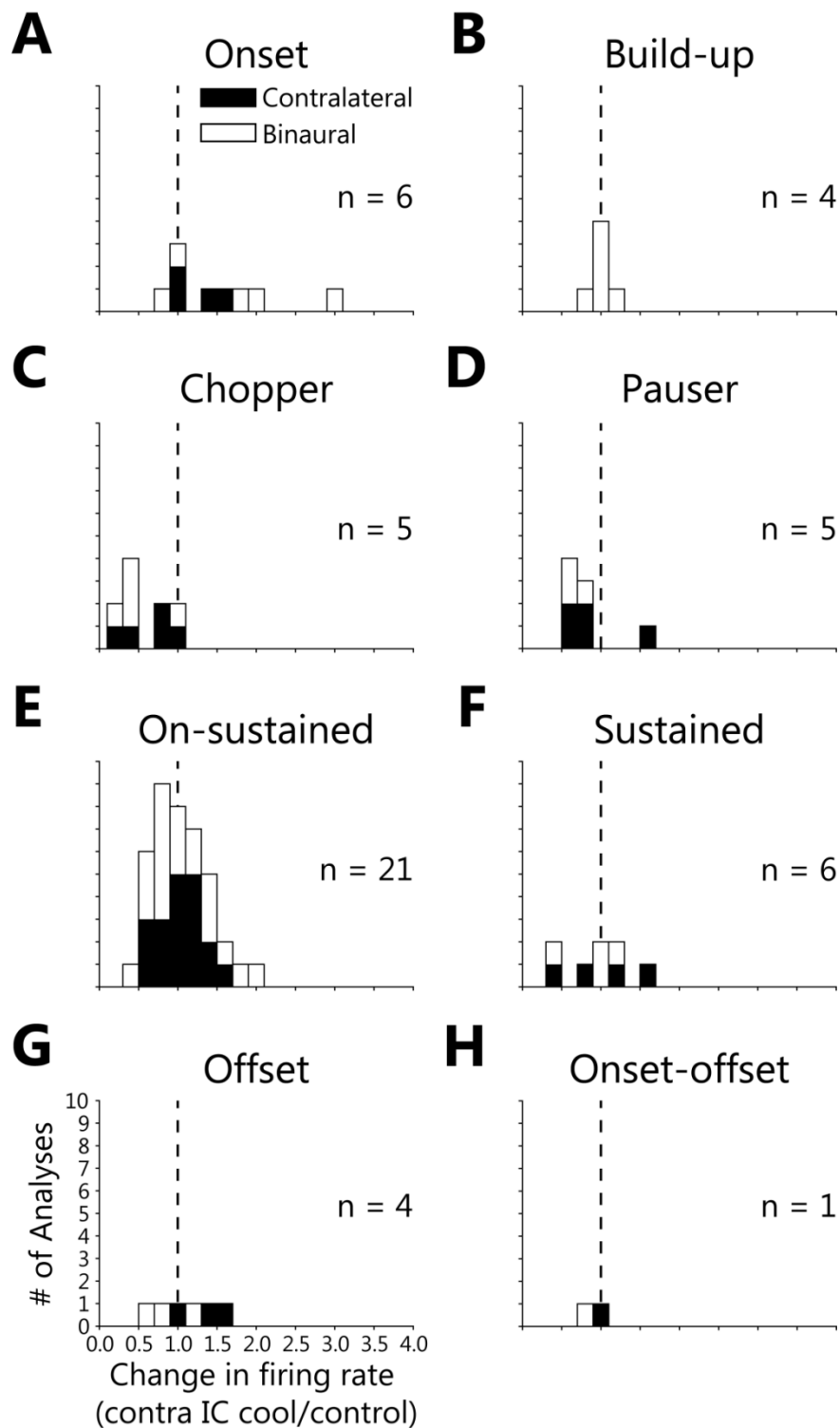


Figure 6.8 Summary of firing rate changes observed across the population of units. (A) Onset units were the only type of PSTH which significantly increased in firing rate as a population. (B) Build-up units showed little change. (C) Choppers showed significant reductions in firing rate. (D) Pausers also reduced in firing rate but this was not significant as a population. (E) On-sustained units exhibited no clear direction of change in firing rate. (F) Sustained, (G) Offset, and (H) Onset-offset types varied in the changes observed during contralateral IC deactivation.

6.3.10 The FRA of a unit had no relationship to its PSTH

As units can be classified based on both their FRA and PSTH, a comparison of the responses of units presented here and in Chapters 4 and 5 was performed. Of the 52 units included in this Chapter, 50 also had FRAs which recovered after cooling. The distribution of each type of FRA and PSTH included in this analysis are shown in table 6.2. There was no apparent relationship between PSTH and FRA responses. The strongest trend was that four of the five Onset units were V-shaped monotonic.

PSTH Type	V monotonic	V non-monotonic	Closed	Narrow	Multi-peaked	Broad	Total
Onset	4	0	0	0	1	0	5
Build-up	0	0	0	1	2	0	3
Chopper	2	0	1	1	1	0	5
Pauser	2	0	0	1	2	0	5
On-sustained	7	1	1	5	5	3	22
Sustained	3	0	1	0	1	0	5
Offset	1	1	0	0	1	1	4
Onset-offset	1	0	0	0	0	0	1
Total	20	2	3	8	13	4	50

Table 6.2 The distribution PSTH and FRA classes in this analysis. V-shaped monotonic and On-sustained were the most numerous FRA and PSTH types observed respectively. There was no relationship between FRA type and PSTH type.

The relationship between FRA type and firing rate was investigated (Fig. 6.9A). There were differences in firing rate between FRA classes: V-shaped monotonic PSTHs had the lowest mean firing rates ($\bar{x} = 2.56$; IQR = 1.78 to 4.80) while V-shaped non-monotonic the highest ($\bar{x} = 6.87$; IQR = 6.27 to 7.47). Most FRA types had a wide range of firing rates and because of this, together with the low totals in some groups, the differences between groups were not significant (Kruskal-Wallis One Way ANOVA: $H(5) = 6.54$, $P = 0.26$).

The change in firing rate measured from the PSTH during the cooling paradigm for each FRA type was also investigated (Fig. 6.9B). V-shaped non-monotonic

PSTHs showed the largest change ($\bar{x} = 1.43$; IQR = 1.37 to 1.52) with all 3 analyses increasing in firing rate. Multi-peaked PSTHs had the lowest median change as most of these units decreased in firing rate ($\bar{x} = 0.84$; IQR = 0.70 to 1.04). The firing rates of units with V-shaped monotonic, Closed, Broad and Narrow FRAs each changed in firing rate with an approximately even split of units increasing and decreasing. The differences in the change in firing rate were not significant between different FRA types ($H(5) = 7.06$, $P = 0.22$).

As summarised above, units with V-shaped non-monotonic FRAs all increased their firing rate while those with Multi-peaked FRAs tended to show a decrease in firing rate – a trend that was more consistent in those units with Multi-peaked FRAs with high control firing rates (Fig. 6.9C). In opposition to the larger changes in FRA area of non-V-shaped FRAs than V-shaped FRAs (see Chapter 4), the range of changes in the firing rate of units with V-shaped FRAs was broader than in those with non-V-shaped FRAs (Fig. 6.9D).

Plotting the change in FRA area as a function of the change in firing rate was possible for 82 analyses (Fig. 6.9D). There was no correlation between the change in FRA area and change in firing rate ($r_s(80) = 0.06$, $P = 0.60$). The range of FRA area changes was greater in non-V shaped than V-shaped FRAs (Fig. 6.9D box plots adjacent to the ordinate). For firing rate the reverse was true - a broader range of changes were found in the PSTHs of units with V-shaped than non-V-shaped FRAs (Fig. 6.9D box plots adjacent to the abscissa). This wider distribution of PSTH firing rate changes for units with V-shaped FRAs ($\bar{x} = 1.07$; IQR = 0.73 to 1.45) relative to non-V-shaped ($\bar{x} = 0.84$; IQR = 0.69 to 1.17) was not statistically significant ($U = 572$, $P = 0.09$). The absolute change in firing rate for the population of units with V-shaped FRAs ($\bar{x} = 0.31$; IQR = 0.16 to 0.58) was greater than for units with non-V-shaped FRAs ($\bar{x} = 0.26$; IQR = 0.16 to 0.40), but not significantly so ($U = 630$, $P = 0.26$).

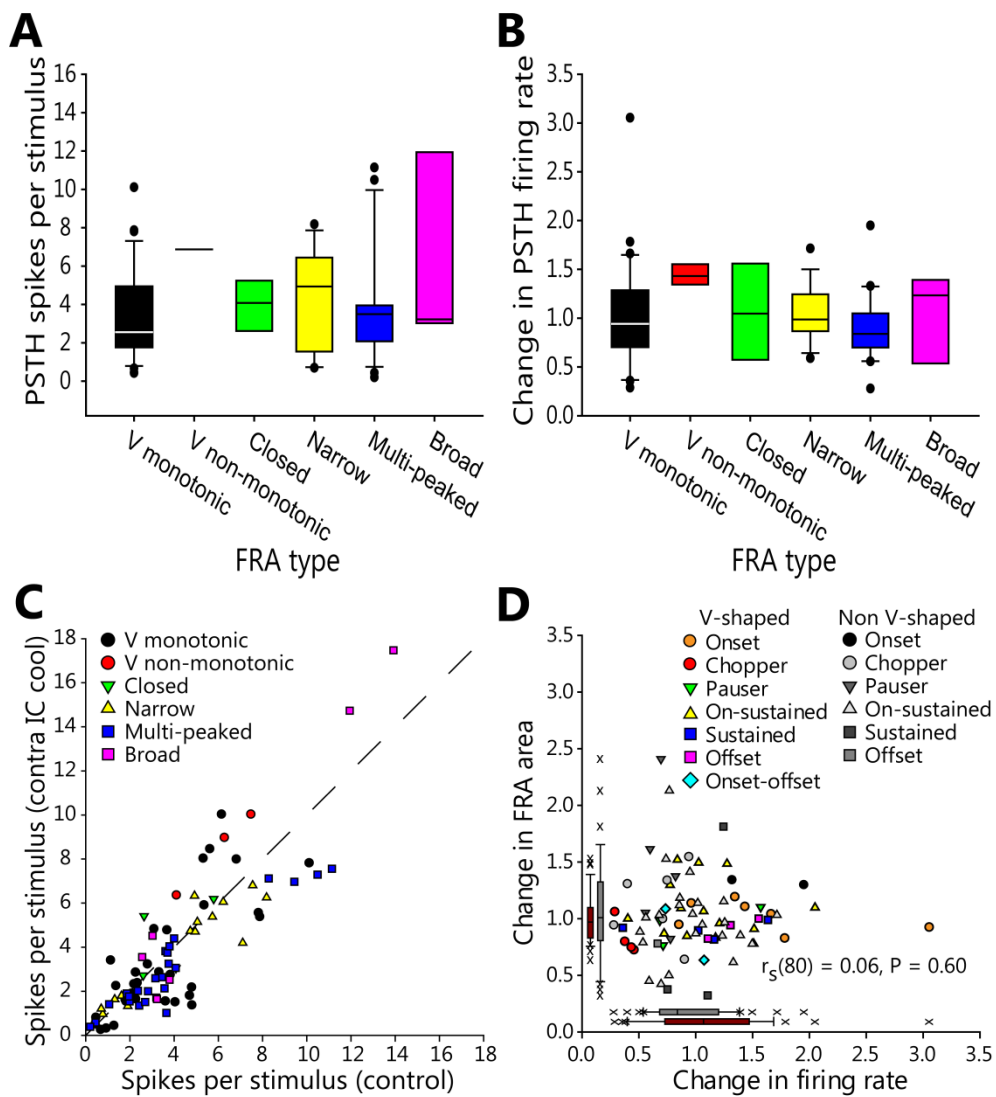


Figure 6.9 (A) A range of control firing rates was observed between different FRA types but these differences were not significant ($H(5) = 6.54; P = 0.26$). (B) The range of changes in PSTH firing rates for units with different FRA classes was also not significantly different ($H(5) = 7.06; P = 0.22$). (C) The range of changes in firing rate of each unit according to PSTH morphology. Note the wide range of changes in V-shaped monotonic FRAs. (D) There was no relationship between the change in PSTH and the change in FRA area. While units with non-V-shaped FRAs (grey box plot; ordinate) showed larger area changes than those with V-shaped FRAs (red box plot; ordinate), the reverse was true for the change in firing rate (abscissa).

6.3.11 Changes in firing rate were not dependent on stimulation type

The possibility that changes in firing rate were different in response to binaural or contralateral stimuli was investigated. Differences between changes in firing rate in response to contralateral and binaural stimuli were variable. The firing rate of the total population of units was similar in the control condition in response to contralateral ($\bar{x} = 3.46$; IQR = 2.13 to 5.23) and binaural ($\bar{x} = 3.56$; IQR = 1.94 to 5.12) stimuli. Cooling the contralateral IC produced a range of changes in firing rate (Fig. 6.10A) and overall reduced the firing rate of the population to both contralateral ($\bar{x} = 3.06$; IQR = 1.75 to 5.18) and binaural ($\bar{x} = 2.52$; IQR = 1.56 to 5.38) stimuli. These changes were not significantly different between the control and contralateral IC cool groups in response to contralateral ($Z = -0.51$, $P = 0.61$) or binaural ($Z = -1.44$, $P = 0.15$) stimuli. Of the 35 units that were tested with both stimulation types, 30 showed the same change (or absence of change) to both stimulus types. Of the remaining 5 units there was no pattern in the differential changes observed to each stimulus type.

Direct comparison of the change in firing rate induced by contralateral and binaural stimulation (Fig. 6.10B) showed similarities between the two distributions. The change to binaural ($\bar{x} = 0.90$; IQR = 0.70 to 1.25) stimuli was slightly smaller than to contralateral ($\bar{x} = 1.01$; IQR = 0.75 to 1.24) stimuli. The changes in firing rate to contralateral stimuli was not significantly different to the changes in response to binaural stimuli ($U = 898$, $P = 0.45$).

Owing to of the wider range of changes in firing rate with binaural stimulation, it was postulated that the absolute change in firing rate might be different between contralateral and binaural stimulation. The maximum absolute change in firing rate to binaural stimulation ($\bar{x} = 0.28$; IQR = 0.14 to 0.53) was larger than to contralateral stimulation ($\bar{x} = 0.25$; IQR = 0.10 to 0.42), but there was a large overlap between the distributions and the two populations were not significantly different ($U = 8.37$, $P = 0.21$).

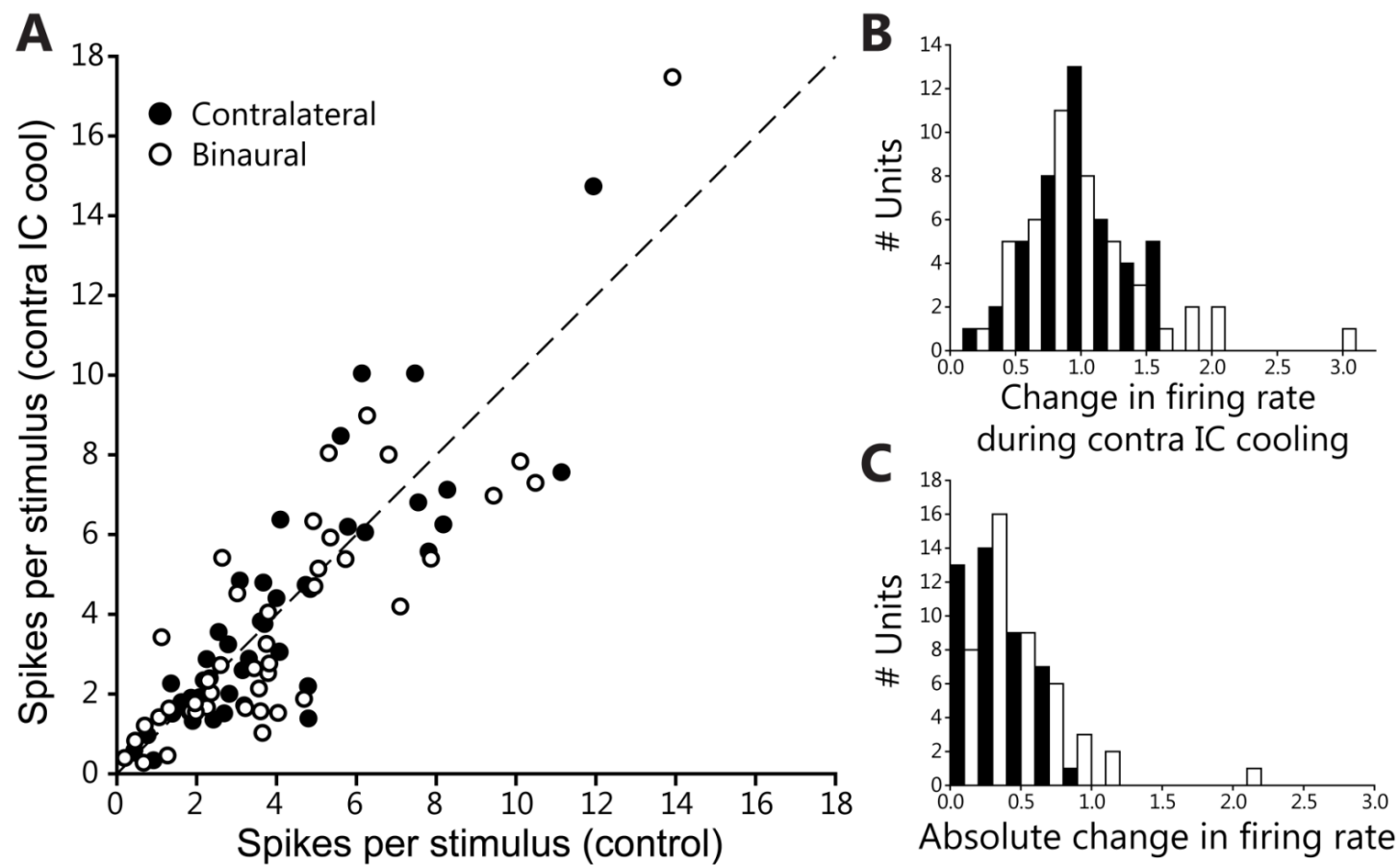


Figure 6.10 (A) Changes in firing rate plotted by the type of stimulation: contralateral (filled circles); binaural (open cycles). The range of changes was similar in response to either stimulus type. (B) The distribution of changes in binaural firing rate had a long tail at the upper end. (C) Absolute changes in firing rate were not significantly different ($U = 8.37$, $P = 0.21$).

6.3.12 Firing rate and first spike latency were negatively related

Each analysis permitted a comparison of the relationship between firing rate and FSL. Figure 6.11A shows the PSTH of a unit which fired throughout the duration of the stimulus ($\tilde{x} = 5.61$; IQR = 4 to 7). The cooling paradigm induced a large increase in the number of spikes fired per stimulus by this unit (Fig. 6.11B; $\tilde{x} = 9$; IQR = 7 to 10) which recovered (not shown; $\tilde{x} = 6$; IQR = 5 to 6). There was a significant difference between the response of the unit between the three conditions of the cooling cycle ($\chi^2(2) = 40.32$, $P < 0.001$). This was due to the increase in firing rate during cooling ($Z = -4.61$, $P < 0.001$) while there was no difference between control and recovery ($Z = 1.12$, $P = 0.27$). The unit had a narrow range of FSLs following stimulus onset (Fig. 6.11C – black trace; $\tilde{x} = 11.44$ ms; IQR = 10.76 to 11.80). During contralateral IC cooling the distribution of FSLs shifted to shorter latencies (Fig. 6.11C – red trace; $\tilde{x} = 10.58$; IQR = 10.15 to 11.32). Following recovery the distribution of FSLs increased (not shown; $\tilde{x} = 11.68$; IQR = 11.33 to 11.98). There was a significant difference between the FSLs of this unit across conditions ($\chi^2(2) = 25.59$, $P < 0.001$). This difference was due to the reduction in FSL re control ($Z = -3.81$, $P < 0.001$). There was no difference between control and recovery FSL ($Z = 1.79$, $P = 0.08$).

The unit plotted in figure 6.11D shows data from another unit which fired with a sharp onset followed by a sustained component ($\tilde{x} = 10$; IQR = 9 to 12). Contralateral IC cooling reduced the firing rate of the unit (Fig. 6.11E; $\tilde{x} = 7$; IQR = 6 to 8), which reversed on recovery (not shown; $\tilde{x} = 9$; IQR = 8 to 11). There was a significant difference across conditions ($\chi^2(2) = 300.55$, $P < 0.001$) which was due to the reduction in firing rate during cooling ($Z = -13.03$, $P < 0.001$) while recovery responses were not different to control ($Z = 1.07$, $P = 0.28$). The FSL of the unit had little variability in the control condition (Fig. 6.11F – black trace; $\tilde{x} = 7.17$ ms; IQR = 6.89 to 7.31). Contralateral IC cooling increased the distributions of FSLs (Fig. 6.11F – red trace; $\tilde{x} = 8.58$; IQR = 8.27 to 8.86). On

recovery the FSL reduced (not shown; $\tilde{x} = 7.12$; IQR = 6.92 to 7.46). There was a significant difference between FSL groups across conditions ($\chi^2(2) = 228.24$, $P < 0.001$), which was due to the increase in FSL during cooling ($Z = 11.69$, $P < 0.001$). Recovery values were not significantly different to control ($Z = 2.69$, $P = 0.09$).

The last example shown in figure 6.11 is from a unit which was unaffected by the contralateral IC cooling paradigm. The unit had a low firing rate with a sharp onset peak with few spikes throughout the sustained component of the response (Fig. 6.11G; $\tilde{x} = 2$; IQR = 1 to 3). Contralateral IC cooling had little effect on the firing rate of the unit (Fig. 6.11H; $\tilde{x} = 3$; IQR = 1 to 4). Following recovery, the firing rate of the unit was similar to the previous two stages (not shown; $\tilde{x} = 2$; IQR = 1 to 3). There was no significant difference between the firing rate across conditions ($\chi^2(2) = 5.37$, $P = 0.07$).

In the control condition the FSL had little jitter (Fig. 6.11 I – black trace; $\tilde{x} = 12.44$; IQR = 12.22 to 12.74). During contralateral IC cooling the latency of the response was unchanged (Fig. 6.11 I – red trace; $\tilde{x} = 12.49$; IQR = 12.16 to 12.76), but the magnitude of the onset response did reduce from 173 to 154 spikes. Throughout recovery the distribution of FSLs was unchanged (not shown; $\tilde{x} = 12.25$; IQR = 11.81 to 12.54). Firing rate was not significantly different between conditions ($\chi^2(2) = 4.77$, $P = 0.09$).

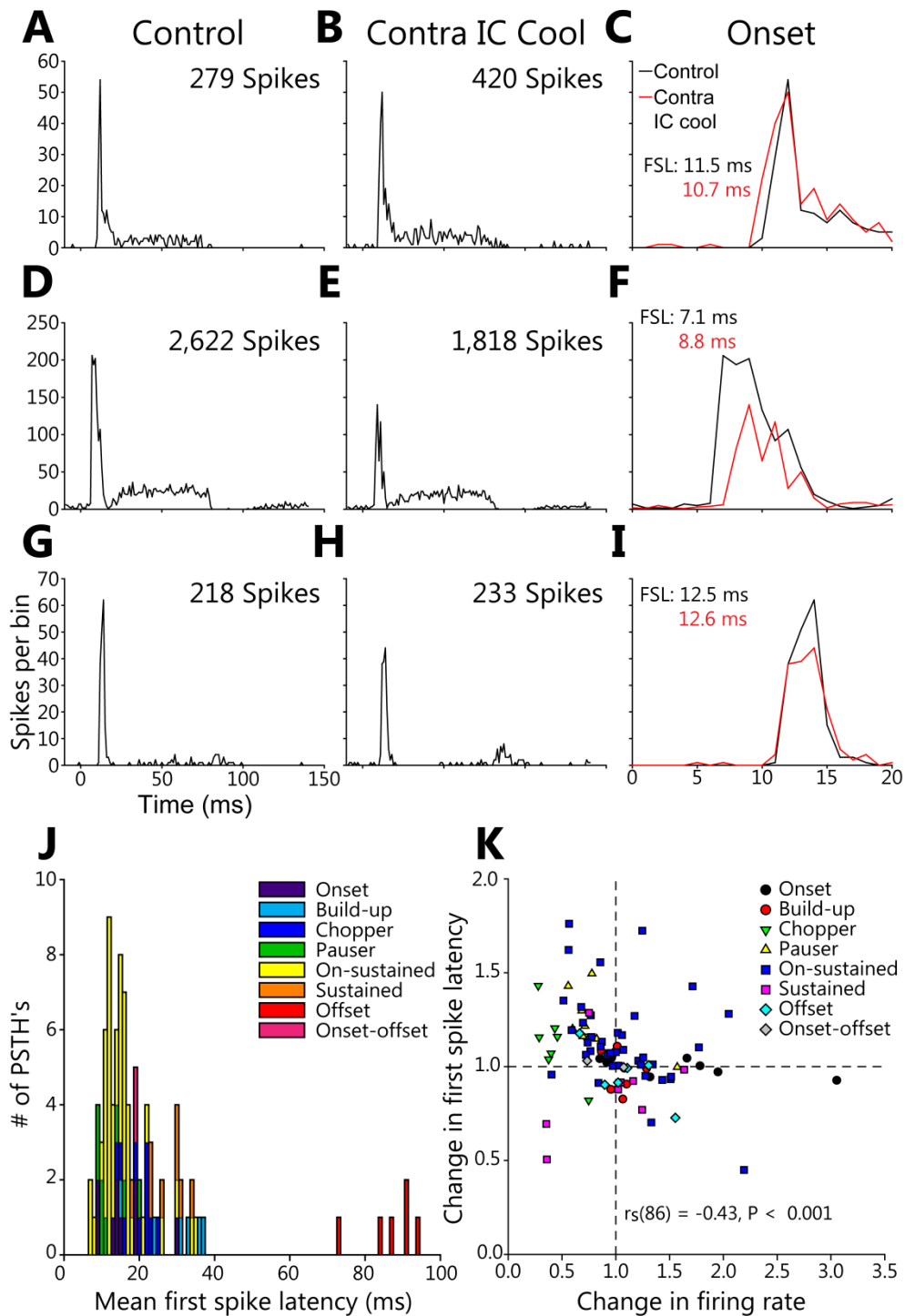


Figure 6.11 Examples of responses from units with sharp onset peaks in their PSTH (A, D, G). The unit in (A; CF = 0.63 kHz) significantly increased in firing rate (B) and had a concomitant reduction in FSL (C). The unit in (D; CF = 3.03 kHz) significantly decreased in firing rate (E) and had an increase in FSL (F). The unit in (G; CF = 1.43 kHz) was unchanged in both firing rate (H) and FSL (I). All units recovered after cooling (not shown – see text). (J) The median FSLs of each unit in the control condition were variable. (K) The change in FSL and change in firing rate were significantly negatively correlated.

Measurement of the FSL of all 52 units produced a population of 88 analyses in response to contralateral and binaural stimuli. The FSLs were broadly spread from 7.10 to 36.61 ms. Offset units formed a separate distribution with median FSLs ranging from 73.33 to 93.93 ms (Fig. 6.11J). The changes in the median FSL of each PSTH type are presented in table 6.3, along with the results from the Friedman test as to whether a significant difference was found in the distributions of FSLs across all conditions. All significant differences were due to changes during contralateral IC cooling.

PSTH type	Control median FSL (ms)	CoIC cool median FSL (ms)	Recovery median FSL (ms)	Significant difference?
Onset	13.82	14.30	14.41	No $\chi^2(2) = 0.00, P = 1.00$
Build-up	32.28	31.42	33.47	No $\chi^2(2) = 1.00, P = 0.74$
Chopper	20.96	22.71	18.89	Yes $\chi^2(2) = 9.60, P = 0.01$
Pauser	10.36	14.02	13.63	No $\chi^2(2) = 5.25, P = 0.08$
On-sustained	13.82	16.66	14.92	Yes $(\chi^2(2) = 23.39, P < 0.001)$
Sustained	29.68	21.57	21.73	Yes $(\chi^2(2) = 6.89, P = 0.03)$
Offset	88.84	83.08	85.67	No $(\chi^2(2) = 4.33, P = 0.14)$

Table 6.3 Different PSTH responses expressed different changes in FSL. Onset responses were almost unchanged throughout all stages. The FSL of Build-up and Offset types reduced but not significantly. The FSLs of Chopper and On-sustained types significantly increased during contralateral IC cooling. Pausers increased in FSL but not significantly. Sustained responses were the only group to significantly reduce in FSL.

The population of Onset units showed a small increase in FSL from control (Fig. 6.11J – purple) during contralateral IC cooling that reversed on recovery. Build-up units had the longest FSLs of any PSTH type other than Offset units (Fig. 6.11J – light blue). Cooling the contralateral IC reduced FSLs slightly and this also reversed on recovery. No significant changes were found in the populations of FSLs of Onset or Build-up responses.

Chopper units had FSL values near the middle of the total population (Fig. 6.11J – navy blue). The cooling paradigm increased the FSL of Chopper units - a trend which reversed on recovery. Statistical analysis found a significant difference between the groups. This difference was found to be between the control and contralateral IC cool groups ($Z = 1.99$, $P = 0.02$) but not between the control and recovery groups ($Z = -1.27$, $P = 0.23$).

Due to their sharp onset peak, Pauser units had the shortest FSLs of any group (Fig. 6.11J – green). Cooling the contralateral IC caused the FSL of Pausers to increase. Recovery shifted the distribution of FSLs back towards control values. Possibly due to the lower number of Pauser analyses than Chopper analyses, there was no significant difference between the control, cool and recovery groups.

In the control condition On-sustained responses had a narrow range of FSLs (Fig. 6.11 J – yellow;). Contralateral IC cooling induced an increase in latency across the population which recovered on cessation of cooling. A significant difference was found between the control and contralateral IC groups ($Z = 3.94$, $P < 0.001$) with no difference between the control and recovery groups ($Z = 2.00$, $P = 0.06$).

The FSL of Sustained units was variable (Fig. 6.11J – orange; $\bar{x} = 29.68$; IQR = 23.41 to 30.48). The cooling paradigm shifted the distribution to shorter latencies with all but one analysis decreasing in FSL. The distribution shifted back to longer latencies on recovery. There was a significant difference across groups that was due to the reduction in FSL during contralateral IC cooling ($Z = -2.07$, $P = 0.02$) while recovery FSLs were not different to control ($Z = -1.48$, $P = 0.16$).

Offset units were distinct from all other units with all responses having FSLs occurring at times after the termination of the stimulus (Fig. 6.11J – red; $\bar{x} =$

88.84; IQR = 83.65 to 90.94). Cooling reduced the FSL of the population. On recovery the distribution shifted back towards control values. There was no significant difference between any of the three stages of the paradigm.

The one Onset-offset unit reversibly increased in FSL by less than a quarter of a millisecond. There was no significant difference in FSL between the three conditions (Fig. 6.11J – pink; $\chi^2(2) = 2.00$, $P = 0.50$).

6.3.13 First spike latency significantly increased across all units

Analysis of the population of responses found that the total distribution of FSLs ($\bar{x} = 16.08$; IQR = 12.38 to 23.70) increased during contralateral IC cooling ($\bar{x} = 18.31$; IQR = 13.87 to 23.92). On recovery the distribution of FSLs reduced to near control levels ($\bar{x} = 16.82$; IQR = 13.67 to 22.49). There was a significant difference across groups ($\chi^2(2) = 11.34$, $P = 0.003$) due to the difference between the control and contralateral IC cool groups ($Z = 2.37$, $P = 0.02$) while control and recovery FSLs were not significantly different ($Z = 0.14$, $P = 0.89$).

The FSL of 57 analyses increased in latency during contralateral IC cooling while the FSL of the remaining 31 decreased. The firing rate of 46 analyses decreased during contralateral IC cooling, 41 increased while one was unchanged. Of those 46 which decreased in firing rate, 39 also increased in FSL. Of the 41 which increased in firing rate, 22 also decreased in FSL. A comparison of the change in FSL plotted as a function of the change in firing rate (Fig. 6.11K) found a significant negative correlation (Fig. 6.11k; $r_s(86) = -0.43$, $P < 0.001$).

Of those units which changed in FSL, 72/88 (88 %) did so by less than 5 ms. The PSTHs of those units which increased or decreased in FSL by more than 5 ms were different. Of the nine analyses that decreased in FSL by more than 5 ms, 3 were Offset types, 4 were Sustained units, 1 was an On-sustained type, and 1 was a Build-up type. There were 7 units which increased in FSL by more than 5 ms, this population comprised of 6 On-sustained types, and 1 Chopper type.

6.3.14 The firing rate of the population of responses was not changed by contralateral IC deactivation

The mean firing rates of all units were compared in each of the stages of the cooling paradigm. In the control condition there were a wide range of mean spikes per stimulus firing rates ($\bar{x} = 3.56$; IQR = 1.98 to 5.12). The median and lower quartile firing rate were reduced during contralateral IC deactivation but the higher quartile increased ($\bar{x} = 2.76$; IQR = 1.64 to 5.40). These changes reversed in the population of recovered responses ($\bar{x} = 3.18$; IQR = 1.93 to 5.21). There was no significant difference between the groups of mean firing rates across conditions ($\chi^2(2) = 1.94$, $P = 0.38$).

6.3.15 Units which were unchanged in firing rate had higher CFs than those that changed

In Chapter 3 the cooling paradigm was estimated to deactivate neurons in the CNIC with CFs up to 8 kHz by at least 40 % with lower CFs being deactivated to an even greater extent. As the projections from the CNIC through the CoIC to the contralateral IC are tonotopic, it was hypothesised that the neurons in this Chapter which were modulated in firing rate would have CFs below 8 kHz while those that were unchanged would have CFs higher than 8 kHz.

The population of responses to either stimulation type which significantly changed in firing rate were predominantly found to have low CFs ($\bar{x} = 1.24$ kHz; IQR = 0.33 to 3.21). There were 54 of 65 responses which had CFs below 4 kHz in this group. Nine of the remaining responses were Multi-peaked which had their most sensitive peaks at high CFs but also had lower frequency peaks in their FRA.

Responses which were unchanged had higher CFs although some had low CFs ($\bar{x} = 7.77$; IQR = 1.39 to 11.66). A Mann-Whitney test found a significant difference between these groups ($U = 453$; $P = 0.001$).

6.4 Discussion

These results provide evidence for the first time that the CoIC exerts an influence over the firing rate and FSL of the majority of units in the IC. The impact of the CoIC was manifest as a control of firing rate, temporal structure and FSL - with no impact on PSTH morphology. The degree and direction of the change in firing rate did bear some relationship to PSTH morphology suggesting a differential influence of the CoIC on subtypes of IC neurons. The most interesting observation of this type was the significant increase in the population of Onset units and the significant decrease in the temporally regular, duration of stimulus firing, Chopper PSTH response types. Overall the effect of contralateral IC deactivation did not change the firing rate of the population although the median firing rate reduced by almost one spike per stimulus – a change of 22.5 %. The FSL of more neurons increased while some of those that decreased in FSL also increased in firing rate. This produced a significant negative correlation between the change in FSL and the change in firing rate. The population of FSLs were found to be significantly later during contralateral IC cooling, a finding that suggests a greater effect of CoIC input on the onset response of IC neurons than the sustained response. These findings support the hypothesis that the CoIC is integral to the firing rate and FSL of auditory responses of most IC neurons, while it has no influence on the PSTH response type.

6.4.1 Technical limitations of this study

The findings of this Chapter are limited to responses of each IC neuron at 20 dB re threshold at CF. The majority of neurons were recorded in response to both contralateral and binaural FRAs (Fig. 6.9) as well as in response to up to 1,000 repetitions of the PSTH stimulation paradigm. This battery of stimuli took up to 20 minutes to record in each stage. As recovery of the unit was imperative to infer that the changes observed during cooling of the contralateral IC were

caused by the experimental manipulation and not gradual changes in the neuron over the course of recordings, the time to record the neuron had to be optimised. Furthermore, to obviate any chance of longer cooling cycles having a gradually less selective effect in the cooled IC (Fig. 3.2); the duration of cooling was also kept to a minimum. Therefore, recording responses to multiple levels with PSTH stimuli was not feasible. The drawback of this is that the changes reported here reflect those at only one point within the FRA of the unit. There may be selective and differential changes throughout the response area of the neuron. However, the data presented in Chapters 4 and 5 suggests that modulation of most FRAs other than some Multi-peaked types were homogeneous. Yet the chance that greater or lesser effects at different points within the FRA were not seen remains a possibility. FRAs were recorded in response to contralateral and binaural stimuli, but ipsilateral stimuli were also not presented for time reasons. This would have provided more information and would be a useful addition to future work.

A second limitation is that by using strict statistical criteria for inclusion, not all units which were presented with both contralateral and binaural stimulation had both response types included in the final dataset. The statistical test is a more objective and robust inclusion criterion to determine changes from control and recovery than the 20 % criterion employed in Chapters 4 and 5. As it was possible to perform this objective analysis it seemed appropriate even if it led to the exclusion of some data which may have increased the size of the groups in the dataset.

The population size is a possible source of error in the data presented here. When the population of responses were divided according to their respective PSTH type the numbers in some groups were low. This may have produced findings with low statistical power that may be misleading. For instance a subset of 5 randomly selected On-sustained units (Fig. 6.8E) may, by chance, closely

resemble the distributions of change seen either in Onset (Fig. 6.8A) or Chopper (Fig. 6.8C) responses. The issue of statistical power is a confounding factor at this juncture for comparisons between individual PSTH types; however at the population level this is not the case. All claims in the following sections about observed differences in individual PSTH types are made with caution in light of this.

6.4.2 Effects of contralateral IC deactivation on firing rate

This study is the first to have investigated the role of the CoIC on the firing rate of large population of IC neurons. The results have confirmed and expanded the finding of Malmierca *et al.* (2005) that the CoIC mediates both inhibitory and excitatory effects on the firing rate of IC neurons. These data also support the finding of Malmierca *et al.* (2005) that the changes in firing rate with drug deactivation of the contralateral IC are nonspecific to the type of stimulation (Figs. 6.3, 6.4, 6.6, 6.7 & 6.8). The paradigm caused a reduction in the median firing rate of the population of almost one spike per stimulus. This finding is in keeping with the known predominantly excitatory projections from each CNIC via the CoIC to the contralateral CNIC (González-Hernández *et al.*, 1996; Hernández *et al.*, 2006).

The distribution of significant changes in firing rate featured 28 (32 %) analyses increasing, 36 (41 %) analyses decreasing and 24 (27 %) analyses unchanged by contralateral IC cooling (Fig. 6.8). That the overwhelming majority (73 %) of analyses were modulated significantly substantiates the finding that intercollicular connections are extensive, widespread and functionally relevant to the processing of sound in the majority of the IC (Malmierca *et al.*, 2005; Malmierca *et al.*, 2009).

That 32 % of analyses increased significantly in firing rate shows that activity in the contralateral IC can exert an inhibitory effect on a sizable portion of IC

neurons. While it is known that the majority of commissurally projecting IC neurons are glutamatergic (Malmierca *et al.*, 1995; Saint Marie, 1996; Zhang *et al.*, 1998), around 20% of CNIC commissural fibres emanate from GABAergic soma (González-Hernández *et al.*, 1996; Hernández *et al.*, 2006). The two key *in vitro* studies of CoIC input onto IC cells found both a short latency and a prolonged late latency inhibition following CoIC stimulation (Smith, 1992; Moore *et al.*, 1998). This implies that the effects seen here could be mediated by either monosynaptic or polysynaptic circuits. The case for a monosynaptic effect is supported by the finding that glutamate blockade did not eradicate all inhibitory input to IC neurons while the long latency, slow IPSPs are hard to explain by anything but polysynaptic inputs (Smith, 1992). The techniques employed here do not differentiate between these two options, but most likely the responses observed relate to a modulation of the interplay between both excitation and inhibition.

Units which were modulated by cooling had low CFs, supporting the findings presented in Chapter 3 that the cooling method deactivated neurons in one IC with CFs of up to ~8 kHz (see section 6.3.15). Assuming that the neurons recorded here received tonotopic CoIC input, it was hypothesised that those PSTH responses which reversibly changed in firing rate would do so only in lower CF regions. The distribution of CFs of those responses which were modulated and those that were not, were significantly different. Almost all units that were modulated had CFs below 4 kHz or were Multi-peaked with CFs at higher frequencies but a large proportion of their FRA was in low frequency regions. The median of those responses which were not modulated was 7.77 kHz, so more than half of these had CFs higher than 8 kHz. By the same token, almost half of those which were not modulated had CFs below 7.77 kHz, suggesting that the firing rate of some low frequency CNIC neurons were unaffected by the cooling paradigm

The findings of this study are in disagreement with those reported by Mei *et al.* (2012). In a study conducted in mouse, they electrically stimulated one IC in synchrony with auditory stimulation and recorded changes in units in the contralateral IC. They found that 29 % of units were unchanged (using a 30 % change as criterion) and of those which changed in firing rate above this criterion, 89% decreased in firing rate with only 13 % increasing. Thus, their data support an almost entirely inhibitory effect mediated by the CoIC. In the data presented here, 58 % of analyses changed their firing rate by less than 30 %, but statistical analysis found that changes much less than 30 % can be statistically significant. There was an approximately equal representation of increases and decreases in firing rate in the population, suggesting a wide range of commissural effects on the contralateral IC.

The discrepancies between these studies may be due to the model species used. Mice have different audiograms to guinea pig (Prosen *et al.*, 1978; Heffner and Masterton, 1980) however the commissural projections between the colliculi of guinea pig and albino mouse have similar gross anatomy (González-Hernández *et al.*, 1986; Malmierca *et al.*, 1995). Although ~20 % of CoIC projecting IC neurons are known to be GABAergic in rat (Hernández *et al.*, 2006), a figure closely matching the proportion of IC neurons which are GABAergic in rat (Merchán *et al.*, 2005) and cat (Oliver *et al.*, 1994). The relative level of inhibitory projection neurons in guinea pig and mouse are unknown. The conserved macro-structural organisation between species as different as cats and rats, suggests that the anatomy of neither mouse nor guinea pig will vary widely from these findings. Therefore, the likely similar percentage of GABAergic projecting CoIC neurons will not have produced the differences observed.

One possibility is that the electrical stimulation caused non-specific drive to neurons in the circuit which produced an input to the contralateral IC that does not operate during the normal functioning of the system. There was significant

inhibition even with differences of up to 10 kHz between the stimulated and recorded neurons (Mei *et al.*, 2012). While the current spread was claimed to be local, the possibility that the DCIC or other lamiae in the CNIC were stimulated by spreading current is a possibility.

Previous studies realised the importance of matching the frequency of the manipulated IC with that of the recorded IC neuron (Malmierca *et al.*, 2003; Malmierca *et al.*, 2005) as this matches the known anatomical connections between CNICs (Saldaña and Merchán, 1992; Malmierca *et al.*, 1995; Malmierca *et al.*, 2009). Cooling eliminates normally occurring physiological activity, whereas electrical stimulation may stimulate connections that are not otherwise normally active. Deactivation techniques confer this advantage over stimulation techniques when trying to infer functional connectivity between brain regions and this is why both pharmacological and cooling deactivations are much more widely used for this purpose than stimulation, which is more commonly used to induce synaptic plasticity *in vivo* (Suga *et al.*, 2002).

6.4.3 Differential changes in firing rate between PSTH morphologies

Units that fired throughout the duration of tonal stimulation expressed a range of changes during cooling of the contralateral IC. Onset units were distinct from all other PSTH morphologies in that the only significant changes observed in the population of Onset responses were increases in firing rate. Onset units had changes in firing rate which, in percentage terms, increased more than any other PSTH type (Fig. 6.2 and 6.8A). Onset units were also different from other unit types in that the population of firing rates was significantly higher during cooling the contralateral IC than in the control condition.

Overall, the population of Chopper responses showed significant reductions in firing rate (Fig. 6.4 and 6.8C). Chopper units mirrored Onset units in that only decreases or unchanged responses were observed. Furthermore, Chopper units

comprised the most extreme decreases in firing rate of any PSTH type (Fig. 6.8C). Pausers decreased in firing rate and tended to increase in ISI and shift to Onset-offset responses (Fig. 6.6; Fig. 6.11). Pausers are known to express an $I_{K(A)}$ current and the duration of the pause is related to the size of $I_{K(A)}$ (Sivaramakrishnan and Oliver, 2001). The pause acts as an inverse code for intervals between successive afferent inputs - the minimum interval being the time for concurrent drives to the cell separated by at least the minimum time for $I_{K(A)}$ to decay. This integration window extends from a few milliseconds up to a maximum of 80 to 100 ms (Sivaramakrishnan and Oliver, 2001). This property makes them excellent for encoding the interval between successive excitatory and inhibitory inputs. The pause duration of Pausers tended to increase to its maximum possible duration of 80 to 100 ms during CoIC deactivation. This supports the speculation that during contralateral IC cooling the switch to Onset-offset responses was due to the unit rebounding from the decay of a prolonged $I_{K(A)}$ current. Whether this is the case is unknown at present but the data imply that CoIC input influences the balance of excitation and inhibition that determines how Pausers encode auditory stimuli.

On-sustained units had a range of firing rate changes (Fig. 6.7 and 6.8). The population of firing rate changes were not significantly different to the control condition at the population level. Those units which fired more throughout the stimulus tended to decrease in firing rate while those which fired less, tended to increase (Table 6.1). This suggests that normal CoIC input to On-sustained cells broadens the distribution of firing rates of different IC neurons. The wide range of firing rates observed in On-sustained responses is therefore dependent on commissural input.

Sustained, Build-up, Offset and Onset-offset each showed a range of small increases and decreases in firing rates which fell within the range of changes seen in On-sustained units with no obvious trends found amongst them.

The differences observed in firing rate change between Onset and duration firing PSTH response types are interesting as there is evidence that these two populations of neurons have different roles in encoding low and high modulation rates (Zheng and Escabí, 2008). Onset cells are unique in the IC in that they are the only PSTH response which correlates with a unique cellular morphology, being found only in stellate cells (Wallace *et al.*, 2012).

The data presented here suggest a possible selective innervation of different neuron types in the IC via the CoIC. An increase in firing rate of temporally regular, duration tuned units such as Choppers and Pausers would increase the temporal fidelity with which the envelope of low modulation rates could be encoded. Conversely, constraining the regularity with which Onset units fire to repetitive stimuli may be a means to ensure the cell only responds to stimuli which are required to be informative to the system. If Onset neurons fired in response to any stimulus, coupled to their binary output, their response would be effectively redundant. Onset units are known to be more than 10 mV more hyperpolarised at rest *in vitro* than duration firing neurons (Sivaramakrishnan and Oliver, 2001). If the CoIC exerts an inhibitory effect on these neurons, only stimuli which drive the cell strongly, such as novel stimuli (Pérez-González *et al.*, 2012) would elicit spikes, thereby making each spike more informative. Such a mechanism may be needed for Onset units as they have a narrow dynamic range of possible spike outputs to supra-threshold stimulation.

6.4.4 PSTH morphology was unchanged by the cooling paradigm

An observation which was true for all units in the sample was the lack of change in PSTH morphology during cooling of the contralateral IC. The iontophoretic application of Bicuculline has been shown in numerous studies to modulate the PSTH morphology of IC neurons (Faingold *et al.*, 1989; Faingold *et al.*, 1991; Vater *et al.*, 1992; Park and Pollak, 1993; Casseday *et al.*, 1994; LeBeau *et al.*, 1996). As the CoIC is one of many sources of inhibition to IC neurons it is

perhaps surprising that bicuculline like modulations were not seen. The lack of any modulation of PSTH, coupled with the dramatic changes in firing rate observed, suggests that the CoIC modulates the interplay of excitation and inhibition onto the cell without having a dominating effect on the temporal response. Removing input from the contralateral IC likely modified the balance of afferent input to the recorded neuron. The absence of a change in PSTH type suggests that excitation and inhibition from lower centres, or intrinsic connections within the IC, or the channels expressed by each neuron, determine the PSTH type.

6.4.5 FRA and PSTH changes showed no correlation

A finding of this study which is consistent with previous reports is the lack of correlation between the frequency and temporal characteristics (Table 6.2) of IC units (LeBeau *et al.*, 1996; Wallace *et al.*, 2012). Given that all units were stimulated 20 dB above threshold, it is not surprising that V-shaped non-monotonic units had the highest firing rate of any FRA type as they are the only group with a peak in their RLF at CF within 10 to 30 dB of threshold (Fig. 6.9A). There is a broad diversity of combinations of FRA and PSTH types (Table, 6.2; LeBeau *et al.*, 1996) which do not have any apparent underlying morphological or physiological relationship (Wallace *et al.*, 2012). It follows from this that the absence of FRA specific modulation of PSTH firing rate due to the cooling paradigm is not surprising. The absence of any relationship between FRA and PSTH in control conditions, or modulation thereof due to contralateral deactivation underlines the differences between the IC and CN where physiology and cellular morphology are inextricably linked (Rhode and Smith, 1986; Smith and Rhode, 1989; Rhode and Greenberg, 1992).

The finding in Chapter 4 that the area of V-shaped FRAs were modulated significantly less than non-V-shaped FRAs by contralateral IC deactivation was found to be reversed when comparing the changes in firing rate of these two

groups (Fig 6.9C). The greater range of changes in V-shaped FRA firing rates than non-V-shaped FRAs cannot be accounted for by differing control firing rates as the range of control firing rates of both groups were not significantly different (Fig. 6.9A). This finding could suggest that removing CoIC input modulated an inhibitory control that sat atop the entire response area of V-shaped FRAs which has been shown to be influenced by GABAergic input (Vater *et al.*, 1992; Yang *et al.*, 1992; Palombi and Caspary, 1996; LeBeau *et al.*, 2001), while CoIC inhibitory influence on non-V-shaped FRAs was more strongly involved in forming the shape of the response area than containing firing rate.

6.4.6 Magnitude of rate changes were similar to either stimulation type

The magnitudes of change in firing rate in response to either contralateral or binaural stimulation were not significantly different (Fig. 6.10A). The distributions of these changes were approximately Gaussian with the only difference being a greater increase in firing rate of 5 binaural analyses than those seen to contralateral stimuli. The lack of difference in the distributions of firing rate change in response to either stimulation type suggests that commissural effects are activated by both binaural and contralateral stimulation. This conclusion is consistent with the findings of Malmierca *et al.* (2005) who similarly observed that blockade of the contralateral IC influenced responses to both binaural and contralateral stimulation.

6.4.7 Changes in firing rate and FSL implicate the CoIC in temporal integration

The range of FSLs observed in the data presented here (Fig. 6.11J) are qualitatively similar to those published previously in both moustache bat (Park and Pollak, 1993) and guinea pig (LeBeau *et al.*, 1996). FSL is an important feature of neuronal responses across numerous sensory modalities. In the rat somatosensory system, first spikes carry the majority of the information in a

spike train about the stimulus at numerous points in the ascending pathway (Petersen *et al.*, 2001; Bale and Petersen, 2009; Storchi *et al.*, 2012). In primary visual cortex FSL conveys a large portion of the information about stimulus contrast (Reich *et al.*, 2001) and orientation (Shriki *et al.*, 2012). The discriminability of odours in mitral/tufted (M/T) cells in the Leopard frog has been shown to be dependent on a latency code (Junek *et al.*, 2010). In the IC, FSL increases the information conveyed by spike trains encoding ITD and ILD (Chase and Young, 2007), and novelty detection (Pérez-González *et al.*, 2012), while FSLs alone are sufficient for single units to encode IPD with some accuracy (Zohar *et al.*, 2011).

The FSLs in this dataset varied widely between PSTH morphologies, suggesting a functional relationship between the two (Fig. 6.11J). A negative correlation between the change in FSL and the change in firing rate was found for the population of responses, with the relationship strongest for decreases in firing rate and increases in FSL (Fig. 6.11K). The majority of those analyses which increased in firing rate also showed reductions in FSL.

The change in FSL of the vast majority (74 %) of IC neurons during contralateral IC deactivation was less than 4 ms. Disinhibition by iontophoretic application of bicuculline has been shown to modulate the FSL of IC neurons. In the moustache bat IC, the reduction in FSL was substantial in half of all units recorded and caused a significant reduction in FSL of the population by an average of 2.5 ms (Park and Pollak, 1993). In guinea pig IC the majority of units showed little change in latency following bicuculline application save for Sustained and 'unclassified' units which appear to have FSLs similar to the Offset types described in this study (see Fig. 6B in LeBeau *et al.* (1996)). Those units which did not change in latency tended to have sharp onset peaks in their response. Recordings in the IC of the big brown bat showed some reduction in latency following bicuculline application up to 4 ms (Lu *et al.*, 1997). Similarly, in

the pallid and moustached bats, Fuzessery *et al.* (2003) found reductions in FSL of up to 3.8 and 10.3 ms respectively, following bicuculline application.

The shifts in the FSL of units which increased in firing rate in this Chapter chime well with these studies in that the majority (22/31) of FSLs reduced by less than 5 ms. Furthermore, 78 % (7/9) of those which reduced by more than 5 ms were Sustained or Offset units. These reductions match closely those observed by Park and Pollak (1993) and LeBeau *et al.* (1996), where Sustained and Offset units sometimes fired with a much shorter latency following disinhibition. The reductions in FSL in this study were therefore likely caused by a removal of short latency inhibition which in the control condition was able to hyperpolarise the cell enough to delay firing. In intracellular studies short latency IPSPs have been described numerous times *in vivo* (Nelson and Erulkar, 1963; Covey *et al.*, 1996; Kuwada *et al.*, 1997). *In vitro* stimulation of the CoIC is known to elicit a short latency IPSP in IC neurons (Smith, 1992; Moore *et al.*, 1998). Neurons in the IC can receive IPSPs only, EPSPs only or a combination of the two as a result of CoIC stimulation (Li *et al.*, 1999). As inhibition arrives earlier than excitation to IC neurons (Nelson and Erulkar, 1963; Voytenko and Galazyuk, 2008), CoIC mediated inhibition may help regulate the FSL of IC neurons.

While Fuzessery *et al.* (2003) found that inhibition had 'little effect' on the response latency of the vast majority of IC neurons (a result expanded and supported here), the precise timing of first spikes in a spike train carries a huge amount of information about auditory stimuli (see Heil (2004) for review). Shifts of FSL up to 4 ms have been shown to reduce the information content of the majority of single units encoding sound location in auditory cortex of awake cat (Mickey and Middlebrooks, 2003), and FSL is significantly more precise in IC than A1 (Ter-Mikaelian *et al.*, 2007). So while changes in FSL in IC were small for the majority of neurons, they could make a large difference in the ability of the neuron to accurately encode the stimulus.

In the moustache bat (Park and Pollak, 1993; Fuzessery *et al.*, 2003) and big brown bat (Lu *et al.*, 1997), blocking GABAergic inhibition occasionally increased response latency, suggesting that in some neurons the effects on FSL observed here may not be due to modulation of monosynaptic inhibition. The reductions in FSL of Sustained and Offset units indicates that CoIC mediated inhibition may help form these responses. In slice recordings, Offset units have been found to show rebound spikes in response to the removal of hyperpolarisation (Sivaramakrishnan and Oliver, 2001). Commissural inhibitory input appears to enhance the ability of these units to synchronise their response with the end of a stimulus, thus allowing a mechanism that may encode envelope changes with high fidelity to operate with higher accuracy. In SOC it has been shown that Offset cells can encode amplitude modulated sounds, which are a key aspect of natural sounds, with higher synchrony than duration firing neurons (Kuwada and Batra, 1999). A similar finding in IC may be hypothesised and based on the data presented here the fidelity with which these synchronisations may occur would likely depend on CoIC input.

The correlation between the change in FSL and the change in firing rate may not involve a change in inhibition but may be explained by a change in the excitatory drive to the neuron. FSL decreases when firing rate increases in IC in response to higher levels of stimulus in monotonic neurons (Nelson and Erulkar, 1963; Kelly and Kavanagh, 1994). The drive to each neuron which produced the FSL and firing rate in the control condition likely involved both EPSPs and IPSPs. The CoIC contributes to both of these currents (Smith, 1992; Moore *et al.*, 1998; Li *et al.*, 1999). The correlation between the change in both FSL and firing rate likely involved changes to both excitatory and inhibitory currents from the CoIC, but a change in only excitatory drive only cannot be discounted.

As CoIC deactivation induced a significant increase in the FSLs of the population without producing a concomitant significant decrease in firing rate (Fig. 6.11),

suggests that the CoIC may have a more pronounced effect at the onset of IC responses than throughout the sustained component. Short latency ionotropic receptor mediated inhibition and excitation are known to be mediated by the CoIC with inhibition leading (Smith, 1992; Moore *et al.*, 1998). Synchronisation of multiple CoIC projecting neurons could therefore mediate a strong net inhibitory effect at stimulus onset to constrain the gain of onset responses in IC neurons in order to regulate FSL. As natural sounds are made up of constantly fluctuating envelope, frequency bandwidth, and temporal structure, the need for accurate encoding of stimulus onset is essential in the IC. That CoIC deactivation had a greater effect on the population of FSLs than firing rate may therefore be due to the nature of the pure tone stimuli employed in this study.

6.5 Conclusion

The CoIC is essential in the determining both the firing rate and FSL but not the PSTH type of the majority of IC neurons in response to sound. This input is differential depending of the temporal nature of the target neuron, likely subserving the specific roles of the different temporal response characteristics of IC neurons. One effect of the CoIC may be to modulate the firing rate of neurons to influence the encoding of multiple aspects of auditory cues in IC. Thus, inputs from the CoIC participate in the formation of both the latency and rate codes in the IC.

Chapter 7. General Discussion

7.1 Summary of Findings

This thesis has validated cryoloop cooling as a technique by which one IC can be reversibly deactivated in anaesthetised guinea pig. Cryoloop cooling was found to produce selective deactivation of spiking activity throughout the dorsal CNIC, without significantly modulating temperature elsewhere in the ascending auditory system. The method was then applied to investigate the functional influence of the commissural connections between the two ICs in processing spectral and temporal characteristics of pure tones at the level of the IC. This was achieved by recording the electrophysiological responses of single units in the IC contralateral to cooling before, during, and after a cooling cycle. Profound effects were observed in the FRA (Chapters 4 and 5), firing rate and FSL (Chapter 6) of the majority of neurons, indicating that the CoIC plays a fundamental and essential role in the processing of simple auditory stimuli in the IC.

7.2 Cooling as a Means by which to Investigate the CoIC

The functional role of the CoIC in the auditory system has received scant attention. The only behavioural study reported was a lesion study by Moore *et al.* (1974) which found that transection of the trapezoid body had a deleterious effect on sound localisation ability in the cat, while transections of the CoIC or corpus callosum had little effect; although the stimuli used may not have been optimal to assess changes in all forms of sound localisation ability. The lack of an obvious role in the auditory system, coupled with the experimental difficulty in surgically accessing the CoIC in most model species, may be two reasons for the paucity of experimental investigations into the nature of the CoIC. The use of drug injection to block neural activity in the IC was recently pioneered in anaesthetised rat - a similar preparation to that employed in this study

(Malmierca *et al.*, 2003; Malmierca *et al.*, 2005). This method had a sound methodology in theory; however, the method produced few units which were recorded throughout contralateral IC deactivation, due to the mechanical disturbance on pressure injection causing a large number of units to be lost before recordings were completed. My aim was to implement a method that would provide a viable, reversible deactivation of one IC without the complications of mechanical disturbances.

Surgical transection of the CoIC were considered, but with only single channel recordings available, a lesion of the CoIC would only allow for the recording of one neuron before and after the cut. Thus, within cell comparisons like those performed in this study would not be possible. Furthermore, the mechanical disturbance from making the lesion would make it difficult to retain recording contact with the same neuron during the transection. As the ICs are so large and the response types of IC neurons to both FRA and PSTH stimuli are so heterogeneous, a larger number of experiments than those conducted in this study would be needed to obtain the adequate number of neurons to assess the changes imparted. This method would also require histological confirmation of the lesion from every experiment with the high probability that the transection of the CoIC would not be complete in some experiments. The chance of imparting trauma to the tissue by transecting the CoIC would also be present.

Iontophoretic application of drugs is known to have pronounced effects on the responses of IC neurons (Faingold *et al.*, 1989; Faingold *et al.*, 1991; Vater *et al.*, 1992; Park and Pollak, 1993; Casseday *et al.*, 1994; LeBeau *et al.*, 1996). However, attempts to use this approach to study commissurally mediated effects (Rees personal communication) have proved ineffective; probably because the limited spatial extent of drug elution by iontophoresis does not deactivate enough of the IC to eliminate commissural influences.

Electrical stimulation is another method that was considered. This method has been performed previously *in vitro* and proved to be highly informative about the influence of the CoIC on IC responses (Smith, 1992; Moore *et al.*, 1998; Li *et al.*, 1999). Another group has recently reported the findings of a series of *in vivo* experiments using such a protocol (Mei *et al.*, 2012; Cheng *et al.*, 2013). Although *in vivo* experiment allows investigation of the intact system in response to auditory stimuli, the application of electrical stimulation would provide additional drive to the intact circuits that might result in specious findings about how the CoIC influences processing in the IC under physiological conditions.

The most attractive model for deactivating one IC would be an optogenetic manipulation (Deisseroth, 2011; Fenno *et al.*, 2011). This would theoretically allow for selective targeting of CoIC projecting neurons in the IC. If one could get expression of a light activated chloride channel such as halorhodopsin into IC neurons, one could deactivate the connections from one IC to the other. The advantages of this method would be numerous. For instance the entire IC could be targeted, allowing for complete deactivation of all IC neurons. Another advantage of this method would be the ability for the experimenter to have precise temporal control over the deactivation. The differential expression of the opsin into different neuron types, such as expression in calbindin or parvalbumin expressing neurons would allow for selective deactivation of DCIC or CNIC neurons respectively (see Fig. 1.3). The neurons projecting via the CoIC form a distinct projection pathway from those that innervate the MGB or the CN (Okoyama *et al.*, 2006). Therefore, if the neuronal population of CoIC projecting neurons could be selectively transfected, a purely CoIC lesion could be induced and controlled experimentally – a step forward that would be superior to any other current method. This method would also confer the advantage of allowing a possible behaving preparation from which both electrophysiological and psychophysical data could be acquired. However, the knowledge of the guinea

pig genome currently lags far behind that of rat, mouse and macaque where optogenetic methods are currently being employed. As such it was not feasible to implement this technique at this time. The time to develop such a model would also be considerable and potentially beyond the scope of a study such as this one which sought to both develop and then employ the deactivation of one IC while observing changes in the contralateral IC.

With these considerations, cooling was hypothesised to be the best option with which to deactivate a large proportion of neuronal responses in one IC. Cryoloop cooling was selected over previously implemented cryoprobe designs (Skinner, 1970; Sherk, 1978; Kayama *et al.*, 1984) due to the simplicity of the design, the ease with which the loop could be formed to suit the shape of the exposed dorsal IC and the lack of trauma imparted to the tissue compared to cryoprobes. The IC in guinea pig provided a useful candidate for cryoloop cooling due to its bulbous shape and because its upper surface projects above the dorsal surface of the brainstem so allowing for IC selective cooling. The vasodilatory capacity of blood vessels in the IC appeared to be efficient as cooling sufficient to cool neural responses was found to be restricted to within 2 mm from the cryoloop. This was found to match with previous measurements in similar experimental models (Lomber *et al.*, 1999; Coomber *et al.*, 2011).

Cryoloop cooling was not a perfect deactivation technique. Cooling the cryoloop to temperatures sufficient to deactivate spiking activity also caused reductions in temperature of a couple of degrees in the IC contralateral to cooling (Fig. 3.2 and Fig. 3.3) and the CN and cochlea (Fig. 3.4) ipsilateral to the cryoloop. While these temperature changes were not large enough to cause either deactivation or the hyperexcitable responses described in Chapter 3, they do show that the method used was not perfectly restricted to the target IC. These changes in temperature were not great enough to confound inferences from the data collected, however, the changes detected did suggest that

cooling cycles had to be restricted to the minimum time possible while useful data were collected. This meant that all well discriminated units (which could have been recorded for a longer period and in response to a wider range of stimuli) were constrained to a maximum cooling duration of ~20 minutes. This meant that IC responses were only recorded in response to two stimulus paradigms, both of which used only pure tones. These data were informative, but to understand the complete nature of the CoIC it will be necessary to assess responses to a much wider range of stimulus types. These stimuli may more accurately model the types of stimuli commonly encountered by animals in their environment. Stimuli such as sound localisation cues, amplitude and frequency modulations, conspecific vocalisations, oddball and stimulus specific adaptation paradigms, as well as broadband and band limited noise may be useful in future experiments.

The major drawback of cryoloop cooling was that it did not deactivate neural activity along the entire tonotopic axis of the IC. This turned out to be useful as it prevented cooling of the DNLL, but did provide a restricted region which was deactivated in the IC. This region did cover around half of the tonotopic range of the IC within which many of the major auditory cues are processed. The use of a penetrating cryoprobe would obviate this problem and was considered, but the disadvantage of this technique is that the trauma imparted to the IC may alter the normal functioning of the system. Cryoprobes would have the advantage of penetrating to deeper regions of the IC, but in order to cause the minimal amount of trauma to the IC, they would have to be narrow. This would create the problem of getting enough coolant flow through the probe to cool sufficiently to deactivate neural activity. The chance of affecting the DNLL would also be much greater with a cryoprobe cooling the ventral IC.

One further drawback is that due to the structure of the guinea pig brain, aspiration is necessary to allow placement of the cryoloop. If one were to wish

to expand this model to an awake behaving preparation, it would not be possible. For animals where the IC is more surgically accessible, such as the mouse, it may be possible to perform such experiments, but the spread of cooling would have to be assessed in a similar manner to that done in Chapter 3. The other small mammals which have low frequency hearing which are common model species used in auditory research are gerbil and chinchilla, both of which have the same surgical accessibility issues as guinea pig. If this model were to be extended into a behaving animal it would probably be best suited to cat or macaque, although the increased financial outlay for these species may serve as an impediment.

Cryoloop cooling provided an adequate means by which to investigate the questions posed in this thesis. The experiments reported in this study provided a corpus of data that may not have been possible using other techniques.

7.3 What Influence does the CoIC have on the Processing of Auditory Stimuli in the IC?

The functional role of the CoIC in the auditory system was a mystery until recently. Anatomical studies involving the CoIC date back at least 40 years (Carey and Webster, 1971) and many detailed descriptions have been made of the interconnectivity of the ICs across several species (Faye-Lund and Osen, 1985; Coleman and Clerici, 1987; Moore, 1988; Saldaña and Merchán, 1992; Malmierca *et al.*, 1995; González-Hernández *et al.*, 1996; Malmierca *et al.*, 2009). In spite of this wealth of anatomical data, there were no studies into the functional role of the CoIC in the analysis of sound *in vivo* until a decade ago – save for the one lesion study which investigated sound localisation in cat after transection of the CoIC (Moore *et al.*, 1974).

The few papers which have investigated the CoIC, both *in vitro* (Smith, 1992; Moore *et al.*, 1998; Li *et al.*, 1999) and *in vivo* (Malmierca *et al.*, 2003; Malmierca *et al.*, 2005; Mei *et al.*, 2012; Cheng *et al.*, 2013), have described a range of

excitatory and inhibitory effects (Section 1.8.3). All studies to date suggest that the CoIC has an important influence in the auditory system on the representation of sound in the IC.

This study has provided evidence for the first time of a range neuronal response changes which are mediated by intercollicular interactions, while also supporting the view that a population of CoIC neurons are not influenced by the CoIC. These changes include changes in FRA area which were significantly larger in non-V-shaped FRAs than V-shaped FRAs (Fig. 4.15) – a finding which implicates the CoIC in the formation of complex FRA response types in the IC (Palmer *et al.*, 2013). This finding provides evidence for the formation of FRA types within the IC, with the CoIC playing an important role in determining the spectral response characteristics of non-V shaped FRAs. Furthermore, the firing rates of the majority of neurons were modulated by removing contralateral IC activity (Fig. 6.8), a finding that matches similar previous reports (Malmierca *et al.*, 2005; Mei *et al.*, 2012).

The findings of the current study contradict a recent report that the CoIC has an almost entirely inhibitory influence (Mei *et al.*, 2012). That study found that 86 % of IC units which were modulated by electrical stimulation of the contralateral IC were inhibited. In the present study there were an almost equal number of units that increased as decreased their firing rate when the other IC was deactivated. This suggests CoIC influences on firing rate are more heterogeneous than suggested by Mei *et al.* (2012) and is consistent with the data of Malmierca *et al.* (2005). The data reported here are also consistent with the anatomical descriptions of commissural connections showing that many are excitatory (González-Hernández *et al.*, 1996; Hernández *et al.*, 2006), although the possible contribution of polysynaptic influences cannot be discounted. Amongst the specific changes in populations of response types were significant increases in firing rate of the population of Onset responses and significant decreases in the

population of Chopper units – both of which may reduce the ability of those response types to optimally encode auditory stimuli.

While the findings reported here have expanded and elaborated the field of knowledge of the CoIC, this study has merely scratched the surface of the possible experimental manipulations which may be necessary. Due to the wide array of response types found in both the spectral and temporal domains, a large number of cells were needed to be informative about response type specific changes. Even with the sizeable populations of neurons reported here, by the time they had been assigned to their respective FRA and PSTH types, some groups had very low numbers. While these may reflect the relative proportions of each of these types in the IC, more would be needed to make statistical comparisons of each response type with adequate power.

7.4 Possible Functional Roles for the CoIC in the Auditory System

If one were to speculate as to the possible functional roles of the CoIC, the first possibility might be a role in reciprocal gain control between the two ICs (Malmierca *et al.*, 2003; Malmierca *et al.*, 2005). Gain control has been demonstrated within the IC previously (Dean *et al.*, 2005; Robinson and McAlpine, 2009). The mirror image reciprocity of the connections could be hypothesised to be the ideal site for the formation of a representation of the entire auditory environment which could then be passed to the thalamus. Each IC has a bias towards representing the contralateral hemifield of the sound field (Irvine, 1986). Lesions of one IC have been found to produce profound sound localisation deficits of contralateral space both in animal studies with unilateral lesions of one IC (Kelly and Kavanagh, 1994) and in a human patient with a unilateral trauma to one IC (Litovsky *et al.*, 2002). A reciprocal bilateral interaction via the CoIC would allow for the spatial position of a sound or multiple sounds in one hemifield to be calibrated against those in the other hemifield before being passed to the MGB. The function of any reciprocal gain

control mechanism could be assessed by presenting binaural stimuli such as interaural time and level discrepant stimuli which mimic sounds originating from different azimuthal locations.

In addition to commissural gain control, which may operate to enhance sound localisation, the CoIC might mediate gain control across different stimulation levels. This was a limitation of the data presented in Chapter 6, as stimuli were only presented at one level for each neuron. The possibility that CoIC input may shift the RLFs of IC neurons (see Chapter 5), implies that level specific effects may be present and are an obvious direction for further study.

These possibilities, however, do not address the simple nature of the stimuli which have been presented thus far in all studies of the CoIC. The simplicity of pure tones makes them useful experimental tools with which to probe the responses of IC neurons to auditory stimuli. However, sounds in the natural environment are rich and complex in the temporal, spectral and level domains. The key role that intercollicular interactions play in determining the firing rate of IC neurons to pure tone stimuli suggests that changes will be observed in neuronal responses irrespective of the stimulus. It is possible that pure tone stimuli may not be the adequate stimulus to reveal the functional nature of the CoIC and the observations made so far are only incidental to its physiological role.

Neurons in the DCIC are known to be driven more strongly by broadband noise stimuli, while CNIC responses are stronger to pure tones. These two subdivisions both project extensively through the CoIC, although the majority of DCIC neurons receive projections from the CoIC with little from other nuclei, the CNIC receives input from both ascending nuclei and the CoIC (González-Hernández *et al.*, 1996). This suggests a functional difference between these regions that may be reflected in the respective changes in firing rate during contralateral IC deactivation. Perhaps the influence of removing CoIC input would be greater in

DCIC neurons than CNIC neurons as the CoIC represents a larger percentage of the input to each cell in DCIC. Studying neurons in both the DCIC and CNIC in response to noise and pure tone stimuli using the deactivation protocol outlined here may be informative.

7.5 Future Work Using Current Methods

As with all projects, given more time there are a multitude of further experiments that would improve the power of the inferences gleaned from the data gathered thus far. The first step I would take would be an increase in the number of neurons sampled. Due to the many FRA and PSTH response types in IC, gathering a sizeable population of each response type requires greater numbers of experiments than were performed in the course of this research project. For example, larger number of Closed neurons would allow for more information as to whether the disinhibition observed in the few neurons recorded here are representative of the entire population. The increase in sample size would not need to expand greatly to permit bootstrapping estimates of whether the differential changes in different response types hold true over the entire population.

7.6 Future Work Using Different Methods

In addition to the above there are numerous aspects of fundamental auditory processing that CoIC input likely influences. Simple extensions of the experiments reported here could shed light upon these. Possible further experiments include:

- 1) Employing sound localisation stimuli such as interaural time and/or level differences before, during and following recovery from contralateral IC deactivation. As outlined above, a commissural influence of the gain of IC neurons, especially their representation of sound position would be a logical role for the CoIC to play in the auditory system. A rescaling of the firing rates and therefore a decrement in the dynamic ranges and discriminability of ITD and ILD functions would be hypothesised to occur during contralateral IC deactivation. As the IC receives information about azimuthal sound localisation cues which have been extracted in the superior olive, transformations in the

shapes of the sound localisation functions of IC neurons would not be predicted, but rescaling may be commonplace.

2) As significant changes were detected in the frequency analyses and temporal responses of IC neurons, this raises the issue of the encoding of frequency and amplitude modulations. Therefore, an investigation into the encoding of both to noise and/or tone carriers would likely find changes in the modulation transfer functions and possibly the best modulation frequency of some IC neurons. As opposing changes in firing rate were found in Chopper and Onset responses, the different roles these neurons are hypothesised to have in encoding low and high temporal modulation rates (Zheng and Escabí, 2008), would allow the hypothesis that the changes in firing rate in both would result in a decrease in the ability of each type response type to optimally encode its preferred modulation rate.

3) The lack of statistical analysis with the FRA presentation paradigm was a drawback to the analyses performed. If FRA analysis was performed in conjunction with the collection of multiple repetitions of iso-level frequency tuning curves, this would provide both the overall picture of the response of the neuron in frequency-level space, and allow statistical testing of bandwidth and rate changes across the range of responses of each neuron.

4) The relationship between level and rate was not investigated here, yet RLFs are a fundamental paradigm which are commonly employed to characterise auditory neuronal responses. A key point of interest would be the relationship between firing rate and FSL as a function of stimulus level. The majority of IC neurons decrease in latency as level re threshold is increased (Nelson and Erulkar, 1963; Klug *et al.*, 2000; Tan *et al.*, 2008). Due to the negative correlation between shifts in FSL and firing rate found here, the relationship between the two would likely be changed by contralateral IC deactivation. Due to the lower variance of FSL than firing rate, it has been proposed to be a more suitable

parameter than firing rate in the evaluation of neuronal responses to frequency and amplitude of stimuli in IC than firing rate (Tan *et al.*, 2008). Firing rate and FSL are both measures of the excitatory drive to a neuron. If the CoIC improves the ability of the auditory system to represent stimuli, it would be expected that the changes in FSL and firing rate induced by contralateral IC deactivation would decrease of the ability of IC neurons to represent said stimuli.

5) A further development of these studies would be an investigation into the representation of sound duration in IC. Bauer *et al.* (2000) found that as well as being level dependent, inhibition in IC was also sensitive to the duration of stimuli. It was found that short latency tones (5 ms) were less effective in generating inhibition than longer ones (20 ms). As the CoIC provides both short and long latency inhibition (Smith, 1992; Moore *et al.*, 1998), contralateral IC deactivation could modulate the balance of inhibition and excitation over different durations of stimulation.

6) The development of multi-channel recording systems allows for wider sampling of the changes imparted by an experimental manipulation. With a shank electrode which spanned at least 2 millimetres, it would be possible to record from both the DCIC and CNIC simultaneously to assess the different contributions of the CoIC to these different neurons.

References

- Adams, J.C. (1979) 'Ascending projections to the inferior colliculus', *Journal of comparative neurology*, 183(3), pp. 519-538.
- Adams, J.C. (1980) 'Crossed and descending projections to the inferior colliculus', *Neuroscience letters*, 19(1), pp. 1-5.
- Adams, J.C. and Mugnaini, E. (1984) 'Dorsal nucleus of the lateral lemniscus: a nucleus of GABAergic projection neurons', *Brain research bulletin*, 13(4), pp. 585-590.
- Adams, J.C. and Wenthold, R.J. (1979) 'Distribution of putative amino acid transmitters, choline acetyltransferase and glutamate decarboxylase in the inferior colliculus', *Neuroscience*, 4(12), pp. 1947-1951.
- Aitkin, L.M., Anderson, D.J. and Brugge, J.F. (1970) 'Tonotopic organization and discharge characteristics of single neurons in nuclei of the lateral lemniscus of the cat', *Journal of neurophysiology*, 33(3), pp. 421-440.
- Aitkin, L.M., Fryman, S., Blake, D.W. and Webster, W.R. (1972) 'Responses of neurones in the rabbit inferior colliculus. I. Frequency-specificity and topographic arrangement', *Brain research*, 47(1), pp. 77-90.
- Aitkin, L.M. and Moore, D.R. (1975) 'Inferior colliculus. II. Development of tuning characteristics and tonotopic organization in central nucleus of the neonatal cat', *Journal of neurophysiology*, 38(5), pp. 1208-1216.
- Aitkin, L.M. and Phillips, S.C. (1984) 'The interconnections of the inferior colliculi through their commissure', *Journal of comparative neurology*, 228(2), pp. 210-216.

Aitkin, L.M. and Schuck, D. (1985) 'Low frequency neurons in the lateral central nucleus of the cat inferior colliculus receive their input predominantly from the medial superior olive', *Hearing research*, 17(1), pp. 87-93.

Aitkin, L.M., Webster, W.R., Veale, J.L. and Crosby, D.C. (1975) 'Inferior colliculus. I. Comparison of response properties of neurons in central, pericentral, and external nuclei of adult cat', *Journal of neurophysiology*, 38(5), pp. 1196-1207.

Alibardi, L. (1998) 'Ultrastructural and immunocytochemical characterization of neurons in the rat ventral cochlear nucleus projecting to the inferior colliculus', *Annals of Anatomy*, 180(5), pp. 415-426.

Alkhatib, A., Biebel, U. and Smolders, J.T. (2006) 'Inhibitory and excitatory response areas of neurons in the central nucleus of the inferior colliculus in unanesthetized chinchillas', *Experimental Brain Research*, 174(1), pp. 124-143.

Anderson, L.A. and Linden, J.F. (2011) 'Physiological differences between histologically defined subdivisions in the mouse auditory thalamus', *Hearing research*, 274(1), pp. 48-60.

Anderson, L.A. and Malmierca, M.S. (2013) 'The effect of auditory cortex deactivation on stimulus-specific adaptation in the inferior colliculus of the rat', *European Journal of Neuroscience*, 37(1), pp. 52-62.

Antunes, F.M. and Malmierca, M.S. (2011) 'Effect of auditory cortex deactivation on stimulus-specific adaptation in the medial geniculate body', *The Journal of Neuroscience*, 31(47), pp. 17306-17316.

Aparicio, M.A., Viñuela, A. and Saldaña, E. (2010) 'Projections from the inferior colliculus to the tectal longitudinal column in the rat', *Neuroscience*, 166(2), pp. 653-664.

Ashmore, J.F. (1987) 'A fast motile response in guinea-pig outer hair cells: the cellular basis of the cochlear amplifier', *The Journal of physiology*, 388(1), pp. 323-347.

Bajo, V.M., Merchán, M.A., López, D.E. and Rouiller, E.M. (1993) 'Neuronal morphology and efferent projections of the dorsal nucleus of the lateral lemniscus in the rat', *Journal of comparative neurology*, 334(2), pp. 241-262.

Bajo, V.M., Merchán, M.A., Malmierca, M.S., Nodal, F.R. and Bjaalie, J.G. (1999) 'Topographic organization of the dorsal nucleus of the lateral lemniscus in the cat', *Journal of comparative neurology*, 407(3), pp. 349-366.

Bajo, V.M. and Moore, D.R. (2005) 'Descending projections from the auditory cortex to the inferior colliculus in the gerbil, *Meriones unguiculatus*', *Journal of comparative neurology*, 486(2), pp. 101-116.

Bajo, V.M., Nodal, F.R., Bizley, J.K., Moore, D.R. and King, A.J. (2007) 'The ferret auditory cortex: descending projections to the inferior colliculus', *Cerebral Cortex*, 17(2), pp. 475-491.

Bajo, V.M., Nodal, F.R., Moore, D.R. and King, A.J. (2009) 'The descending corticocollicular pathway mediates learning-induced auditory plasticity', *Nature neuroscience*, 13(2), pp. 253-260.

Bajo, V.M., Villa, A.E.P., de Ribaupierre, F. and Rouiller, E.M. (1998) 'Discharge properties of single neurons in the dorsal nucleus of the lateral lemniscus of the rat', *Brain research bulletin*, 47(6), pp. 595-610.

Baldwin, H.A., Frenk, S. and Lettvin, J.Y. (1965) 'Glass-coated tungsten microelectrodes', *Science*, 148(3676), pp. 1462-1464.

Bale, M.R. and Petersen, R.S. (2009) 'Transformation in the Neural Code for Whisker Deflection Direction Along the Lemniscal Pathway', *Journal of neurophysiology*, 102(5), pp. 2771-2780.

Batra, R. and Fitzpatrick, D.C. (2002) 'Monaural and binaural processing in the ventral nucleus of the lateral lemniscus: a major source of inhibition to the inferior colliculus', *Hearing research*, 168(1), pp. 90-97.

Bauer, E.E., Klug, A. and Pollak, G.D. (2000) 'Features of contralaterally evoked inhibition in the inferior colliculus', *Hearing research*, 141(1), pp. 80-96.

Bauer, E.E., Klug, A. and Pollak, G.D. (2002) 'Spectral determination of responses to species-specific calls in the dorsal nucleus of the lateral lemniscus', *Journal of neurophysiology*, 88(4), pp. 1955-1967.

Baumann, S., Griffiths, T.D., Sun, L., Petkov, C.I., Thiele, A. and Rees, A. (2011) 'Orthogonal representation of sound dimensions in the primate midbrain', *Nature neuroscience*, 14(4), pp. 423-425.

Benson, C.G. and Cant, N.B. (2008) 'The ventral nucleus of the lateral lemniscus of the gerbil (*Meriones unguiculatus*): organization of connections with the cochlear nucleus and the inferior colliculus', *Journal of comparative neurology*, 510(6), pp. 673-690.

Berman, A.L. (1968) *The brain stem of the cat. A cytoarchitectonic atlas with stereotaxic coordinates*. University of Wisconsin Press.

Beyerl, B.D. (1978) 'Afferent projections to the central nucleus of the inferior colliculus in the rat', *Brain research*, 145(2), pp. 209-223.

Blackburn, C.C. and Sachs, M.B. (1989) 'Classification of unit types in the anteroventral cochlear nucleus: PST histograms and regularity analysis', *Journal of neurophysiology*, 62(6), pp. 1303-1329.

- Bock, G.R., Webster, W.R. and Aitkin, L.M. (1972) 'Discharge patterns of single units in inferior colliculus of the alert cat', *Journal of neurophysiology*, 35(2), pp. 265-277.
- Boudreau, J.C. and Tsuchitani, C. (1968) 'Binaural interaction in the cat superior olive S segment', *Journal of neurophysiology*, 31(3), pp. 442-54.
- Bourk, T.R., Mielcarz, J.P. and Norris, B.E. (1981) 'Tonotopic organization of the anteroventral cochlear nucleus of the cat', *Hearing research*, 4(3), pp. 215-241.
- Brand, A., Behrend, O., Marquardt, T., McAlpine, D. and Grothe, B. (2002) 'Precise inhibition is essential for microsecond interaural time difference coding', *Nature*, 417(6888), pp. 543-547.
- Brawer, J.R., Morest, D.K. and Kane, E.C. (1974) 'The neuronal architecture of the cochlear nucleus of the cat', *Journal of comparative neurology*, 155(3), pp. 251-300.
- Brooks, V.B. (1983) 'Study of brain function by local, reversible cooling', in *Reviews of Physiology, Biochemistry and Pharmacology, Volume 95*. Springer, pp. 1-109.
- Brugge, J.F., Anderson, D.J. and Aitkin, L.M. (1970) 'Responses of neurons in the dorsal nucleus of the lateral lemniscus of cat to binaural tonal stimulation', *Journal of neurophysiology*, 33(3), pp. 441-458.
- Brunso-Bechtold, J.K., Thompson, G.C. and Masterton, R.B. (1981) 'HRP study of the organization of auditory afferents ascending to central nucleus of inferior colliculus in cat', *Journal of comparative neurology*, 197(4), pp. 705-722.
- Burger, R.M. and Pollak, G.D. (2001) 'Reversible inactivation of the dorsal nucleus of the lateral lemniscus reveals its role in the processing of multiple sound

sources in the inferior colliculus of bats', *The Journal of Neuroscience*, 21(13), pp. 4830-4843.

Caicedo, A. and Herbert, H. (1993) 'Topography of descending projections from the inferior colliculus to auditory brainstem nuclei in the rat', *Journal of comparative neurology*, 328(3), pp. 377-392.

Calford, M.B. and Aitkin, L.M. (1983) 'Ascending projections to the medial geniculate body of the cat: evidence for multiple, parallel auditory pathways through thalamus', *The Journal of Neuroscience*, 3(11), pp. 2365-2380.

Calford, M.B. and Webster, W.R. (1981) 'Auditory representation within principal division of cat medial geniculate body: an electrophysiology study', *Journal of neurophysiology*, 45(6), pp. 1013-1028.

Calford, M.B., Webster, W.R. and Semple, M.M. (1983) 'Measurement of frequency selectivity of single neurons in the central auditory pathway', *Hearing research*, 11(3), pp. 395-401.

Cant, N.B. and Benson, C.G. (2006) 'Organization of the inferior colliculus of the gerbil (*Meriones unguiculatus*): Differences in distribution of projections from the cochlear nuclei and the superior olivary complex', *Journal of comparative neurology*, 495(5), pp. 511-528.

Cant, N.B. and Casseday, J.H. (1986) 'Projections from the anteroventral cochlear nucleus to the lateral and medial superior olivary nuclei', *Journal of comparative neurology*, 247(4), pp. 457-476.

Cao, X.-J. and Oertel, D. (2005) 'Temperature affects voltage-sensitive conductances differentially in octopus cells of the mammalian cochlear nucleus', *Journal of neurophysiology*, 94(1), pp. 821-832.

Carey, C.L. and Webster, D.B. (1971) 'Ascending and Descending Projections of the Inferior Colliculus in the Kangaroo Rat (*Dipodomys merriami*)', *Brain, behavior and evolution*, 4(6), pp. 401-412.

Carrasco, A., Brown, T.A., Kok, M.A., Chabot, N., Kral, A. and Lomber, S.G. (2013) 'Influence of Core Auditory Cortical Areas on Acoustically Evoked Activity in Contralateral Primary Auditory Cortex', *The Journal of Neuroscience*, 33(2), pp. 776-789.

Carrasco, A. and Lomber, S.G. (2009a) 'Differential Modulatory Influences between Primary Auditory Cortex and the Anterior Auditory Field', *The Journal of Neuroscience*, 29(26), pp. 8350-8362.

Carrasco, A. and Lomber, S.G. (2009b) 'Evidence for hierarchical processing in cat auditory cortex: nonreciprocal influence of primary auditory cortex on the posterior auditory field', *The Journal of Neuroscience*, 29(45), pp. 14323-14333.

Casseday, J.H. and Covey, E. (1992) 'Frequency tuning properties of neurons in the inferior colliculus of an FM bat', *Journal of comparative neurology*, 319(1), pp. 34-50.

Casseday, J.H., Ehrlich, D. and Covey, E. (1994) 'Neural tuning for sound duration: role of inhibitory mechanisms in the inferior colliculus', *Science*, 264(5160), pp. 847-849.

Chase, S.M. and Young, E.D. (2005) 'Limited Segregation of Different Types of Sound Localization Information among Classes of Units in the Inferior Colliculus', *The Journal of Neuroscience*, 25(33), pp. 7575-7585.

Chase, S.M. and Young, E.D. (2007) 'First-spike latency information in single neurons increases when referenced to population onset', *Proceedings of the National Academy of Sciences*, 104(12), pp. 5175-5180.

- Chen, G.-D., Manohar, S. and Salvi, R. (2012) 'Amygdala hyperactivity and tonotopic shift after salicylate exposure', *Brain research*, 1485, pp. 63-76.
- Cheng, L., Mei, H.-X., Tang, J., Fu, Z.-Y., Jen, P.H.-S. and Chen, Q.-C. (2013) 'Bilateral collicular interaction: Modulation of auditory signal processing in frequency domain', *Neuroscience*, 235, pp. 27-39.
- Clark, G.M. (1969) 'The ultrastructure of nerve endings in the medial superior olive of the cat', *Brain research*, 14(2), pp. 293-305.
- Clerici, W.J. and Coleman, J.R. (1990) 'Anatomy of the rat medial geniculate body: I. Cytoarchitecture, myeloarchitecture, and neocortical connectivity', *Journal of comparative neurology*, 297(1), pp. 14-31.
- Clopton, B.M. and Winfield, J.A. (1973) 'Tonotopic organization in the inferior colliculus of the rat', *Brain research*, 56, pp. 355-358.
- Coleman, J.R. and Clerici, W.J. (1987) 'Sources of projections to subdivisions of the inferior colliculus in the rat', *Journal of comparative neurology*, 262(2), pp. 215-226.
- Coleman, J.R., McDonald, A.J., Pinek, B. and Zrull, M.C. (1992) 'The inferior colliculus: Calbindin and parvalbumin immunoreactivity in neural grafts', *Experimental neurology*, 115(1), pp. 142-145.
- Coomber, B., Edwards, D., Jones, S.J., Shackleton, T.M., Goldschmidt, J., Wallace, M.N. and Palmer, A.R. (2011) 'Cortical inactivation by cooling in small animals', *Frontiers in systems neuroscience*, 5.
- Coote, E.J. and Rees, A. (2008) 'The distribution of nitric oxide synthase in the inferior colliculus of guinea pig', *Neuroscience*, 154(1), pp. 218-225.

Covey, E., Kauer, J.A. and Casseday, J.H. (1996) 'Whole-cell patch-clamp recording reveals subthreshold sound-evoked postsynaptic currents in the inferior colliculus of awake bats', *The Journal of Neuroscience*, 16(9), pp. 3009-3018.

Davis, K.A. (2002) 'Evidence of a Functionally Segregated Pathway From Dorsal Cochlear Nucleus to Inferior Colliculus', *Journal of neurophysiology*, 87(4), pp. 1824-1835.

De No, R.L. (1933) 'Anatomy of the eighth nerve: III.—General plan of structure of the primary cochlear nuclei', *The Laryngoscope*, 43(4), pp. 327-350.

Dean, I., Harper, N.S. and McAlpine, D. (2005) 'Neural population coding of sound level adapts to stimulus statistics', *Nature Neuroscience*, 8(12), pp. 1684-1689.

Deisseroth, K. (2011) 'Optogenetics', *Nature Methods*, 8(1), pp. 26-29.

Dorr, A., Sled, J.G. and Kabani, N. (2007) 'Three-dimensional cerebral vasculature of the CBA mouse brain: A magnetic resonance imaging and micro computed tomography study', *NeuroImage*, 35(4), pp. 1409-1423.

Dum, N., Schmidt, U. and Von Wedel, H. (1981) 'Scalp distribution of the auditory evoked brainstem potentials in the guinea pig during monaural and binaural stimulation', *Hearing research*, 5(2), pp. 271-284.

Edeline, J.-M., Manunta, Y., Nodal, F.R. and Bajo, V.M. (1999) 'Do auditory responses recorded from awake animals reflect the anatomical parcellation of the auditory thalamus?', *Hearing research*, 131(1), pp. 135-152.

Egorova, M., Ehret, G., Vartanian, I. and Esser, K.-H. (2001) 'Frequency response areas of neurons in the mouse inferior colliculus. I. Threshold and tuning characteristics', *Experimental Brain Research*, 140(2), pp. 145-161.

Ehret, G. and Fischer, R. (1991) 'Neuronal activity and tonotopy in the auditory system visualized by c-fos gene expression', *Brain research*, 567(2), pp. 350-354.

Ehret, G. and Merzenich, M.M. (1988) 'Complex sound analysis (frequency resolution, filtering and spectral integration) by single units of the inferior colliculus of the cat', *Brain Research Reviews*, 13(2), pp. 139-163.

Ehret, G. and Moffat, A.J.M. (1985) 'Inferior colliculus of the house mouse', *Journal of Comparative Physiology A*, 156(5), pp. 619-635.

Ehret, G. and Schreiner, C.E. (2005) 'Spectral and intensity coding in the auditory midbrain', in Winer, J.A. and Schreiner, C. (eds.) *The Inferior Colliculus*. Springer, pp. 312-345.

Erulkar, S.D. (1959) 'The responses of single units of the inferior colliculus of the cat to acoustic stimulation', *Proceedings of the Royal Society of London. Series B*, 150(940), pp. 336-355.

Evans, E.F. (1972) 'The frequency response and other properties of single fibres in the guinea-pig cochlear nerve', *The Journal of physiology*, 226(1), pp. 263-287.

Evans, E.F. and Nelson, P.G. (1973) 'The responses of single neurones in the cochlear nucleus of the cat as a function of their location and the anaesthetic state', *Experimental Brain Research*, 17(4), pp. 402-427.

Faingold, C.L., Anderson, C.A.B. and Randall, M.E. (1993) 'Stimulation or blockade of the dorsal nucleus of the lateral lemniscus alters binaural and tonic inhibition in contralateral inferior colliculus neurons', *Hearing research*, 69(1), pp. 98-106.

Faingold, C.L., Boersma Anderson, C.A. and Caspary, D.M. (1991) 'Involvement of GABA in acoustically-evoked inhibition in inferior colliculus neurons', *Hearing research*, 52(1), pp. 201-216.

- Faingold, C.L., Gehlbach, G. and Casparly, D.M. (1989) 'On the role of GABA as an inhibitory neurotransmitter in inferior colliculus neurons: iontophoretic studies', *Brain research*, 500(1), pp. 302-312.
- Faye-Lund, H. and Osen, K.K. (1985) 'Anatomy of the inferior colliculus in rat', *Anatomy and Embryology*, 171(1), pp. 1-20.
- Feliciano, M. and Potashner, S.J. (1995) 'Evidence for a glutamatergic pathway from the guinea pig auditory cortex to the inferior colliculus', *Journal of neurochemistry*, 65(3), pp. 1348-1357.
- Fenko, L., Yizhar, O. and Deisseroth, K. (2011) 'The Development and Application of Optogenetics', *Annual Review of Neuroscience*, 34(1), pp. 389-412.
- Ferster, D., Chung, S. and Wheat, H. (1996) 'Orientation selectivity of thalamic input to simple cells of cat visual cortex', *Nature*, 380(6571), pp. 249-252.
- Fitzpatrick, K.A. (1975) 'Cellular architecture and topographic organization of the inferior colliculus of the squirrel monkey', *Journal of comparative neurology*, 164(2), pp. 185-207.
- Friauf, E. (1992) 'Tonotopic Order in the Adult and Developing Auditory System of the Rat as Shown by c-fos Immunocytochemistry', *European Journal of Neuroscience*, 4(9), pp. 798-812.
- Fuzessery, Z.M., Wenstrup, J.J., Hall, J.C. and Leroy, S. (2003) 'Inhibition has little effect on response latencies in the inferior colliculus', *Journal of the Association for Research in Otolaryngology*, 4(1), pp. 60-73.
- Gaese, B.H. and Ostwald, J. (2001) 'Anesthesia Changes Frequency Tuning of Neurons in the Rat Primary Auditory Cortex', *Journal of neurophysiology*, 86(2), pp. 1062-1066.

- Games, K.D. and Winer, J.A. (1988) 'Layer V in rat auditory cortex: projections to the inferior colliculus and contralateral cortex', *Hearing research*, 34(1), pp. 1-25.
- Gao, E. and Suga, N. (1998) 'Experience-dependent corticofugal adjustment of midbrain frequency map in bat auditory system', *Proceedings of the National Academy of Sciences*, 95(21), pp. 12663-12670.
- Gao, E. and Suga, N. (2000) 'Experience-dependent plasticity in the auditory cortex and the inferior colliculus of bats: role of the corticofugal system', *Proceedings of the National Academy of Sciences*, 97(14), pp. 8081-8086.
- Girard, P. and Bullier, J. (1989) 'Visual activity in area V2 during reversible inactivation of area 17 in the macaque monkey', *Journal of neurophysiology*, 62(6), pp. 1287-1302.
- Girardin, C.C. and Martin, K.A.C. (2009) 'Cooling in cat visual cortex: stability of orientation selectivity despite changes in responsiveness and spike width', *Neuroscience*, 164(2), pp. 777-787.
- Glendenning, K.K. and Hutson, K.A. (1998) 'Lack of topography in the ventral nucleus of the lateral lemniscus', *Microscopy research and technique*, 41(4), pp. 298-312.
- Glendenning, K.K. and Masterton, R.B. (1983) 'Acoustic chiasm: efferent projections of the lateral superior olive', *The Journal of Neuroscience*, 3(8), pp. 1521-1537.
- Goldberg, J.M. and Brown, P.B. (1969) 'Response of binaural neurons of dog superior olivary complex to dichotic tonal stimuli: some physiological mechanisms of sound localization', *Journal of neurophysiology*, 32(4), pp. 613-636.

Goldberg, J.M. and Brownell, W.E. (1973) 'Discharge characteristics of neurons in anteroventral and dorsal cochlear nuclei of cat', *Brain research*, 64, pp. 35-54.

González-Hernández, T.H., Galindo-Mireles, D., Castañeyra-Perdomo, A. and Ferres-Torres, R. (1991) 'Divergent projections of projecting neurons of the inferior colliculus to the medial geniculate body and the contralateral inferior colliculus in the rat', *Hearing research*, 52(1), pp. 17-21.

Gonzalez-Lima, F. and Cada, A. (1994) 'Cytochrome oxidase activity in the auditory system of the mouse: a qualitative and quantitative histochemical study', *Neuroscience*, 63(2), pp. 559-578.

González-Hernández, T., Mantolán-Sarmiento, B., González-González, B. and Pérez-González, H. (1996) 'Sources of GABAergic input to the inferior colliculus of the rat', *Journal of comparative neurology*, 372(2), pp. 309-326.

González-Hernández, T., Meyer, G. and Ferres-Torres, R. (1986) 'The commissural interconnections of the inferior colliculus in the albino mouse', *Brain research*, 368(2), pp. 268-276.

Gross, P.M., Sposito, N.M., Pettersen, S.E., Panton, D.G. and Fenstermacher, J.D. (1987) 'Topography of Capillary Density, Glucose Metabolism, and Microvascular Function Within the Rat Inferior Colliculus', *Journal of Cerebral Blood Flow & Metabolism*, 7(2), pp. 154-160.

Grothe, B. and Sanes, D.H. (1993) 'Bilateral inhibition by glycinergic afferents in the medial superior olive', *Journal of neurophysiology*, 69(4), pp. 1192-1196.

Hackney, C.M., Osen, K.K. and Kolston, J. (1990) 'Anatomy of the cochlear nuclear complex of guinea pig', *Anatomy and Embryology*, 182(2), pp. 123-149.

- Hall, J.C. (1999) 'GABAergic inhibition shapes frequency tuning and modifies response properties in the auditory midbrain of the leopard frog', *Journal of Comparative Physiology A*, 185(5), pp. 479-491.
- Hardingham, N.R. and Larkman, A.U. (1998) 'The reliability of excitatory synaptic transmission in slices of rat visual cortex in vitro is temperature dependent', *The Journal of physiology*, 507(1), pp. 249-256.
- Harnischfeger, G. (1978) 'Single unit study in the inferior colliculus of the house mouse (*Mus musculus*)', *Neuroscience letters*, 9(4), pp. 279-284.
- Harrison, J.M. and Warr, W.B. (1962) 'A study of the cochlear nuclei and ascending auditory pathways of the medulla', *Journal of comparative neurology*, 119(3), pp. 341-379.
- Harrison, R.V. and Palmer, A.R. (1984) 'Neurone response latency in the inferior colliculus in relation to the auditory brainstem responses (ABR) in the guinea pig', *Scandinavian audiology*, 13(4), pp. 275-281.
- Heffner, H. and Masterton, B. (1980) 'Hearing in Glires: Domestic rabbit, cotton rat, feral house mouse, and kangaroo rat', *The Journal of the Acoustical Society of America*, 68(6), pp. 1584-1599.
- Heffner, R., Heffner, H. and Masterton, B. (1971) 'Behavioral Measurements of Absolute and Frequency-Difference Thresholds in Guinea Pig', *The Journal of the Acoustical Society of America*, 49(6B), pp. 1888-1895.
- Hefti, B.J. and Smith, P.H. (2000) 'Anatomy, Physiology, and Synaptic Responses of Rat Layer V Auditory Cortical Cells and Effects of Intracellular GABA Blockade', *Journal of neurophysiology*, 83(5), pp. 2626-2638.
- Heil, P. (2004) 'First-spike latency of auditory neurons revisited', *Current opinion in neurobiology*, 14(4), pp. 461-467.

Helfert, R.H., Bonneau, J.M., Wenthold, R.J. and Altschuler, R.A. (1989) 'GABA and glycine immunoreactivity in the guinea pig superior olivary complex', *Brain research*, 501(2), pp. 269-286.

Henkel, C.K., Fuentes-Santamaria, V., Alvarado, J.C. and Brunso-Bechtold, J.K. (2003) 'Quantitative measurement of afferent layers in the ferret inferior colliculus: DNLL projections to sublayers', *Hearing research*, 177(1), pp. 32-42.

Henkel, C.K. and Shneiderman, A. (1988) 'Nucleus sagulum: projections of a lateral tegmental area to the inferior colliculus in the cat', *Journal of comparative neurology*, 271(4), pp. 577-588.

Hernández, O., Espinosa, N., Pérez-González, D. and Malmierca, M.S. (2005) 'The inferior colliculus of the rat: a quantitative analysis of monaural frequency response areas', *Neuroscience*, 132(1), pp. 203-217.

Hernández, O., Rees, A. and Malmierca, M.S. (2006) 'A GABAergic component in the commissure of the inferior colliculus in rat', *Neuroreport*, 17(15), pp. 1611-1614.

Hind, J.E., Goldberg, J.M., Greenwood, D.D. and Rose, J.E. (1963) 'Some discharge characteristics of single neurons in the inferior colliculus of the cat. II. Timing of the discharges and observations on binaural stimulation', *Journal of neurophysiology*, 26(2), pp. 321-341.

Huang, C.-M. and Fex, J. (1986) 'Tonotopic organization in the inferior colliculus of the rat demonstrated with the 2-deoxyglucose method', *Experimental Brain Research*, 61(3), pp. 506-512.

Huffman, R.F., Argeles, P.C. and Covey, E. (1998) 'Processing of sinusoidally amplitude modulated signals in the nuclei of the lateral lemniscus of the big brown bat, *Eptesicus fuscus*', *Hearing research*, 126(1), pp. 181-200.

Ingham, N.J., Bleeck, S. and Winter, I.M. (2006) 'Contralateral inhibitory and excitatory frequency response maps in the mammalian cochlear nucleus', *European Journal of Neuroscience*, 24(9), pp. 2515-2529.

Irvine, D.R.F. (1986) *The auditory brainstem*. Springer-Verlag.

Ito, M., van Adel, B. and Kelly, J.B. (1996) 'Sound localization after transection of the commissure of Probst in the albino rat', *Journal of neurophysiology*, 76(5), pp. 3493-3502.

Josephson, E.M. and Morest, D.K. (1998) 'A quantitative profile of the synapses on the stellate cell body and axon in the cochlear nucleus of the chinchilla', *Journal of neurocytology*, 27(11), pp. 841-864.

Junek, S., Kludt, E., Wolf, F. and Schild, D. (2010) 'Olfactory coding with patterns of response latencies', *Neuron*, 67(5), pp. 872-884.

Kapfer, C., Seidl, A.H., Schweizer, H. and Grothe, B. (2002) 'Experience-dependent refinement of inhibitory inputs to auditory coincidence-detector neurons', *Nature Neuroscience*, 5(3), pp. 247-253.

Katsuki, Y., Sumi, T., Uchiyama, H. and Watanabe, T. (1958) 'Electric responses of auditory neurons in cat to sound stimulation', *Journal of neurophysiology*, 21(6), pp. 569-588.

Kayama, Y., Shosaku, A. and Doty, R.W. (1984) 'Cryogenic blockade of the visual cortico-thalamic projection in the rat', *Experimental Brain Research*, 54(1), pp. 157-165.

Keating, G.E. and Gooley, S.G. (1988) 'Saccadic disorders caused by cooling the superior colliculus or the frontal eye field, or from combined lesions of both structures', *Brain research*, 438(1), pp. 247-255.

Keithley, E.M., Lo, J. and Ryan, A.F. (1994) '2-Deoxyglucose uptake patterns in response to pure tone stimuli in the aged rat inferior colliculus', *Hearing research*, 80(1), pp. 79-85.

Keithley, E.M. and Schreiber, R.C. (1987) 'Frequency map of the spiral ganglion in the cat', *The Journal of the Acoustical Society of America*, 81, p. 1036.

Kelly, J.B., Glenn, S.L. and Beaver, C.J. (1991) 'Sound frequency and binaural response properties of single neurons in rat inferior colliculus', *Hearing research*, 56(1), pp. 273-280.

Kelly, J.B. and Kavanagh, G.L. (1994) 'Sound localization after unilateral lesions of inferior colliculus in the ferret (*Mustela putorius*)', *Journal of neurophysiology*, 71(3), pp. 1078-1087.

Kelly, J.B., Li, L. and van Adel, B. (1996) 'Sound localizations after kainic acid lesions of the dorsal nucleus of the lateral lemniscus in the albino rat', *Behavioral neuroscience*, 110(6), pp. 1445-1455.

Kelly, J.B., van Adel, B.A. and Ito, M. (2009) 'Anatomical projections of the nuclei of the lateral lemniscus in the albino rat (*Rattus norvegicus*)', *Journal of comparative neurology*, 512(4), pp. 573-593.

Kiang, N.Y.-S. (1965) *Discharge Patterns of Single Fibers in the Cat's Auditory Nerve*. MIT Press.

Kidd, S.A. and Kelly, J.B. (1996) 'Contribution of the dorsal nucleus of the lateral lemniscus to binaural responses in the inferior colliculus of the rat: interaural time delays', *The Journal of Neuroscience*, 16(22), pp. 7390-7397.

Kitzes, L.M. and Semple, M.N. (1985) 'Single-unit responses in the inferior colliculus: effects of neonatal unilateral cochlear ablation', *Journal of neurophysiology*, 53(6), pp. 1483-1500.

Klug, A., Khan, A., Burger, R.M., Bauer, E.E., Hurley, L.M., Yang, L., Grothe, B., Halvorsen, M.B. and Park, T.J. (2000) 'Latency as a function of intensity in auditory neurons: influences of central processing', *Hearing research*, 148(1), pp. 107-123.

Koch, U. and Grothe, B. (2003) 'Hyperpolarization-Activated Current (I_h) in the Inferior Colliculus: Distribution and Contribution to Temporal Processing', *Journal of neurophysiology*, 90(6), pp. 3679-3687.

Kössl, M. and Vater, M. (1985) 'The cochlear frequency map of the mustache bat, *Pteronotus parnellii*', *Journal of Comparative Physiology A*, 157(5), pp. 687-697.

Kudo, M. and Niimi, K. (1978) 'Ascending projections of the inferior colliculus onto the medial geniculate body in the cat studied by anterograde and retrograde tracing techniques', *Brain research*, 155(1), pp. 113-117.

Kumoi, K., Saito, N. and Tanaka, C. (1993) 'Immunohistochemical localization of γ -aminobutyric acid and aspartate-containing neurons in the guinea pig superior olivary complex', *Hearing research*, 68(2), pp. 173-179.

Kuwabara, N. and Zook, J.M. (2000) 'Geniculo-collicular descending projections in the gerbil', *Brain research*, 878(1), pp. 79-87.

Kuwada, S. and Batra, R. (1999) 'Coding of sound envelopes by inhibitory rebound in neurons of the superior olivary complex in the unanesthetized rabbit', *The Journal of Neuroscience*, 19(6), pp. 2273-2287.

Kuwada, S., Batra, R., Yin, T.C.T., Oliver, D.L., Haberly, L.B. and Stanford, T.R. (1997) 'Intracellular recordings in response to monaural and binaural stimulation of neurons in the inferior colliculus of the cat', *The Journal of Neuroscience*, 17(19), pp. 7565-7581.

Kuwada, S., Fitzpatrick, D.C., Batra, R. and Ostapoff, E.-M. (2006) 'Sensitivity to interaural time differences in the dorsal nucleus of the lateral lemniscus of the unanesthetized rabbit: comparison with other structures', *Journal of neurophysiology*, 95(3), pp. 1309-1322.

Kuwada, S., Yin, T.C.T., Syka, J., Buunen, T.J. and Wickesberg, R.E. (1984) 'Binaural interaction in low-frequency neurons in inferior colliculus of the cat. IV. Comparison of monaural and binaural response properties', *Journal of neurophysiology*, 51(6), pp. 1306-1325.

Langner, G. (1992) 'Periodicity coding in the auditory system', *Hearing research*, 60(2), pp. 115-142.

Langner, G., Schreiner, C. and Merzenich, M.M. (1987) 'Covariation of latency and temporal resolution in the inferior colliculus of the cat', *Hearing research*, 31(2), pp. 197-201.

LeBeau, F.E.N., Malmierca, M.S. and Rees, A. (2001) 'Iontophoresis in vivo demonstrates a key role for GABAA and glycinergic inhibition in shaping frequency response areas in the inferior colliculus of guinea pig', *The Journal of Neuroscience*, 21(18), pp. 7303-7312.

LeBeau, F.E.N., Rees, A. and Malmierca, M.S. (1996) 'Contribution of GABA and glycine-mediated inhibition to the monaural temporal response properties of neurons in the inferior colliculus', *Journal of neurophysiology*, 75(2), pp. 902-919.

Li, L. and Kelly, J.B. (1992) 'Inhibitory influence of the dorsal nucleus of the lateral lemniscus on binaural responses in the rat's inferior colliculus', *The Journal of Neuroscience*, 12(11), pp. 4530-4539.

Li, Y., Evans, M.S. and Faingold, C.L. (1999) 'Synaptic response patterns of neurons in the cortex of rat inferior colliculus', *Hearing research*, 137(1), pp. 15-28.

Litovsky, R.Y., Fligor, B.J. and Tramo, M.J. (2002) 'Functional role of the human inferior colliculus in binaural hearing', *Hearing research*, 165(1-2), pp. 177-188.

Loftus, W.C., Malmierca, M.S., Bishop, D.C. and Oliver, D.L. (2008) 'The cytoarchitecture of the inferior colliculus revisited: a common organization of the lateral cortex in rat and cat', *Neuroscience*, 154(1), pp. 196-205.

Lohmann, C. and Friauf, E. (1996) 'Distribution of the calcium-binding proteins parvalbumin and calretinin in the auditory brainstem of adult and developing rats', *Journal of comparative neurology*, 367(1), pp. 90-109.

Lomber, S.G., Malhotra, S. and Hall, A.J. (2007a) 'Functional specialization in non-primary auditory cortex of the cat: areal and laminar contributions to sound localization', *Hearing research*, 229(1), pp. 31-45.

Lomber, S.G., Malhotra, S. and Sprague, J.M. (2007b) 'Restoration of acoustic orienting into a cortically deaf hemifield by reversible deactivation of the contralesional superior colliculus: the acoustic "Sprague effect"', *Journal of neurophysiology*, 97(2), pp. 979-993.

Lomber, S.G. and Payne, B.R. (1996) 'Removal of two halves restores the whole: reversal of visual hemineglect during bilateral cortical or collicular inactivation in the cat', *Visual neuroscience*, 13, pp. 1143-1156.

Lomber, S.G., Payne, B.R. and Cornwell, P. (2001) 'Role of the superior colliculus in analyses of space: superficial and intermediate layer contributions to visual orienting, auditory orienting, and visuospatial discriminations during unilateral and bilateral deactivations', *Journal of comparative neurology*, 441(1), pp. 44-57.

Lomber, S.G., Payne, B.R. and Horel, J.A. (1999) 'The cryoloop: an adaptable reversible cooling deactivation method for behavioral or electrophysiological assessment of neural function', *Journal of neuroscience methods*, 86(2), pp. 179-194.

Lu, Y., Jen, P.-S. and Zheng, Q.Y. (1997) 'GABAergic disinhibition changes the recovery cycle of bat inferior collicular neurons', *Journal of Comparative Physiology A*, 181(4), pp. 331-341.

Lu, Y. and Jen, P.H.S. (2003) 'Binaural interaction in the inferior colliculus of the big brown bat, *Eptesicus fuscus*', *Hearing research*, 177(1), pp. 100-110.

Ma, X. and Suga, N. (2001) 'Plasticity of Bat's Central Auditory System Evoked by Focal Electric Stimulation of Auditory and/or Somatosensory Cortices', *Journal of neurophysiology*, 85(3), pp. 1078-1087.

Malmierca, M.S. (2004) 'The Inferior Colliculus: A Center for Convergence of Ascending and Descending Auditory Information', *Neuroembryology and Aging*, 3(4), pp. 215-229.

Malmierca, M.S., Blackstad, T.W. and Osen, K.K. (2011) 'Computer-assisted 3-D reconstructions of Golgi-impregnated neurons in the cortical regions of the inferior colliculus of rat', *Hearing research*, 274(1), pp. 13-26.

Malmierca, M.S. and Hackett, T.A. (2010) 'Structural organization of the ascending auditory pathway', in Rees, A. and Palmer, A.R. (eds.) *The Auditory Brain*. Oxford University Press, pp. 9-41.

Malmierca, M.S., Hernández, O., Antunes, F.M. and Rees, A. (2009) 'Divergent and point-to-point connections in the commissural pathway between the inferior colliculi', *Journal of comparative neurology*, 514(3), pp. 226-239.

Malmierca, M.S., Hernández, O., Falconi, A., Lopez-Poveda, E.A., Merchán, M. and Rees, A. (2003) 'The commissure of the inferior colliculus shapes frequency response areas in rat: an in vivo study using reversible blockade with microinjection of kynurenic acid', *Experimental Brain Research*, 153(4), pp. 522-529.

Malmierca, M.S., Hernández, O. and Rees, A. (2005) 'Intercollicular commissural projections modulate neuronal responses in the inferior colliculus', *European Journal of Neuroscience*, 21(10), pp. 2701-2710.

Malmierca, M.S., Izquierdo, M.A., Cristaudo, S., Hernández, O., Pérez-González, D., Covey, E. and Oliver, D.L. (2008) 'A discontinuous tonotopic organization in the inferior colliculus of the rat', *The Journal of Neuroscience*, 28(18), pp. 4767-4776.

Malmierca, M.S., LeBeau, F.E.N. and Rees, A. (1996) 'The topographical organization of descending projections from the central nucleus of the inferior colliculus in guinea pig', *Hearing research*, 93(1), pp. 167-180.

Malmierca, M.S., Leergaard, T.B., Bajo, V.M., Bjaalie, J.G. and Merchán, M.A. (1998) 'Anatomic evidence of a three-dimensional mosaic pattern of tonotopic organization in the ventral complex of the lateral lemniscus in cat', *The Journal of Neuroscience*, 18(24), pp. 10603-10618.

Malmierca, M.S., Rees, A., LeBeau, F.E.N. and Bjaalie, J.G. (1995) 'Laminar organization of frequency-defined local axons within and between the inferior colliculi of the guinea pig', *Journal of comparative neurology*, 357(1), pp. 124-144.

Manis, P.B. (1990) 'Membrane properties and discharge characteristics of guinea pig dorsal cochlear nucleus neurons studied in vitro', *The Journal of Neuroscience*, 10(7), pp. 2338-2351.

- Masterton, B., Thompson, G.C., Bechtold, J.K. and RoBards, M.J. (1975) 'Neuroanatomical basis of binaural phase-difference analysis for sound localization: a comparative study', *Journal of comparative and physiological psychology*, 89(5), pp. 379-386.
- May, B.J., Le Prell, G.S. and Sachs, M.B. (1998) 'Vowel representations in the ventral cochlear nucleus of the cat: effects of level, background noise, and behavioral state', *Journal of neurophysiology*, 79(4), pp. 1755-1767.
- Meffin, H. and Grothe, B. (2009) 'Selective filtering to spurious localization cues in the mammalian auditory brainstem', *The Journal of the Acoustical Society of America*, 126, pp. 2437-2454.
- Mei, H.-X., Cheng, L., Tang, J., Fu, Z.-Y., Jen, P.H.-S. and Chen, Q.-C. (2012) 'Modulation of amplitude sensitivity by bilateral collicular interaction among different frequency laminae', *Neuroscience letters*, 517(1), pp. 13-17.
- Meininger, V., Pol, D. and Derer, P. (1986) 'The inferior colliculus of the mouse. A Nissl and Golgi study', *Neuroscience*, 17(4), pp. 1159-1179.
- Merchán, M., Aguilar, L.A., Lopez-Poveda, E.A. and Malmierca, M.S. (2005) 'The inferior colliculus of the rat: quantitative immunocytochemical study of GABA and glycine', *Neuroscience*, 136(3), pp. 907-925.
- Merchán, M.A. and Berbel, P. (1996) 'Anatomy of the ventral nucleus of the lateral lemniscus in rats: a nucleus with a concentric laminar organization', *Journal of comparative neurology*, 372(2), pp. 245-263.
- Merrill, E.G. and Ainsworth, A. (1972) 'Glass-coated platinum-plated tungsten microelectrodes', *Medical and Biological Engineering*, 10(5), pp. 662-672.
- Merzenich, M.M. and Reid, M.D. (1974) 'Representation of the cochlea within the inferior colliculus of the cat', *Brain research*, 77(3), pp. 397-415.

Michalski, A., Wimborne, B.M. and Henry, G.H. (1993) 'The effect of reversible cooling of cat's primary visual cortex on the responses of area 21a neurons', *The Journal of physiology*, 466(1), pp. 133-156.

Mickey, B.J. and Middlebrooks, J.C. (2003) 'Representation of auditory space by cortical neurons in awake cats', *The Journal of Neuroscience*, 23(25), pp. 8649-8663.

Miller, K.E., Casseday, J.H. and Covey, E. (2005) 'Relation between intrinsic connections and isofrequency contours in the inferior colliculus of the big brown bat, *Eptesicus fuscus*', *Neuroscience*, 136(3), pp. 895-905.

Mitani, A., Shimokouchi, M. and Nomura, S. (1983) 'Effects of stimulation of the primary auditory cortex upon colliculogeniculate neurons in the inferior colliculus of the cat', *Neuroscience letters*, 42(2), pp. 185-189.

Miyazaki, Y., Ervin, F., Siegfried, J., Richardson, E.P. and Mark, V.H. (1963) 'Localized cooling in the central nervous system: Part ii. histopathological results', *Archives of Neurology*, 9(4), pp. 392-399.

Moore, C.N., Casseday, J.H. and Neff, W.D. (1974) 'Sound localization: the role of the commissural pathways of the auditory system of the cat', *Brain research*, 82(1), pp. 13-26.

Moore, D.R. (1988) 'Auditory brainstem of the ferret: sources of projections to the inferior colliculus', *Journal of comparative neurology*, 269(3), pp. 342-354.

Moore, D.R., Kotak, V.C. and Sanes, D.H. (1998) 'Commissural and lemniscal synaptic input to the gerbil inferior colliculus', *Journal of neurophysiology*, 80(5), pp. 2229-2236.

Moore, D.R., Semple, M.N. and Addison, P.D. (1983) 'Some acoustic properties of neurones in the ferret inferior colliculus', *Brain research*, 269(1), pp. 69-82.

- Moore, R.Y. and Goldberg, J.M. (1966) 'Projections of the inferior colliculus in the monkey', *Experimental neurology*, 14(4), pp. 429-438.
- Morest, D.K. and Oliver, D.L. (1984) 'The neuronal architecture of the inferior colliculus in the cat: Defining the functional anatomy of the auditory midbrain', *Journal of comparative neurology*, 222(2), pp. 209-236.
- Nakamoto, K.T., Jones, S.J. and Palmer, A.R. (2008) 'Descending projections from auditory cortex modulate sensitivity in the midbrain to cues for spatial position', *Journal of neurophysiology*, 99(5), pp. 2347-2356.
- Nakamoto, K.T., Mellott, J.G., Killius, J., Storey-Workley, M.E., Sowick, C.S. and Schofield, B.R. (2013) 'Ultrastructural examination of the corticocollicular pathway in the guinea pig: a study using electron microscopy, neural tracers, and GABA immunocytochemistry', *Frontiers in Neuroanatomy*, 7.
- Nakamoto, K.T., Shackleton, T.M. and Palmer, A.R. (2010) 'Responses in the inferior colliculus of the guinea pig to concurrent harmonic series and the effect of inactivation of descending controls', *Journal of neurophysiology*, 103(4), pp. 2050-2061.
- Nelson, P.G. and Erulkar, S.D. (1963) 'Synaptic mechanisms of excitation and inhibition in the central auditory pathway', *Journal of neurophysiology*, 26(6), pp. 908-923.
- Oertel, D. and Young, E.D. (2004) 'What's a cerebellar circuit doing in the auditory system?', *Trends in neurosciences*, 27(2), pp. 104-110.
- Okoyama, S., Ohbayashi, M., Ito, M. and Harada, S. (2006) 'Neuronal organization of the rat inferior colliculus participating in four major auditory pathways', *Hearing research*, 218(1), pp. 72-80.

Oldfield, S.R. and Parker, S.P. (1984) 'Acuity of sound localisation: A topography of auditory space: II. Pinna cues absent', *Perception*, 13(5), pp. 601-617.

Oliver, D.L. (1984a) 'Dorsal cochlear nucleus projections to the inferior colliculus in the cat: a light and electron microscopic study', *Journal of comparative neurology*, 224(2), pp. 155-172.

Oliver, D.L. (1984b) 'Neuron types in the central nucleus of the inferior colliculus that project to the medial geniculate body', *Neuroscience*, 11(2), pp. 409-424.

Oliver, D.L. (1985) 'Quantitative analyses of axonal endings in the central nucleus of the inferior colliculus and distribution of 3H-labeling after injections in the dorsal cochlear nucleus', *Journal of comparative neurology*, 237(3), pp. 343-359.

Oliver, D.L. (1987) 'Projections to the inferior colliculus from the anteroventral cochlear nucleus in the cat: possible substrates for binaural interaction', *Journal of comparative neurology*, 264(1), pp. 24-46.

Oliver, D.L., Beckius, G.E. and Shneiderman, A. (1995) 'Axonal projections from the lateral and medial superior olive to the inferior colliculus of the cat: a study using electron microscopic autoradiography', *Journal of comparative neurology*, 360(1), pp. 17-32.

Oliver, D.L., Kuwada, S., Yin, T.C.T., Haberly, L.B. and Henkel, C.K. (1991) 'Dendritic and axonal morphology of HRP-injected neurons in the inferior colliculus of the cat', *Journal of comparative neurology*, 303(1), pp. 75-100.

Oliver, D.L., Ostapoff, E.M. and Beckius, G.E. (1999) 'Direct innervation of identified tectothalamic neurons in the inferior colliculus by axons from the cochlear nucleus', *Neuroscience*, 93(2), pp. 643-658.

Oliver, D.L., Winer, J.A., Beckius, G.E. and Saint Marie, R.L. (1994) 'Morphology of GABAergic neurons in the inferior colliculus of the cat', *Journal of comparative neurology*, 340(1), pp. 27-42.

Osen, K.K. (1969) 'Cytoarchitecture of the cochlear nuclei in the cat', *Journal of comparative neurology*, 136(4), pp. 453-483.

Osen, K.K. (1970) 'Course and termination of the primary afferents in the cochlear nuclei of the cat. An experimental anatomical study', *Archives italiennes de biologie*, 108(1), pp. 21-51.

Osen, K.K. (1972) 'Projection of the cochlear nuclei on the inferior colliculus in the cat', *Journal of comparative neurology*, 144(3), pp. 355-371.

Palmer, A.R., Jiang, D. and Marshall, D.H. (1996) 'Responses of ventral cochlear nucleus onset and chopper units as a function of signal bandwidth', *Journal of neurophysiology*, 75(2), pp. 780-794.

Palmer, A.R., Shackleton, T.M., Sumner, C.J., Zobay, O. and Rees, A. (2013) 'Classification of frequency response areas in the IC reveals continua not discrete classes', *The Journal of physiology*, Epub ahead of print.

Palombi, P.S. and Caspary, D.M. (1996) 'GABA inputs control discharge rate primarily within frequency receptive fields of inferior colliculus neurons', *Journal of neurophysiology*, 75(6), pp. 2211-2219.

Park, T.J., Brand, A., Koch, U., Ikebuchi, M. and Grothe, B. (2008) 'Dynamic changes in level influence spatial coding in the lateral superior olive', *Hearing research*, 238(1), pp. 58-67.

Park, T.J. and Pollak, G.D. (1993) 'GABA shapes a topographic organization of response latency in the mustache bat's inferior colliculus', *The Journal of Neuroscience*, 13(12), pp. 5172-5187.

Pecka, M., Brand, A., Behrend, O. and Grothe, B. (2008) 'Interaural Time Difference Processing in the Mammalian Medial Superior Olive: The Role of Glycinergic Inhibition', *The Journal of Neuroscience*, 28(27), pp. 6914-6925.

Pecka, M., Siveke, I., Grothe, B. and Lesica, N.A. (2010) 'Enhancement of ITD coding within the initial stages of the auditory pathway', *Journal of neurophysiology*, 103(1), pp. 38-46.

Pérez-González, D., Hernández, O., Covey, E. and Malmierca, M.S. (2012) 'GABAA-mediated inhibition modulates stimulus-specific adaptation in the inferior colliculus', *PloS one*, 7(3), p. e34297.

Peruzzi, D., Bartlett, E., Smith, P.H. and Oliver, D.L. (1997) 'A monosynaptic GABAergic input from the inferior colliculus to the medial geniculate body in rat', *The Journal of Neuroscience*, 17(10), pp. 3766-3777.

Peruzzi, D., Sivaramakrishnan, S. and Oliver, D.L. (2000) 'Identification of cell types in brain slices of the inferior colliculus', *Neuroscience*, 101(2), pp. 403-416.

Petersen, R.S., Panzeri, S. and Diamond, M.E. (2001) 'Population Coding of Stimulus Location in Rat Somatosensory Cortex', *Neuron*, 32(3), pp. 503-514.

Phillips, D.P. and Irvine, D.R. (1981) 'Responses of single neurons in physiologically defined primary auditory cortex (AI) of the cat: frequency tuning and responses to intensity', *Journal of neurophysiology*, 45(1), pp. 48-58.

Phillips, D.P. and Irvine, D.R.F. (1982) 'Properties of single neurons in the anterior auditory field (AAF) of cat cerebral cortex', *Brain research*, 248(2), pp. 237-244.

Pollak, G.D. (2013) 'The Dominant Role of Inhibition in Creating Response Selectivities for Communication Calls in the Brainstem Auditory System', *Hearing research*, Epub ahead of print.

Pollak, G.D., Burger, R.M. and Klug, A. (2003) 'Dissecting the circuitry of the auditory system', *Trends in neurosciences*, 26(1), pp. 33-39.

Pollak, G.D., Burger, R.M., Park, T.J., Klug, A. and Bauer, E.E. (2002) 'Roles of inhibition for transforming binaural properties in the brainstem auditory system', *Hearing research*, 168(1-2), pp. 60-78.

Pollak, G.D., Gittelman, J.X., Li, N. and Xie, R. (2011) 'Inhibitory projections from the ventral nucleus of the lateral lemniscus and superior paraolivary nucleus create directional selectivity of frequency modulations in the inferior colliculus: a comparison of bats with other mammals', *Hearing research*, 273(1), pp. 134-144.

Popelar, J. and Syka, J. (1982) 'Response properties of neurons in the inferior colliculus of the guinea-pig', *Acta Neurobiologiae Experimentalis*, 42, pp. 299-310.

Portfors, C.V. and Wenstrup, J.J. (2002) 'Excitatory and facilitatory frequency response areas in the inferior colliculus of the mustached bat', *Hearing research*, 168(1), pp. 131-138.

Powell, T.P.S. and Cowan, W.M. (1962) 'An experimental study of the projection of the cochlea', *Journal of anatomy*, 96(Pt 2), pp. 269-284.

Prosen, C.A., Petersen, M.R., Moody, D.B. and Stebbins, W.C. (1978) 'Auditory thresholds and kanamycin-induced hearing loss in the guinea pig assessed by a positive reinforcement procedure', *The Journal of the Acoustical Society of America*, 63(2), pp. 559-566.

Ramachandran, R., Davis, K.A. and May, B.J. (1999) 'Single-unit responses in the inferior colliculus of decerebrate cats I. Classification based on frequency response maps', *Journal of neurophysiology*, 82(1), pp. 152-163.

Ramon y Cajal, S. (1995) 'Histology of the nervous system of man and vertebrates', *Oxford Univ. Press, New York*.

Rees, A., Sarbaz, A., Malmierca, M.S. and Le Beau, F.E.N. (1997) 'Regularity of firing of neurons in the inferior colliculus', *Journal of neurophysiology*, 77(6), pp. 2945-2965.

Reich, D.S., Mechler, F. and Victor, J.D. (2001) 'Temporal Coding of Contrast in Primary Visual Cortex: When, What, and Why', *Journal of neurophysiology*, 85(3), pp. 1039-1050.

Reivich, M., Jehle, J., Sokoloff, L. and Kety, S.S. (1969) 'Measurement of regional cerebral blood flow with antipyrine-14C in awake cats', *Journal of Applied Physiology*, 27(2), pp. 296-300.

Reynolds Jr, A.F., Ojemann, G.A. and Ward Jr, A.A. (1975) 'Intracellular recording during focal hypothermia in cat pericruciate cortex', *Experimental neurology*, 46(3), pp. 566-582.

Rhode, W.S. and Greenberg, S. (1992) 'Physiology of the cochlear nuclei', in Fay, R.R. (ed.) *The mammalian auditory pathway: Neurophysiology*. Springer, pp. 94-152.

Rhode, W.S. and Smith, P.H. (1986) 'Encoding timing and intensity in the ventral cochlear nucleus of the cat', *Journal of neurophysiology*, 56(2), pp. 261-286.

Riquelme, R., Saldaña, E., Osen, K.K., Ottersen, O.P. and Merchán, M.A. (2001) 'Colocalization of GABA and glycine in the ventral nucleus of the lateral lemniscus in rat: An in situ hybridization and semiquantitative immunocytochemical study', *Journal of comparative neurology*, 432(4), pp. 409-424.

Roberts, M.T., Seeman, S.C. and Golding, N.L. (2013) 'A Mechanistic Understanding of the Role of Feedforward Inhibition in the Mammalian Sound Localization Circuitry', *Neuron*, 78(5), pp. 923-935.

Robinson, B.L. and McAlpine, D. (2009) 'Gain control mechanisms in the auditory pathway', *Current opinion in neurobiology*, 19(4), pp. 402-407.

Rockel, A.J. and Jones, E.G. (1973a) 'The neuronal organization of the inferior colliculus of the adult cat. I. The central nucleus', *Journal of comparative neurology*, 147(1), pp. 11-59.

Rockel, A.J. and Jones, E.G. (1973b) 'The neuronal organization of the inferior colliculus of the adult cat. II. The pericentral nucleus', *Journal of comparative neurology*, 149(3), pp. 301-333.

Rockel, A.J. and Jones, E.G. (1973c) 'Observations on the fine structure of the central nucleus of the inferior colliculus of the cat', *Journal of comparative neurology*, 147(1), pp. 61-91.

Romand, R. (1997) 'Modification of tonotopic representation in the auditory system during development', *Progress in neurobiology*, 51(1), pp. 1-17.

Romand, R. and Ehret, G. (1990) 'Development of tonotopy in the inferior colliculus. I. Electrophysiological mapping in house mice', *Developmental Brain Research*, 54(2), pp. 221-234.

Rose, J.E., Galambos, R. and Hughes, J.R. (1959) 'Microelectrode studies of the cochlear nuclei of the cat', *Bulletin of the Johns Hopkins Hospital*, 104(5), p. 211.

Rose, J.E., Greenwood, D.D., Goldberg, J.M. and Hind, J.E. (1963) 'Some discharge characteristics of single neurons in the inferior colliculus of the cat. I. Tonotopical organization, relation of spike-counts to tone intensity, and firing patterns of single elements', *Journal of neurophysiology*, 26(2), pp. 294-320.

Rose, J.E., Gross, N.B., Geisler, C.D. and Hind, J.E. (1966) 'Some neural mechanisms in the inferior colliculus of the cat which may be relevant to localization of a sound source', *Journal of neurophysiology*, 29(2), pp. 288-314.

Rouiller, E.M. and De Ribaupierre, F. (1985) 'Origin of afferents to physiologically defined regions of the medial geniculate body of the cat: ventral and dorsal divisions', *Hearing research*, 19(2), pp. 97-114.

Rübsamen, R. (1992) 'Postnatal development of central auditory frequency maps', *Journal of Comparative Physiology A*, 170(2), pp. 129-143.

Rutkowski, R.G., Miasnikov, A.A. and Weinberger, N.M. (2003) 'Characterisation of multiple physiological fields within the anatomical core of rat auditory cortex', *Hearing research*, 181(1), pp. 116-130.

Ryan, A. and Miller, J. (1978) 'Single unit responses in the inferior colliculus of the awake and performing rhesus monkey', *Experimental Brain Research*, 32(3), pp. 389-407.

Ryugo, D.K., Willard, F.H. and Fekete, D.M. (1981) 'Differential afferent projections to the inferior colliculus from the cochlear nucleus in the albino mouse', *Brain research*, 210(1), pp. 342-349.

Saint Marie, R.L. (1996) 'Glutamatergic connections of the auditory midbrain: Selective uptake and axonal transport of D-[3H] aspartate', *Journal of comparative neurology*, 373(2), pp. 255-270.

Saint Marie, R.L., Ostapoff, E., Morest, D.K. and Wenthold, R.J. (1989) 'Glycine-immunoreactive projection of the cat lateral superior olive: Possible role in midbrain ear dominance', *Journal of comparative neurology*, 279(3), pp. 382-396.

Saint Marie, R.L., Shneiderman, A. and Stanforth, D.A. (1997) 'Patterns of γ -aminobutyric acid and glycine immunoreactivities reflect structural and functional differences of the cat lateral lemniscal nuclei', *Journal of comparative neurology*, 389(2), pp. 264-276.

Saldaña, E., Aparicio, M.A., Fuentes-Santamaría, V. and Berrebi, A.S. (2009) 'Connections of the superior paraolivary nucleus of the rat: projections to the inferior colliculus', *Neuroscience*, 163(1), pp. 372-387.

Saldaña, E., Feliciano, M. and Mugnaini, E. (1996) 'Distribution of descending projections from primary auditory neocortex to inferior colliculus mimics the topography of intracollicular projections', *Journal of comparative neurology*, 371(1), pp. 15-40.

Saldaña, E. and Merchán, M.A. (1992) 'Intrinsic and commissural connections of the rat inferior colliculus', *Journal of comparative neurology*, 319(3), pp. 417-437.

Sando, I. (1965) 'The anatomical interrelationships of the cochlear nerve fibers', *Acta Oto-Laryngologica*, 59(2-6), pp. 417-436.

Schiller, P.H. and Malpeli, J.G. (1977) 'The effect of striate cortex cooling on area 18 cells in the monkey', *Brain research*, 126(2), pp. 366-69.

Schofield, B.R. (2001) 'Origins of projections from the inferior colliculus to the cochlear nucleus in guinea pigs', *Journal of comparative neurology*, 429(2), pp. 206-220.

Schofield, B.R. (2002) 'Ascending and descending projections from the superior olivary complex in guinea pigs: different cells project to the cochlear nucleus and the inferior colliculus', *Journal of comparative neurology*, 453(3), pp. 217-225.

Schofield, B.R. (2010) 'Structural organization of the descending auditory pathway', in Rees, A. and Palmer, A.R. (eds.) *The Auditory Brain*. Oxford University Press, pp. 43-64.

Schofield, B.R. and Cant, N.B. (1992) 'Organization of the superior olivary complex in the guinea pig: II. Patterns of projection from the periolivary nuclei to the inferior colliculus', *Journal of comparative neurology*, 317(4), pp. 438-455.

Schofield, B.R. and Cant, N.B. (1999) 'Descending auditory pathways: projections from the inferior colliculus contact superior olivary cells that project bilaterally to the cochlear nuclei', *Journal of comparative neurology*, 409(2), pp. 210-223.

Schreiner, C.E. and Langner, G. (1997) 'Laminar fine structure of frequency organization in auditory midbrain', *Nature*, 388(6640), pp. 383-386.

Semple, M.N. and Aitkin, L.M. (1979) 'Representation of sound frequency and laterality by units in central nucleus of cat inferior colliculus', *Journal of neurophysiology*, 42(6), pp. 1626-1639.

Semple, M.N. and Kitzes, L.M. (1985) 'Single-unit responses in the inferior colliculus: different consequences of contralateral and ipsilateral auditory stimulation', *Journal of neurophysiology*, 53(6), pp. 1467-1482.

Sherk, H. (1978) 'Area 18 cell responses in cat during reversible inactivation of area 17', *Journal of neurophysiology*, 41(1), pp. 204-215.

Shneiderman, A., Stanforth, D.A., Henkel, C.K. and Saint Marie, R.L. (1999) 'Input-output relationships of the dorsal nucleus of the lateral lemniscus: Possible substrate for the processing of dynamic spatial cues', *Journal of comparative neurology*, 410(2), pp. 265-276.

Shriki, O., Kohn, A. and Shamir, M. (2012) 'Fast coding of orientation in primary visual cortex', *PLoS Computational Biology*, 8(6), p. e1002536.

- Sivaramakrishnan, S. and Oliver, D.L. (2001) 'Distinct K currents result in physiologically distinct cell types in the inferior colliculus of the rat', *The Journal of Neuroscience*, 21(8), pp. 2861-2877.
- Siveke, I., Pecka, M., Seidl, A.H., Baudoux, S. and Grothe, B. (2006) 'Binaural response properties of low-frequency neurons in the gerbil dorsal nucleus of the lateral lemniscus', *Journal of neurophysiology*, 96(3), pp. 1425-1440.
- Skinner, J.E. (1970) 'A cryoprobe and cryoplate for reversible functional blockade in the brains of chronic animal preparations', *Electroencephalography and Clinical Neurophysiology*, 29(2), pp. 204-205.
- Slater, B.J., Willis, A.M. and Llano, D.A. (2013) 'Evidence for layer-specific differences in auditory corticocollicular neurons', *Neuroscience*, 229, pp. 144-154.
- Smith, P.H. (1992) 'Anatomy and physiology of multipolar cells in the rat inferior collicular cortex using the in vitro brain slice technique', *The Journal of Neuroscience*, 12(9), pp. 3700-3715.
- Smith, P.H. and Rhode, W.S. (1989) 'Structural and functional properties distinguish two types of multipolar cells in the ventral cochlear nucleus', *Journal of comparative neurology*, 282(4), pp. 595-616.
- Song, Y., Mellott, J.G. and Winer, J.A. (2011) 'Microvascular organization of the cat inferior colliculus', *Hearing research*, 274(1), pp. 5-12.
- Stiebler, I. and Ehret, G. (1985) 'Inferior colliculus of the house mouse. I. A quantitative study of tonotopic organization, frequency representation, and tone-threshold distribution', *Journal of comparative neurology*, 238(1), pp. 65-76.

Storchi, R., Bale, M.R., Biella, G.E.M. and Petersen, R.S. (2012) 'Comparison of latency and rate coding for the direction of whisker deflection in the subcortical somatosensory pathway', *Journal of neurophysiology*, 108(7), pp. 1810-1821.

Strominger, N.L., Nelson, L.R. and Dougherty, W.J. (1977) 'Second order auditory pathways in the chimpanzee', *Journal of comparative neurology*, 172(2), pp. 349-365.

Suga, N., Xiao, Z., Ma, X. and Ji, W. (2002) 'Plasticity and corticofugal modulation for hearing in adult animals', *Neuron*, 36(1), pp. 9-18.

Suga, N., Zhang, Y. and Yan, J. (1997) 'Sharpening of Frequency Tuning by Inhibition in the Thalamic Auditory Nucleus of the Mustached Bat', *Journal of neurophysiology*, 77(4), pp. 2098-2114.

Sumner, C.J. and Palmer, A.R. (2012) 'Auditory nerve fibre responses in the ferret', *European Journal of Neuroscience*, 36(4), pp. 2428-2439.

Sun, Y.J., Kim, Y.-J., Ibrahim, L.A., Tao, H.W. and Zhang, L.I. (2013) 'Synaptic Mechanisms Underlying Functional Dichotomy between Intrinsic-Bursting and Regular-Spiking Neurons in Auditory Cortical Layer 5', *The Journal of Neuroscience*, 33(12), pp. 5326-5339.

Sutter, M.L. (2000) 'Shapes and level tolerances of frequency tuning curves in primary auditory cortex: quantitative measures and population codes', *Journal of neurophysiology*, 84(2), pp. 1012-1025.

Sutter, M.L. and Schreiner, C.E. (1991) 'Physiology and topography of neurons with multipeaked tuning curves in cat primary auditory cortex', *Journal of neurophysiology*, 65(5), pp. 1207-1226.

Syka, J. and Popelář, J. (1984) 'Inferior colliculus in the rat: neuronal responses to stimulation of the auditory cortex', *Neuroscience letters*, 51(2), pp. 235-240.

Syka, J., Popelář, J., Kvašňák, E. and Astl, J. (2000) 'Response properties of neurons in the central nucleus and external and dorsal cortices of the inferior colliculus in guinea pig', *Experimental Brain Research*, 133(2), pp. 254-266.

Symmes, D., Alexander, G.E. and Newman, J.D. (1980) 'Neural processing of vocalizations and artificial stimuli in the medial geniculate body of squirrel monkey', *Hearing research*, 3(2), pp. 133-146.

Szczepaniak, W.S. and Møller, A.R. (1993) 'Interaction between auditory and somatosensory systems: a study of evoked potentials in the inferior colliculus', *Electroencephalography and Clinical Neurophysiology*, 88(6), pp. 508-515.

Tan, M.L., Theeuwes, H.P., Feenstra, L. and Borst, J.G.G. (2007) 'Membrane Properties and Firing Patterns of Inferior Colliculus Neurons: An In Vivo Patch-Clamp Study in Rodents', *Journal of neurophysiology*, 98(1), pp. 443-453.

Tan, X., Wang, X., Yang, W. and Xiao, Z. (2008) 'First spike latency and spike count as functions of tone amplitude and frequency in the inferior colliculus of mice', *Hearing research*, 235(1-2), pp. 90-104.

Tardif, E., Chiry, O., Probst, A., Magistretti, P.J. and Clarke, S. (2003) 'Patterns of calcium-binding proteins in human inferior colliculus: identification of subdivisions and evidence for putative parallel systems', *Neuroscience*, 116(4), pp. 1111-1121.

Tasaki, I. (1954) 'Nerve impulses in individual auditory nerve fibers of guinea pig', *Journal of Neurophysiology*, 17(2), pp. 97-122.

Ter-Mikaelian, M., Sanes, D.H. and Semple, M.N. (2007) 'Transformation of temporal properties between auditory midbrain and cortex in the awake Mongolian gerbil', *The Journal of Neuroscience*, 27(23), pp. 6091-6102.

Thompson, A.M. and Thompson, G.C. (1993) 'Relationship of descending inferior colliculus projections to olivocochlear neurons', *Journal of comparative neurology*, 335(3), pp. 402-412.

Trevelyan, A.J. and Jack, J.J. (2002) 'Detailed passive cable models of layer 2/3 pyramidal cells in rat visual cortex at different temperatures', *The Journal of physiology*, 539(2), pp. 623-636.

Tunturi, A.R. (1955) 'Analysis of cortical auditory responses with the probability pulse', *American Journal of Physiology*, 181(3), pp. 630-638.

Turner, J.G., Hughes, L.F. and Caspary, D.M. (2005) 'Divergent response properties of layer-V neurons in rat primary auditory cortex', *Hearing research*, 202(1), pp. 129-140.

van Adel, B.A., Kidd, S.A. and Kelly, J.B. (1999) 'Contribution of the commissure of Probst to binaural evoked responses in the rat's inferior colliculus: interaural time differences', *Hearing research*, 130(1), pp. 115-130.

van der Heijden, M., Lorteije, J.A.M., Plauška, A., Roberts, M.T., Golding, N.L. and Borst, J.G.G. (2013) 'Directional Hearing by Linear Summation of Binaural Inputs at the Medial Superior Olive', *Neuron*, 78(5), pp. 936-948.

Vater, M., Habbicht, H., Kössl, M. and Grothe, B. (1992) 'The functional role of GABA and glycine in monaural and binaural processing in the inferior colliculus of horseshoe bats', *Journal of Comparative Physiology A*, 171(4), pp. 541-553.

Vater, M., Schlegel, P. and Zöllner, H. (1979) 'Comparative auditory neurophysiology of the inferior colliculus of two molossid bats, *molossus ater* and *molossus molossus*', *Journal of comparative physiology*, 131(2), pp. 137-145.

Vetter, D.E., Saldaña, E. and Mugnaini, E. (1993) 'Input from the inferior colliculus to medial olivocochlear neurons in the rat: a double label study with PHA-L and cholera toxin', *Hearing research*, 70(2), pp. 173-186.

Villa, A.E.P., Rouiller, E.M., Simm, G.M., Zurita, P., De Ribaupierre, Y. and De Ribaupierre, F. (1991) 'Corticofugal modulation of the information processing in the auditory thalamus of the cat', *Experimental Brain Research*, 86(3), pp. 506-517.

Villa, A.E.P., Tetko, I.V., Dutoit, P., De Ribaupierre, Y. and De Ribaupierre, F. (1999) 'Corticofugal modulation of functional connectivity within the auditory thalamus of rat, guinea pig and cat revealed by cooling deactivation', *Journal of neuroscience methods*, 86(2), pp. 161-178.

Volgushev, M., Vidyasagar, T.R., Chistiakova, M. and Eysel, U.T. (2000a) 'Synaptic transmission in the neocortex during reversible cooling', *Neuroscience*, 98(1), pp. 9-22.

Volgushev, M., Vidyasagar, T.R., Chistiakova, M., Yousef, T. and Eysel, U.T. (2000b) 'Membrane properties and spike generation in rat visual cortical cells during reversible cooling', *The Journal of physiology*, 522(1), pp. 59-76.

von Békésy, G. (1960) *Experiments in hearing*. McGraw-Hill.

Voytenko, S.V. and Galazyuk, A.V. (2008) 'Timing of sound-evoked potentials and spike responses in the inferior colliculus of awake bats', *Neuroscience*, 155(3), pp. 923-936.

Wallace, M.N., Shackleton, T.M. and Palmer, A.R. (2012) 'Morphological and physiological characteristics of laminar cells in the central nucleus of the inferior colliculus', *Frontiers in neural circuits*, 6.

Wang, J., Salvi, R.J. and Powers, N. (1996) 'Plasticity of response properties of inferior colliculus neurons following acute cochlear damage', *Journal of neurophysiology*, 75(1), pp. 171-183.

Warr, W.B. (1966) 'Fiber degeneration following lesions in the anterior ventral cochlear nucleus of the cat', *Experimental neurology*, 14(4), pp. 453-474.

Webster, W.R., Serviere, J., Martin, R. and Hartley, E. (1983) 'Tonotopic bands produced by tones commenced long after 2-deoxyglucose injection', *Neuroscience letters*, 40(3), pp. 281-286.

Whitfield, I.C. (1968) 'The functional organization of the auditory pathways', *Journal of Sound and Vibration*, 8(1), pp. 108-117.

Whitfield, I.C. and Purser, D. (1972) 'Microelectrode Study of the Medial Geniculate Body in Unanaesthetized Free-Moving Cats', *Brain, behavior and evolution*, 6(1-6), pp. 311-322.

Whitley, J.M. and Henkel, C.K. (1984) 'Topographical organization of the inferior collicular projection and other connections of the ventral nucleus of the lateral lemniscus in the cat', *Journal of comparative neurology*, 229(2), pp. 257-270.

Willott, J.F., Parham, K. and Hunter, K.P. (1991) 'Comparison of the auditory sensitivity of neurons in the cochlear nucleus and inferior colliculus of young and aging C57BL/6J and CBA/J mice', *Hearing research*, 53(1), pp. 78-94.

Willott, J.F. and Urban, G.P. (1978) 'Response properties of neurons in nuclei of the mouse inferior colliculus', *Journal of comparative physiology*, 127(2), pp. 175-184.

Winer, J.A., Chernock, M.L., Larue, D.T. and Cheung, S.W. (2002) 'Descending projections to the inferior colliculus from the posterior thalamus and the auditory cortex in rat, cat, and monkey', *Hearing research*, 168(1), pp. 181-195.

Winer, J.A., Larue, D.T., Diehl, J.J. and Hefti, B.J. (1998) 'Auditory cortical projections to the cat inferior colliculus', *Journal of comparative neurology*, 400(2), pp. 147-174.

Winer, J.A., Larue, D.T. and Pollak, G.D. (1995) 'GABA and glycine in the central auditory system of the mustache bat: structural substrates for inhibitory neuronal organization', *Journal of comparative neurology*, 355(3), pp. 317-353.

Winer, J.A. and Prieto, J.J. (2001) 'Layer V in cat primary auditory cortex (AI): cellular architecture and identification of projection neurons', *Journal of comparative neurology*, 434(4), pp. 379-412.

Winer, J.A., Saint Marie, R.L., Larue, D.T. and Oliver, D.L. (1996) 'GABAergic feedforward projections from the inferior colliculus to the medial geniculate body', *Proceedings of the National Academy of Sciences*, 93(15), pp. 8005-8010.

Xie, R., Meitzen, J. and Pollak, G.D. (2005) 'Differing roles of inhibition in hierarchical processing of species-specific calls in auditory brainstem nuclei', *Journal of neurophysiology*, 94(6), pp. 4019-4037.

Yan, W. and Suga, N. (1998) 'Corticofugal modulation of the midbrain frequency map in the bat auditory system', *Nature neuroscience*, 1(1), pp. 54-58.

Yang, L., Pollak, G.D. and Resler, C. (1992) 'GABAergic circuits sharpen tuning curves and modify response properties in the mustache bat inferior colliculus', *Journal of neurophysiology*, 68(5), pp. 1760-1774.

Yang, X.-F., Kennedy, B.R., Lomber, S.G., Schmidt, R.E. and Rothman, S.M. (2006) 'Cooling produces minimal neuropathology in neocortex and hippocampus', *Neurobiology of disease*, 23(3), pp. 637-643.

Yin, T.C.T. and Chan, J.C. (1990) 'Interaural time sensitivity in medial superior olive of cat', *Journal of neurophysiology*, 64(2), pp. 465-488.

- Yin, T.C.T. and Kuwada, S. (2010) 'Binaural localization cues', in Rees, A. and Palmer, A.R. (eds.) *The Auditory Brain*. Oxford University Press, pp. 271-302.
- Young, E.D., Spirou, G.A., Rice, J.J. and Voigt, H.F. (1992) 'Neural organization and responses to complex stimuli in the dorsal cochlear nucleus', *Philosophical Transactions of the Royal Society of London. Series B*, 336(1278), pp. 407-413.
- Yuan, B., Morrow, T.J. and Casey, K.L. (1986) 'Corticofugal influences of S1 cortex on ventrobasal thalamic neurons in the awake rat', *The Journal of Neuroscience*, 6(12), pp. 3611-3617.
- Zhang, D.X., Li, L., Kelly, J.B. and Wu, S.H. (1998) 'GABAergic projections from the lateral lemniscus to the inferior colliculus of the rat', *Hearing research*, 117(1), pp. 1-12.
- Zhang, H. and Kelly, J.B. (2006) 'Responses of neurons in the rat's ventral nucleus of the lateral lemniscus to monaural and binaural tone bursts', *Journal of neurophysiology*, 95(4), pp. 2501-2512.
- Zheng, Y. and Escabí, M.A. (2008) 'Distinct roles for onset and sustained activity in the neuronal code for temporal periodicity and acoustic envelope shape', *The Journal of Neuroscience*, 28(52), pp. 14230-14244.
- Zohar, O., Shackleton, T.M., Nelken, I., Palmer, A.R. and Shamir, M. (2011) 'First spike latency code for interaural phase difference discrimination in the guinea pig inferior colliculus', *The Journal of Neuroscience*, 31(25), pp. 9192-9204.